# P and S-centred reactions in a thiazole-fused 1,4-diphosphinine: insights into addition and redox chemistry

Dissertation

zur

Erlangung des Doktorgrades (Dr. rer. nat.)

der

Mathematisch-Naturwissenschaftlichen Fakultät

der

Rheinischen Friedrich-Wilhelms-Universität Bonn

vorgelegt von

Tim Achim Kalisch

aus

Bonn

Bonn 2024

Angefertigt mit Genehmigung der Mathematisch-Naturwissenschaftlichen Fakultät
der Rheinischen Friedrich-Wilhelms-Universität Bonn

Gutachter/Betreuer: Prof. Dr. Rainer Streubel
Gutachter: Prof. Dr. Sigurd Höger

Tag der Promotion: 14.10.2024
Erscheinungsjahr: 2024

Hiermit versichere ich, dass ich die vorliegende Arbeit unter Einhaltung der Regeln guter wissenschaftlicher Praxis selbständig verfasst, keine anderen als die angegebenen Quellen und Hilfsmittel benutzt und die Zitate kenntlich gemacht habe.

*For even the very wise cannot see all ends.*

— J. R. R. TOLKIEN

# Publications and conference contributions

## Publications

- *“New frontiers: 1,4-diphosphinines and P-bridged bis(NHCs)”* D. Welideniya, M. R. K. Ramachandran, T. Kalisch, R. Streubel, *Dalton Trans.* **2021**, *50*, 9345–9366. DOI: 10.1039/D1DT01624E

- *“[4 + 2]-Cycloadditions of a thiazol-based tricyclic 1,4-diphosphinine and a new easy 1,4-diphosphinine protection deprotection strategy”* I. Begum, T. Kalisch, G. Schnakenburg, Z. Kelemen, L. Nyulászi, R. Streubel, *Dalton Trans.* **2020**, *49*, 12776–12779. DOI: 10.1039/D0DT02529A

## Conference contributions

- European Workshop on Phosphorus Chemistry 2020 EWPC-17, Rennes (France), 26–28 February, **2020**, *"Cycloaddition and S-methylation reactions of a thiazole-2-thione-based tricyclic 1,4-diphosphinine"* (**Poster presentation**).

- Online Workshop on Phosphorus Chemistry 2021 (online), 29–31 March, **2021**, *"A thiazole-2-thione-based 1,4-diphosphinine anion and its conversion into a derivative with mixed P-valency"* (**Poster presentation**).

- International Conference on Phosphorus Chemistry 2021 ICPC23 (online), 04–09 July, **2021**, *"Surprising cycloaddition pathways of a 1,3-thiazole-2-thione based 1,4-diphosphinine"* (**Poster presentation**).

- Deutsch-Österreichischer Mitarbeiterworkshop 2021 MHC-11, Bonn (Germany), 02–05 September, **2021**, *"Novel cycloaddition reactions of a 1,3-thiazole-2-thione based 1,4-diphosphinine affording a mixed-valence product"* (**Oral presentation**).

- PacifiChem **2021** (online), Honolulu/Hawaii (United States of America), 16–21 December, *"Unveiling a novel oxidation-cycloaddition of a 1,4-diphosphinine"* (**Poster presentation**).

- International Symposium on Inorganic Ring Systems 2022 IRIS16, Graz (Austria), 24–29 July, **2022**, *"Synthesis of P(III) and P(III)/P(V) 1,4-diphosphabarrelenes"* (**Poster presentation**).

- American Chemical Society, ACS, Fall meeting - Sustainability in a Changing World, Chicago/Illinois (United States of America), 21–25 August, **2022**, *"Why bent, unstable P-linked 1,3-thiazole-2-thione-based bis(NHCs)?"* (**Poster presentation**).

- European Workshop on Phosphorus Chemistry 2022 EWPC-18, Rostock (Germany), 14–16 September, **2022**, *"Study on cycloaddition chemistry of a thiazole-2-thione based 1,4-diphosphinine"* (**Poster presentation**).

- European Workshop on Phosphorus Chemistry 2022 EWPC-19, San Sebastian (Spain), 28–30 March, **2023**, *"Local vs global: on the aromaticity in 1,4-diphosphinines"* (**Poster presentation**).

- European Workshop on Phosphorus Chemistry 2022 EWPC-20, Würzburg (Germany), 04–06 March, **2024**, *"Sequential 1,4-additions of a tricyclic, thiazole-2-thione based 1,4-diphosphinine"* (**Poster presentation**).

# CONTENT

# 1 INTRODUCTION

## 1.1 FROM APPLICATIONS OF MATERIALS TO MODERN CHEMISTRY

Since the very early beginnings, mankind has used and transformed natural resources for their purposes, starting with basic materials like stone and wood and working their way up to more complex processes such as charcoal burning and metallurgy. As progress continued, more and more natural products were used in various applications. Aztecs learned to use natural rubber in order to manufacture waterproof clothing,[1] while the Chinese wrote on paper made from the bast of paper mulberry.[2] In Europe, the practice of alchemy saw a plethora of (pseudo-) scientific studies from the late Medieval times to the later modern period, many of which were focused on creating gold from ignoble precursors or on finding the so-called Philosopher's Stone.[3] Numerous serendipitous findings were made in this context, *e.g.*, the discovery of the element Phosphorus by Henning Brand in 1669. He had boiled down urine and observed that the white residue gave off light. The process had involved generating sodium ammonium hydrogen phosphate ($Na(NH_4)HPO_4$), which was reduced to white phosphorus ($P_4$) by organic materials present in the urine. The white phosphorus in turn was oxidised to phosphorus oxides ($P_2O_3$ and $P_2O_5$), emitting light in the process and, thus, giving the element phosphorus its name.[4]

As alchemy slowly transformed into chemistry in the late 17$^{th}$ and 18$^{th}$ century, the knowledge about the nature of materials and compounds which were investigated expanded more quickly. This gave rise to a better understanding of structural features and their importance regarding chemical properties and reactivity. One example were nitrogen-containing heterocycles, being present in many of the commonly used natural products. In 1887 and 1888, respectively, Hantzsch and Widman independently suggested methods for the systematic nomenclature of such heterocyclic compounds,[5] which were later combined and expanded into the still-used Hantzsch-Widman nomenclature in a revised version.[6] Remnants of its origin in the naming of nitrogen-containing compounds persist to this day, with the names of these heterocycles consistently differing from those of cycles containing different heteroelements.

## 1.2 NITROGEN-CONTAINING HETEROCYCLES

### 1.2.1 Azines and diazines

With the first isolation in 1846 and the structural elucidation around 1870, pyridine **I** (or azine according to IUPAC nomenclature) became one of the first heteroaromatic compounds structurally known to literature (Figure 1).[7] Today, its importance for coordination chemistry,

catalysis and pharmacology cannot be overstated.[7,8] Synthetic routes to pyridine derivatives and their properties and reactivities have been studied in detail for over 100 years,[9,10] making it one of the most versatile building blocks particularly in the design of antibacterial, -viral and -fungal drugs.[7] Although isoelectronic to benzene, the substitution of a methyne group for a nitrogen atom has important implications for the reactivity of pyridine, making it a π-deficient aromatic compound and more prone to nucleophilic substitutions, while the degree of aromaticity remains similar to that of benzene.[11]

The formal substitution of a second methyne group for nitrogen in pyridine gives a diazine. Three diazine isomers are possible, 1,2- (pyridazine) **II**, 1,3- (pyrimidine) **III** and 1,4-diazine (pyrazine) **IV**. Effects of pyridine are exaggerated in these compounds: the effect of π-deficiency is stronger, making diazines better electrophiles than the corresponding pyridines, and reducing basicity on the nitrogen centre(s).[12] However, similar to pyridine, diazines have found applications in many different fields, *e.g.* biochemical and biomedical applications, non-linear optical materials, as well as organometallic and polymer chemistry.[13]

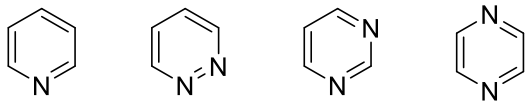


**I** **II** **III** **IV**

*Figure 1:* Pyridine **I**, pyridazine **II**, pyrimidine **III** and pyrazine **IV**.

One of the most prominent features contributing to the remarkable stability of such cyclic systems is aromaticity.[14] This concept was introduced more than 150 years ago when some compounds showed an unusual stabilisation that was significantly stronger than expected. In 1865, Kekulé recognised the structure of benzene, giving birth to the first structural description of an aromatic compound.[15] A more general approach was used by Hückel in 1931 when he published his theory, using a molecular orbital (MO) approach to predict the aromaticity of a compound. This method, known as the “Hückel-rule”, works by simply counting the number of π-electrons in a given conjugated ring system (to 4n+2 for aromatic compounds),[16] yet, although it provides a reliable indication of the presence or absence of an (anti-)aromatic effect in a molecule, it does not directly address the intensity of this effect. Pauling and Mulliken expanded on this theory, but a quantification of aromaticity remained a challenge.[17,18] To tackle this problem, a number of methods have been developed since, using several different approaches,[19] including (but not limited to) energetic criteria such as the aromatic stabilisation energy (ASE),[20] geometry-based investigations such as the harmonic oscillator model of aromaticity (HOMA),[21] electronic assessments like the electron localisation function (ELF)[22] or magnetics-based indices like the nucleus independent chemical shift (NICS).[23] As the number of different indices to describe aromaticity continued to increased, the discussion about the

strengths and weaknesses of said descriptors and about the nature of aromaticity itself has been reignited and is currently a topic of intense debate.[24]

One of the most commonly used methods to gauge aromaticity is NICS (nucleus independent chemical shift). This technique was introduced by P. v. R. Schleyer in 1996[23] and has been used for many different classes of aromatic compounds.[14,25,26] Consequently, many tweaks and improvements to this approach have been published since its first report, mainly pushed by Stanger.[27–30] The big problem of σ-electron density contaminating the assessment of the aromatic (π-)ring current was overcome by introducing sigma-contribution- and off-centre effect-free methods such as the σ-only model (SOM).[28] While still encountered to this date, the original NICS calculations are being phased out and replaced by $NICS_{\pi,zz}$.[30] A recent addition to this field was presented recently in form of $\int NICS_{\pi,zz}$,[29] and even further expansion of NICS was achieved when calculating trajectories across the XY plane of multicyclic systems, opening the door for the understanding of aromaticity as a global feature of polycyclic compounds.[31] Additionally, two-dimensional NICS scans have been performed across the whole ring area of a given molecule.[32]

### 1.2.2 *N*-heterocyclic carbenes

Nowadays, one class of nitrogen-containing cyclic compounds has risen to extraordinary prominence, namely, *N*-heterocyclic carbenes (NHCs), which are most commonly derived from imidazoles, *i.e.*, 1,3-diazoles. Although first indirect studies on the class of carbenes, compounds containing a carbon atom with an electron sextet, had been done in the early 1800s,[33] the first fundamental research towards NHCs was conducted by Wanzlick in the 1960s, who thermally cleaved off chloroform from 1,3-diphenyl-2-trichloromethyl-imidazoline to *in situ* generate 1,3-diphenyl-imidazoline-2-ylidene. However, he observed the rapid dimerisation of this NHC to **V** (Figure 2).[34]

Much later, the work on carbenes was extended by Bertrand who reported on the synthesis of the first isolable carbene **VI**.[35] However, a significant P-C double- and triple-bond character was found in **VI**, so the bonding situation and, hence, the presence of a carbene centre remained under intense discussion. Shortly afterwards, the breakthrough in this field was achieved by Arduengo in 1991.[36] He synthesised the first crystalline carbene **VII**, which led to a rapid expansion of the field in both theoretical and experimental studies.[37] Several different synthetic approaches to such (and other) NHCs have been developed since (Figure 2, bottom), the most prominent being deprotonation of 1,3-imidazolium salts **VIII**,[38–43] or reductive desulfurisation of 1,3-imidazole-2-thiones **X** (in the following, "1,3-" will be omitted for 1,3-imidazoles and related compounds in order to increase readability).[44–46]

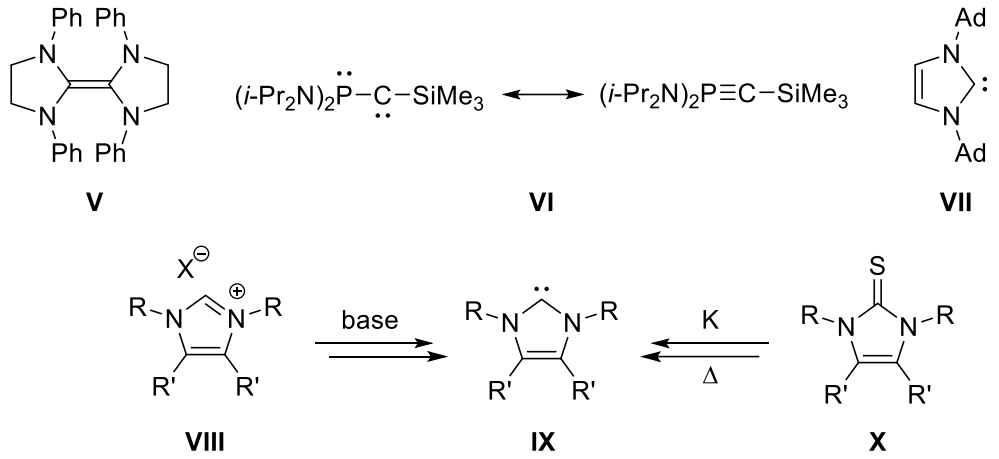


*Figure 2:* Stuctures of important contributions to the carbene development (top, Ad = adamantyl)[34–36] and general synthetic approaches to NHCs (bottom).[38–46]

The remarkable stability of NHCs can be attributed to the electronic effect of the nitrogen atoms neighbouring the low-valent carbon atom, stabilising the latter both mesomerically via π-donation into its empty p-orbital as well as inductively by withdrawing σ-electron density from carbene carbon atom.[47,48] Substituents at nitrogen further stabilise NHCs kinetically by disfavouring their dimerisation due to steric hindrance.[47] The resulting versatility of NHCs towards substituents and synthetic routes led to the development of a multitude of variants of the classical NHCs, like the cyclic (alkyl)(amino)carbenes (CAACs) **XI**[49] or mesoionic carbenes (MICs, also called abnormal carbenes) **XII** (Figure 3).[50,51]

Another noteworthy addition to this field was the development of multitopic bis-NHCs which are of great interest in organometallic chemistry and catalysis due to their flexible backbone allowing a bidentate behaviour.[52] Conversely, bis-NHCs possessing a rigid backbone were much less explored.

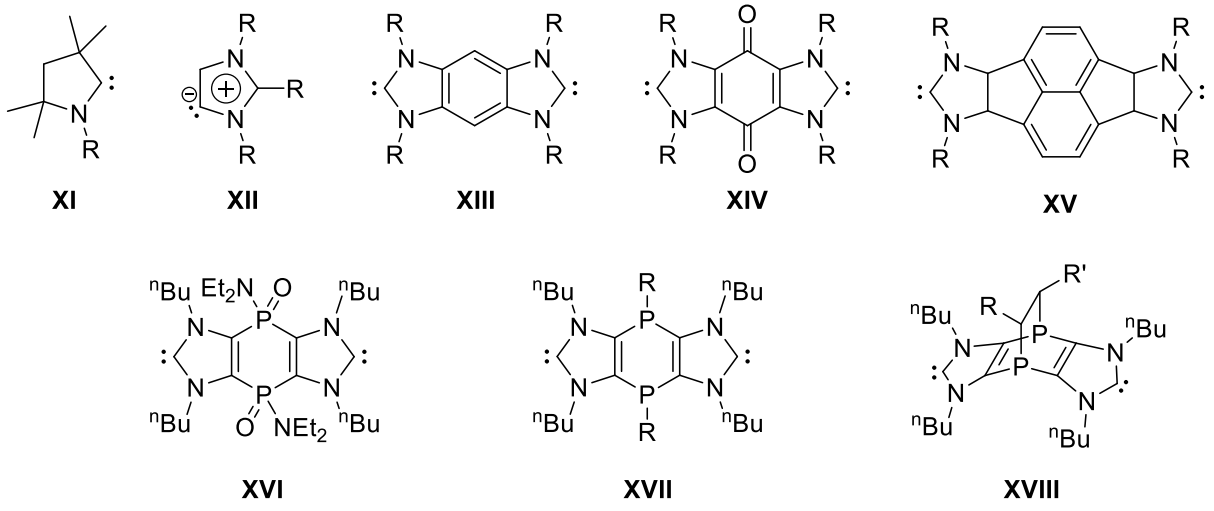


*Figure 3:* Examples of CAAC (**XI**),[49] mesoionic NHC (**XII**)[50,51] and rigid bis-NHCs (**XIII–XV**) (top)[53–58] and P-bridged bis-NHCs **XVI–XVII** (bottom).[59,60]

It was only in the last two decades that some derivatives of these so-called Janus-type[61] compounds were reported, mainly by Bielawski and Peris (Figure 3, **XIII–XV**).[53–58,62] Until very recently, almost no rigid, heteroatom-linked bis-NHCs were known.[63] In 2020 and 2021, Streubel published the first P-bridged rigid bis-NHCs **XVI,XVII**,[59,60] and was recently able to expand on this finding with the isolation of rigid-bent bis-NHCs **XVIII** (Figure 3, bottom).[64]

While all previously discussed (bis-)NHCs are based on an imidazole-framework, the effect of different heteroelements in the five-membered rings was also explored, the most common approach being the formal substitution of one nitrogen unit by a sulfur atom. The first stable thiazole-2-ylidene **XX** was synthesised by Arduengo by deprotonation of a thiazolium salt with potassium hydride (Scheme 2, top).[65] He observed a fast dimerisation of the carbene in the presence of trace amounts of Brønsted acids to form the respective *E*-dithiadiazafulvalene (DTDAF) **XXI**, which was strongly dependent on the substituent at nitrogen. While bulky aryl groups primarily led to the formation of the thiazole-2-ylidene, only the dimeric form was observed when employing alkyl substituents. This tendency for dimerisation was confirmed by later reports and was found to be a general trend upon substitution of one or both nitrogen atoms for a different pnictogen/chalcogen.[66,67,68] Nevertheless, thiazole-2-ylidenes could be generated *in situ* and used in different applications, *e.g.*, in organocatalysis.[69] Synthesis of these transient carbenes was most commonly done by deprotonation of the respective thiazolium salts **XXIII** which in turn were generated directly from thiazole derivatives or from thiazole-2-thiones or -selones (Scheme 1, bottom).[65,66,68,70–73] However, compared to imidazole-2-ylidenes, only very few such compounds have been synthesised to date.

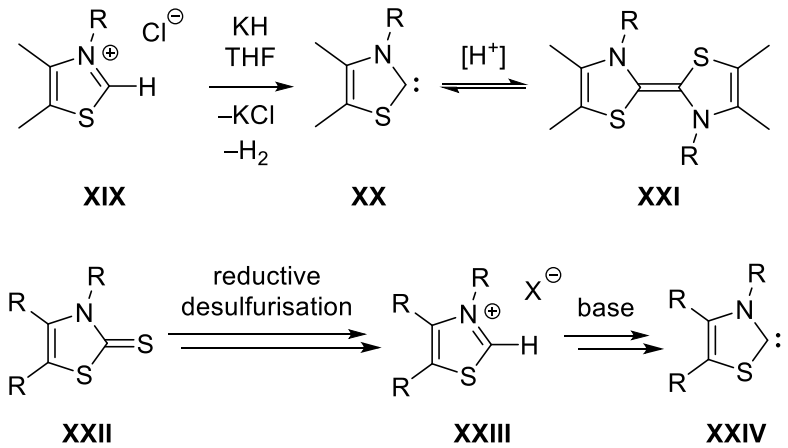


*Scheme 1:* Synthesis and dimerisation of the first thiazole-2-ylidene **XX** (top, R = aryl, Me)[65] and proven synthetic procedure for thiazole-2-ylidenes **XXIV** from thiazole-2-thiones **XXII** (bottom, R = aryl, alkyl).[65,66,68,70–73]

## 1.3 PHOSPHORUS-CONTAINING HETEROCYCLES

### 1.3.1 Phosphinines

The first example of a derivative of the heavier homolog of pyridine, the $\sigma^2\lambda^3$-phosphinine, was synthesised in 1966 by Märkl by reacting the pyrylium salt **XXV** with tris(hydroxymethyl)phosphane to give **XXVI** (Figure 4, top left).[74]

Five years later, Ashe was able to report on the parent-compound **XXVIII**, providing a synthetic pathway via 1,4-dihydro-stannine **XXVII** (Figure 4, bottom left).[75] Since then, the properties and reactivity of phosphinines have been extensively studied. This class of compounds contains a low-coordinate $\sigma^2\lambda^3$-phosphorus atom in the aromatic ring, disturbing the $\pi$-conjugation and, hence, phosphinines were reported to possess a lower degree of aromaticity (90%) compared to benzene and pyridine.[26] Additionally, this disturbance of $\pi$-conjugation effects the frontier molecular orbitals (FMOs) of phosphinines compared to their nitrogen-analogues (Figure 4, right).[17,76] While the general shape of the FMOs remains the same in pyridine and phosphinine, their relative energetic order changes drastically. Most notably, the P-lone pair does not constitute the highest occupied molecular orbital (HOMO) like in pyridine, but the lower-lying HOMO−2. Additionally, upon formal substitution of N for P, the lowest unoccupied molecular orbital (LUMO) is lowered dramatically. These effects combined make phosphinine a worse $\sigma$-donor, but a better $\pi$-acceptor than pyridine.

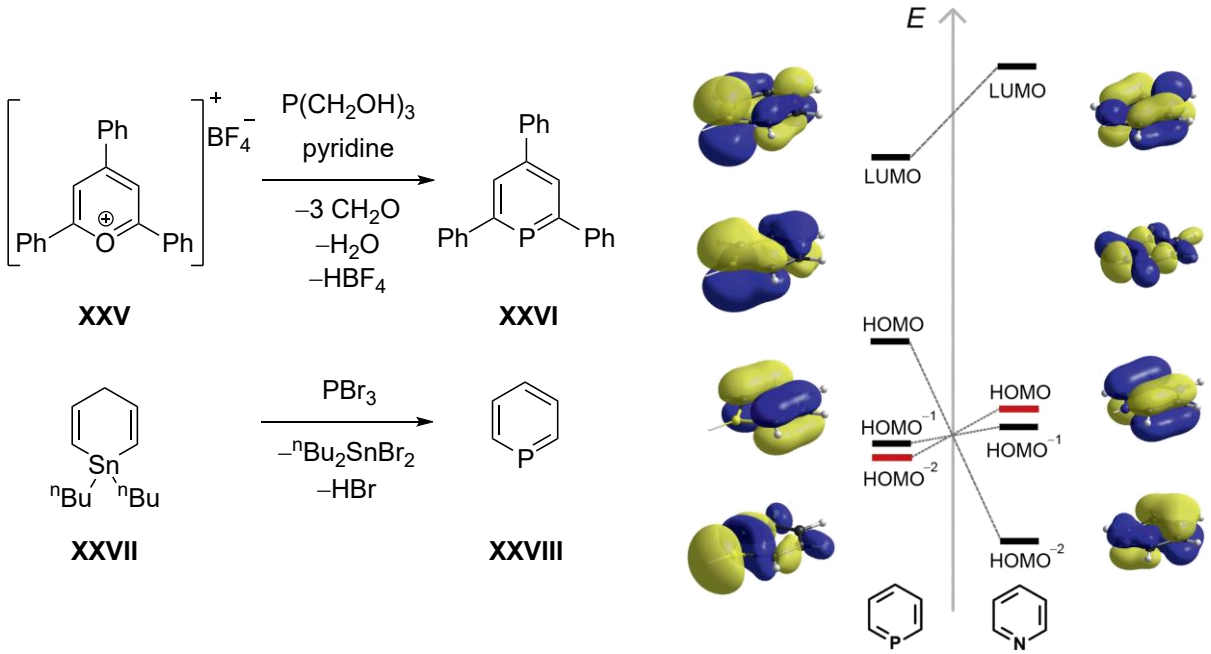


*Figure 4:* First synthesis of a phosphinine (**XXVI**, top left),[74] synthesis of parent phosphinine **XXVIII** (bottom left)[75] and electronic structures of frontier molecular orbitals (FMOs) of phosphinine compared to pyridine (right, respective lone pair levels are shown in red; taken form a literature contribution from C. Müller).[17,76]

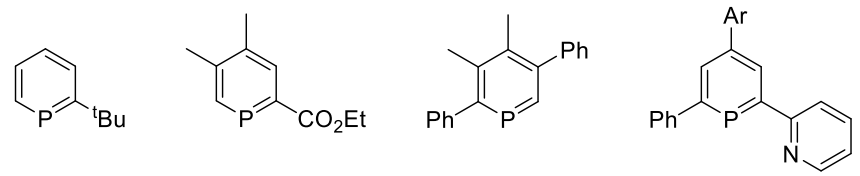


**XXIX** **XXX** **XXXI** **XXXII**

*Figure 5:* Selected examples of phosphinines synthesised via different synthetic routes.[77–80]

Since their first report, several different synthetic routes to phosphinines have been found,[81,82] *e.g.*, the reaction of pyrones with phosphaalkynes to give substituted phosphinines like **XXIX** (Figure 5).[77] The thermal reaction of a phosphole sulfide with ethyldiazoacetate and subsequent reduction with triphenylphosphite was found to form **XXX**,[78] while several metal-mediated pathways were reported, *e.g.*, yielding **XXXI**.[80] Furthermore, phosphinines like **XXXII**, carrying additional functional groups, are used in transition metal complexes.[79]

Reactivity studies of phosphinines were performed with different focuses in mind. Firstly, various organic transformations and functionalisations have been reported, like reactions with nucleophiles such as Grignard reagents or organolithium compounds to afford (anionic) $\lambda^4$-phosphinine salts which can successively be reacted with electrophiles giving access to substitution products with different regiochemistry (Figure 6, **XXXIII–XXXV**).[17,82–85] Moreover, multiple P-oxidation reactions are known, yielding phosphoranes and phosphane oxides (**XXXVI,XXXVII**).[86] Besides a great variety of applications in organometallic chemistry,[79,80,87] phosphinines are known to undergo Diels-Alder type [4+2]-cycloadditions[88] forming phospha-barrelenes. Although other synthetic approaches have been studied,[89] this is the most common route to this type of structural motif (Figure 6, bottom).[90] As sterically demanding phosphine ligands, phosphabarrelenes have been used in organometallic chemistry, *e.g.*, for hydroformylations.[89,91] Yet, the number of phosphabarrelene structures remains small to this day.

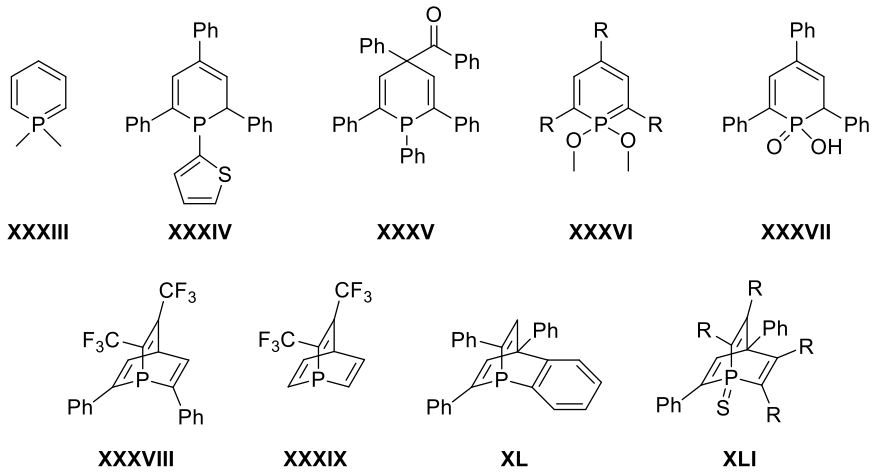


**XXXIII** **XXXIV** **XXXV** **XXXVI** **XXXVII**

**XXXVIII** **XXXIX** **XL** **XLI**

*Figure 6:* Selected examples of addition reactions to phosphinines (top) and phosphabarrelenes (bottom, R = $CF_3$).[17,83–85]

### 1.3.2 Diphosphinines

While phosphinines, compared to pyridines, represent a relatively established class of compounds, only a few derivatives of the heavy homologs of diazines, the diphosphinines, are known to literature. Like for the diazines, three substitution patterns are possible: 1,2-, 1,3- and 1,4-diphosphinines.[10] In 1991, Bickelhaupt published the synthesis of $1\lambda^5,2\lambda^3$-diphosphinine **XLIV** in successive reaction of **XLII** with hydrogen chloride (HCl) to achieve a ring closure affording **XLIII** and magnesium to reduce the intermediate to **XLIV** (Scheme 2, top).[92] Isolation of **XLIV** was not possible due to a side product present in the final mixture and the structure of **XLIV** was postulated via $^{31}$P nuclear magnetic resonance (NMR) spectroscopy. To this day, this compound remains the only example of a 1,2-diphosphinine known to literature.

The synthesis and reactivity of 1,3-diphosphinines has been comparatively more explored. Although $1\lambda^5,3\lambda^5$-diphosphinines were known as early as the late 1980s,[93] the first $1\lambda^3,3\lambda^3$-diphosphinine **XLVII** was reported in 1995 by Zenneck by cyclodi- and -trimerising alkynes and phosphaalkynes at an iron centre (Scheme 2, bottom).[94] Schmidpeter followed shortly after by preparing the dicationic 1,3-diphosphininium salts **XLIX** in a dechlorination reaction of the 1,3-diphosphatetralines **XLVIII** with two equivalents of gallium trichloride (Scheme 3, top).[95] The only other $1\lambda^3,3\lambda^3$-diphosphinines **LI** were published in 2000 by Heydt, forming in a reaction of cyclopropene **L** with phosphaalkynes (Scheme 3, bottom).[96]

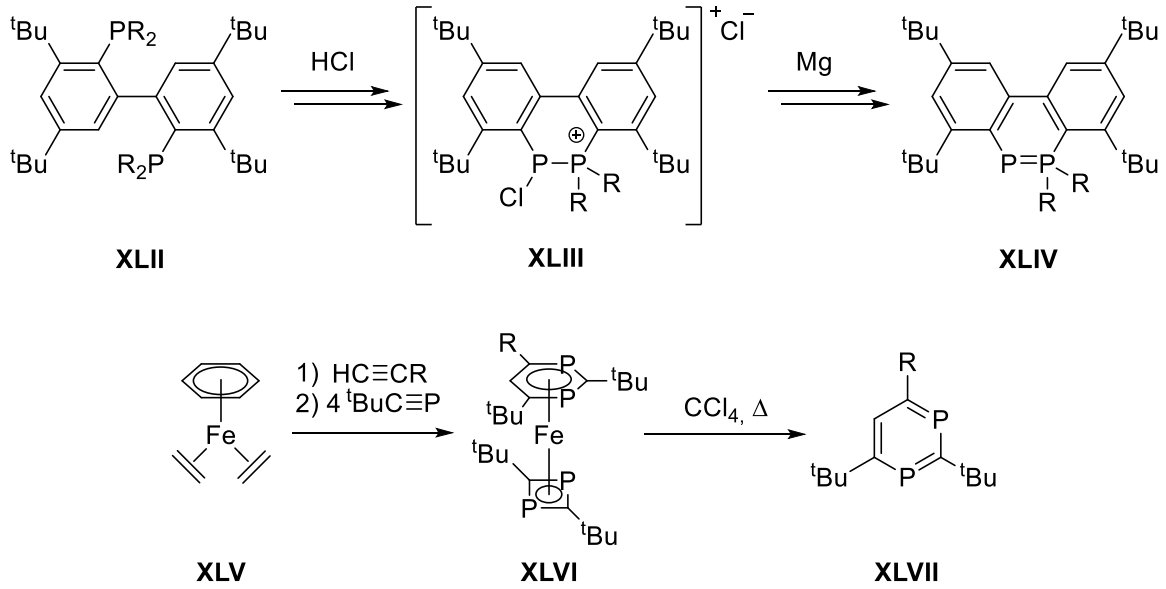


*Scheme 2:* Synthesis of the only 1,2-diphosphinine **XLIV** (top, R = $NMe_2$)[92] and the first 1,3-diphosphinine **XLVII** (bottom, R = H,$CH_2OC(O)CH_3$).[94]

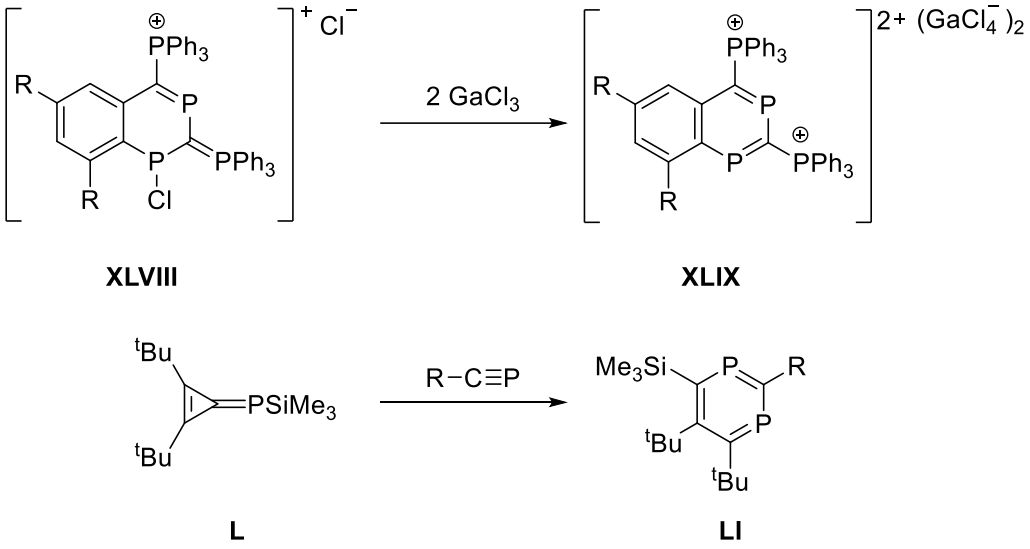


*Scheme 3:* Synthesis of dicationic 1,3-diphosphininine **XLIX** from precursor **XLVIII** (top, R = H, Me)[95] and 1,3-diphosphinine **LI** from **L** (bottom, R = alkyl).[96]

The third regioisomer of diphosphinines, the 1,4-diphosphinine, is known to literature since 1976.[97] Kobayashi synthesised the first example starting from hexafluoro-2-butyne which upon treatment with red phosphorus and catalytic amounts of iodine forms **LII** at 200 °C under pressure.[98] **LII** was then reacted with rhodium trichloride in methanol, affording **LIV** under reflux conditions via intermediate **LIII** (Scheme 4).[97] However, due to its instability, **LIV** could not be isolated and was only handled as a *n*-hexane solution. After this first report, it took until 2017 for the first stable 1,4-diphosphinine **LVI** to be isolated by Streubel (Figure 7).[99] The synthesis of this imidazole-based tricyclic compound involved 1,4-dihydro-1,4-diphosphinine precursors which were reduced using tri-*n*-butylphosphane to give **LVI**.

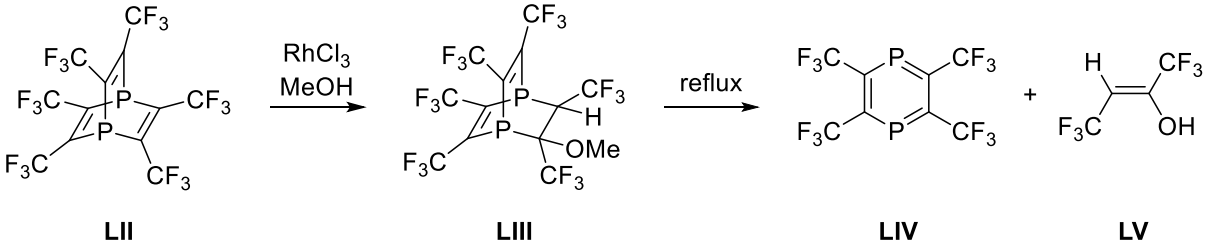


*Scheme 4:* Synthesis of the first 1,4-diphosphinine **LIV** from 1,4-diphosphabarrelene **LII**.[97]

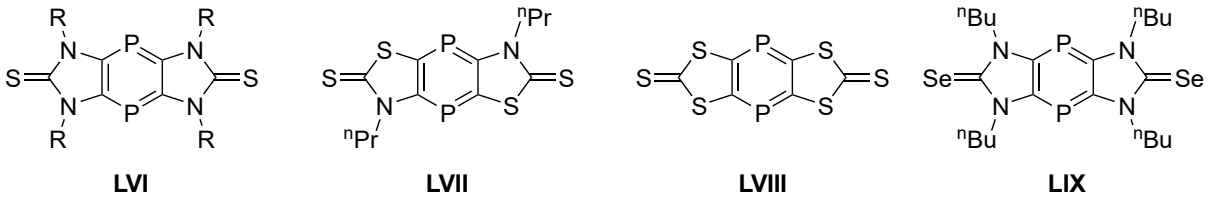


*Figure 7:* Stable, tricyclic 1,4-diphosphinines **LVI–LIX** synthesised by Streubel (R = Me, *n*-Bu).[59,99–101]

Shortly after, a very similar approach was used in the synthesis of related tricyclic 1,4-diphosphinines based on imidazole-2-selones (**LIX**),[59] thiazole-2-thiones (**LVII**),[100] or dithiol-2-thiones (**LVIII**),[101] as well as indications for a tetrathiafulvalene-based 1,4-diphosphinine.[102] Another contribution to the field was a dicationic tricyclic 1,4-diphosphinine synthesised by Ghadwal.[103] It has to be noted, that in the case of **LVIII**, the 1,4-diphosphinine product could not be isolated due to insolubility, but the presence of **LVIII** in the mixture was confirmed by a [4+2]-cycloaddition with diethylacetylene dicarboxylate (DEAD), where the respective 1,4-diphosphabarrelene was formed. Different theoretical and experimental studies on the properties and reactions of the 1,4-diphosphinines synthesised by Streubel were carried out since their first report. A look into the FMOs of **LVI$^{Me}$–LVIII** (the N-methyl derivatives of **LVI–LVII**) compared to the parent compound, 1,4-diphosphinine (**LIV$^{H}$**, "$^{H}$" denoting all-hydrogen substitution), can (to some extent) be an indicator for the expected reactivity (Figure 8).[104]

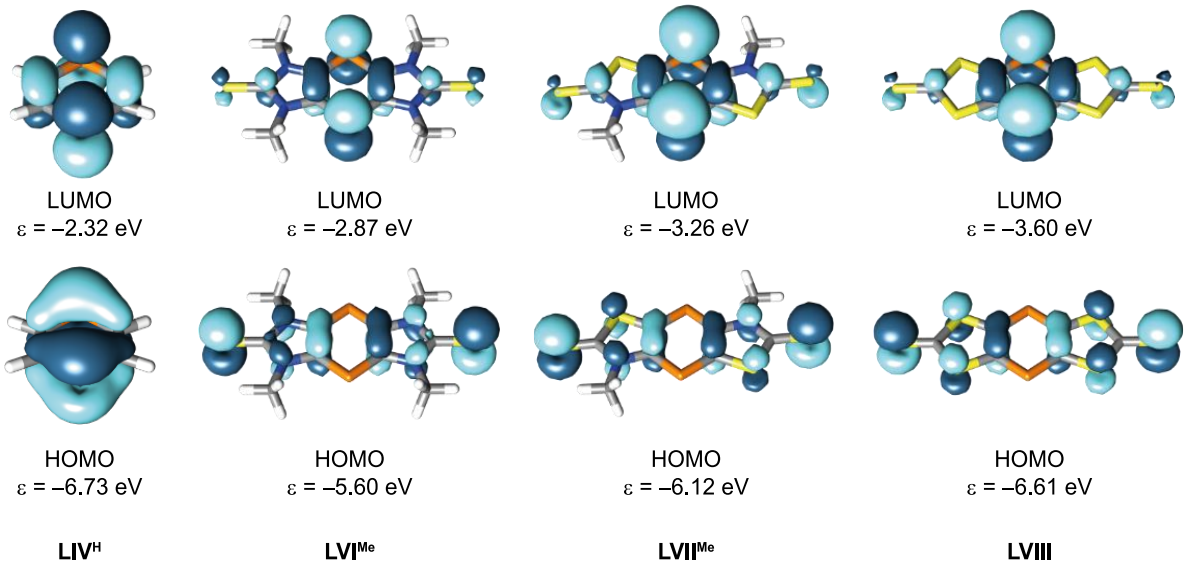


*Figure 8:* FMOs with their respective energies of 1,4-diphosphinine (denoted as **LIV$^{H}$**) and methyl derivatives (denoted as $^{Me}$) of tricyclic 1,4-diphosphinines **LVI–LVII**, as well as **LVIII**.[104]

*Table 1:* HOMO/LUMO gaps and NICS(1)-values of benzene ($C_6H_6$), parent phosphinine **XXVIII**, parent 1,4-diphosphinine **LIV$^{H}$** and **LVI$^{Me}$**, **LVII$^{Me}$** and **LVIII**.[104]

| | HOMO/LUMO gap / eV | central ring NICS(1) / ppm | outer ring NICS(1) / ppm |
|---|---|---|---|
| $C_6H_6$ | — | −12.8 | |
| **XXVIII** | — | −11.4 | |
| **LIV$^{H}$** | 4.41 | −10.4 | |
| **LVI$^{Me}$** | 2.73 | −8.5 | −6.1 |
| **LVII$^{Me}$** | 2.86 | −7.6 | −4.4 |
| **LVIII** | 3.01 | −6.6 | −2.8 |

The HOMOs of **LVI$^{Me}$–LVIII** are all comprised of the $\pi$-symmetric anti-bonding combination of the respective five-membered rings (imidazole-2-thione, thiazole-2-thione or dithiole-2-thione) and are significantly higher in energy than the HOMO of **LIV$^{H}$**. Conversely, the LUMOs of **LVI$^{Me}$–LVIII** are stabilised compared to the parent-compound's LUMO, but are very similar in shape, consisting mainly of the $\pi^*$-symmetric LUMO of parent 1,4-diphopsphinine **LIV$^{H}$**. Additionally, the HOMO/LUMO gaps of tricyclic **LVI$^{Me}$–LVIII** are much smaller than that of **LIV$^{H}$**, though increasing for a higher sulfur content in the annulated rings (Table 1).[104] The P-lone pairs of these three compounds are represented in energetically low lying FMOs being HOMO−6 (**LVI$^{Me}$**, $\varepsilon$ = −8.40 eV), HOMO−7 (**LVII$^{Me}$**, $\varepsilon$ = −8.85 eV) and HOMO−5 (**LVIII**, $\varepsilon$ = −8.89 eV), respectively, hinting at a poor $\sigma$-donor strength for these 1,4-diphosphinines. The effect of the fused heterocycles on the central ring is also apparent in NICS(1) values (Table 1). A decrease of aromaticity upon formal substitution of methyne units for phosphorus atoms can be found when comparing benzene to **XXVIII** and **LIV$^{H}$**. Similarly, NICS(1) values of **LVI$^{Me}$–LVIII** are less negative for a higher sulfur content, implying a further diminishing of the degree of aromaticity. However, the outer heterocycles were also found to possess a certain degree of aromaticity as indicated by the (albeit small) negative NICS(1) values.[104]

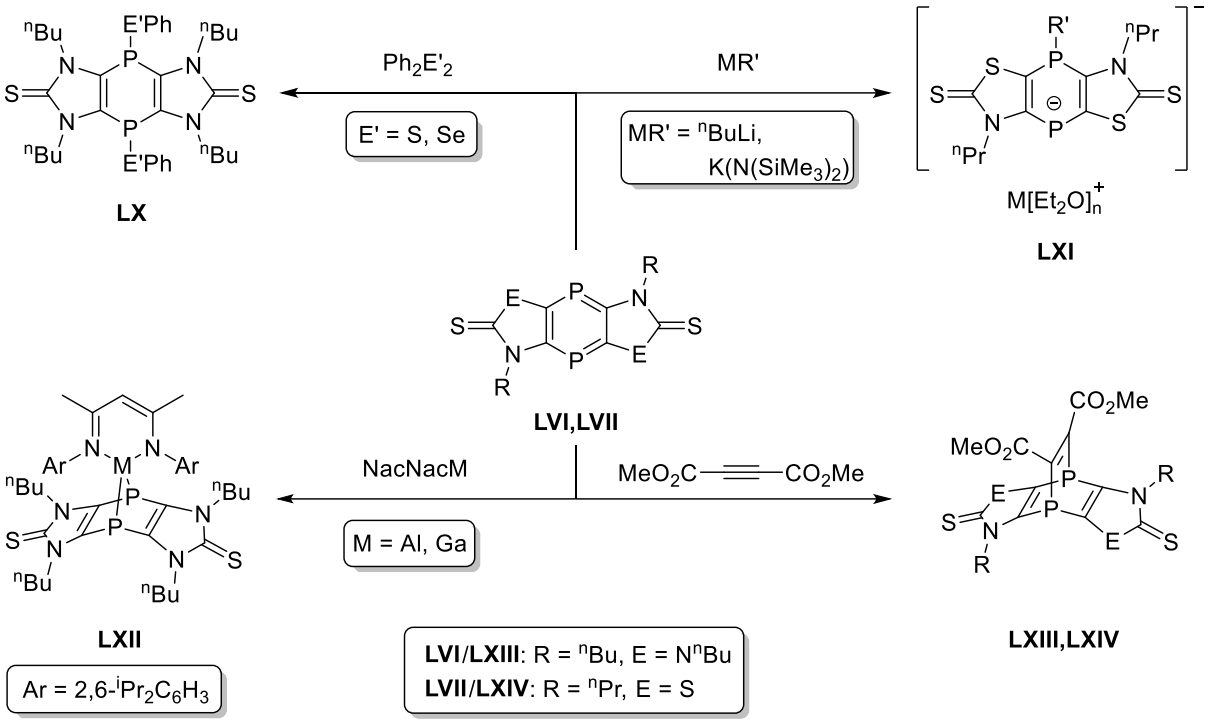


*Scheme 5:* Addition reactions to 1,4-diphosphinines **LVI,LVII** to form 1,4-addition products **LX**[105] and P-anionic **LXI**[100] (top) and cycloaddition reactions to give 1,4-diphosphanorbornadienes **LXII**[106] (NacNacM = 1,2-dihydro-1,3-bis(2,6-di-*i*-propylphenyl)-4,6-dimethyl-1,3,2-diazametalinine) and -barrelenes **LXIII,LXIV**[100–102,105]

In addition to theoretical investigations, compounds **LVI–LIX** have been studied extensively with regard of their reactivities. Among these are 1,4-addition reactions with dichalcogenides to form ***trans*-LX** (Scheme 5),[105] additions of nucleophiles affording the respective P-anionic compounds **LXI**, which could subsequently be reacted with electrophiles to 1,4-dihydro-1,4-diphosphinines,[100] as well as cycloaddition reactions with low-coordinate group 13 compounds to 7-metalla-1,4-diphosphanorbornadienes **LXII**[106] (in analogy to the all-carbon system norbornadiene[107] while having phosphorus atoms at the fusion positions) or 1,4-diphospha-barrelenes (in analogy to the all-carbon system barrelene[108]) like **LXIII** and **LXIV**.[100–102,105] Furthermore, pseudo-dimerisation reactions of anionic 1,4-dihydro-1,4-diphosphinines were observed after oxidation, as well as reactions with electrophiles at the thione/selone moieties.[59,100,109]

# 2 OBJECTIVE OF THIS WORK

The main focus of this work lay on reactivity studies of a tricyclic thiazole-2-thione-based 1,4-diphosphinine. As this class of compounds has only seen initial research efforts in the last few years and, hence, knowledge remains very scarce to this day, several goals were set out:

1. Addition reactions of a thiazole-2-thione based 1,4-diphosphinine and comparison of its reactivity to differently substituted 1,4-diphosphinines, mainly, an imidazole-2-thione-based 1,4-diphosphinine.
2. [4+1]- and [4+2]-cycloaddition reactions and assessment of the tendency to form 1,4-diphosphanorbornadienes and 1,4-diphosphabarrelenes.
3. Investigation of the formed cycloaddition products with regard to reactivity both at phosphorus and at the thione moieties.
4. Desulfurisation of the thione moieties to form thiazolium salts and, further, thiazole-based carbene centres with the goal of di- or oligomerising these reactive bis-carbenes.

# 3 RESULTS AND DISCUSSION

## 3.1 1,4-ADDITION REACTIONS

### 3.1.1 Synchronous additions

As the tricyclic 1,4-diphosphinine **LVII** is the basis for the following work, it will be denoted as **1** in the following. In a seven-step synthesis, 1,4-diphosphinine **1** was synthesised from *n*-propylamine and carbon disulfide following a literature-known protocol.[100] Although some sequential additions of nucleophiles and electrophiles to **1** were reported earlier, no thermal synchronous [4π+2σ]-cycloaddition reaction of **1** to a 1,4-dihydro-type structure of **1** had been performed.[100] In order to study the P-centred reactivity of **1** different 1,4-addition reactions were carried out. In analogy to **LVI**,[105] **1** was treated with diphenyldisulfane under thermal conditions in order to form 1,4-dihydro compound **2** (Scheme 6).

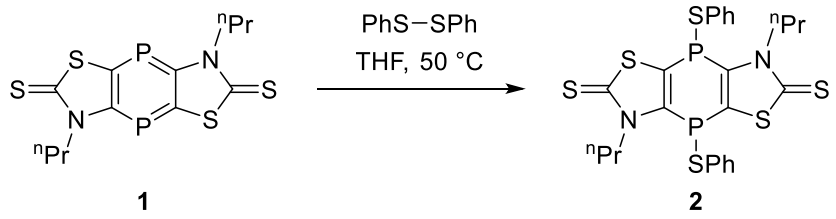


*Scheme 6:* Reaction of **1** with diphenyldisulfane.

In contrast to the reaction observed for the imidazole-based **LVI**, the conversion to **2** proceeded already at 50 °C in THF, and after stirring for 3 h the red suspension had turned yellow. $^{31}P\{^{1}H\}$ NMR spectroscopic monitoring of the reaction mixture revealed a full conversion of **1** to the product **2** which appeared in the spectrum as a singlet at a chemical shift of −20.8 ppm. Volatiles were removed *in vacuo* ($10^{-2}$ mbar) and the residue was washed with *n*-pentane. **2** was fully characterised by multinuclear NMR spectroscopy, MS, IR spectroscopy and EA. Interestingly, in analogy to **LVI**, only one diastereomer of **2** was obtained in the reaction.[105] As no crystal structure could be obtained from the product, the exact nature of the diastereomer could not be determined. However, in spite the close relation of **2** to **LVI**, the assumption of the *trans* diastereomer being formed cannot be made. While the formation of **2** is thought to proceed analogously to that of **LX**, namely, via a [4π+2σ]-cycloaddition to initially form the *cis* isomer ***cis*-2**,[105] the succeeding conversion to the 0.4 kcal/mol more stable ***trans*-2** likely does not take place in this case as the temperature of 50 °C does not allow for an easy isomerisation overcoming a barrier of 31.2 kcal/mol according to theoretical calculations of the N-methyl substituted systems (**"Me"**, PW6B95-D3(BJ)/def2-QZVP($CPCM_{THF}$)//TPSS-D3(BJ)/def2-TZVP($CPCM_{THF}$), for a detailed description of theoretical methods see section 5.5).

As a P-silyl structural motif can be a valuable precursor for further conversions, a reaction of **1** with reducing agents, namely, magnesium and potassium graphite ($KC_8$), forming literature-known **3**,[110] and subsequent addition of trimethylsilyl chloride (TMS-Cl) was performed in order to get the formal 1,4-addition product **4a** (Scheme 7).

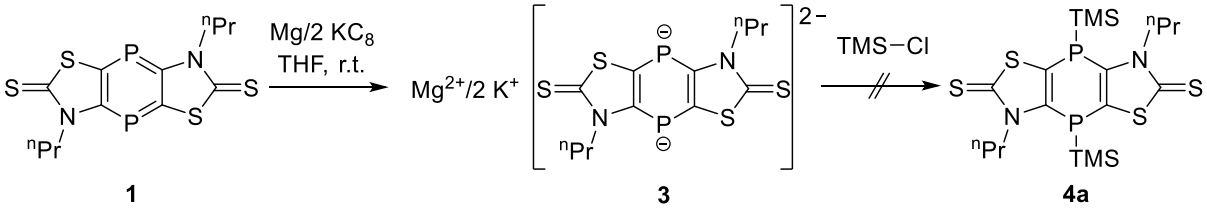


*Scheme 7:* Reaction of **1** with magnesium or potassium graphite and trimethylsilyl chloride.

Initially, **1** was treated with an excess of Mg (26 eq.), followed by addition of a slight excess of TMS-Cl after 15 min. While the reaction was found to proceed slowly, $^{31}P\{^1H\}$ NMR spectroscopic monitoring showed the selective formation of one product after 24 h (Figure 9, top). However, the observed two doublets were not assigned to the desired product as **4a** is expected to have a chemical shift in the highfield region of the $^{31}P$ NMR spectrum (between −80 to −120ppm). Instead, as the formed product showed an AB-type spin system with a coupling constant of 7.85 Hz, the signals were tentatively assigned to the mono-silylated product **4a'** in analogy to similar known structures (Figure 10, left).[100]

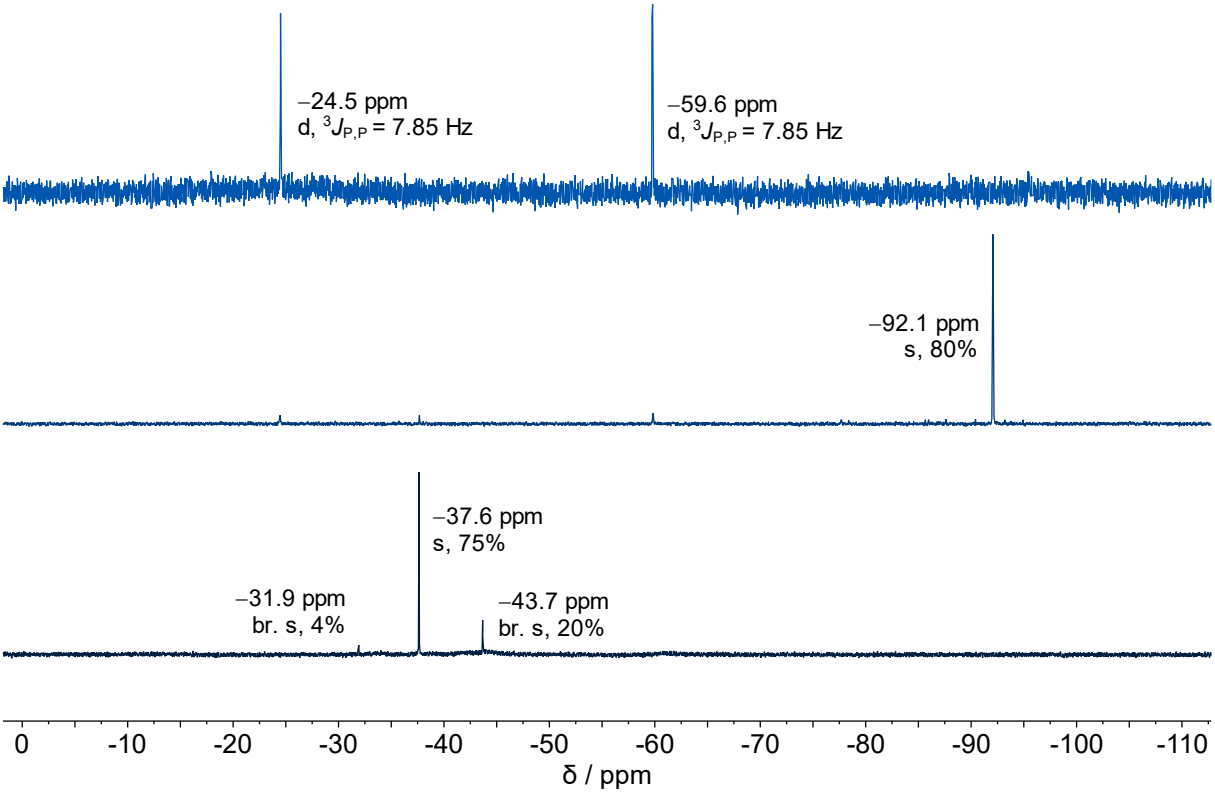


*Figure 9:* $^{31}P\{^1H\}$ NMR spectra of the reaction mixture of **1** with Mg/TMS-Cl (top), a small scale of **1** with $KC_8$/TMS-Cl (middle) and upscaling of the latter reaction (bottom).

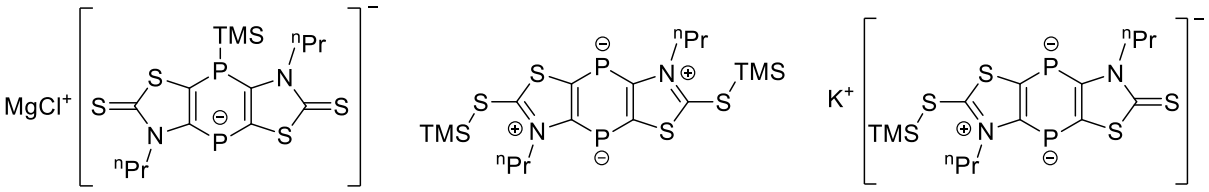


*Figure 10:* Possible (intermediate) products in reactions of **1** with $Mg/KC_8$ and TMS-Cl.

**4a'** can be an intermediate in the silylation step of the performed reaction and its formation would suggest an incomplete reaction with just one equivalent of TMS-Cl. However, stirring the reaction mixture for a longer time as well as addition of a further excess of TMS-Cl led to an unselective decomposition of **4a'** to give different products with resonances in the highfield as well as the lowfield region. This decomposition may be attributed to the large excess of magnesium metal still present in the mixture which can reduce potential formed intermediates. Hence, $KC_8$ was chosen as a different reducing agent for the first step, to increase both the reductive potential and the preparatory ease of weighing the reagent. Addition of a slight excess led to the clean formation of **3** which has already been described before.[110] $^{31}P\{^1H\}$ NMR spectroscopic monitoring of the reaction revealed **3** as broad singlets at −40.5 and −39.0 ppm in the NMR spectrum, which fits well to the reported values of −43.7 and −40.7 ppm in diethyl ether ($Et_2O$).[110] Subsequently, TMS-Cl was added to **3** after 10 min. The almost black solution turned blue-violet and the $^{31}P\{^1H\}$ NMR spectrum showed one singlet at −92.1 ppm (Figure 9, centre), which is in good agreement with a reaction which had previously been observed for the imidazole-based system **LVI**.[111] Due to a very small reaction scale, the product could not be isolated from the reaction mixture and the reaction was repeated whilst scaling up by a factor of 6. This led to a colour change to wine-red after addition of TMS-Cl and three signals appeared in $^{31}P\{^1H\}$ NMR spectra between −30 and −45 ppm (Figure 9, bottom). While not fitting to the composition of **4a**, these signals were assigned to dianionic compounds as the chemical shifts lie in close proximity to that of **3**. The main signal showed no splitting due to P,P-couplings and, hence, was assigned to the symmetrically silylated **3-TMS$_2$**, corresponding to a literature-known imidazolium-based dianionic 1,4-dihydro-1,4-diphosphinine (Figure 10, centre).[103] The apparent shoulders of the two other broad singlets led to the tentative assignment of both signals to the mono-silylated **3-TMS** which would display a small P-P coupling in the NMR spectrum (Figure 10, right). Interestingly, the two major side products in all three reactions also appear in the $^{31}P\{^1H\}$ NMR spectrum of the possible formation of **4a**, albeit in small concentrations (Figure 9, centre). This outcome shows the very high sensitivity of the performed reaction with regard to (local) concentrations and stoichiometries.

In order to eliminate possible systematic errors during the course of the reaction, a control experiment was performed using the respective imidazole-based 1,4-diphosphinine **LVI** as its 1,4-disilylation product had already been known (Scheme 8).[111]

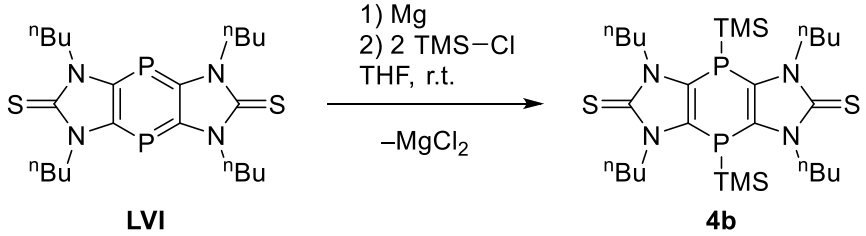


**LVI** **4b**

*Scheme 8:* Reaction of **LVI** with Mg and TMS-Cl.

The experiment was carried out using analogous to the conditions discussed first, *i.e.*, using a high excess of magnesium for the reduction of the respective 1,4-diphosphinine. After 15 min, TMS-Cl was added at ambient temperature. The addition was observed to proceed much faster than for **3**, the respective dianionic intermediate being fully consumed after 2 h. Instead, one main signal was visible as a singlet in the $^{31}P\{^{1}H\}$ NMR spectrum at −114.2 ppm, having formed in a ratio of 66% by integration. This singlet was confidently assigned to the desired 1,4-addition product **4b**, reproducing the already known reactivity of **LVI** and confirming the absence of experimental problems during the procedure.[111] However, this result speaks for a significant difference in electronic structure and reactivity of thiazole-based **1** to imidazole-based **LVI**, the nature of which has not been determined yet.

### 3.1.2 Sequential additions

#### *3.1.2.1 Adduct formations*

The reaction of tricyclic 1,4-diphosphinines **LVI** and **1** with nucleophiles to mono-anionic compounds is known to literature, as well as subsequent conversions with electrophiles to afford 1,4-dihydro-type compounds of **1**.[100,109] In the case of imidazole-based **LVI**, the scope of this reactivity was probed by employing several different heteroatom-nucleophiles such as potassium bis(trimethylsilyl)amide (KHMDS) or lithium di-*i*-propylamide (LDA) and subsequent methylation of the anions to form the final P-adducts.[109] Conversely, in the case of **1** the only nucleophiles used were *n*-butyllithium and KHMDS. Therefore, a systematic screening study was conducted in order to test the availability of different P-adducts and their methylations to 1,4-addition products. For this purpose, **1** was treated with two NHCs ($IMe_4$ and $CAAC^{Pr,Me}$) as well as four different N- and O-nucleophilic salts (Scheme 9).

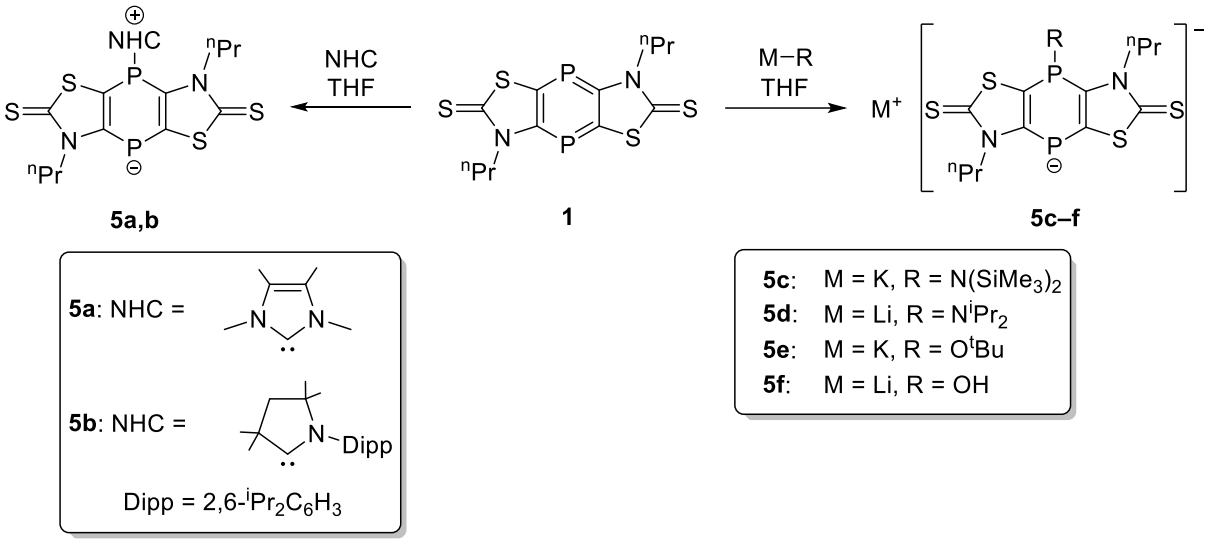


*Scheme 9:* Additions of nucleophilic reagents to **1** to form P-adducts **5**.

All reactions were carried out in THF and at ambient temperature ($IMe_4$, $KO^tBu$, LiOH) or cooled to temperatures below −60 °C ($CAAC^{Pr,Me}$, LDA, KHMDS) during the addition of 1 eq. of reagent. In all cases, the reaction afforded a very dark, green solution. Interestingly, in the case of **5f**, the green colour vanished in favour of a yellow-orange solution after about 15 min. $^{31}P\{^1H\}$ NMR spectroscopic experiments were carried out at ambient temperature for all reactions and generally showed signals around or below 0 ppm (Figure 11). As the bis(trimethylsilyl)amide (HMDS) adduct **5c** is known to literature,[100] its features can be used to determine the composition of the other 5 adducts. In general, the more highfield-shifted signal in the $^{31}P\{^1H\}$ NMR spectra can be attributed to the anionic P atom while the lowfield-shifted one belongs to the comparatively deshielded P atom of the nucleophilic attack. Especially in **5b,c**, the products show very broad resonances, which is in line with findings in the literature.[100]

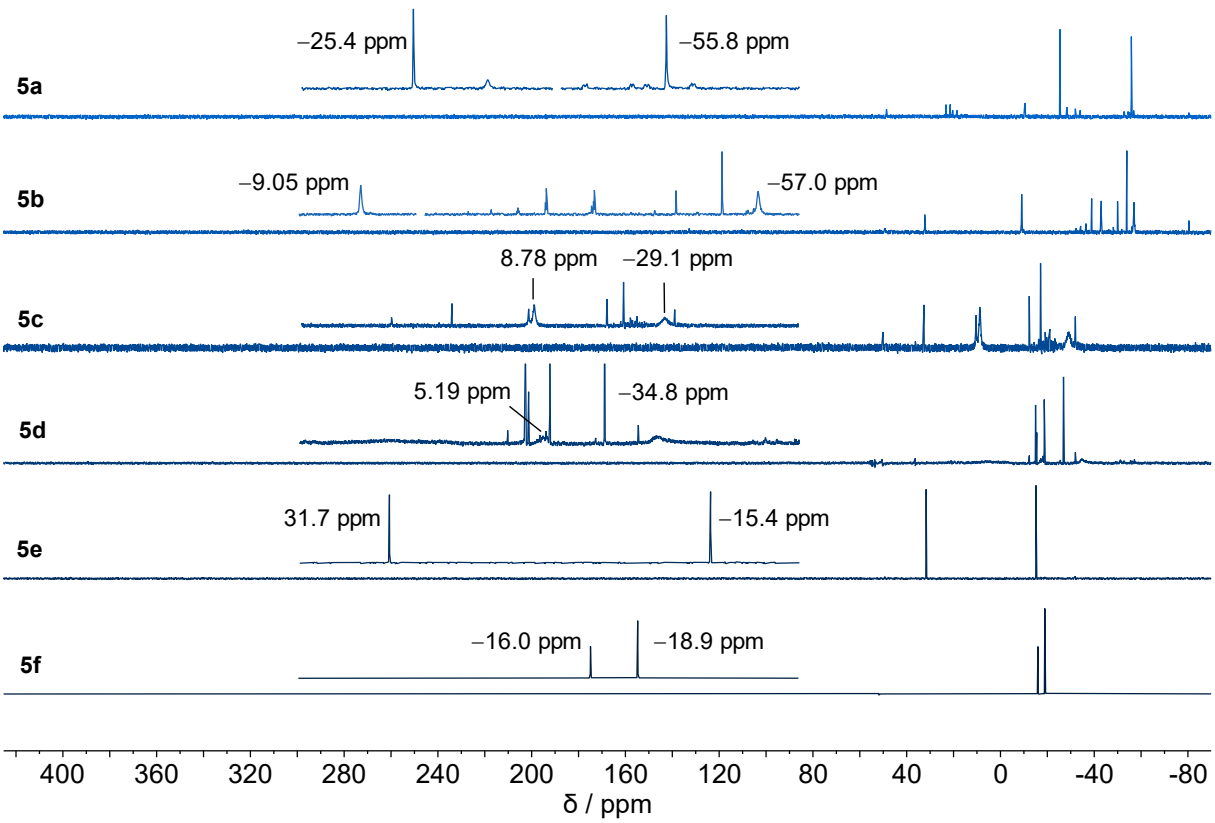


*Figure 11:* $^{31}P\{^{1}H\}$ NMR spectra of reaction mixtures of **5a–f**.

While **5c,d** showed several side products in their respective $^{31}P\{^{1}H\}$ NMR spectra, the formation of the P-adducts went smoothly especially in the case of $IMe_4$ (**5a**) and $KO^tBu$ (**5e**). While **5a** was found to be prone to decomposition upon removal or change of solvent and, hence, only NMR spectroscopic characterisations could be done, **5e** could be isolated in an excellent yield of 90% and was fully characterised.

A remarkable feature of **5f** was observed when conducting $^{31}P$ NMR spectroscopic experiments as the spectra showed a large P,H-coupling of the resonance at −18.9 ppm with a coupling constant of 544.9 Hz, clearly pointing to the $^{1}J_{P,H}$ coupling between a P(IV) and a directly bound H atom. Thus, it became clear that the reaction of **1** with LiOH did not form the expected P-OH motif, but rather a compound resembling the structure of **5f'** (Scheme 10). The colour change from green to orange points towards the initial formation of green **5f** (a structure similar to **5a−e**), which then rearranges to form yellow **5f'** within minutes, as neutral hydroxyphosphanes are well known to undergo this rearrangement.[112]

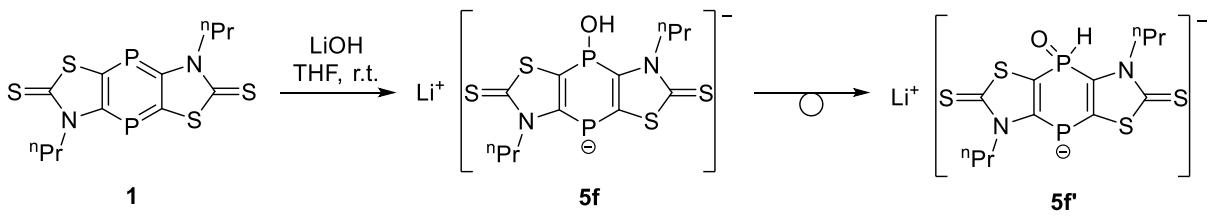


*Scheme 10:* Formation of **5a** and subsequent rearrangement to form **5f'**.

Theoretical investigations were conducted to understand the reactvity and the formed structure. Indeed, phosphane oxide **5f'$^{Me}$** is 7.2 kcal/mol more favoured compared to the hydroxyphosphane **5f$^{Me}$** which in itself is favoured by 33.4 kcal/mol in comparison to the starting materials, underlining the proposed rearrangement. Gauging different isomeric structures of **5f'$^{Me}$** showed the isomer **Li[5f'$^{Me}$]** with O-Li linkage (= **5f'$^{Me}$-OLi**) to be 23.8 kcal/mol more stable than **Li[5f'$^{Me}$]** with ion pair separation (= **5f'$^{Me}$-Li**) and 10.8 kcal/mol more stable than **Li[5f'$^{Me}$]** with P-Li linkage (= **5f'$^{Me}$-PLi**), suggesting the structure of **5f'** is actually the one of **Li[5f'$^{Me}$]** with O-Li linkage (Figure 12). However, the depiction of an aromatic central ring remains very questionable as the P(IV) atom does not reside within the ring plane in any of the three isomers, and it is bent towards oxygen with an out-of-plane angle φ between 8° and 12°. P-C and C-C bond lengths in the central ring are different to the aromatic structure of **1$^{Me}$**, C-C bonds being shorter and P-C bonds being longer (Table 2). These bond lengths remain the closest to **1$^{Me}$** for **Li[5f'$^{Me}$]** with O-Li linkage, indicating that some degree of π-delocalisation is still present in the central ring, causing P-C bonds to shorten and C-C bonds to elongate compared to **Li[5f'$^{Me}$]** with ion pair separation and **Li[5f'$^{Me}$]** with P-Li linkage.

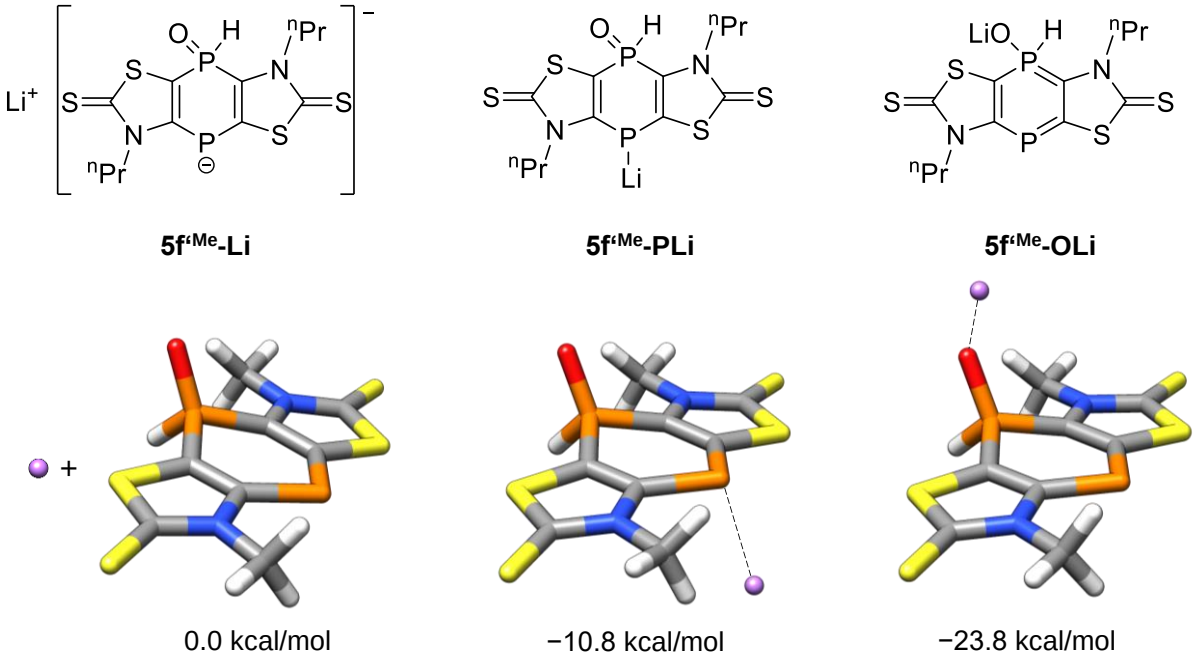


*Figure 12:* Lewis formulae and computed structures (including relative free enthalpies ΔG) of three different isomers of **Li[5f'$^{Me}$]**.

*Table 2:* Out-of-plane angles φ and average C-C and P-C bond distances for **1** and isomers of **5f'**.

| | **1$^{Me}$** | **5f'$^{Me}$** | **5f'$^{Me}$-PLi** | **5f'$^{Me}$-OLi** |
|---|---|---|---|---|
| φ | 0.0° | 10.9° | 8.8° | 11.7° |
| Ø d(C-C) / Å | 1.410 | 1.391 | 1.383 | 1.393 |
| Ø d(P-C) / Å | 1.751 | 1.773 | 1.781 | 1.765 |

### *3.1.2.2 Methylations*

The formation of P-adducts **5a–e** in solution was confirmed via $^{31}P\{^{1}H\}$ NMR spectroscopy, but only one example (**5e**) could be isolated and fully characterised. Therefore, P-methylation reactions were carried out for all investigated anionic/zwitterionic systems to afford the respective 1,4-addition products **6a–e** (Scheme 11). Like for the formation of **5a–e**, different temperatures were employed for different P-adducts (**5a,d**: > 10 °C, **5b,c,e**: < −50 °C). After warming up to ambient temperature, the reaction mixtures were examined via $^{31}P\{^{1}H\}$ NMR spectroscopy (Figure 13).

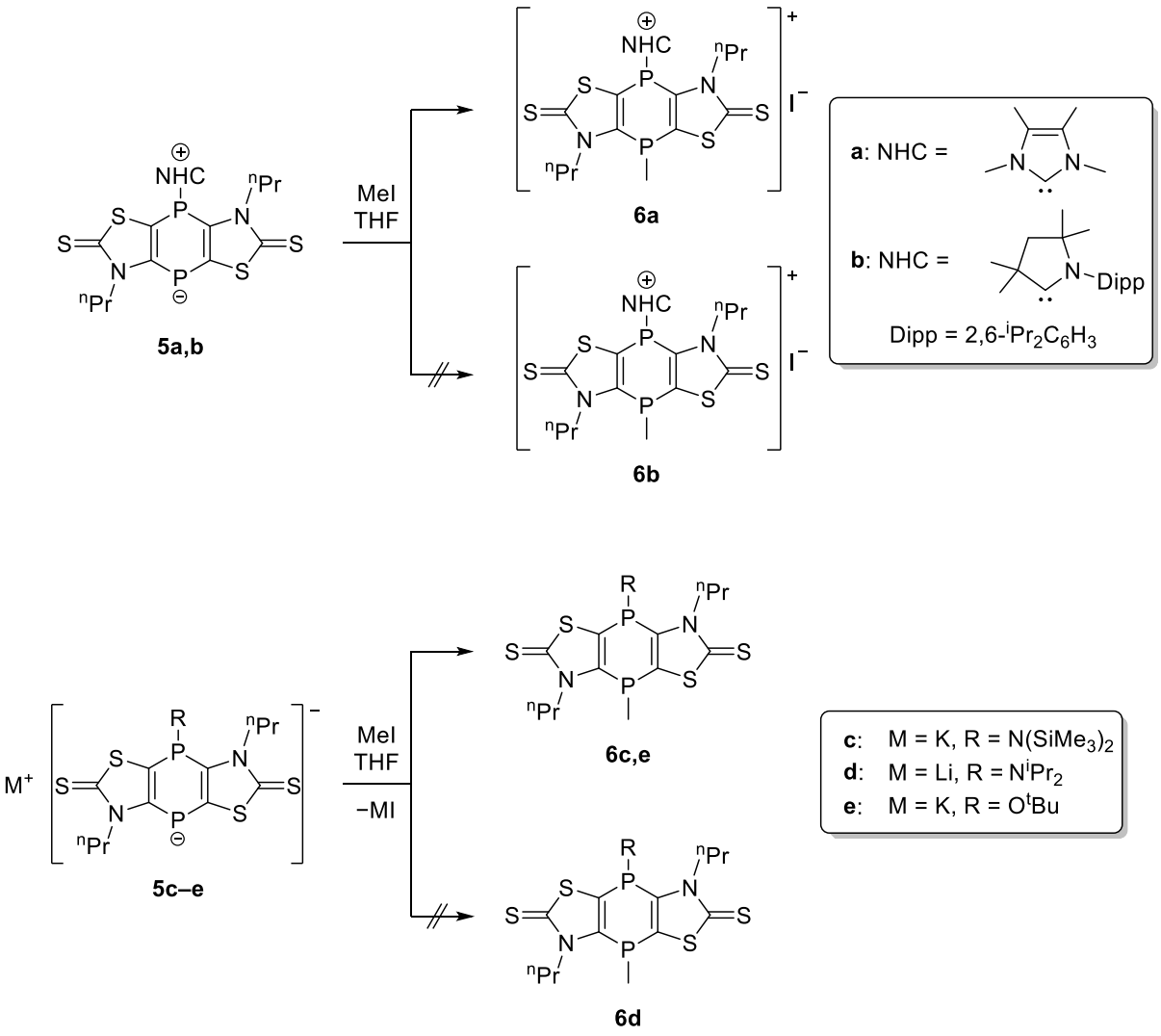


*Scheme 11:* Methylation reactions of **5a–e** to form 1,4-addition products **6a–e**.

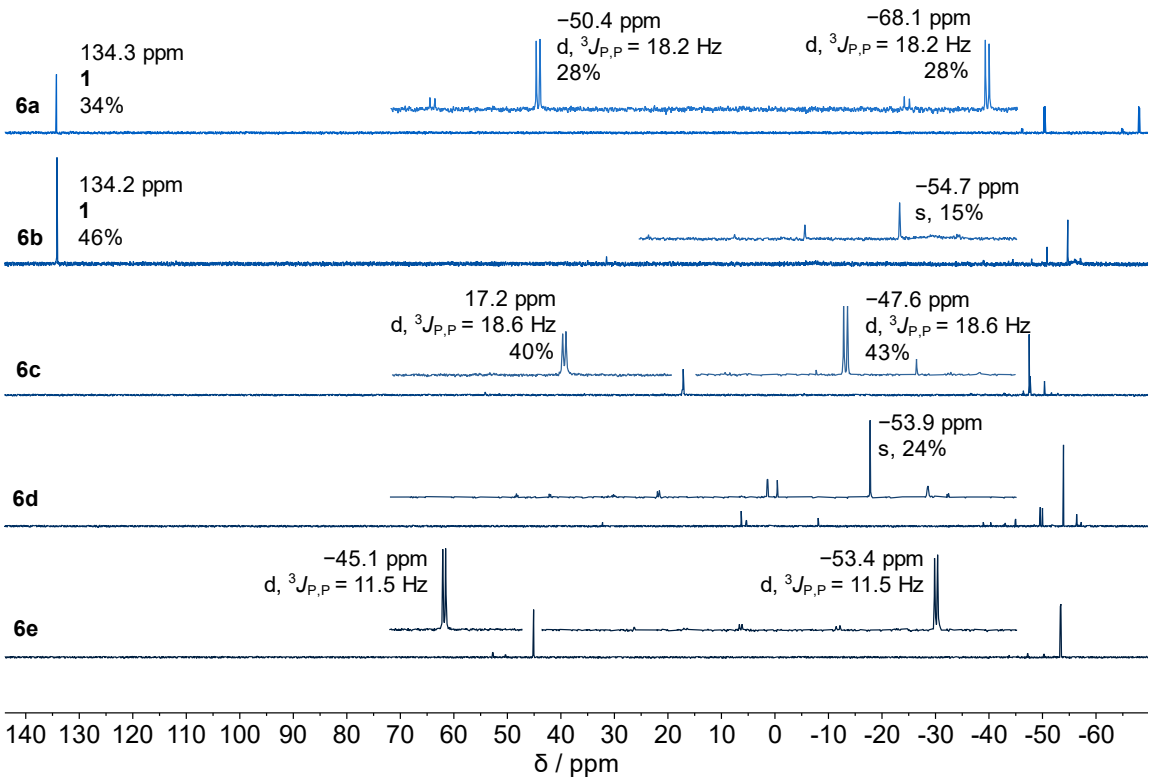


*Figure 13:* $^{31}P\{^1H\}$ NMR spectra of reaction mixtures of **6a–e**.

Two different trends became apparent when analysing the spectra: firstly, for both NHC-adducts, the formation of **1** ($\delta \approx 134$ ppm) was observed, while the other three adducts showed virtually no signals in the lowfield region of the respective $^{31}P\{^1H\}$ NMR spectrum. Secondly, the adducts formed with $IMe_4$, KHMDS and KO$^t$Bu furnished products appearing as AB-type spin systems, while the CAAC$^{Pr,Me}$ and LDA-adducts did not form any products of this type. The formed AB-spin systems fit well to the expected asymmetric substitutions at the two P atoms for **6a,c,e**. While the P,P-coupling constants of all three systems lie in the range of 10–12 Hz, their respective $^{31}P$ NMR spectra show the quartet splitting of a P-Me moiety for the resonances lying at chemical shifts of around −50 ppm. In all three cases, these P,H-coupling constants are small (~5 Hz). The second $^{31}P$-resonances show no P,H-couplings and lie at −45.1 and 17.2 ppm for the heteroatom-substituted **6c,e**, respectively; the NHC-substituted P atom in **6a** is even more high-field shifted than its P-Me counterpart, appearing at −68.1 ppm. Remarkably, only one isomer was formed in all cases, likely, the *trans* isomer, due to the sterically demanding reagents in the P-adduct formations. Isolation attempts were made for all three products, however, only **6c** could be isolated with a yield of 54% after filtration of the product and subsequent washing with THF and *n*-pentane. As the reaction mixture suggested, a strong tendency of **6a** to form back 1,4-diphosphinine **1** was found, hence, it was not possible to isolate the clean compound. A similar observation was made for **6e**. Although the desired product had formed almost exclusively in the reaction mixture, removal of solvent *in vacuo*

($10^{-2}$ mbar) led to a decomposition of **6e** to a very complicated mixture containing upwards of 20 resonances in the $^{31}P\{^{1}H\}$ NMR spectrum, some of which showed multiple P,P-couplings.

In order to explain the different observations, theoretical calculations were performed for all five systems, including the formation of the P-adducts, P-methylations and the decomposition to **1** (Figure 14). A comparison of the free reaction enthalpies ($\Delta_r G$) of the adduct formations reveals significant differences between **5a–e$^{Me}$**. The formation of NHC-adducts is comparatively less favoured than that of P-heteroatom adducts. While **5c,e$^{Me}$** possess similar values for $\Delta_r G$, a striking exception is the formation of **5d$^{Me}$** at a very exergonic value of −44.7 kcal/mol.

The methylation step from **5a–e$^{Me}$** to **6a–e$^{Me}$** is exergonic for all investigated systems. However, the difference between NHC-adducts **6a,b$^{Me}$** and base-adducts **6c–e$^{Me}$** becomes very large in this step, as the values of $\Delta_r G$ in the methylation reaction for **6a$^{Me}$** and **b$^{Me}$** are only −6.4 and −0.4 kcal/mol, respectively, while all other derivatives exhibit very exergonic methylation steps of up to −52 kcal/mol. This trend is reversed when examining the decomposition of methylated products **6a–e$^{Me}$** to **1$^{Me}$** and the respective (imid-)azolium salts, amines and ethers. The decomposition of the NHC-substituted **6a,b$^{Me}$** are exergonic by about −20 kcal/mol, explaining the prominent presence of **1** in their $^{31}P$ NMR spectra. In the three other cases, the decompositions are endergonic between 7 and 13 kcal/mol. While this is in line with the absence of **1** and the isolation of **6c$^{Me}$**, the reasons for the decomposition of **6e** upon removal of solvent and the unsuccessful attempt to synthesise **6d** remain elusive.

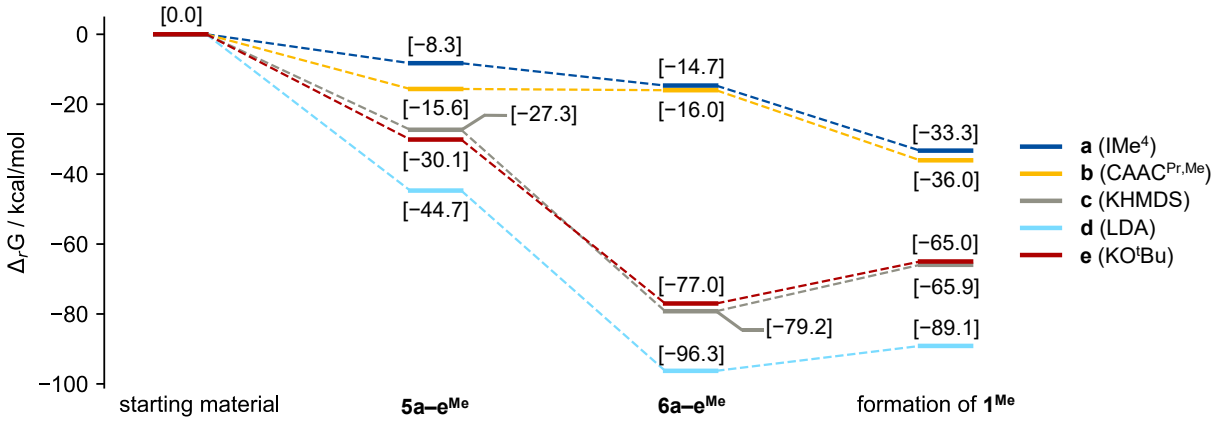


*Figure 14:* Relative free enthalpies of the formation of **5a–e$^{Me}$** and **6a–e$^{Me}$** and their decompositions to **1$^{Me}$**.

In addition to **5a–e**, the mixed-valent adduct **5f'** was also subjected to methylation attempts in order to form **7a**. Initially, methyl iodide was employed as a methylating agent at ambient temperature (Scheme 12).

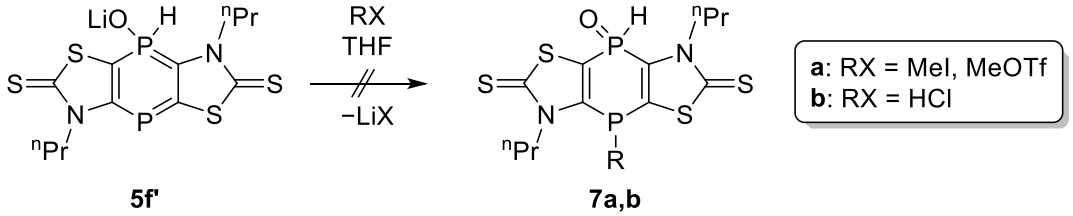


**5f'** **7a,b**

*Scheme 12:* Targeted methylation and protonation reactions of **5f'** to form 1,4-addition products **7a,b**.

$^{31}P\{^{1}H\}$ NMR spectroscopic monitoring of the reaction mixture revealed the reluctance of methyl iodide to react with **5f'** as it remained the sole product in the mixture. Consequently, the reaction was repeated using the more potent methylation agent methyl trifluoromethane-sulfonate (methyl triflate, MeOTf). However, the reaction did not proceed with methyl triflate, either, and **5f'** was the only compound evident in the $^{31}P\{^{1}H\}$ NMR spectrum. Suspecting a tight ion pair as one of the reasons for this lack of reaction, 12-crown-4 was utilised in order to separate the lithium cation from the molecular anion before adding methyl iodide or -triflate at −80 °C. Yet, this incorporation of 12-crown-4 was unselective for both cases and yielded $^{31}P\{^{1}H\}$ NMR spectra with no resonance fitting to **7a**.

As an alternative for methylation reactions, tests towards the protonation of **5f'** were conducted. The addition of hydrogen chloride solution in dioxane to the adduct immediately produced a bright red suspension and $^{31}P\{^{1}H\}$ NMR spectroscopy confirmed the formation of **1** as the major product of this reaction, alongside a second unknown product at −95.9 ppm, which was generated in 25% by integration, and traces of **5f'** (Figure 15).

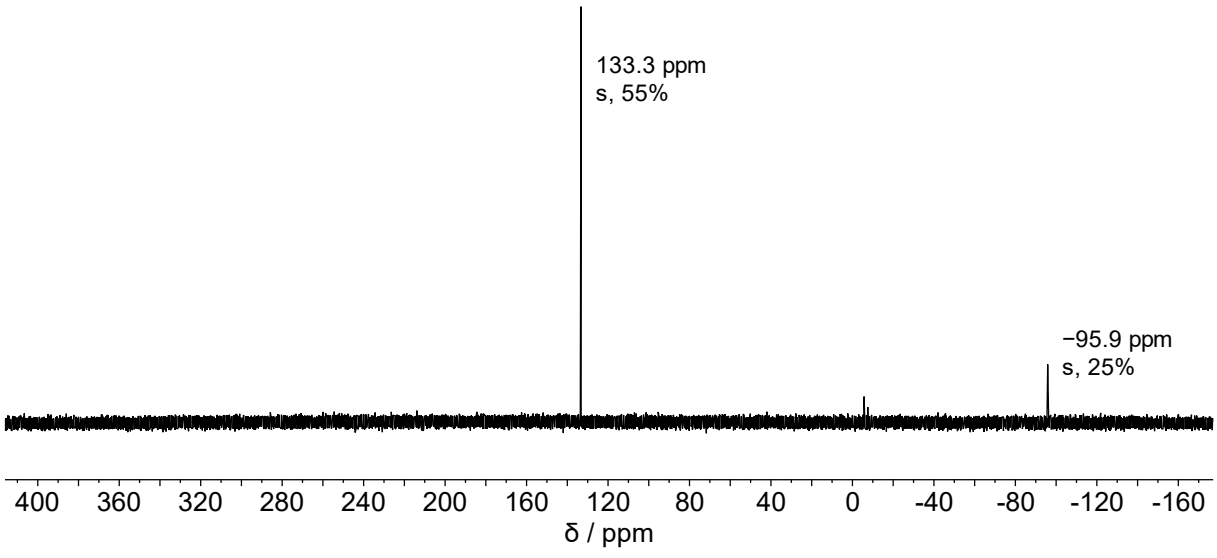


*Figure 15:* $^{31}P\{^{1}H\}$ NMR spectrum of the reaction mixture of **7b**.

Theoretical investigations were again used to get a more detailed picture of the P-methylation and protonation attempts of **5f'** (Figure 16). A possible reaction mechanism from **5f'** to **1** can proceed via the protonation/methylation of the P(III) atom to give **7a,b** in the first step (Scheme 13). Following this, a rearrangement can take place in the *cis* isomer, affording **8a,b** by migration of the methyl group or proton to the oxygen atom. These intermediates can then eliminate methanol or water, two very good leaving groups, and form back 1,4-diphosphinine **1**, the driving force being (in part) the re-aromatisation in **1**.

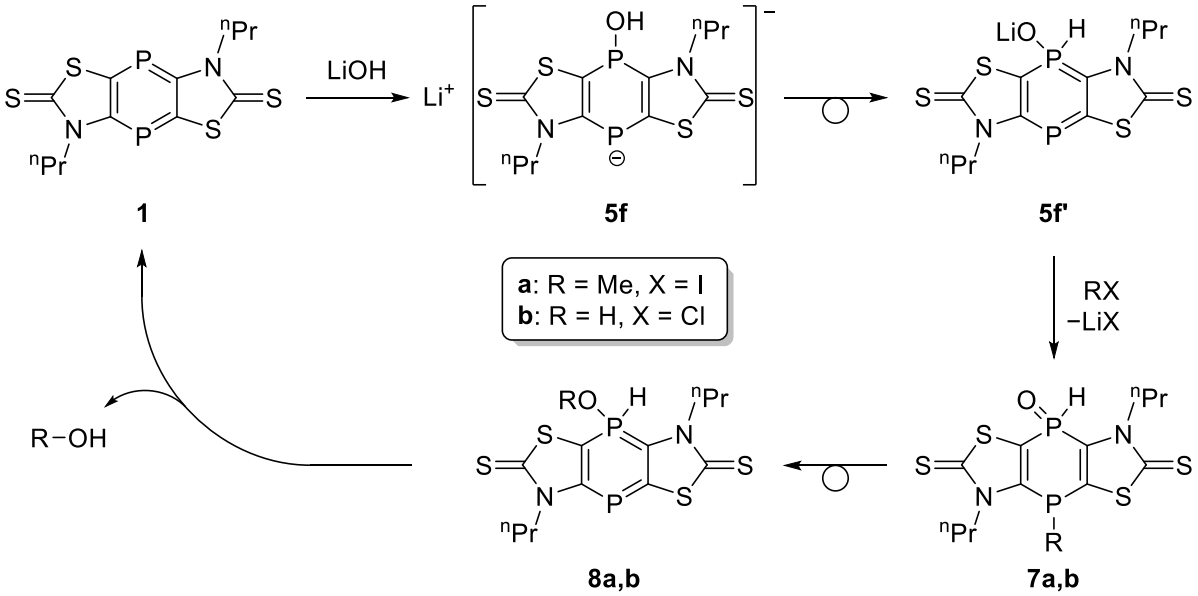


*Scheme 13:* Possible reaction mechanism of the formation of **1** in the methylation/protonation reactions of **5f'**.

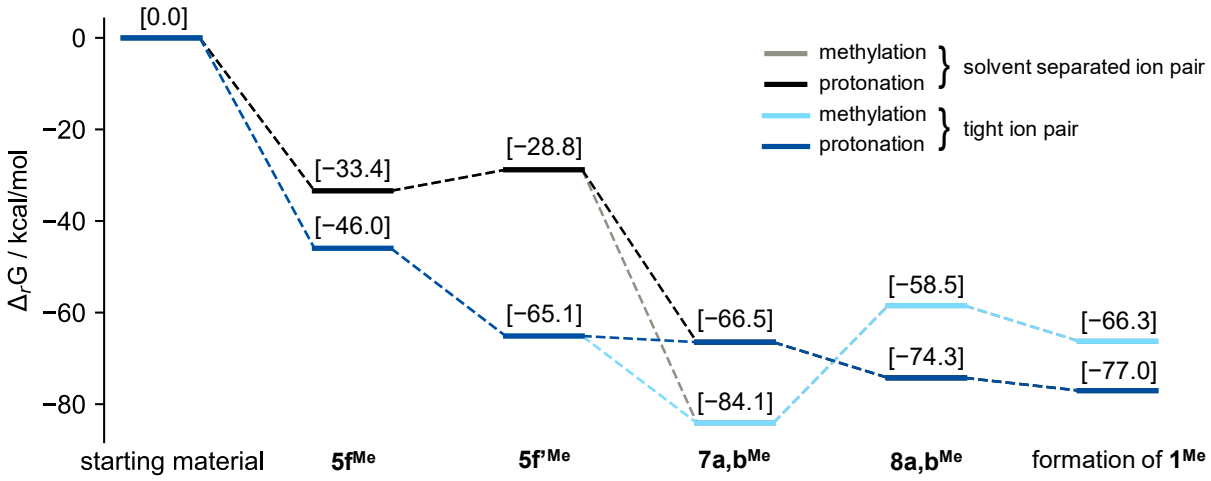


*Figure 16:* Relative free enthalpies for the proposed mechanism (cf. Scheme 13) of the formation of $\mathbf{1}^{Me}$ in methylation/protonation reactions of $\mathbf{5f'}^{Me}$.

Examining the mechanism described above, $\Delta_r G$ values were calculated for each step of both pathways, *i.e.*, the methylation and the protonation (Figure 16). A differentiation between tight ion pairs (blue) and solvent-separated ion pairs (black/grey) was made for **5f$^{Me}$** and **5f'$^{Me}$** to assess the influence of 12-crown-4 on the reaction. Without addition of 12-crown-4, the formation of **5f$^{Me}$** and its rearrangement to **5f'$^{Me}$** in total has a total free reaction enthalpy of −65.1 kcal/mol with the intermediate **5f$^{Me}$** residing at a $\Delta_r G$ value of −33.4 kcal/mol (as already described for the formation of **5f'$^{Me}$**). Protonation and methylation of the tight ion pair **5f'$^{Me}$** are both exergonic in nature, the methylation being favoured by 19 kcal/mol while the protonation is almost thermoneutral at a $\Delta_r G$ of −1.4 kcal/mol. However, the rearrangement of **7a,b$^{Me}$** to form the respective **8a,b$^{Me}$** was found to be clearly endergonic in the case of methylated **7a$^{Me}$**, going 25.4 kcal/mol uphill to **8a$^{Me}$**. $\Delta_r G$ of the theoretical decomposition of **8a$^{Me}$** to form **1$^{Me}$** and methanol turned out to be −7.8 kcal/mol. In comparison, the protonation pathway from **7b$^{Me}$** over **8b$^{Me}$** to **1$^{Me}$** and water is strictly exergonic in every step, the rearrangement being favoured by 7.8 kcal/mol and the elimination of water by 2.7 kcal/mol.
While the methylation and protonation of **5f'$^{Me}$** remains the same when investigating solvent-separated ion pairs, the energy profile of the adduct formation itself changes drastically. Remarkably, a rearrangement of **5f$^{Me}$** to the P-oxide **5f'$^{Me}$** is disfavoured in this case as the latter is higher in energy compared to the former by 4.6 kcal/mol. Both structures are less stabilised compared to the tight ion pairs, differing by as much as 36.6 kcal/mol for **5f'$^{Me}$**.

Comparing the obtained theoretical findings with experimental observations, it is evident that the reactive centre in the formed adduct distinctly lies on the oxygen atom, as the theoretically exergonic P-methylation is not observed experimentally. Instead, a direct O-methylation affording **8a$^{Me}$** is endergonic by 6.4 kcal/mol, the value being consistent with the experiment where no reaction of **5f'$^{Me}$** with methyl iodide or methyl triflate was observed. This is in line with the adduct isomer **Li[5f'$^{Me}$]** with O-Li linkage being 13 kcal/mol more stable than **Li[5f'$^{Me}$]** with P-Li linkage (Figure 12). When employing 12-crown-4 in the reactions, reactivity is likely enhanced due to the increased stability of **5f$^{Me}$**, however, many different reaction pathways of **5f$^{Me}$** with methyl iodide or methyl triflate seem to exist, preventing the selective formation of **8a$^{Me}$**. The formation of **1** when protonating **5f'$^{Me}$** is very feasible from an energetic point of view as every step in the proposed mechanism is exergonic in both cases of tight or solvent separated ion pairs.

### *3.1.2.3 Silylations*

Beyond methylations, adducts **5a–e** were subjected to reactions with TMS-Cl to achieve P-silylated derivatives **9a–e** (Scheme 14). The reactions were carried out in THF at ambient temperature (**5a**) or between −40/−80 °C (**5b–e**) using a small excess of TMS-Cl of ca. 1.3 eq.

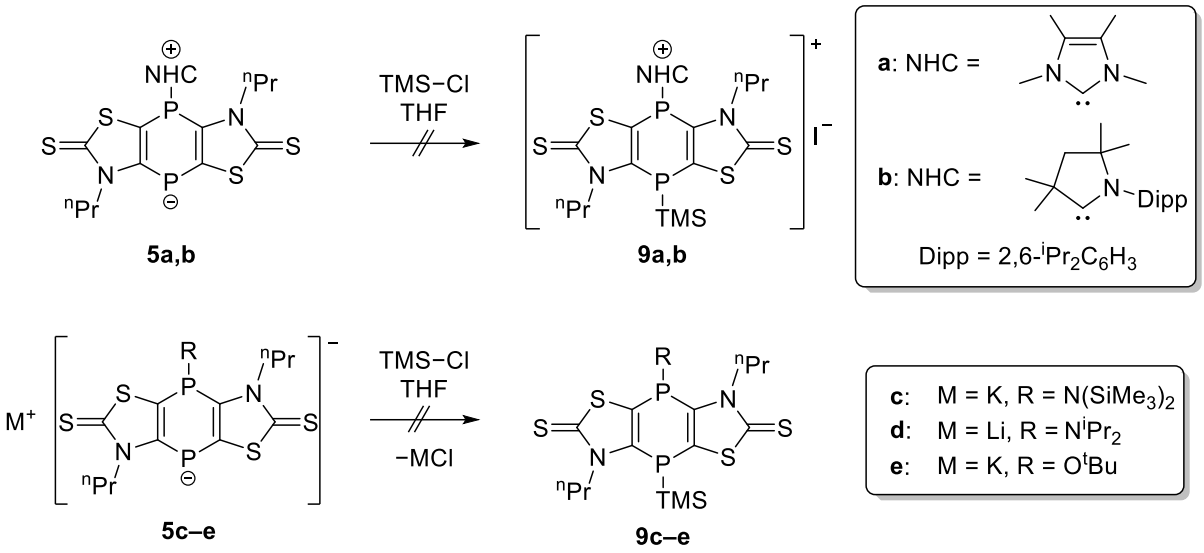


*Scheme 14:* Targeted silylation reactions of **5a–e** to form 1,4-addition products **9a–e**.

Throughout all reactions, the conversions were monitored using $^{31}P\{^{1}H\}$ NMR spectroscopy (Figure 17). Similar to the methylation, the two NHC-adducts primarily formed **1** upon addition of TMS-Cl, in this case even more prominent than in the attempted syntheses of **6a,b** with close to 70% (compare Figure 13). Surprisingly, a very similar outcome was observed when using the *t*-butoxy substituted adduct **5e**. While the methylation afforded **6e**, which was not stable upon removal of solvent, the addition of TMS-Cl led to the formation of **1** in a content of over 80% by integration. In all three cases **9a,b,e**, one other $^{31}P$ resonance is visible in the $^{31}P\{^{1}H\}$ NMR spectra. The chemical shifts of these three resonances are similar, appearing around 50 ppm, indicating a similar structural motif being formed in all cases. While none of the corresponding reaction products could be isolated, the singlet multiplicity of all three resonances is a clear confirmation that the formed products are not the expected **9a,b,e** as these would exhibit AB-type spin systems in analogy to their methylated counterparts.

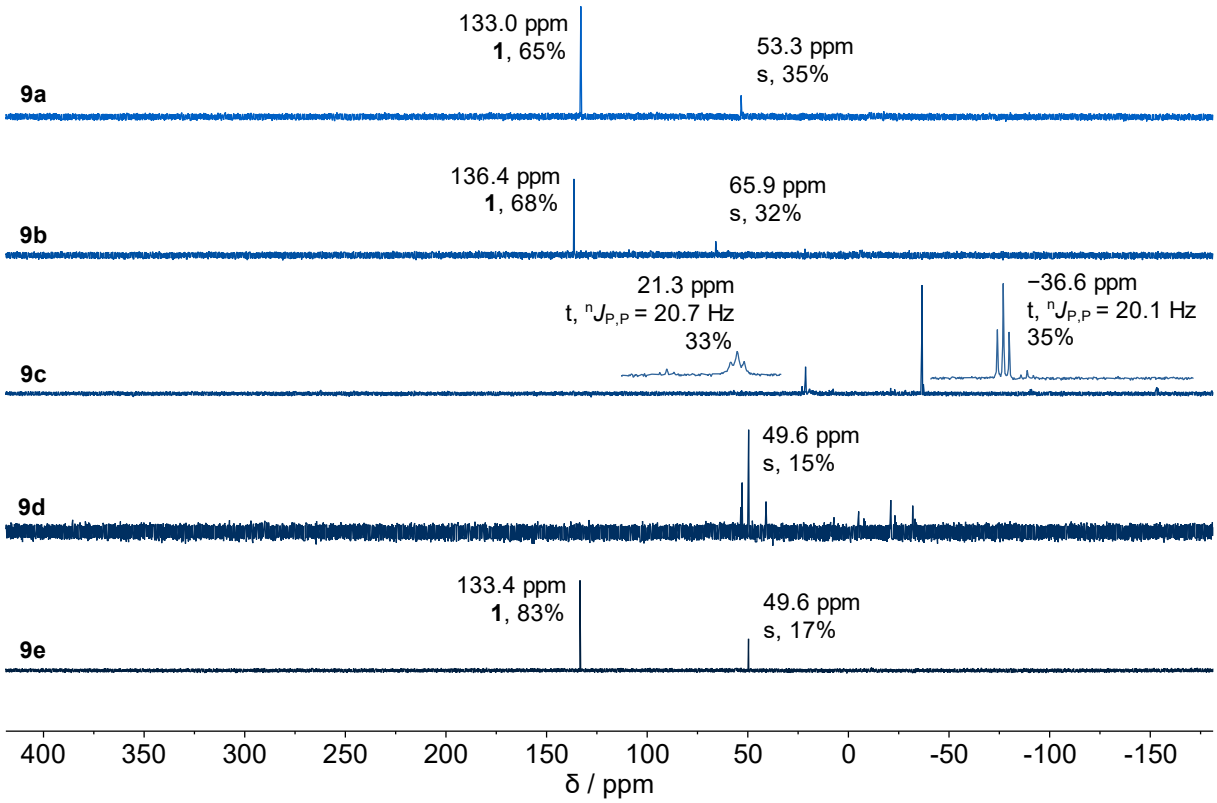


*Figure 17:* $^{31}P\{^{1}H\}$ NMR spectra of reaction mixtures of **9a–e**.

While the treatment of the di-*i*-propylamino substituted **5d** with TMS-Cl lead to an unselective mixture of products, the major one having an integral ratio of 15% in the respective $^{31}P\{^{1}H\}$ NMR spectrum, one major product is visible in the case of **9c**. The resonances seemingly show a triplet multiplicity with a P,P-coupling constant of around 20 Hz. As their integral ratios are similar, the respective structure either has to contain two sets of two magnetically equivalent phosphorus atoms, or the multiplicity is in fact comprised of doublets of doublets in the AB-type spin systems of two isomers. However, as this product was not isolated, a concrete suggestion of its structure cannot be made at this point.

Mimicking the approach taken for the methylation reactions, the silylations of adducts **5a–e** and their subsequent decompositions to 1,4-diphosphinine **1** were investigated theoretically (Figure 18). While there is obviously no change in the formation of **5a–e$^{Me}$**, $\Delta_r G$ values diverge greatly in the silylation step compared to the methylation reactions (compare Figure 14). All silylations are about 30 kcal/mol less favoured than their methylation counterparts, however, **9c–e$^{Me}$** are still significantly more stable than **5c–e$^{Me}$**. The decomposition of these P-silylated compounds to **1$^{Me}$** are all exergonic, however, only favoured by less than 5 kcal/mol for **9c,d$^{Me}$**, while the *t*-butoxy-substituted **9e$^{Me}$** displays a $\Delta_r G$ value of −19.1 kcal/mol for the elimination of trimethylsilyl *t*-butyl ether and the formation of **1$^{Me}$**.

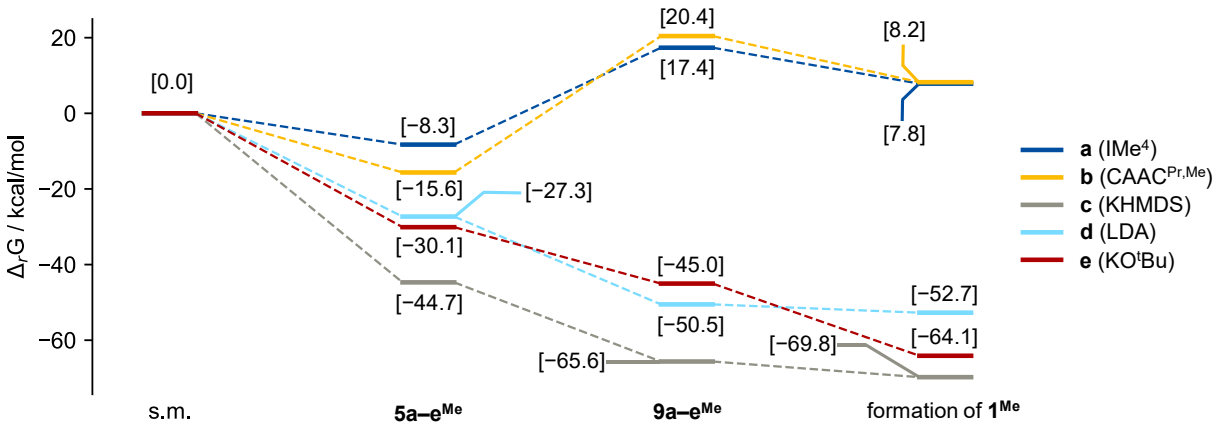


*Figure 18:* Relative free enthalpies of the formation of **5a–e$^{Me}$** and **9a–e$^{Me}$** and their decompositions to **1$^{Me}$**.

Examination of the NHC-substituted **5a,b$^{Me}$** gave a surprising result: the silylations of the adducts were found to be highly endergonic in both cases, having $\Delta_r G$ values of 25.7 and 36.0 kcal/mol, respectively. Additionally, in the exemplary investigation into the barrier of the silylation of **5a$^{Me}$**, no transition state could be located. A barrier-free process leads to the reaction equilibrium lying almost exclusively on the side of the respective adduct **5a,b$^{Me}$**. Addition of TMS-Cl then directly forms the respective *C*-trimethylsilyl (imid-)azolium chloride with free carbene still present in the mixture. Although this process is also endergonic by 16.1 and 23.9 kcal/mol, respectively, the formed salts precipitate and are removed from the reaction, pulling the equilibrium towards the formation of **1**, as is evident by the $^{31}P\{^1H\}$ NMR spectra. These processes can explain the differences in reactivity between the adducts **5a–e** and show the comparatively lower tendency of **5a–e** to form silylated products as opposed to methylated ones.

## 3.2 1,4-DIPHOSPHANORBORNADIENES

### 3.2.1 Carbon tetrachloride

To date, only six isolated 1,4-diphosphanorbornadienes are known to the literature,[106,113–116] two of them being products of the few reactivity studies that were performed on the first 1,4-diphosphinine **LIV**.[113,114] At 130 °C **LIV** reacted with $CCl_4$ in a formal [4+1]-cycloaddition reaction to form the 1,4-diphosphanorbornadiene **10** containing a $CCl_2$ moiety in the bridge (Scheme 15, top). However, the product was only ever characterised using $^{19}F$ NMR spectroscopy, mass spectrometry and melting point measurements. Additionally, the 1,4-dichloro-1,4-dihydro compound **11** was postulated as a side product, but the reaction mechanism was never verified.

In order to test this type of reaction using the tricyclic derivative **1**, the literature protocol was mimicked by using a sealed Schlenk tube containing a suspension of **1** in $CCl_4$ which was heated to 130 °C for 2 h (Scheme 15, bottom). Surprisingly, no evidence for the formation of a hetero-norbornadiene derivative was obtained. $^{31}P\{^1H\}$ NMR spectroscopic investigations during the reaction did not reveal the formation of a resonance attributable to the expected product. Instead, two sets of AB-type spin systems were visible at −9.5/29.2 ppm (86%, $^3J_{P,P}$ = 6.72 Hz) and 1.3/27.7 ppm (14%, $^3J_{P,P}$ = 5.62 Hz), respectively, hinting at the formation of two isomers with a 1,4-dihydro-1,4-diphosphinine structural motif (Figure 19, top). Consequently, the signals were assigned to the 1,4-addition product **12,12'** which appears in the $^{31}P\{^1H\}$ NMR spectrum as *cis/trans* isomers in an isomeric ratio of 86:14, the major diastereomer likely being the *trans* isomer as it is favoured by 2.0 kcal/mol and the relatively high inversion barrier at 43.2 kcal/mol can be overcome by the reaction temperature of 130 °C.

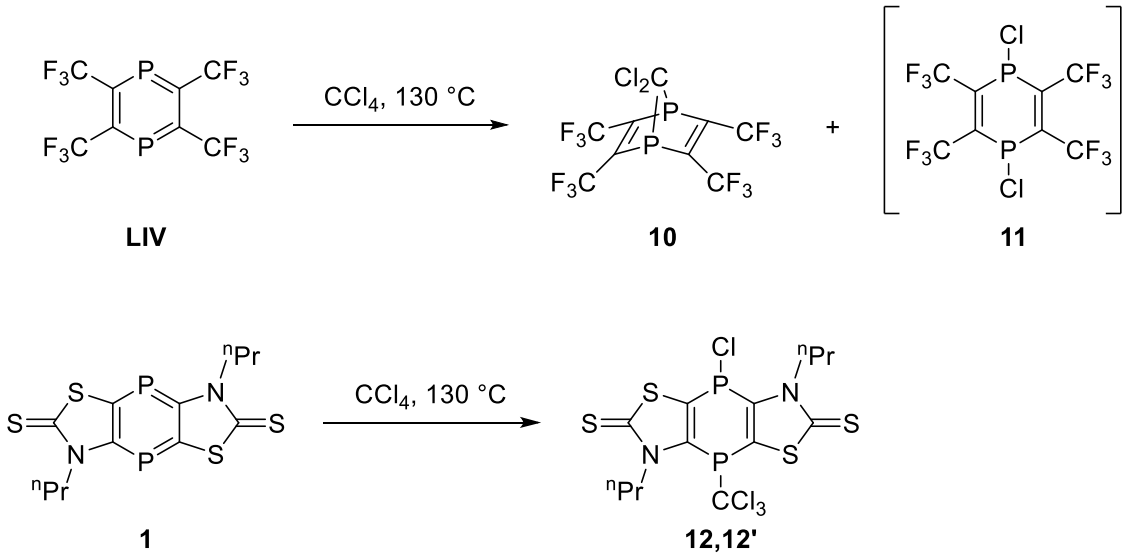


*Scheme 15:* 1,4-addition of $CCl_4$ to the two phosphorus centers of **LIV** (top)[113] and **1**.

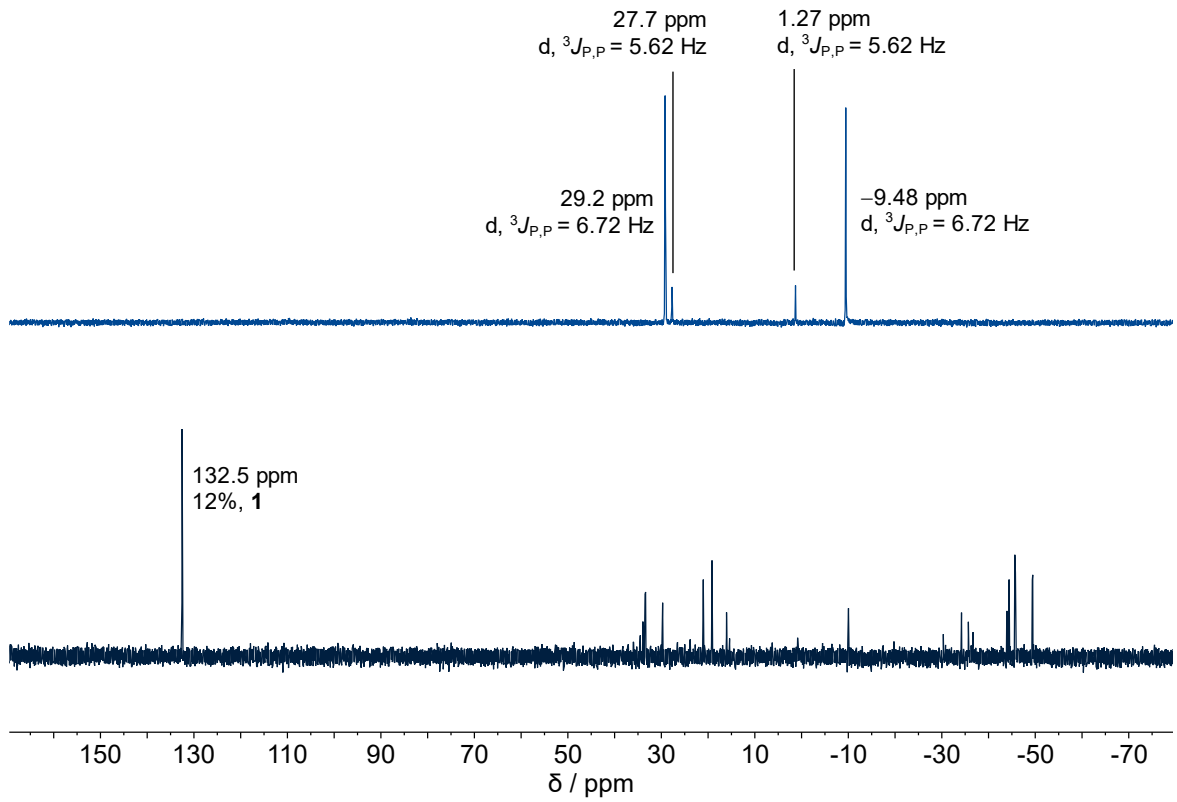


*Figure 19:* $^{31}P\{^1H\}$ NMR spectra of isolated **10** (top) and thermal decomposition after 5 h at 100 °C in xylenes (bottom).

Multinuclear NMR studies showed a signal in the $^{13}C\{^1H\}$ NMR spectrum at 116.3 ppm (d, $^1J_{P,C}$ = 23.6 Hz) which can be assigned to the $CCl_3$ moiety of **12,12'** as it is in good agreement with similar trichloro compounds $R_2PCCl_3$ (R = alkyl) found in the literature.[117] The formation of **12,12'** was confirmed via further characterisations like mass spectrometry, showing fragmentations of the *n*-propyl groups as well as one chlorine atom. On the other hand, no fragmentation of the $CCl_3$ unit could be detected in the mass spectrum. Investigations on the thermal stability were performed in order to examine elimination processes, such as elemental chlorine to give the desired 1,4-diphosphanorbornadiene. Therefore, **12,12'** was heated in xylenes to 100 °C. $^{31}P\{^1H\}$ NMR spectroscopic monitoring showed a slow but unselective decomposition of **12,12'**, resulting in a mixture of compounds and a multitude of resonances in the region between −50 and 50 ppm (Figure 19, bottom). Yet, no signal for the respective 1,4,-dichloro-1,4-dihydro-1,4-diphosphinine could be observed,[100,113] which could have been formed alongside the 1,4-diphosphanorbornadiene. Interestingly, the primary decomposition product was observed to be **1**, appearing at 132.5 ppm with a content of 12% in the spectrum. This suggests a partially reversible reaction, possibly similar to the syntheses of tricyclic 1,4-diphosphinines **LVI–LIX** which proceeds via the somewhat spontaneous elimination of $Cl_2$ from the respective 1,4,-dichloro-1,4-dihydro-1,4-diphosphinine.[118] However, due to the otherwise unselective thermal decomposition a concise statement on reversibility cannot be made.

### 3.2.2 Sulfur

As the study of Kobayashi on the formation of a 1,4-diphosphanorbornadiene could not be verified by using **1** and $CCl_4$ under thermal conditions, different reagents were then tested. Kobayashi had also reported on the [4+1]-cycloaddition of the 1,4-diphosphinine derivative (**LIV**) with elemental sulfur when heated to 100 °C for 48 h.[114] Therefore, a toluene suspension of **1** with an excess of sulfur was heated until reflux conditions (Scheme 16).

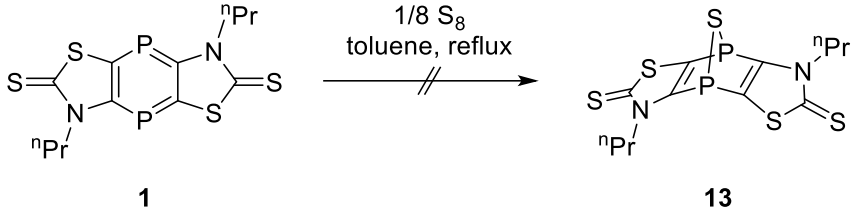


**1** **13**

*Scheme 16:* Targeted reaction of **1** with elemental sulfur.

$^{31}P\{^{1}H\}$ NMR spectroscopic monitoring of the reaction showed a slow consumption of **1** while, after three days at 120 °C, signals in low intensity appeared in the region expected for 1,4-diphosphanorbornadienes, but these resonances were not in line with the expected singlet multiplicity of the symmetrically bridged compound **13** and, instead, AB-type spin systems together with other signals in the range from −100 to 170 ppm appeared in the spectrum. Although $^{31}P\{^{1}H\}$ NMR spectroscopic data do not exist for 7-thio-1,4-diphosphanorbornadienes, the shift of carbon-bridged compounds can be expected around 30 ppm.[115] Extrapolation of this shift to a sulfur-bridged system in analogy to non-cyclic compounds leads to an expected $^{31}P$ chemical shift for **13** of ~40 ppm.[119] When stirring was continued for three more days the content of the asymmetric products increased but no resonance that might fit to the structure of **13** could be observed.

In order to understand these findings, $\mathbf{13^{Me}}$ was theoretically compared to the respective derivative of **LIV**. The reaction of **LIV** with sulfur to form the respective 1,4-diphosphanorbornadiene is energetically favoured by 12.9 kcal/mol, which is almost three times the $\Delta_r G$ of $\mathbf{1^{Me}}$ to $\mathbf{13^{Me}}$ of only −4.6 kcal/mol. These results clearly support the difference(s) in the outcome of these experiments, and should have their origin in the different electronic nature between monocyclic **LIV** and tricyclic **1**, especially pointing to a comparatively larger stability of the latter. The small value for $\Delta_r G$ for the formation of $\mathbf{13^{Me}}$ may also explain the presence of numerous side products, as it may allow for different possible and energetically competing reaction paths which then led to the observed low selectivity.

### 3.2.3 Group 13 ylidenes

The only known 1,4-diphosphanorbornadienes, formed from tricyclic 1,4-diphosphinines, are 7-metalla-1,4-diphosphanorbornadienes which were published by the Streubel group in 2019.[106] The synthesis of these compounds was achieved by reacting 1,4-diphosphinine **LVI** with two low-valent group 13 ylidenes (NacNacGa, NacNacAl, see Scheme 17) in benzene or diethyl ether, and the respective products **LXII** showed $^{31}P\{^{1}H\}$ NMR resonances at very high field (beyond −100 ppm). Therefore, it deemed promising to carry out analogous reactions using **1** (Scheme 17).

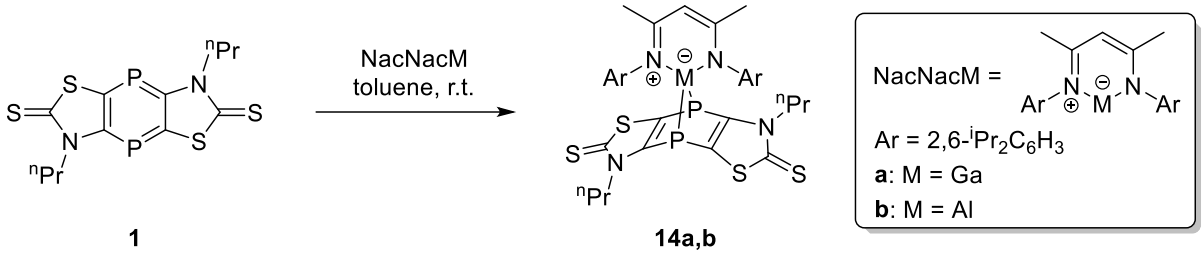


*Scheme 17:* Reactions of **1** with NacNacGa (**a**) and NacNacAl (**b**).

Upon addition of a suspension of **1** to a solution of NacNacGa in toluene an immediate colour change from red to yellow was observed. The full conversion of **1** was confirmed by the selective formation of **14a** having a chemical shift of −81.7 ppm in $^{31}P\{^{1}H\}$ NMR spectra. Following this observation, excess NacNacGa was removed by repeated precipitation of **14a** from cold diethyl ether as an off-white powder and its composition was confirmed by multinuclear NMR spectroscopy as well as (high resolution) MS and IR spectroscopy. No crystal structure could be obtained for **14a**, but results from theoretical calculations suggest a very similar structure compared to the imidazole-based analogue **LXII-Ga** with P-Ga bond lengths of 2.44 Å and a P-Ga-P angle of 85.9°, both being significantly different from P-Ga bond lengths and angles at the gallium centre in related NacNacGa(X)($PPh_2$) compounds (X = H, $SO_3CF_3$).[120] P-Ga bond lengths in these compounds tend to lie below 2.4 Å and angles above 90°. This effect is likely caused by ring strain due to the multicyclic nature of **14a** thus also pointing to effects of the fused thiazole rings onto the bond lengths of the central 1,4-diphosphanorbornadiene moiety.

Compound **1** was also reacted with NacNacAl in toluene in order to form the respective 7-aluma-1,4-norbornadiene **14b**. In contrast to **LVI** though, this reaction under dropwise addition of NacNacAl did not lead to the clean formation of **14b**. While the resonance of a main product (with a content of 62%) in the $^{31}P\{^{1}H\}$ NMR spectrum at −100.6 ppm was observed which may correspond to **14b** (the difference in chemical shifts compared to **14a** agrees very well with literature-known values),[106] there was also an unknown product (38%) presenting an AB-type spin system at −108.5 and −88.1 ppm with a $^{3}J_{P,P}$ coupling of 20.8 Hz (Figure 20, top).

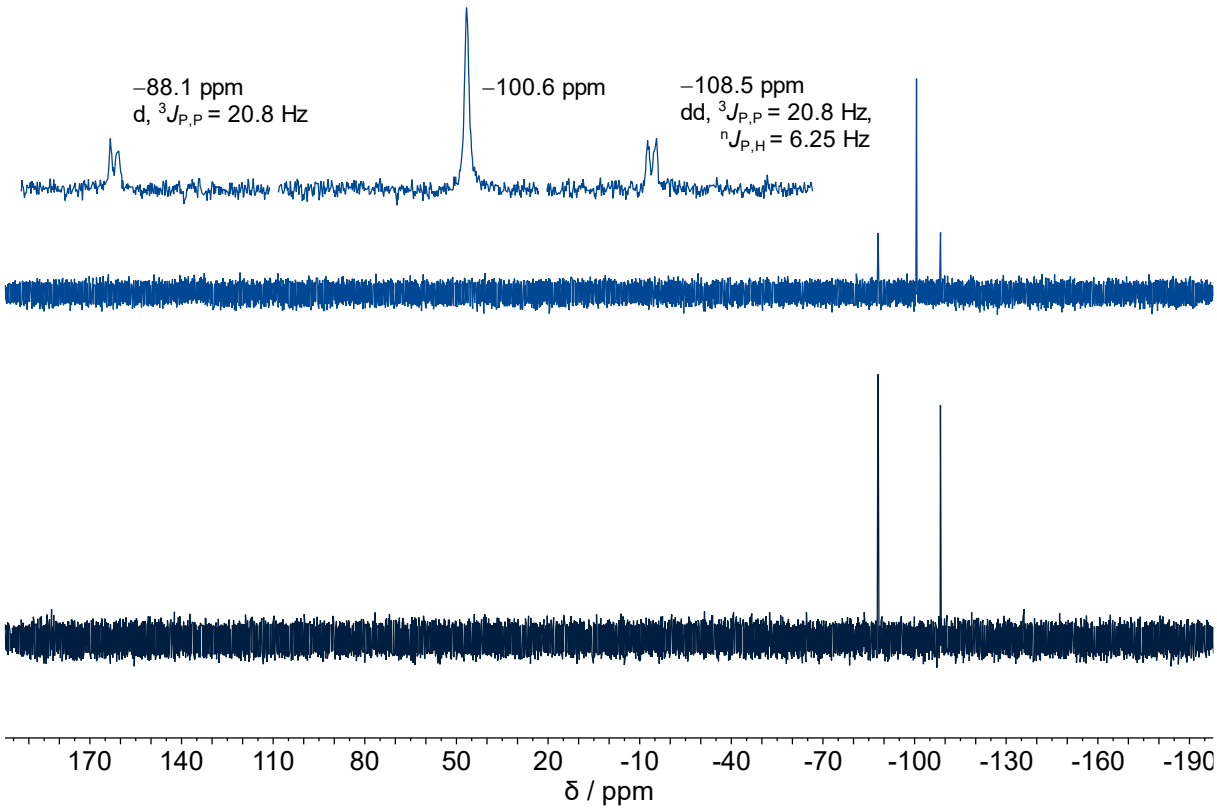


*Figure 20:* $^{31}$P NMR spectra of the reaction of **1** with NacNacAl in benzene (top) and diethyl ether (bottom).

The resonance shifted more to the highfield region additionally displayed a P,H-coupling of 6.2 Hz in the $^{31}$P NMR spectrum. Employing an excess (2 eq.) of NacNacAl led to an increase in content of the asymmetric AB-type spin system to 45%, yet, an even larger excess did not lead to a further raise of its content. The possibility of trace amounts of water leading to partial hydrolysis of **14b** would explain the presence of a P,H-coupling and asymmetry of the formed product, however, a definitive statement about the observed reactivity cannot be made. Remarkably, repeating the reaction in diethyl ether led to the selective formation of the asymmetric AB-spin system (Figure 20, bottom). While the latter can be caused by effects such as solubility differences between benzene and diethyl ether, the nature and formation mechanism of this unknown product could not be determined and it was not possible to isolate either of the formed compounds.

### 3.2.4 Group 14 ylidenes

In addition to group 13 low-valent NacNacM reagents, selected low-valent group 14 compounds were used in order to target the 1,4-diphosphanorbornadiene structural motif. Here, a focus lay on stabilised and/or singlet heterocyclic silylenes, the heavier homologues of carbenes, as they are highly reactive, low-valent reagents and are known to undergo—among other things—bond activation and [4+1]-cycloaddition reactions.[121] First, a reaction of

**1** with the NHC-stabilised dichlorosilylene IPr−$SiCl_2$ (IPr = 1,3-bis(2,6-diisopropylphenyl)imidazole-2-ylidene) in toluene was performed to give dichlorosilyl-bridged **15a** (Scheme 18).[122]

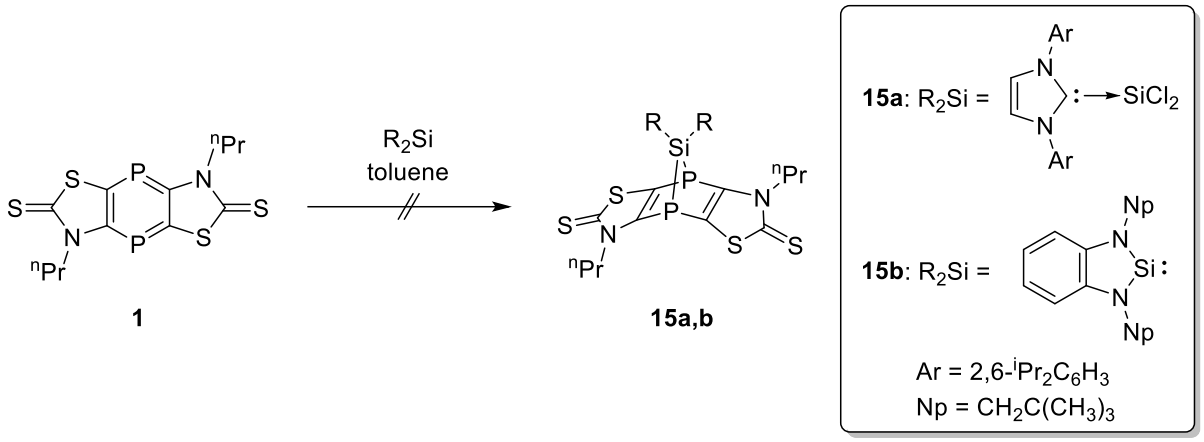


*Scheme 18:* Targeted reactions of **1** with different silylenes.

The reaction was carried out at ambient temperature in toluene. After an immediate colour change from a red suspension to an orange solution, $^{31}P\{^1H\}$ NMR spectroscopic investigations were carried out which revealed the formation of several products. Firstly, multiple signals with a singlet multiplicity appeared in the $^{31}P\{^1H\}$ NMR spectrum between −10 and −75 ppm, as well as an AB-type spin system as a minor product very close to 0 ppm with a P,P- coupling constant of 21.4 Hz (Figure 22, top). The main product of the reaction was found with a content of 24% by integration as an AB-type spin system at −91.3 and −85.8 ppm showing a P,P-coupling of 10.4 Hz. While the chemical shift of this resonance could fit to a P-bridged compound, the $C_2$-symmetric **15a** should produce a singlet in $^{31}P\{^1H\}$ NMR spectra, Instead, the observed resonance could fit to an asymmetrically bridged compound such as **15a'** (Figure 21).

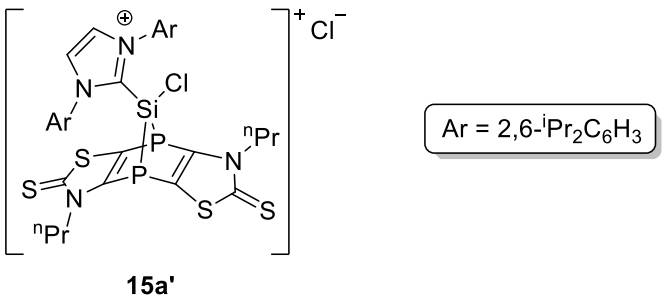


**15a'**

*Figure 21:* Possible product **15a'** of the reaction of **1** with IPr−$SiCl_2$.

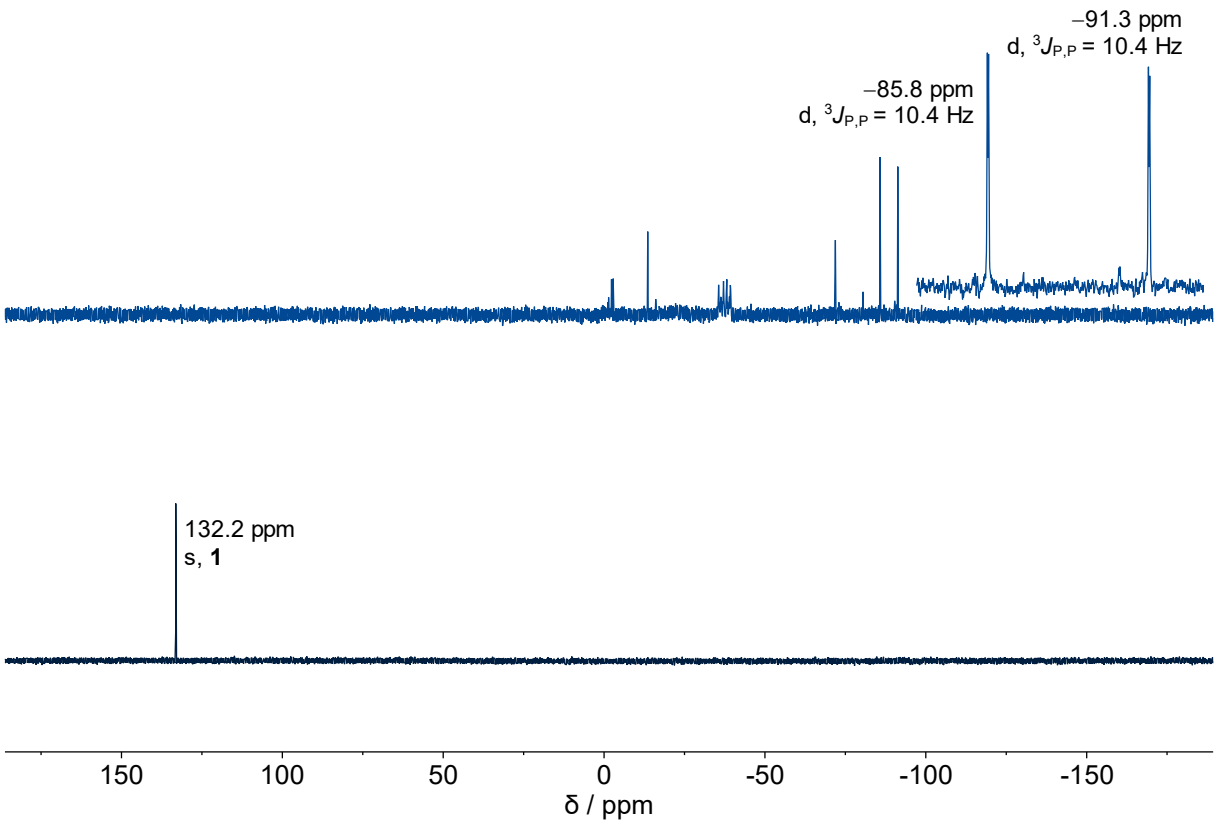


*Figure 22:* $^{31}P\{^1H\}$ NMR spectra of reactions of **1** with an IPr−$SiCl_2$ (top) and $ZnCl_2$/IPr−$SiCl_2$ (bottom).

As a one-step reaction of **1** with IPr−$SiCl_2$ did not yield the desired product, the reaction was repeated while adding $ZnCl_2$ to the mixture in order to form an insoluble IPr−$ZnCl_2$ complex,[123] thus liberating the transient dichlorosilylene and significantly increasing its reactivity (Scheme 19).

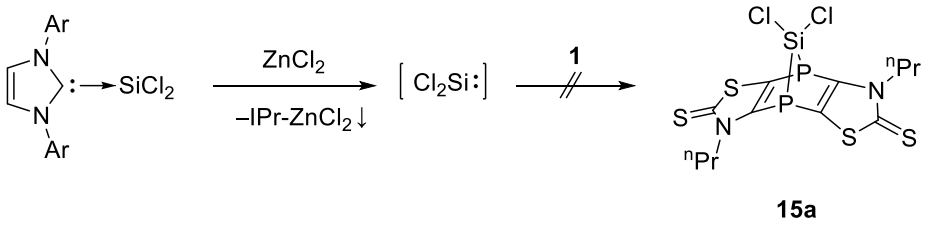


**15a**

*Scheme 19:* Targeted reaction of IPr−$SiCl_2$ with $ZnCl_2$ to form transient dichlorosilylene and, upon addition to **1**, **15a**.

Additionally, competing reactions forming asymmetric products like **15a'** should be suppressed by removing the NHC from the reaction mixture. During the addition of IPr−$SiCl_2$ to a suspension of **1** and a small excess of $ZnCl_2$ in diethyl ether or toluene at −90 °C led to no immediate colour change. Indeed, even after warming up to ambient temperature over the course of 19 h, no reaction was observed, and **1** remained the only present P-containing compound in $^{31}P\{^1H\}$ NMR experiments (Figure 22, bottom). A likely explanation for this

behaviour can be a side reaction of the very reactive $SiCl_2$ intermediate with itself or other compounds present in the mixture, suppressing a reaction with **1**.

In addition to IPr−$SiCl_2$, **1** was reacted with an 1,3-bis(2,2-dimethylpropyl)-1,3-dihydro-2*H*-1,3,2-benzodiazasilol-2-ylidene, originally synthesised by Gehrhus and Lappert in 1995,[124] in order to furnish **15b** (Scheme 18). The addition of the silylene was carried out at −80 °C to suppress unwanted side reactions and then slowly warmed up to ambient temperature. The indication of the obtained red suspension was corroborated by $^{31}P\{^1H\}$ NMR studies which revealed that **1** remained the most prominent compound at about 69% (Figure 23, top). Besides, two singlets were visible at −105.1 and −97.9 ppm (approximately 15%). As these chemical shifts were found in a reasonable region for **15b**, the integrals pointed to a very slow reaction, hence, the reaction mixture was heated to 80 °C and stirred at this temperature for 18 h. $^{31}P\{^1H\}$ NMR experiments were repeated, however, the two resonances appearing in the highfield region of the spectrum emerged with significantly lower content of about 5% each, while that of **1** had risen to over 90% (Figure 23, bottom). This points towards a shift of the reaction equilibrium away from the product **15b** at higher temperatures, possibly due to a steric repulsion between the very bulky *neo*-pentyl groups in the used silylene which facilitate [4+1]-cycloreversion giving back the starting materials. However, a conversion of more than 31% of **1** was not observed at lower temperatures and, hence, **15b** could not be isolated.

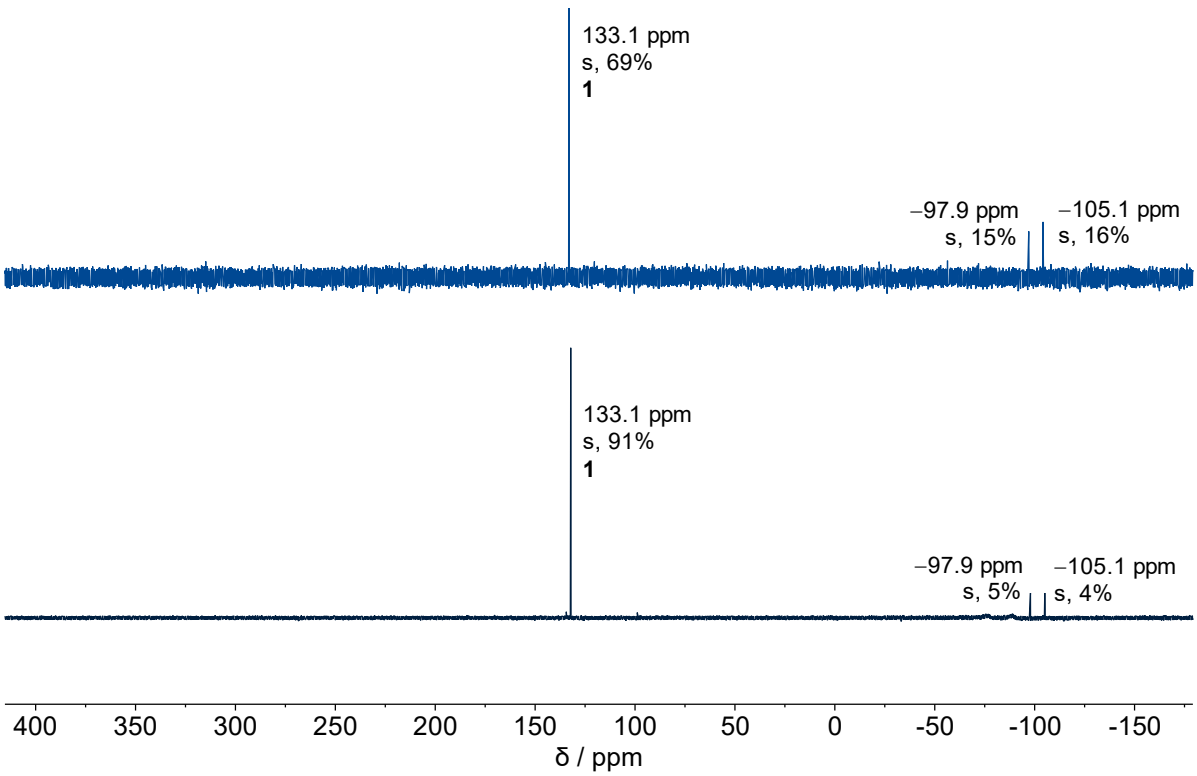


*Figure 23:* $^{31}P\{^1H\}$ NMR spectra of the reaction of **1** with an N-heterocyclic silylene (NHSi) at ambient temperature (top) and 80 °C (bottom).

Going to the heavier homologs of silylenes, germylenes are also known to undergo [4+1]-cycloaddition reactions with dienes, and related 7-germanorbornadiene motifs have been reported to the literature.[125] Therefore, a reaction with germanium dichloride dioxane complex ($GeCl_2$ · dioxane) was performed (Scheme 20, top). The reaction was performed at room temperature, however, under these conditions, no reaction could be observed and **1** remained unchanged in the $^{31}P\{^1H\}$ NMR spectrum. Therefore, the reaction was repeated and $GeCl_2$ · dioxane was first reacted with sodium tetrakis(3,5-bis(trifluoromethyl)phenyl)borate ($NaBAr^F$) in order to form highly reactive $[GeCl]^+$ which—as a more active species—could facilitate the desired [4+1]-cycloaddition reaction (Scheme 20, bottom).

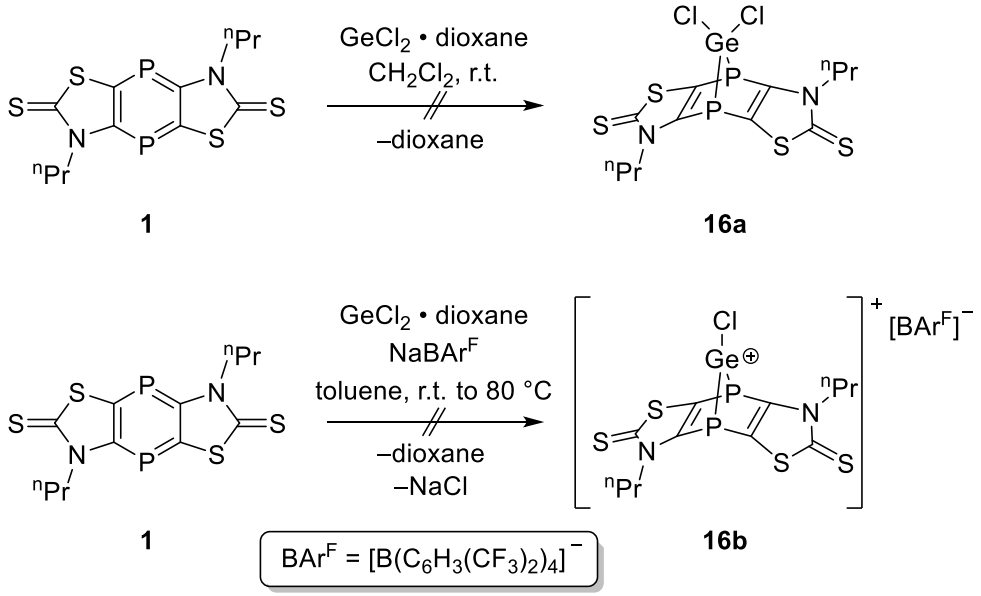


*Scheme 20:* Targeted reactions of **1** with germanium dichloride dioxane complex (top) and further addition of sodium tetrakis(3,5-bis(trifluoromethyl)phenyl)borate (bottom).

After addition of **1** and stirring for 5.5 h $^{31}P\{^1H\}$ NMR spectra showed the formation of small quantities (7% and 8% by integration, respectively) of two products in the highfield region at the same chemical shifts as the observed products of the previously described reaction with an NHSi. This is a strong indication that the observed products are indeed not 7-tetrelano-1,4-diphosphabarrelenes as the chemical shifts of a silicon-bridged and a germanium-bridged compound are expected to differ significantly. Instead, a reaction at the two thione moieties could be possible, explaining the still present main signal of **1**. In accordance to the observations in the case of the NHSi, heating to 80 °C yielded the single resonance of **1** in $^{31}P\{^1H\}$ NMR spectra, further corroborating the resemblance of the formed products in both cases. However, as these products were only formed *in situ* in small quantities, no attempt for their isolation was made.

## 3.3 1,4-DIPHOSPHABARRELENES

While 1,4-diphosphabarrelenes have been known to the literature since 1961,[98] their synthesis and reactivity has remained a very narrow niche of research with only few examples published to date. Most early syntheses focused on building the barrelene scaffold directly from phosphanes/phosphites and the targeted peripheral moieties[126,127] and this approach remains relevant today.[128] The first preparation of a 1,4-diphosphabarrelene from a 1,4-diphosphinine was achieved by Kobayashi with the first 1,4-diphosphinine **LIV** in a [4+2]-cycloaddition reaction.[114] After four decades, the group of Streubel expanded on the preparation of 1,4-diphosphabarrelenes by reporting on some of these structures based on their tricyclic 1,4-diphosphinines.[64,101,102,105,129] However, the reversibility of these [4+2]-cycloadditions was addressed only in two communications.[64,129] Hence, a broader study on the formation and decomposition of 1,4-diphosphabarrelenes based on **1** was conducted.

### 3.3.1 [4+2]-cycloadditions with alkynes

Firstly, the scope of unsaturated bridges was expanded beyond the only literature-known example[101,105,129] by reacting 1,4-diphosphinine **1** with differently substituted alkynes, *i.e.*, diethyl acetylene dicarboxylate (DEAD, **a**), ethyl propiolate (**b**) and 3-hexyne (**c**). The reactions were carried out in toluene at elevated temperatures, as no reaction of **1** with the employed alkynes was observed at ambient temperature (Scheme 21).

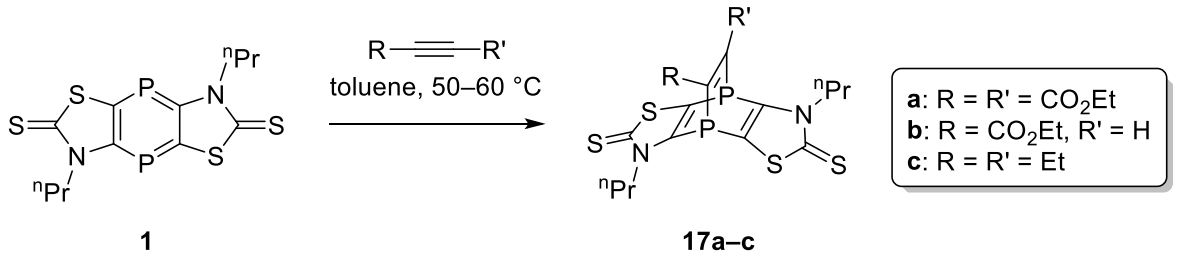


**1** **17a–c**

*Scheme 21:* Reactions of **1** with different alkynes to form 9,10-unsaturated 1,4-diphosphabarrelenes **17a–c**.

As the colour of the reaction mixtures changed from red (**1**) to yellow/orange, differences in the rate of the conversions were noticed depending on the alkyne substituents R,R'. While ester substitution led to reaction times of 1.5–6.5 h in order to reach full conversion to the respective barrelene, the alkyl substituted 3-hexyne needed a reaction time of over three weeks to furnish **17c**. However, once the starting material was fully consumed, $^{31}P\{^{1}H\}$ NMR spectroscopy revealed the selective formation of a single product in all three reactions. These products appeared as singlets for the symmetrically substituted bridges of **17a,c** (−75.5 and −71.2 ppm, respectively), while the asymmetrically bridged **17b** showed an AB-system (−87.1/−84.0 ppm) with a P,P-coupling constant of 26.0 Hz, the latter being in the expected range of a $^{3}J_{P,P}$ coupling for this class of compounds. Due to the volatile nature of the employed

alkynes, isolation of the three products was straight-forward and **17a–c** could be fully characterised. The structure of **17c** was confirmed via single crystal X-ray diffraction analysis (Figure 24). As expected, bond lengths and angles of the barrelene framework are very similar to analogous structures reported in the literature with differences in P-C bonds of below 0.002 Å and endocyclic C-P-C angle differences of about 1°.[129]

Theoretically, all three reactions were found to be clearly exergonic in nature. **17b$^{Me}$** possesses a remarkable stability compared to the other two derivatives, its $\Delta_r G$ being significantly more negative at −23.2 kcal/mol. The two products with either a more or a less electron-deficient alkyne are comparatively less favoured at −14.4 kcal/mol for **17a$^{Me}$** and −11.7 kcal/mol for **17b$^{Me}$**. Investigating the transition state structures revealed a relatively low barrier for **17b$^{Me}$** at 18.5 kcal/mol, while **17a$^{Me}$** and **17b$^{Me}$** are formed via transition states at 27.7 and 20.3 kcal/mol, respectively, explaining the vastly different conversion rates of the three reactions, **17b** being formed after 1.5 h at 50 °C while **17c** was stirred at 60 °C for 22 d to achieve complete conversion.

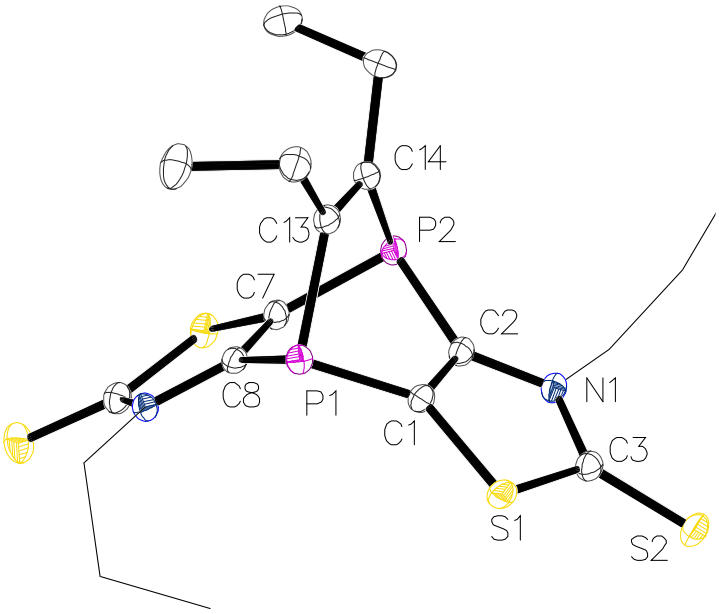


*Figure 24:* Molecular structure of **17c** in the single crystal lattice at 100 K. Thermal ellipsoids are set at 50% probability level. Hydrogen atoms were omitted and *n*-propyl groups are shown as wire-frames for clarity. Selected bond lengths (Å) and bond angles (°): P1−C1 1.8193(13), P1−C8 1.8458(13), C1−C2 1.3491(18), P1−C13 1.8682(14), C13−C14 1.338(2), C1−P1−C8 94.52(6).

### 3.3.2 [4+2]-cycloadditions with alkenes

Compared to 1,4-diphosphabarrelenes containing a C-C unsaturated bridge, reaction products of [4+2]-cycloadditions with alkenes are found much more scarcely in the literature. The only reagents ever to be probed for tricyclic 1,4-diphosphinines were alkenes such as 1-hexene and *N*-phenyl-pyrrole-2,5-dione.[64,105,129] Interestingly, while this reaction was described to proceed at much higher temperatures than the reaction with an alkyne in the case of imidazole-based **LVI**, the thiazole-based **1** reacted at ambient temperature with the pyrrole-2,5-dione, while alkynes required a temperature of 50 °C to furnish the respective 1,4-diphosphabarrelenes. Hence, reactions of **1** with differently substituted alkenes were studied in more detail in order to get a better understanding of the substituent effects on [4+2]-cycloadditions and the comparison to the previously discussed alkynes. To accomplish this, seven different alkenes were employed, ranging from ethene and alkyl substituted derivatives to doubly ester substituted ones like diethyl maleate (*Z*-diethyl ethene dicarboxylate) and diethyl fumarate (*E*-diethyl ethene dicarboxylate, Scheme 22).

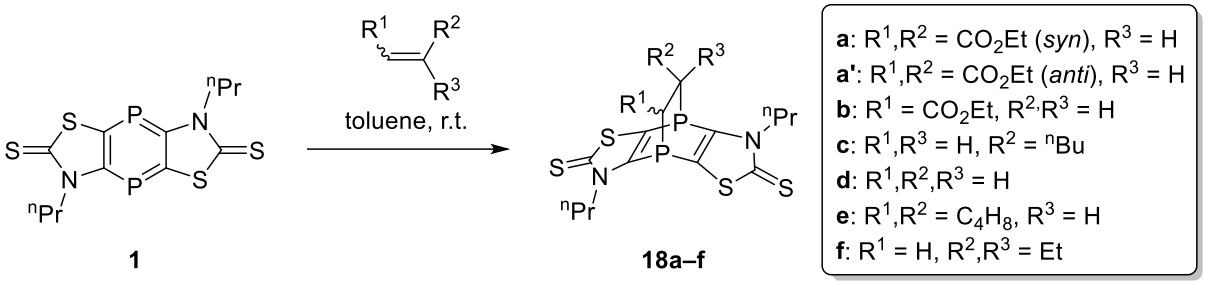


*Scheme 22:* Reactions of **1** with different alkenes to form 9,10-saturated 1,4-diphosphabarrelenes **18a–f**.

All reactions were carried out at ambient temperature and, in analogy to the previously reported example of a 1,4-diphosphabarrelene of **1** having a saturated bridge, all reactions proceeded forming colourless to off-white suspensions without visible traces of **1** left. Indeed, $^{31}$P NMR spectroscopic monitoring revealed the selective appearance of sets of resonances in the highfield region of the spectra, corresponding well to literature-known derivatives.[129] All seven examples could be isolated in good yields and were fully characterised. Depending on the nature of the bridges, **18a–f** appear in $^{31}$P NMR spectra as different spin systems (Table 3): while the C2-symmetric bridges derived from ethene (**18d**) and diethyl fumarate (**18a'**) resulted in one (for **18d**) or two (for the diastereomers (47:53) of **18a'**) singlets in $^{31}$P{$^{1}$H} NMR spectra which show further splitting in $^{31}$P NMR spectra, *Z*-alkenes such as diethyl maleate (**18a**) and cyclohexene (**18e**) as well as the doubly-substituted 2-ethyl-1-butene (**18f**) result in one set of AB-type spin systems each.

*Table 3:* $^{31}$P NMR data of 1,4-diphosphabarrelenes **18a–f** (all spectra were measured in $CDCl_3$).

| compound | alkene | δ($^{31}$P) / ppm | multiplicity[a] | $^3J_{P,P}$ / Hz | $^nJ_{P,H}$ / Hz |
|---|---|---|---|---|---|
| **18a** | diethyl maleate | −75.8/−73.3 | dm/dd | 28.7 | —/6.23 |
| **18a'** | diethyl fumarate | −72.5<br>−72.3 | br. s<br>br. s | —<br>— | —<br>— |
| **18b** | ethyl acrylate | −80.0/−75.4<br>−79.7/−74.1 | dm/dd<br>dm/dt | 29.3<br>28.9 | —/4.76<br>—/3.75 |
| **18c** | 1-hexene | −77.7/−72.6<br>−77.0/−73.5 | dt/dm<br>dt/dm | 24.5<br>24.3 | 7.90/—<br>8.15/— |
| **18d** | ethene | −82.0 | m | — | — |
| **18e** | cyclohexene | −69.4/−68.4 | dm/dm | 20.4 | — |
| **18f** | 2-ethyl-1-butene | −73.4/−63.4 | dt/dq | 23.4 | 7.54/11.4 |

[a]) s = singlet, d = doublet, t = triplet, q = quartet, m = multiplet, br. = broad

Singly-substituted bridges such as the ones derived from ethyl acrylate (**18b**) or 1-hexene (**18c**) are formed in two diastereomers (with diastereomeric ratios of roughly 40:60) both displaying AB-systems in $^{31}$P{$^1$H} NMR spectra. $^3J_{P,P}$ couplings for all products displaying AB-spin systems lie between 20 and 30 Hz, being in the same range as similar known compounds.[127,129] Notably, while less electronegative substituents in the bridge cause the corresponding $^{31}$P signal to appear more highfield-shifted, P,P-coupling constants are smaller for these systems, being closer to 20 Hz, whereas systems with ester-substituted bridges display P,P-coupling constants closer to 30 Hz. While many examples did not allow a clear-cut analysis of P,H-coupling constants in their $^{31}$P NMR spectra due to broadening of the respective signals, some $^2J_{P,H}$ couplings were resolved and lie in the range of a few Hertz.

It was possible to confirm the molecular structure of the 9,9-diethyl-substituted **18f** via single crystal X-ray diffraction analysis (Figure 25). A comparison of bond lengths and angles between **18f** and the alkyne-based **18c** shows the diphosphinine-based moiety virtually unchanged for both a saturated and an unsaturated bridge (compare Figure 24). Significant changes in the geometry of the scaffold only appear in the C-C bond of the bridge, where **18f** shows an expected elongation of the C-C bond compared to **17c** (1.556(3) Å *vs.* 1.338(2) Å). Additionally, the P-C bonds to the bridge atoms are somewhat elongated in **18f**, however, this difference remains small at only 0.035 Å.

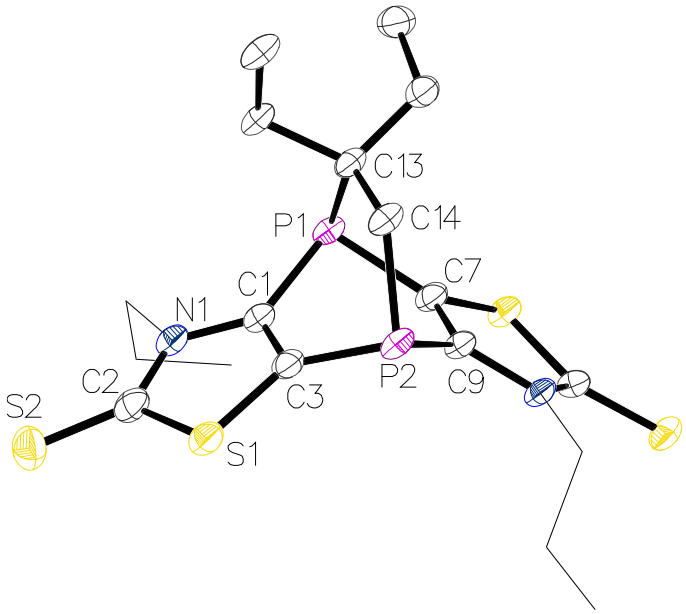


*Figure 25:* Molecular structure of **18f** in the single crystal lattice at 100 K. Thermal ellipsoids are set at 50% probability level. Hydrogen atoms were omitted and *n*-propyl groups are shown as wire-frames for clarity. Selected bond lengths (Å) and bond angles (°): P1−C1 1.832(2), P1−C7 1.818(2), C1−C3 1.351(3), P1−C13 1.903(2), C13−C14 1.554(3), C1−P1−C7 95.11(10).

Similar to the alkyne-based **17a–c$^{Me}$**, theoretical investigations revealed the formations of alkene based **18a–f$^{Me}$** to be exergonic, albeit $\Delta_rG$ values were closer to 0 for compounds **18a–f$^{Me}$** (Table 4) On the other hand, the while being less exergonic, these [4+2]-cycloadditions also showed lower barriers down to 10.8 kcal/mol for **18a$^{Me}$**, explaining the conversion to the products already at ambient temperature. Compounds **18a',b,c$^{Me}$** show the expected (but very small) differences in $\Delta_rG^{‡}$ and $\Delta_rG$ for the two diastereomers.

*Table 4:* $\Delta_rG^{‡}$ and $\Delta_rG$ of the formation of compounds **18a–f$^{Me}$**.

| compound | Alkene | $\Delta_rG^{‡}$ / kcal/mol | $\Delta_rG$ / kcal/mol |
|---|---|---|---|
| **18a$^{Me}$** | diethyl maleate | 10.8 | −13.0 |
| **18a'$^{Me}$** | diethyl fumarate | 18.6<br>14.8 | −3.1<br>−4.4 |
| **18b$^{Me}$** | ethyl acrylate | 19.8<br>18.8 | −4.9<br>−6.1 |
| **18c$^{Me}$** | 1-hexene | 21.0<br>19.5 | −6.8<br>−7.1 |
| **18d$^{Me}$** | Ethene | 19.8 | −11.2 |
| **18e$^{Me}$** | Cyclohexene | 23.4 | −3.0 |
| **18f$^{Me}$** | 2-ethyl-1-butene | 20.6 | −5.4 |

However, contrary to the obvious assumption of steric repulsion between the bridge-substituent and the *n*-propyl group(s), the diastereomers with a *syn*-arrangement of these groups are the more stable ones in all three cases, likely due to dispersion interactions between the substituents. The small differences in energy correspond well to the observed ratios of the formed diastereomers which lie between 40:60 and 50:50 for all cases, corroborating the small differences in barrier and stability.

### 3.3.3 Experimental and theoretical investigations on the thermal reversibility of [4+2]-cycloadditions

As numerous different examples of 1,4-diphosphabarrelenes were achieved experimentally, a systematic experimental and theoretical study on the effects of substituents and the nature of the bridge was carried out with respect to their stability and, consequently, the reversibility of the [4+2]-cycloaddition reactions forming **17,18**. For completeness, the hypothetical ethyne-based 1,4-diphosphabarrelene (named **17d$^{Me}$**) containing an unsaturated, unsubstituted bridge was included in the calculations, allowing comparisons to the synthesised ethene-based derivative **18d$^{Me}$**.

A comparing overview over the free reaction enthalpies $\Delta_rG$ and barriers $\Delta_rG^{‡}$ of 1,4-diphosphabarrelenes having an unsaturated (**17a–d$^{Me}$**) *vs.* a saturated (**18a–f$^{Me}$**) bridge underlines the experimental observations (Figure 26, left). Generally, $\Delta_rG^{‡}$ values of **18a–f$^{Me}$** (diastereomers were averaged) are smaller than those of **17a–d$^{Me}$**, agreeing well with fast reactions at ambient temperature in the syntheses of the former, while the latter needed elevated temperatures to furnish the respective products. Conversely, an unsaturated bridge seems to stabilise the 1,4-diphosphabarrelene moiety as **17a–d$^{Me}$** are formed in more exergonic reactions than **17a–f$^{Me}$**. Another trend is visible in a more detailed comparison of compounds having the same substituent pattern on the bridge (Figure 26, right).

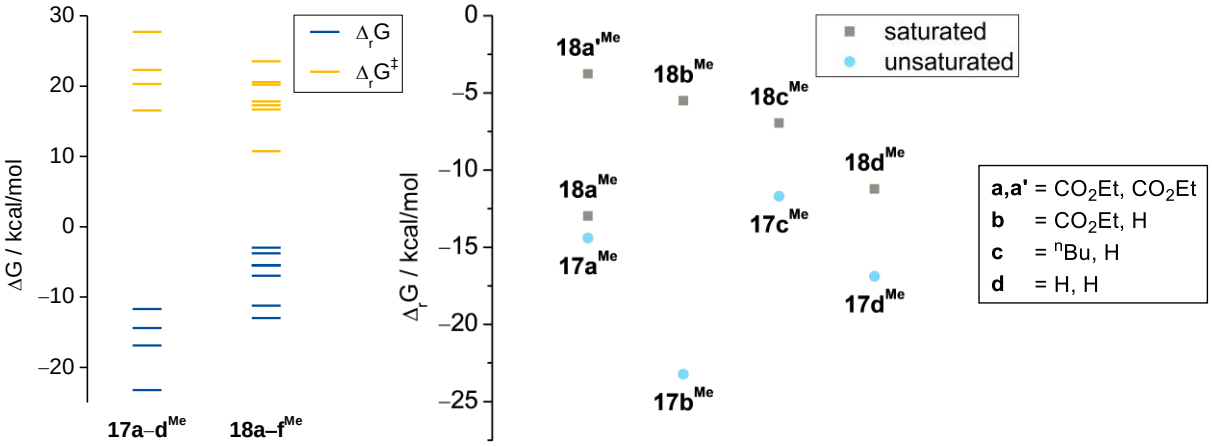


*Figure 26:* $\Delta_rG$ and $\Delta_rG^{‡}$ of 1,4-diphosphabarrelenes having an unsaturated (**17a–d$^{Me}$**) or saturated (**18a–f$^{Me}$**) bridge (left) and $\Delta_rG$ of **17a–d$^{Me}$** and **18a–d$^{Me}$** (right).

In the case of **18a–d$^{Me}$**, derivatives with smaller and less electron-withdrawing substituents are more stabilised, albeit with one notable exception: **18a$^{Me}$** displays a significantly more negative value of $\Delta_r G$ compared to the electronically very similar **18a'$^{Me}$**, indicating a steric effect between the bridge and the diphosphinine moiety. Although **18a'$^{Me}$** is energetically more favoured than the least stabilised unsaturated **17c$^{Me}$**, all other derivatives of **17** show lower values of $\Delta_r G$. However, no correlation between $\Delta_r G$ and the bridge substituents is visible here as the four examples show no trend comparable to that of **18a–d**.

Due to the reasonably small barriers of the investigated [4+2]-cycloadditions and the differences in stability of **17$^{Me}$,18$^{Me}$**, the synthesised 1,4-diphosphabarrelenes were expected to be prone to thermal decomposition, forming back starting material **1** in a [4+2]-cycloreversion. Indeed, multiple derivatives had been found to show a reddish colour upon heating, indicating that **1** was partially forming in the mixture. Hence, a reversibility study was carried out, heating solutions of all ten isolated derivatives in xylenes (up to a maximum of 190 °C in a sealed NMR tube) until a reddening of the solution was observed. Due to large differences in solubility, the same concentration could not be maintained in all reactions, however, it was kept as close as possible to ensure comparability.
Cycloreversion temperatures ($T_{rev}$) were obtained for most of the synthesised 1,4-diphospha-barrelenes (Table 5). The exceptions were **17a** and **17c**, which showed no reddening of the solution even at the solvent limit of 190 °C. The third derivative with an unsaturated bridge, **17b**, possesses a cycloreversion temperature of 180 °C. Compounds with saturated bridges exhibited lower cycloreversion temperatures, apparent from the highest value of 135 °C in the case of **18d**. The other derivatives of **18** display even lower temperatures down to as low as 45 °C for **18a'**. The trend of more negative free reaction enthalpies for less bridge-substitution is mirrored in $T_{rev}$ as higher temperatures, *i.e.*, more energy, is needed to afford **1** in systems with smaller substituents.

*Table 5:* Cycloreversion temperatures ($T_{rev}$, accuracy of ±5 °C) of 1,4-diphosphabarrelenes **17,18**.

| compound | alkyne/alkene | $T_{rev}$ / °C |
|---|---|---|
| **17a** | DEAD | >190 |
| **17b** | ethyl propiolate | 180 |
| **17c** | 3-hexyne | >190 |
| **18a** | diethyl maleate | 60 |
| **18a'** | diethyl fumarate | 45 |
| **18b** | ethyl acrylate | 75 |
| **18c** | 1-hexene | 90 |
| **18d** | ethene | 135 |
| **18e** | cyclohexene | 80 |
| **18f** | 2-ethyl-1-butene | 70 |

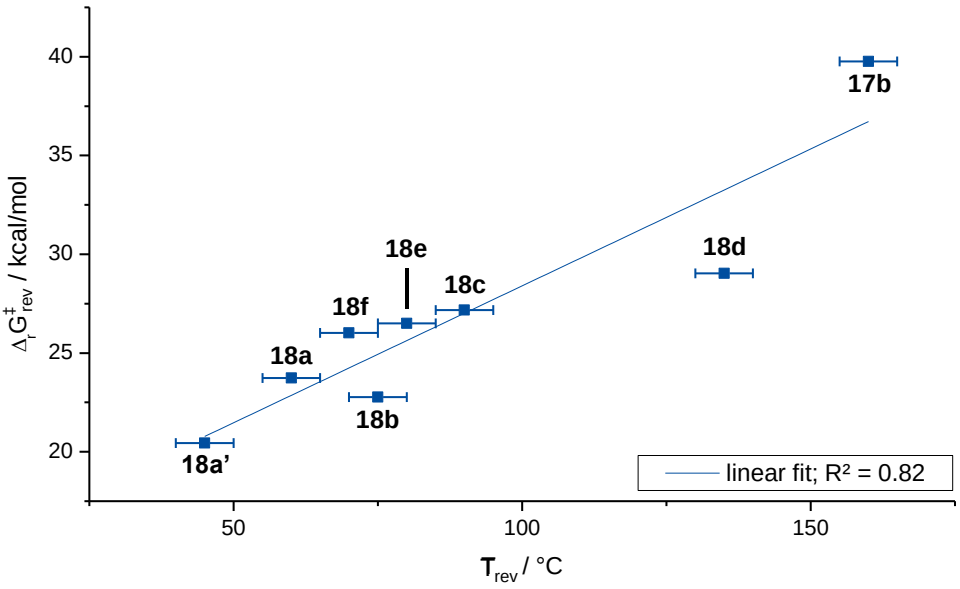


*Figure 27:* $\Delta_r G^{\ddagger}_{rev}$ of **17$^{Me}$,18$^{Me}$** plotted against $T_{rev}$ (below 170 °C) of **17,18** together with a linear fitting function.

A correlation of the obtained cycloreversion temperatures (below 190 °C) to the barrier of the reaction to **1**, $\Delta_r G^{\ddagger}_{rev}$, revealed a clear trend which could be fitted with a linear function with a correlation coefficient of 82% (Figure 27). While most derivatives of **18** were found to lie close to one another, two outliers become apparent: the ethene-bridged **18d**, showing a significantly lower barrier compared to its cycloreversion temperature, and the ethyl propiolate-bridged **17b** for which the opposite is true: its value of $\Delta_r G^{\ddagger}_{rev}$ points towards a cycloreversion temperature that is significantly higher than the observed $T_{rev}$. Additionally, the linear fitting allows a prediction of the decomposition temperatures of **17a,c**, which could not be obtained experimentally. Extrapolation to the respective values of $\Delta_r G^{\ddagger}_{rev}$ yields a $T_{rev}$ of 145 ± 9 °C for **17a**, while **17c** is expected to form back **1** at 180 ± 15 °C. While the latter does lie outside of the measurable temperature window, the cycloreversion of **17a** should be observable according to these calculations. However, a deviation from the expected value similar to the one found for **18d** is possible, pushing the actual $T_{rev}$ beyond 190 °C. Application of the same extrapolation to the theoretical ethyne-bridged compound **17d** gives a value for $T_{rev}$ of 198 ± 15 °C, similar to the value for **17c**. This differs significantly to the case of saturated bridges as ethene-bridged **18d** displays a significantly higher cycloreversion temperature than 1-hexene-bridged **18c**. However, it is possible that the actual values of **17c,d** are distinctly different from the extrapolated ones based on a linear regression.

In order to take a more detailed look at the formation of **17,18**, distortion energies $\Delta G_{dist}$ at the transition state were calculated for **17a–d$^{Me}$** and **18a–f$^{Me}$** for both the diphosphinine and alkene/alkyne fragment (Figure 28, left) to get a better understanding of the differences in reactivity between saturated and unsaturated bridges and the value of $\Delta_r G^{\ddagger}$. A comparison between unsaturated (**17**) and saturated (**18**) bridges reveals the trend of higher distortion of the diphosphinine fragment for **18a–f$^{Me}$**. In both cases, the distortion of the alkene/alkyne fragment varies significantly for the investigated systems, indicating that the total distortion energy is mostly dependent on the substitution in the 1,4-diphosphabarrelene bridge.

A comparison of $\Delta G_{dist}$ to the respective $\Delta_r G^{\ddagger}$ revealed further trends (Figure 28, right). In spite of a substantial variation in the total distortion energies, a larger value of $\Delta G_{dist}$ correlates with a larger value of $\Delta_r G^{\ddagger}$, indicating that the interaction energy (derived from $\Delta G^{\ddagger} = \Delta G_{dist} + \Delta G_{int}$)[130] remains similar for differently substituted alkenes/alkynes. Yet, fitting a linear function to the obtained values reveals the correlation between $\Delta G_{dist}$ and $\Delta_r G^{\ddagger}$ to be rather weak, especially for **18a–f$^{Me}$**, as the correlation coefficient is small (67%). The unsaturated **17a–d$^{Me}$** give a better correlation of 86% with generally higher values of $\Delta_r G^{\ddagger}$. As $\Delta G_{dist}$ lie in a similar range compared to **18a–f$^{Me}$**, the higher reaction barriers can be attributed to lower interaction energies between **1** and alkynes as opposed to alkenes.

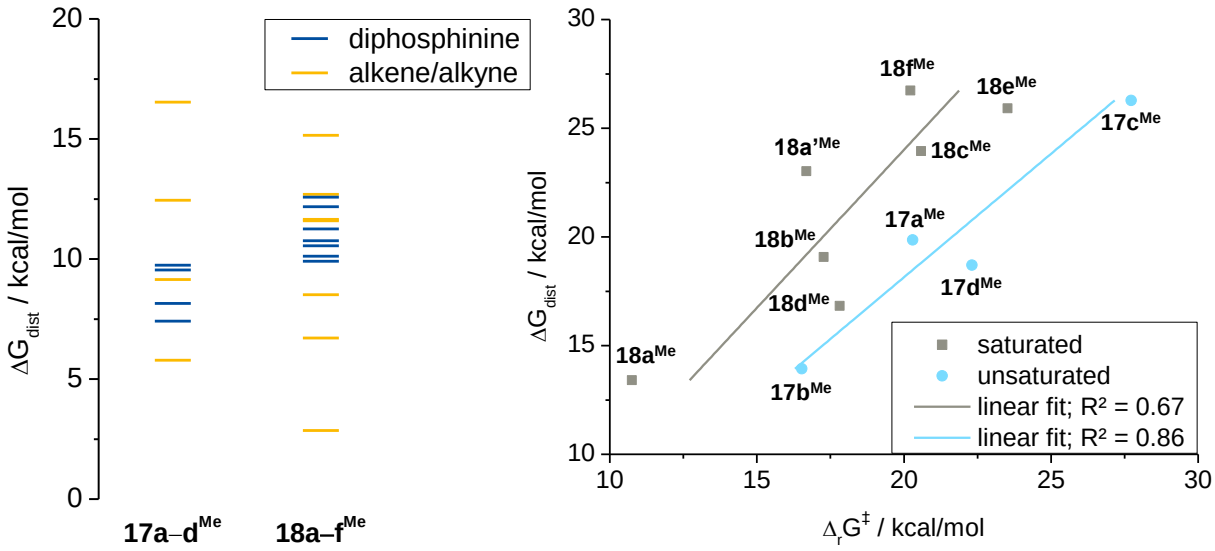


*Figure 28:* $\Delta G_{dist}$ of diphosphinine and alkene/alkyne (left) and $\Delta G_{dist}$ plotted against $\Delta_r G^{\ddagger}$ **18a–f$^{Me}$** and **17a–d$^{Me}$** together with linear fitting functions (right).

### 3.3.4 [4+2]-cycloadditions with nitrogen-containing π-systems

#### *3.3.4.1 Reaction with 5,5-dimethyl-pyrroline-N-oxide*

In order to probe its reactivity towards heteroatom-containing dienophiles, **1** was reacted with different nitrogen-containing π-systems. First, reactions with C=N double bond-containing systems were examined. As **1** did not react with imines such as *N*-methyl-phenylimine at all, the concept emerged to use related classes of compounds such as more activated 1,3-dipoles, *e.g.*, 5,5-dimethyl-pyrroline-*N*-oxide (DMPO). Indeed, the addition of DMPO to **1** led to a full conversion after stirring for 20 h at ambient temperature (Scheme 23).

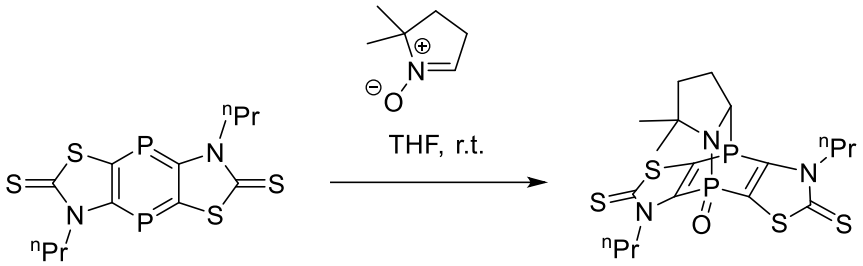


**1** **19**

*Scheme 23:* Reaction of **1** with 5,5-dimethyl-pyrroline-*N*-oxide to form 1,4-diphosphabarrelene oxide **19**.

$^{31}P\{^{1}H\}$ NMR spectroscopic investigations revealed the formation of two AB-type spin systems in a diastereomeric ratio of 2:1 having small P,P-coupling constants of around 4 Hz, with one set of nuclei appearing in the highfield beyond −80 ppm while the other set was close to 0 ppm (Figure 29). **19** could be purified column chromatographically, however, the product was found to be very sensitive and, hence, a full characterisation beyond NMR and IR spectroscopy as well as MS was not possible. Still, the proposed structure of **19** could be confirmed by multinuclear NMR experiments, as a P,H-coupling to the bridge-carbon atom was only visible for the P(III) nucleus, verifying the P-N connectivity at the P(V) atom. Calculated $^{31}P$ chemical shifts of $\mathbf{19^{Me}}$ (B97-D3/def2-TZVP($CPCM_{THF}$)) further supported this assignment as the two diastereomers were found to have theoretical $^{31}P$ chemical shifts of −64/−54 ppm for P(III) and 1.4/0.3 ppm for P(V), the values being referenced to the $^{31}P$ chemical shift of **1**. Within the accuracy of calculated $^{31}P$ NMR shifts, the data fits well to the experimental values.

Mass spectrometric experiments using electron ionisation (EI, 70 eV) revealed—apart from the molecular ion peak and an oxidised species—multiple fragmentations, mainly of the bridging pyrrolidinyl moiety. Additionally, similar to **17** and **18**, 1,4-diphosphinine **1** was visible in the mass spectrum as the bridge and oxygen atom are cleaved off under EI conditions.

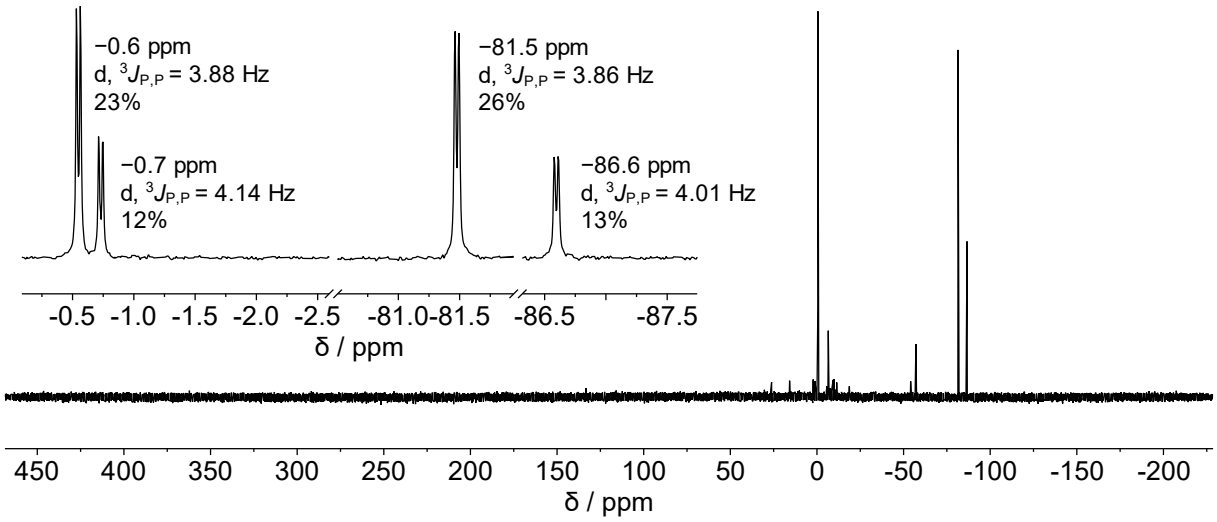


*Figure 29:* $^{31}P\{^1H\}$ NMR of spectrum of reaction mixture of **19**.

More detailed theoretical investigations were carried out to gain insight into a possible formation mechanism of **19**. After initial studies suggested a two-step mechanism, an intermediate structure was found at −43.5 kcal/mol, comprising of an adduct of 5,5-dimethyl-pyrroline to a mixed-valent, bent 1,4-diphosphinine (Figure 30). The formation of this adduct can proceed over a barrier of 29.0 kcal/mol. In the transition state, the N-O bond length of the DMPO fragment is significantly elongated at 1.70 Å (compared to 1.29 Å in DMPO) while the P-O distance is about 0.1 Å longer than in the N→P adduct (1.65 Å *vs.* 1.48 Å). The intermediate could not be detected in $^{31}P$ NMR experiments, being in line with the very small barrier (5.2 kcal/mol for the *anti*-conformation of the alkyl groups, 2.1 kcal/mol for *syn*) in the second step, *i.e.*, the barrelene formation. The final product **19$^{Me}$** was found to be a total of 54.5 kcal/mol (*anti*) and 55.8 kcal/mol (*syn*) more favoured than the **1$^{Me}$**, the difference to the intermediate adduct being −12.3 kcal/mol (*anti*) and 11.0 kcal/mol (*syn*).

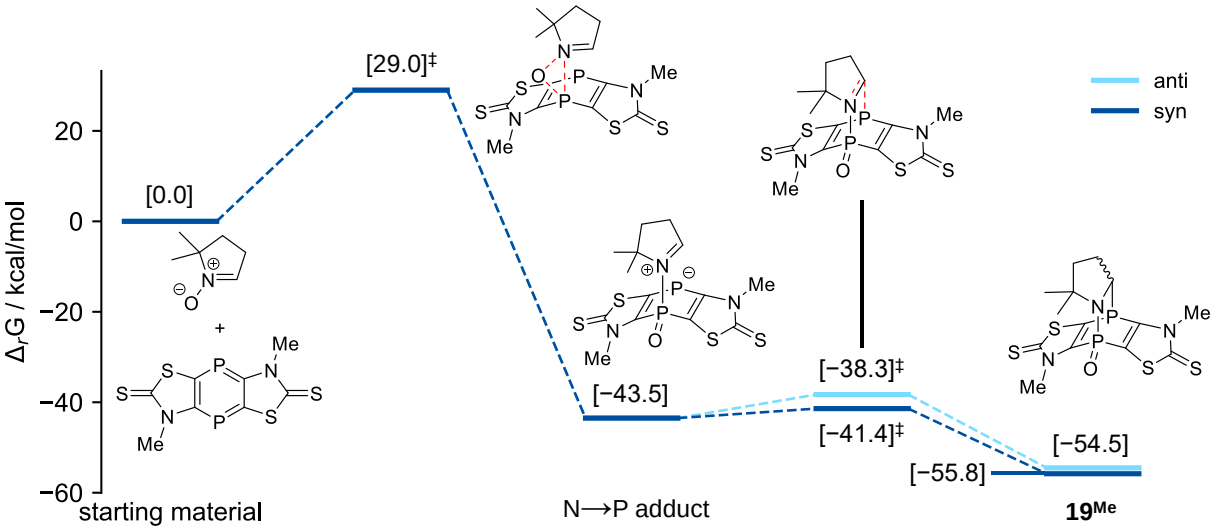


*Figure 30:* Proposed reaction mechanism of the formation of **19$^{Me}$** via an intermediate N→P adduct.

### *3.3.4.2 Reaction with 4-phenyl-1,2,4-triazoline-3,5-dione*

As reactions with imines did not result in successful [4+2]-cycloadditions, the investigations on the reactivity of **1** towards heteroatom-containing double bonds were continued by using the very strong dienophile 4-phenyl-1,2,4-triazoline-3,5-dione (in the following: triazoline), which was employed to probe the addition of an activated N=N double bond to **1**.[129] Although **20** started forming at −20 °C already, the reaction was carried out in toluene at 90 °C to achieve full conversion (Scheme 24).

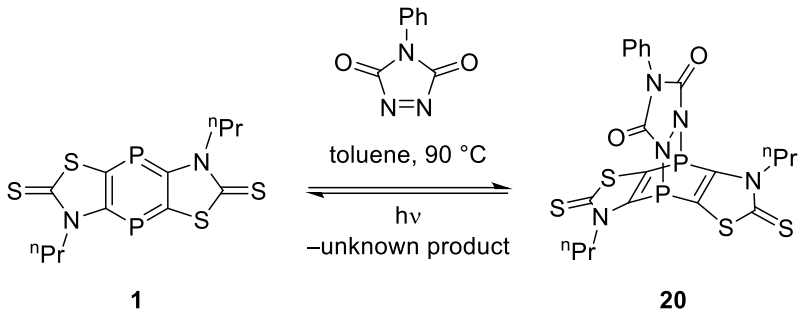


*Scheme 24:* Reversible reaction of **1** with 4-phenyl-1,2,4-triazoline-3,5-dione to form **20**.[129]

The product **20** was formed selectively, showing a $^{31}P\{^{1}H\}$ NMR resonance at −45.8 ppm (Figure 31, top), could be isolated by filtration and was obtained as a yellow solid. As only one singlet was observed, a low barrier for the inversion at the N,N-bridge was assumed. Theoretical calculations showed that the transition state for the formation of **20$^{Me}$** lies very low at only 2.2 kcal/mol, explaining the partial formation of **20** at −20 °C, while $\Delta_r G$ of the [4+2]-cycloaddition has a value of −32.3 kcal/mol.

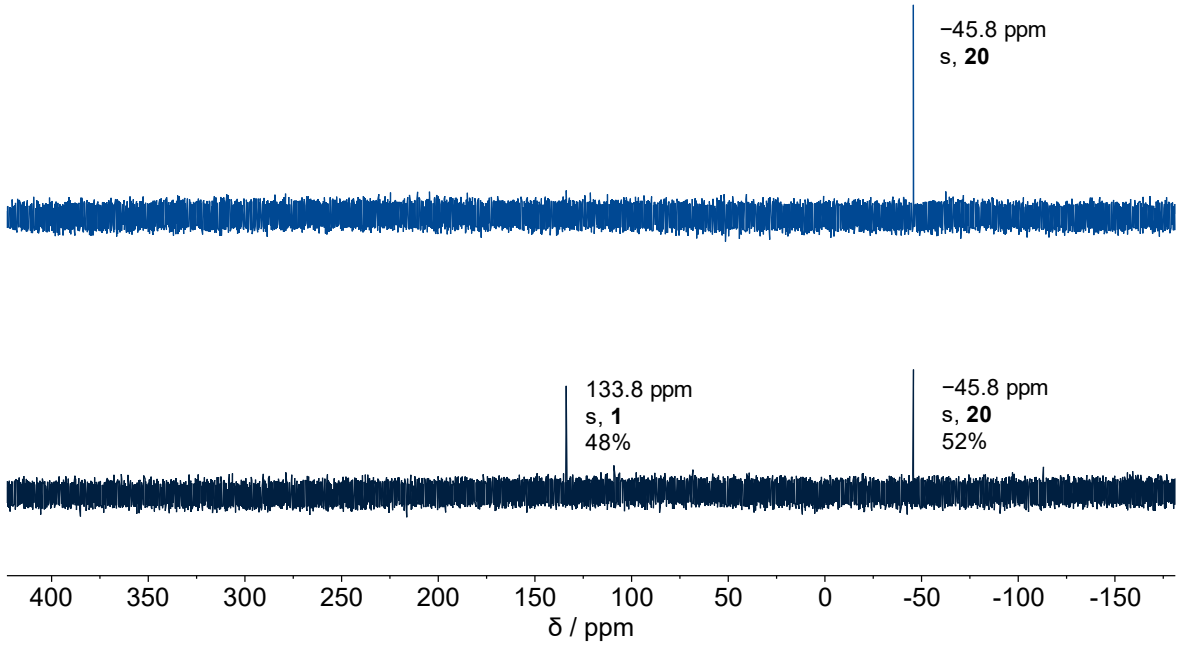


*Figure 31:* $^{31}P\{^{1}H\}$ NMR spectra of the reaction mixture of **20** (top, toluene) and mixture after irradiation (bottom, $CH_2Cl_2$).

During work-up and characterisation, an unexpected instability of **20** towards light was observed in solution and, to an extent, in the solid. Hence, a complete characterisation was impossible and only multinuclear NMR, IR and MS[110] data could be obtained. Upon irradiation with day light, the formation of **1** was observed. This finding was confirmed by irradiation of a solution of **20** in $CH_2Cl_2$ with UV light (of a Hg lamp) for 90 min. $^{31}P\{^1H\}$ NMR spectroscopic monitoring showed **1** being present in the resulting solution at a content of 48% by integration, yet, **20** was not fully consumed (Figure 31. bottom). Remarkably, **20** was not forming again after the photochemical reaction, suggesting that no clean [4+2]-cycloreversion reaction took place during irradiation, but the light induced a decomposition of **20** or the triazoline. In order to confirm this theory, UV/vis experiments were carried out as all involved species are intensely coloured. Both **1** (Figure 32, dark blue) and the triazoline (Figure 32, yellow) showed characteristic absorption bands which could be used to identify the respective compounds in the irradiated mixture (Figure 32, light blue). While the latter showed the absorption bands of both **1** and **20** (matching the corresponding $^{31}P\{^1H\}$ NMR spectrum, Figure 31, bottom), no absorption band at 545 nm was observed, suggesting that no triazoline had been formed and, thus, confirming its decomposition during the irradiation. Additionally, the decomposed mixture was split and exposed to the formation conditions of **20** while adding triazoline to one batch. As expected, **20** was selectively formed again in this batch, while no addition of triazoline resulted in no change in the $^{31}P\{^1H\}$ NMR spectrum as before heating in toluene, further corroborating the theory of decomposition of triazoline during the photochemical reaction.

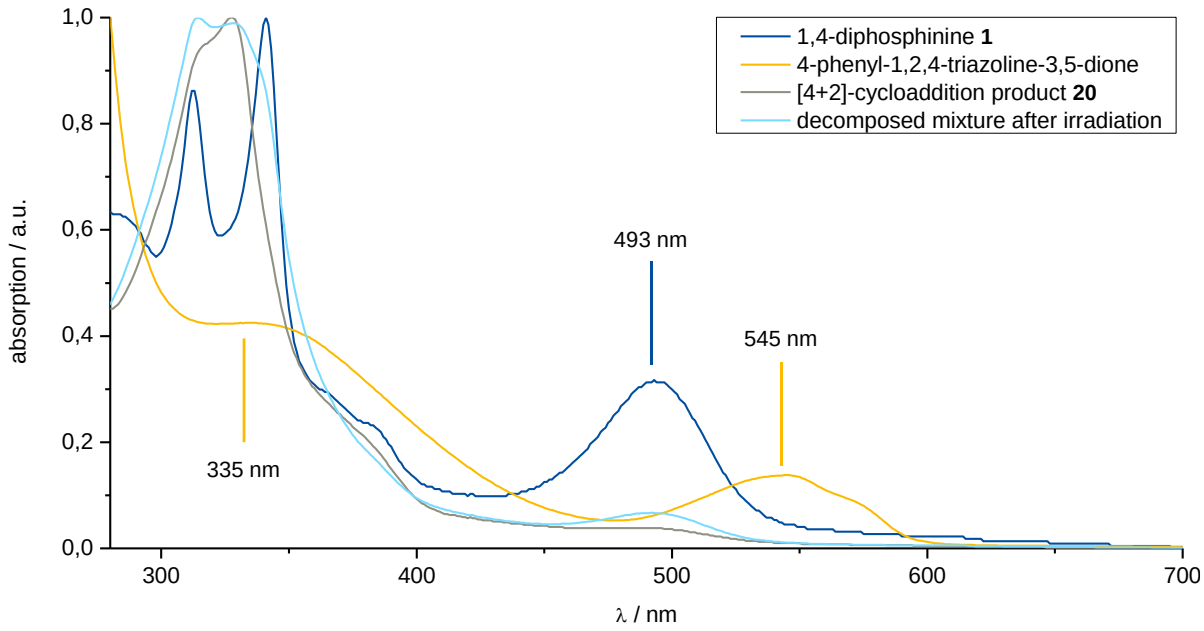


*Figure 32:* UV/vis studies ($CH_2Cl_2$) of **1**, triazoline, **20** and the decomposed mixture after irradiation. All curves were normalised to the highest respective value.

## 3.4 P-OXIDATION REACTIONS OF 1,4-DIPHOSPHABARRELENES

The synthesised 1,4-diphosphabarrelenes **17,18** can conceptually be further functionalised at two different moieties: the two phosphorus atoms as well as the thione groups at the outer rings. For the first reactivity studies of **17,18**, the emphasis was set on the former, *i.e.*, carrying out P-oxidation reactions. In order to ensure the highest tolerance towards chemical and thermal conditions, the alkyl-substituted **17c** and **18c** were chosen as the focus of the study.

### 3.4.1 Targeting a P-oxide structural motif

After the successful synthesis of 1,4-diphosphabarrelene P-oxide **19**, first reactions were aimed at the synthesis of this structural motif via one-fold oxidation of 1,4-diphosphabarrelene **18c**. Initial tests of reactions of **18c** with DMPO, pyridine-N-oxide and dimethylsulfoxide (DMSO) did not show any conversion. However, the addition of one equivalent of hydrogen peroxide-urea adduct revealed a reaction to three different main products (Scheme 25).

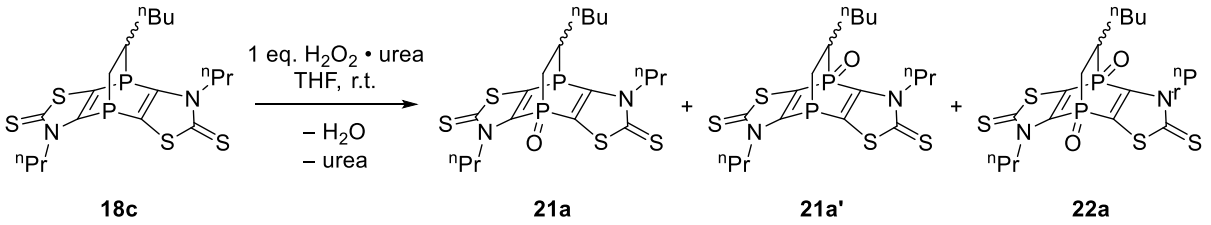


*Scheme 25:* Reaction of **18c** with one equivalent of hydrogen peroxide-urea.

$^{31}P\{^{1}H\}$ NMR spectroscopic monitoring of the reaction showed a content of 24% of **18c** remaining in the reaction solution (Figure 33). The major product of the oxidation was the targeted **21a** (Figure 33, grey) with a content of almost 40%, whose constitution could be confirmed via multinuclear NMR spectroscopy.

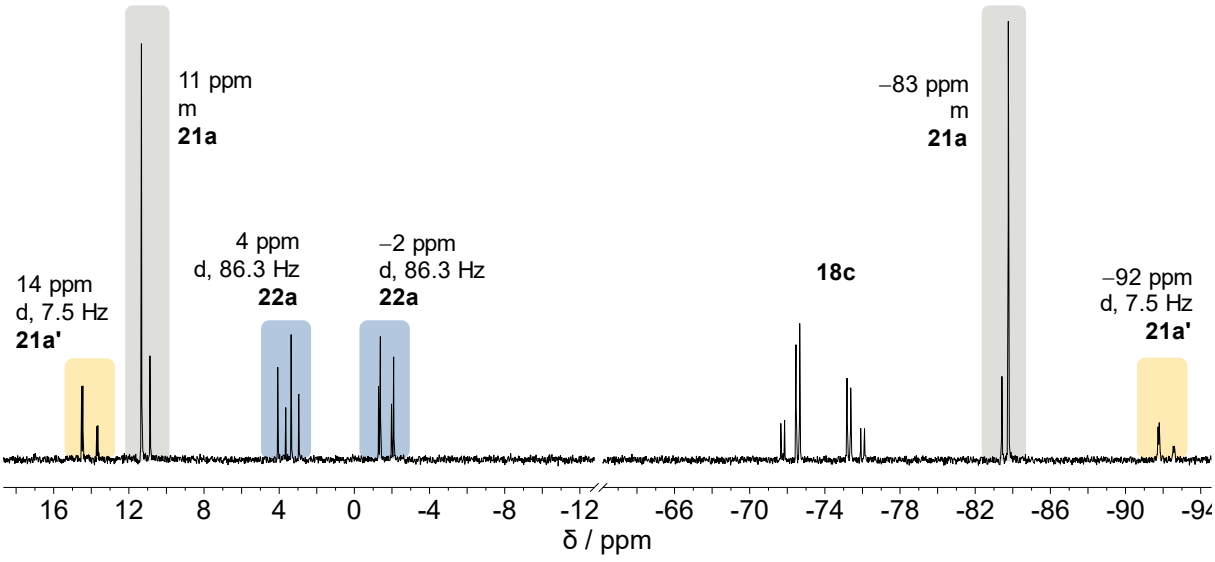


*Figure 33:* $^{31}P\{^{1}H\}$ NMR of reaction mixture containing differently oxidised 1,4-diphosphabarrelenes.

Yet, an assignment of the two formed diastereomers was not possible. The same holds true for the regioisomer **21a'**, which was formed in the reaction with a content of 14% (Figure 33, yellow). The significant difference in content between **21a** and **21a'** can be explained by the presence of the *n*-butyl group, sterically hindering the attack of hydrogen peroxide to the neighbouring phosphorus centre. While the formation of these two products was promising, a third compound was visible in the $^{31}P\{^{1}H\}$ NMR spectrum, *i.e.*, the doubly oxidised **22a** (Figure 33, blue). As expected, at 23% its content was very close to the one of **18c**, explaining the residual starting material. Although the presence of **21a,a'** and **22a** allow the proposal of a stepwise mechanism for the up to two-fold oxidation of 1,4-diphosphabarrelenes, the mixture also points towards a challenging synthesis of mono-oxidised species since these species did not form selectively before the second oxidation. Hence, the target of the study was shifted to 1,4-diphosphabarrelene dioxide structures like **22a**, accessible by the two-fold oxidation of **18c**. In order to simplify the $^{31}P\{^{1}H\}$ NMR data during following reactions, the symmetric **17c** was used in a reaction with an excess of hydrogen peroxide-urea, ensuring a complete oxidation of the two phosphorus centres (Scheme 26). As early studies had shown a more selective conversion under these conditions, molecular sieves (3 Å) were added to the reaction mixture to trap the formed water and prevent hydrolysis.

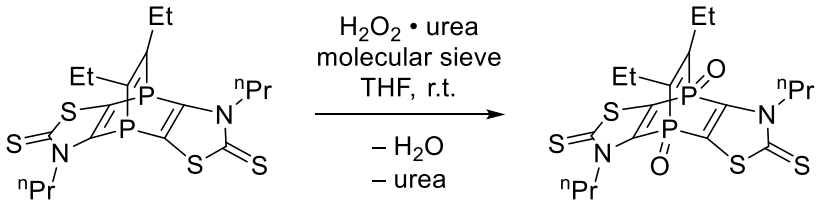


**17c** **22b**

*Scheme 26:* Reaction of **17c** with hydrogen peroxide-urea and molecular sieve to form **22b**.

$^{31}P\{^{1}H\}$ NMR spectroscopic monitoring of the mixture showed the slow but selective formation of a singlet at −12.3 ppm (Figure 34, top). A full conversion was achieved after 24 h and **22b** could be isolated and characterised. A structural characterisation using single crystal X-ray diffraction methods was not possible, but high-resolution mass spectrometry confirmed the composition of **22b** and eliminated the possibility of an additional oxidation at the thione moieties to sulfites or related structural motifs. Interestingly, although both phosphorus centres of **22b** are fully oxidised to P(V), **22b** displayed a remarkable sensitivity towards water. Upon addition of a drop of water to a sample of isolated **22b**, the formation of a set of two AB-spin systems was observed in the $^{31}P\{^{1}H\}$ NMR spectra (Figure 34, bottom). These resonances lay in close vicinity to the singlet of **22b** and showed P,P-coupling constants of more than 40 Hz.

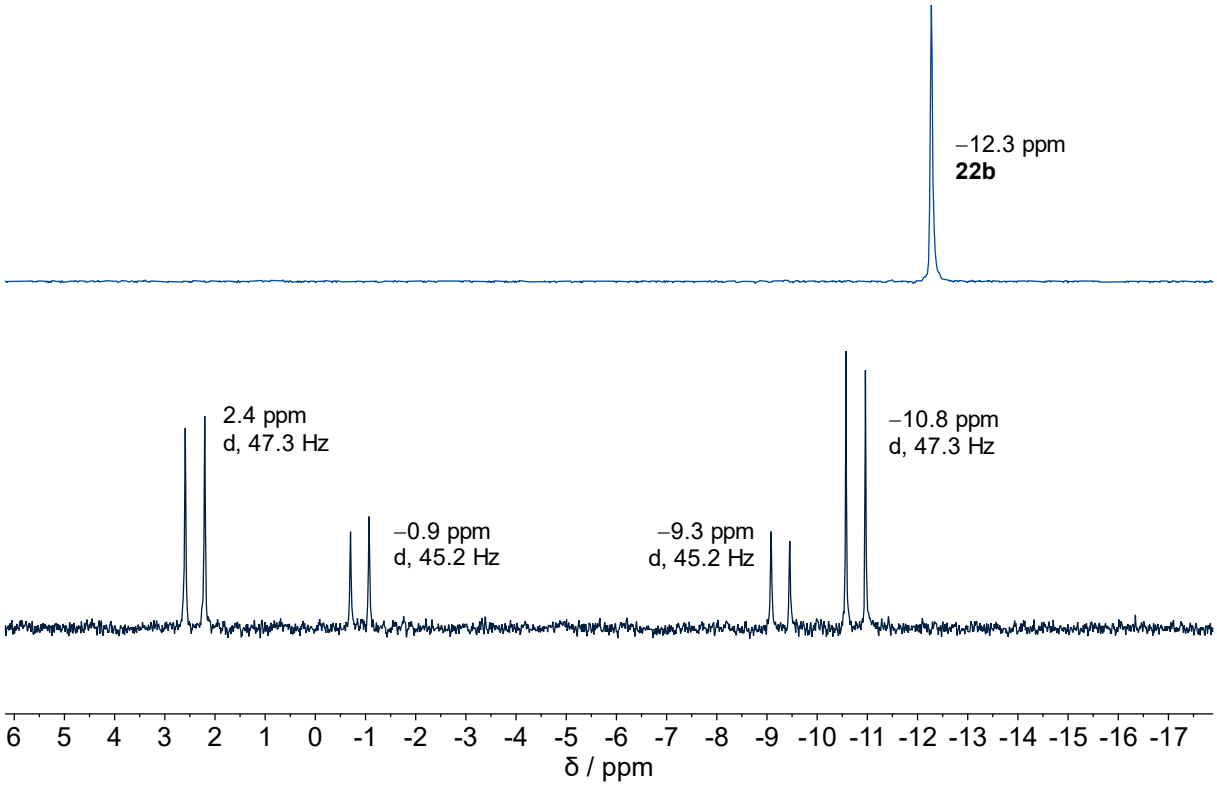


*Figure 34:* $^{31}P\{^{1}H\}$ NMR spectra of isolated **22b** (top) and reaction mixture of **22b** after hydrolysis (bottom).

While the more highfield-shifted resonances of these AB-spin systems remain close to the signal of **22b**, the more lowfield-shifted ones are located very close to 0 ppm. In the context of hydrolysis, cleaving one P-C bond and forming a phosphoric acid at one P centre can explain both the location of these lowfield-shifted doublets, as well as the asymmetric nature of the product itself. The presence of two AB-type spin systems can stem from the cleavage of different rings of **22b**, resulting in three different possible regioisomers of the hydrolysed product **23** (Figure 35). Yet, only two of the possible isomers seem to form in the reaction. Unfortunately, no $^{1}H$ NMR resonance for a thiazole-2-thione backbone proton in **23/23'** or the 3-hexene moiety in **23''** could be found. As a result, the structure of the hydrolysed product remains unknown, as all other $^{1}H$ and $^{13}C\{^{1}H\}$ data speak for an unaltered connectivity compared to **22b**.

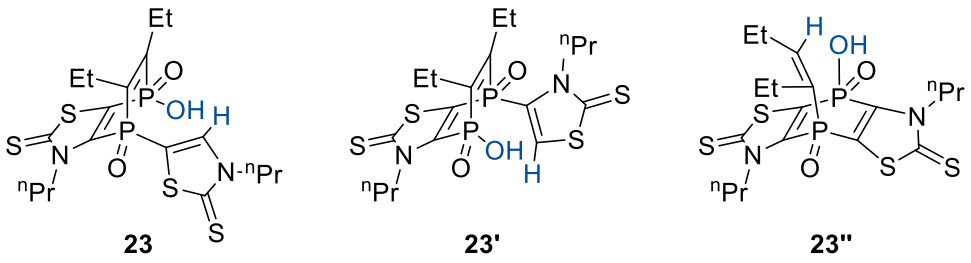


*Figure 35:* Possible asymmetric hydrolysis products of **22b** after cleavage of one ring system.

### 3.4.2 Targeting a P-sulfide structural motif

In addition to P-oxidations using hydrogen peroxide, investigations into the feasibility of the synthesis of 1,4-diphosphabarrelene disulfides were also conducted. These studies began by looking into the oxidation with an excess of elemental sulfur (Scheme 27).

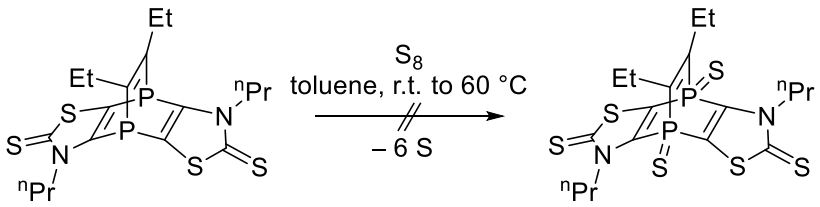


**17c** **24a**

*Scheme 27:* Targeted reaction of **18c** with elemental sulfur to form 1,4-diphosphabarrelene disulfide **24a**.

The reaction was initially carried out at ambient temperature, but no conversion was observed under these conditions. Therefore, the mixture was heated to 60 °C. Yet, this treatment led to an unselective reaction with multiple broad resonances around 30 ppm in the $^{31}P\{^{1}H\}$ NMR spectrum. While in the expected region for compound **24a**, no product could be isolated from this mixture. Hence, the reaction was repeated using a different sulfur atom source, *i.e.*, cyclohexene sulfide, which is known to cleave off its sulfur atom upon heating, forming cyclohexene in the process. The reaction was carried out with an excess of cyclohexene sulfide and while heating the mixture to 80 °C in toluene (Scheme 28).

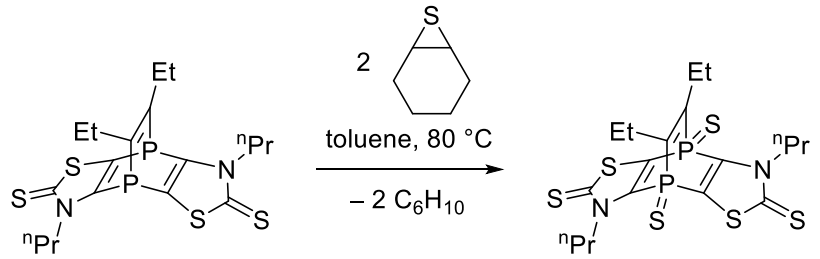


**17c** **24a**

*Scheme 28:* Reaction of **18c** with cyclohexene sulfide to form **24a**.

After initially, no reaction could be detected, stirring the reaction mixture at 80 °C for multiple weeks led to the slow consumption of **17c** and the formation of **24a**. After about 50 d, the conversion did not proceed any further. $^{31}P\{^{1}H\}$ NMR spectroscopic studies showed the full consumption of **17c**. However, the desired product **24a** was present in the spectrum with a content of only 83% as a singlet at −4.7 ppm, while a side product was visible as an AB-spin system at −94.4 and 6.6 ppm with a P,P-coupling constant of 5.72 Hz. This product was identified as the mono-oxidised compound, indicating an incomplete conversion to **24a**. Stirring the reaction mixture for even longer periods of time did not lead to a quantitative formation of

**24a** and the compound was characterised from the mixture. In this way, multinuclear NMR data as well as IR spectroscopic studies and (HR)MS data could be obtained for **24a**, confirming its formation in the reaction. P,C-coupling constants of **24a** were found to be increased compared to **17c**, appearing at about 35 Hz compared to ~12 Hz in **17c**.

With cyclohexene sulfide dissociating into elemental sulfur and cyclohexene under thermal conditions, the possible stepwise formation of 1,4-diphosphabarrelene disulfide **24b** was investigated (Scheme 29). While the P-oxidation had been found to be slow, taking almost two months to reach 83% completion in the case of **24a**, the formation of 1,4-diphosphabarrelene **18e** had been observed to proceed comparatively much faster, achieving full conversion to **18e** after only 24 h. Therefore, the reaction was expected to proceed first via the formation of **18e** which would then be singly and doubly oxidised to form **24b** with 1,4-diphosphabarrelene sulfide **25** as an intermediate in the P-oxidation reaction.

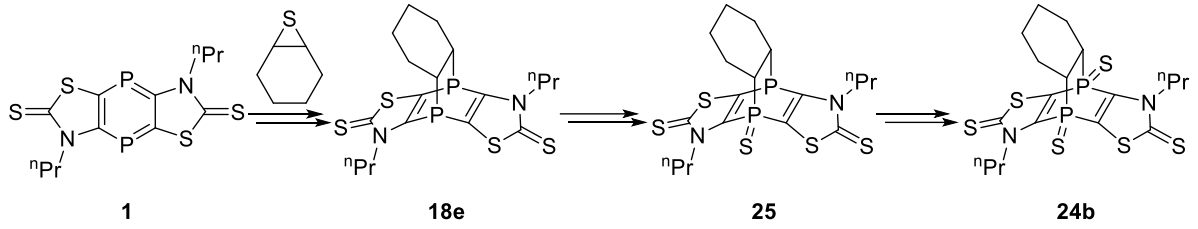


*Scheme 29:* Stepwise formation of **24b** from **1** via 1,4-diphosphabarrelene **18e** and 1,4-diphosphabarrelene sulfide **25**.

The reaction mixture was stirred at 80 °C for multiple days and $^{31}P\{^{1}H\}$ NMR spectroscopic experiments were carried out in regular intervals to check the progress of the reaction. Indeed, a $^{31}P\{^{1}H\}$ NMR spectrum recorded after 1 d of stirring at 80 °C revealed the formation of multiple products in the mixture (Figure 36, top). While a content of 15% of **1** was still visible in the spectrum, the main product of the reaction at this stage was found to be 1,4-diphosphabarrelene **18e** with a content of 34%. As expected, the [4+2]-cycloaddition reaction was found to proceed faster than the P-oxidation, leading to the initial formation of **18e**. Interestingly, $^{31}P\{^{1}H\}$ resonances for both the singly oxidised intermediate **25** as well as the 1,4-diphosphabarrelene disulfide **24b** could also be detected, the two regioisomers of **25** appearing at −83.8/15.4 ppm and −82.0/16.1 ppm with small P,P-coupling constants of 5.0 and 6.0 Hz. While this pair of intermediates has the second-most prominent resonances in the $^{31}P\{^{1}H\}$ NMR spectrum with contents of 24% and 16%, respectively, a small signal of **24b** at about 7 ppm with a content of 11% can also be detected already after 1 d. Although showing the same AB-type spin system as 1,4-diphosphabarrelene **18e**, the two doublets of **24b** lie very close to each other, resulting in a huge roof effect with a very low intensity of the outer resonances. The P,P-coupling constant of this AB-spin system is rather large at 81.2 Hz, yet, a large coupling constant between the two P(V) centres is to be expected.

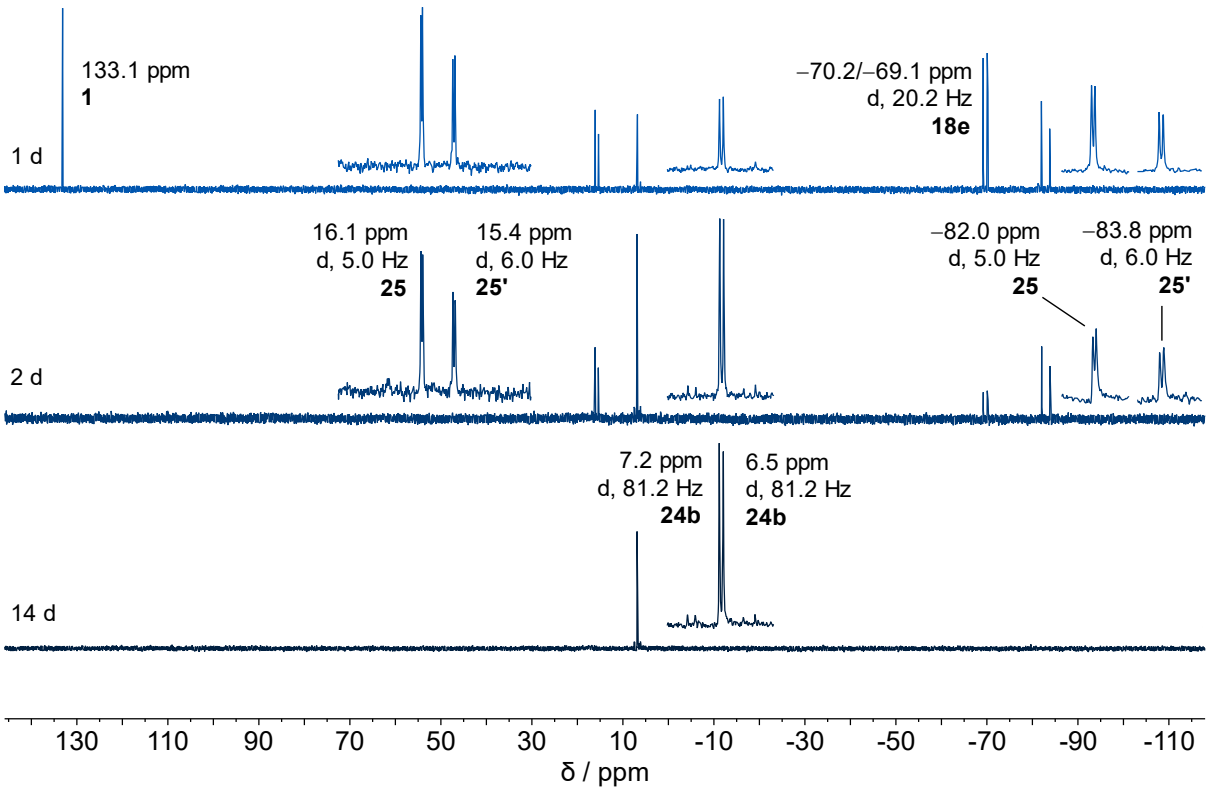


*Figure 36:* $^{31}P\{^{1}H\}$ NMR spectra of the reaction mixture of **24b** after 1 d (top), 2 d (centre) and 14 d (bottom).

When stirring the reaction mixture for another day, $^{31}P\{^{1}H\}$ NMR spectroscopic studies showed that no residual **1** was present in the mixture and the content of **18e** had decreased to only 10% (Figure 36, centre). Conversely, **25** remained almost unchanged at 29% and 23%, and the content of **24b** had risen to 38%. However, even though the initial conversion was fast, the reaction mixture needed to be stirred for 14 d before a quantitative formation of **24b** in the $^{31}P\{^{1}H\}$ NMR spectra had been achieved (Figure 36, bottom). Due to the presence of elemental sulfur, resulting from the thermal decomposition of excess cyclohexene sulfide, **24b** could not be isolated and, hence, only be characterised using multinuclear NMR studies, IR spectroscopy and (HR)MS. The latter showed a peak at 522.9809 compared to a theoretical value of 522.9812 for the protonated molecular ion peak ($[M+H]^{+\bullet}$), allowing an unambiguous confirmation of the composition of **24b**.

## 3.5 DESULFURISATION ATTEMPTS OF 1,4-DIPHOSPHABARRELENES

The presence of two thiones at the $C^2$-positions of the fused thiazole rings of 1,4-diphosphabarrelenes **17,18** has promising implications, as these moieties are known to be precursors for thiazole-based carbenes.[65,66,68,69] While some rigid bis-NHCs are known to literature, either connected via an all-carbon scaffold[53–58] or a P-containing backbone,[59,60] only two rigid, bent bis-NHCs have been reported to date.[64] For this reason, investigations were carried out by exploring the desulfurisation possibilities of **17,18**. The studies were focused on 1,4-diphosphabarrelenes containing an alkyl-substituted bridge, namely, 3-hexyne-based **17c** and 1-hexene-based **18c**, as these bridges are more innocent towards harsh reagents than ester substituted derivatives.

### 3.5.1 Reductive desulfurisations using metals

One established method for the desulfurisation of imidazole-2-thiones is the reaction with strongly reducing metals such as potassium under formation of the respective sulfide salt.[38,44,45] This reactivity was probed for **17c** and **18c** by using potassium metal (i), but also different reagents, *i.e.*, potassium graphite (ii), magnesium metal (iii) and a dispersion of sodium in sodium chloride (iv), in order to use the driving force of precipitating sulfide salts to enable the formation of the bis-NHCs **26a,b** (Scheme 30). All reactions were carried out at ambient temperature ((i)–(iii)) or by warming up from −90 °C (iv), and using a slight excess of the respective reagent.

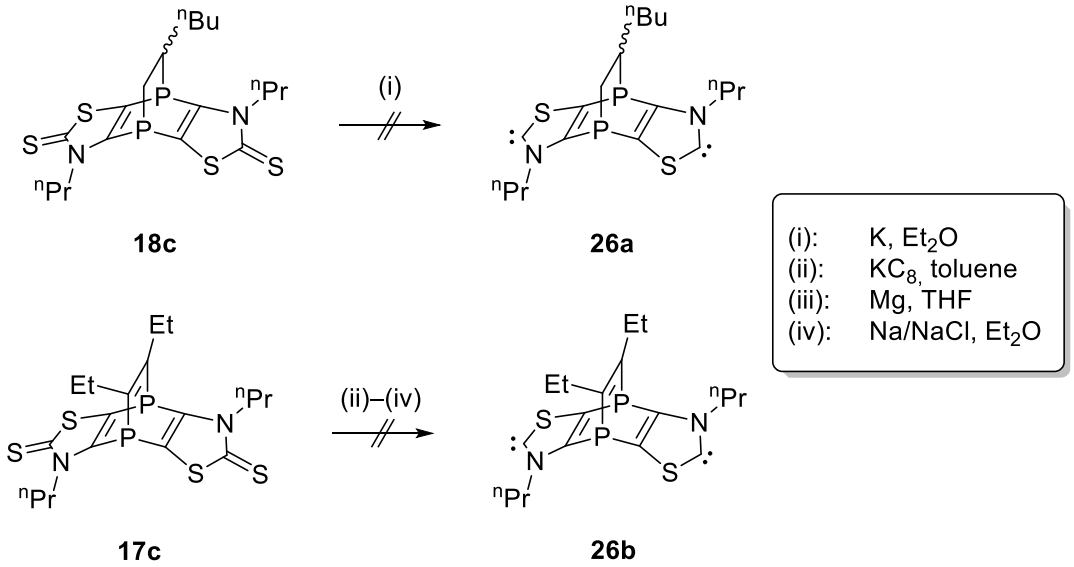


*Scheme 30:* Targeted desulfurisations of **17c,18c** to form **26a,b** using different metals.

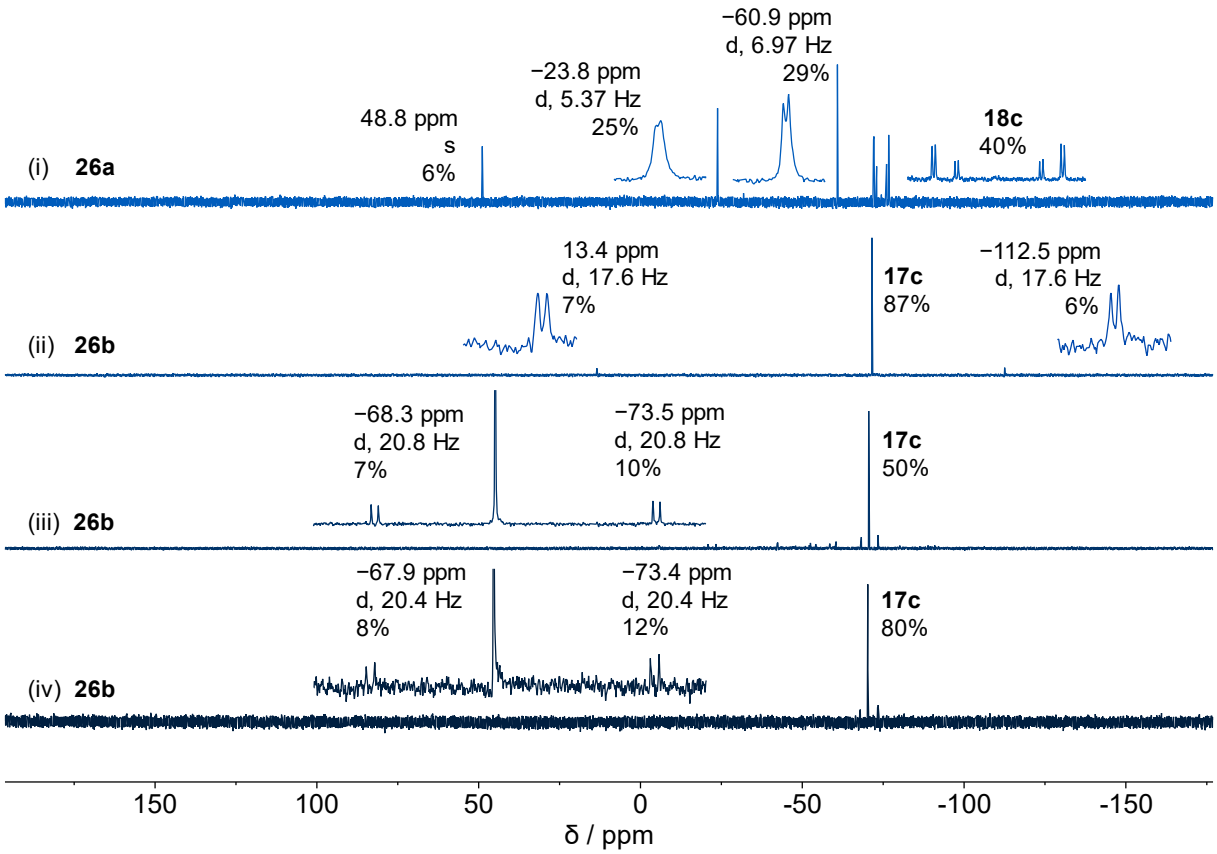


*Figure 37:* $^{31}P\{^{1}H\}$ NMR spectra of the reaction mixtures of **26a,b** using potassium (i), potassium graphite (ii), magnesium (iii) and sodium in sodium chloride (iv).

$^{31}P\{^{1}H\}$ NMR spectroscopic monitoring of the reactions was carried out in all cases, comparing the reactivities of the four reagents (Figure 37). The first striking observation is the significant presence of the respective starting material **17c** or **18c**, the contents being upwards of 40% in all reactions. Additionally, AB-type spin systems are visible in every $^{31}P\{^{1}H\}$ NMR spectrum, however, their nature is different for different reactions. While potassium metal (i) led to the formation of a broad AB-spin system at −60.9 and −23.8 ppm, having a small P,P-coupling of around 6 Hz, the use of potassium graphite (ii) led to a very different AB-spin system at −112.5 and 13.4 ppm with a larger P,P-coupling constant (17.6 Hz). Interestingly, for both magnesium metal (iii) and sodium in sodium chloride (iv), the same AB-spin system (−73.5/−68 ppm, 20.5 Hz) is formed, being very close to the starting material **17c**. However, with the exception of (i) with a content of more than 50% by integration, all AB-spin systems appear in the $^{31}P\{^{1}H\}$ NMR spectra in small contents of 20% or less and the respective starting material remains by far the most prominent species. The formation of asymmetric products points towards an incomplete reaction, possibly forming carbene complexes such as **27b** for the example of magnesium (Scheme 31). As this one-fold desulfurisation does not take place in close vicinity of the phosphorus atoms, a very small change in $^{31}P$ chemical shift is expected, making the AB-spin systems in (iii) and (iv) promising candidates for **27b**.

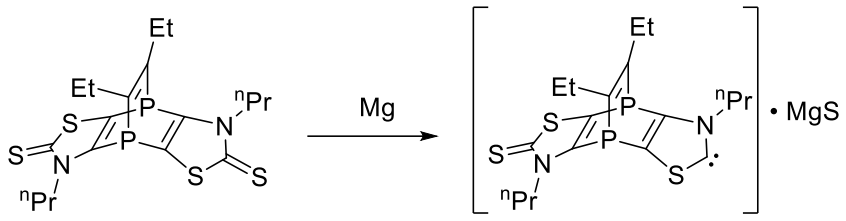


**17c** **27b**

*Scheme 31:* Possible carbene complex formation after singly desulfurising 1,4-diphosphabarrelene **17c** with magnesium metal.

In the other two reactions, using potassium as a reductant, the formed AB-spin systems display a stark difference in $^{31}P$ chemical shifts compared to the respective starting material, indicating a reaction at the phosphorus centres instead of the thione moieties. This theory is corroborated by the absence of two diastereomers when reacting **18c** with potassium metal in (i), since a reaction on (at least) one phosphorus centre cleaving off the labile 1,4-diphosphabarrelene bridge leads to the loss of one stereogenic centre. This fits very well to the observation of a product displaying only one AB-spin system in the $^{31}P\{^{1}H\}$ NMR spectrum in contrast to the two of **18c** (Figure 37, top). A similar situation is present in (ii), where a difference of more than 120 ppm was found between the two centres of the formed AB-spin system, being a certain indication of a reaction at phosphorus instead of sulfur. Hence, the literature-known usage of potassium for the reductive desulfurisation of thiones seems to be impossible when using 1,4-diphosphabarrelenes **17,18** as this strong reductant showed a tendency to react with the fused ring system itself as opposed to the thione moieties. Conversely, milder reducing agents such as magnesium or sodium gave promising results. However, in all studied reactions, no full conversion was achieved even after days and thus, the theory of an incomplete desulfurisation could not be verified by the isolation of **26b** or **27b** as large quantities of starting material remained in the reaction mixture in all four cases.

### 3.5.2 Reductive desulfurisations using phosphanes

In the report on the synthesis of dithiole-2-thione based 1,4-diphosphinine **LVIII**, a dimerisation mechanism was proposed which competes the formation of **LVIII**, initialised by the desulfurisation of one thione by tri-*n*-butylphosphane in dichloromethane at ambient termperature.[101] Due to the very close similarity between **LVIII** and **1**, the use of phosphanes for the desulfurisation of thiazole-2-thiones was investigated in detail. As aminophosphanes and phosphites are known to be stronger desulfurisation agents than alkylphosphanes,[131] in addition to tri-*n*-butylphosphane, tris(diethylamino)phosphane and tri-*n*-butylphosphite were added to **18c** in a ten-fold excess (i)–(iii) and the reaction progress was monitored at different temperatures from ambient to 60 °C (Scheme 32). **18c** was also added to neat tri-*n*-butylphosphite and heated to reflux conditions (iv).

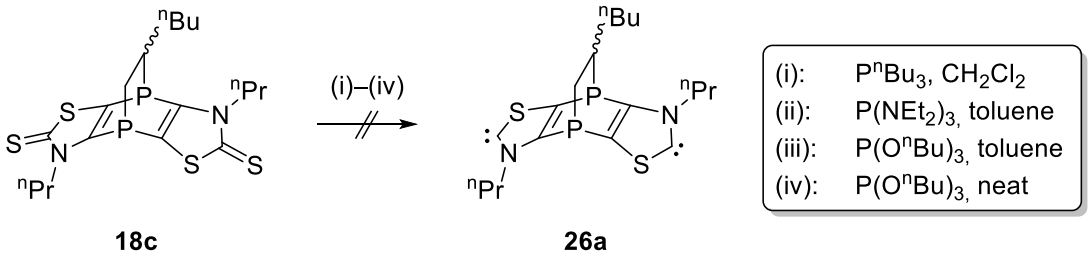


**18c** **26a**

*Scheme 32:* Targeted desulfurisations of **18c** to form **26a** using different phosphanes.

$^{31}P\{^{1}H\}$ NMR spectroscopic monitoring of the reaction mixtures was done after different stirring times (Figure 38, reagent signals are vertically clipped to increase visibility). As for the previously discussed reductions with metals, much of **18c** remains in the reaction mixtures, even after stirring at 60 °C for several days ((i), (ii)) or up to a month (iii). Small quantities of products can be seen in the $^{31}P\{^{1}H\}$ NMR spectra, but these amount to a total content from 9% in the case of (i) to 34% in (iii) and the signals in question lie far from the starting material **18c**, *i.e.*, the region of the spectrum that is expected for **26a**. Moreover, desulfurisations by phosphanes result in the formation of the corresponding phosphane sulfides, all of which are well-known. These side products have $^{31}P$ chemical shifts of about 49 ppm for tri-*n*-butylphosphane sulfide (i),[132,133] 82 ppm for tris(diethylamino)phosphane sulfide (ii)[132] and 66 ppm for tri-*n*-butoxyphosphane sulfide (iii).[134]

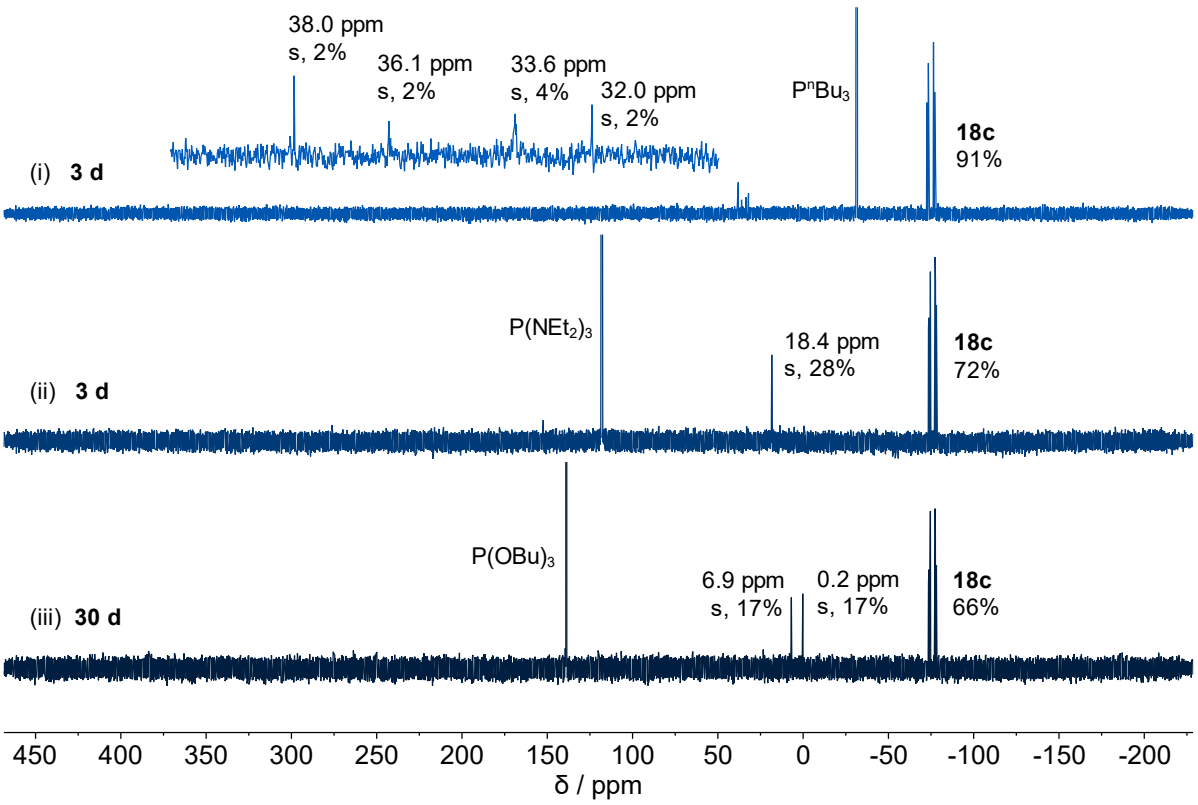


*Figure 38:* $^{31}P\{^{1}H\}$ NMR spectra of the reaction mixtures of **26a** using tri-*n*-butylphosphane (i), tris(diethylamino)-phosphane (ii) and tri-*n*-butylphosphite (iii). Reagent signals are vertically clipped.

However, the $^{31}P\{^{1}H\}$ NMR spectra do not show resonances for any of the respective, known phosphane sulfides, indicating that no significant desulfurisation reaction has taken place. Instead, the long reaction times at elevated temperature can lead to side reactions, explaining the small content of conversion products in all spectra.

In order to check whether a very high reaction barrier was needed to overcome to initiate the desulfurisation of **18c**, it was subjected to a reaction in neat tri-*n*-butylphosphite and heated to 150 °C. But, instead of the targeted reactivity at the thione moieties, the solution turned red, indicating the thermally induced [4+2]-cycloreversion of the 1,4-diphosphabarrelene had taken place, forming **1**. This finding could be confirmed via $^{31}P\{^{1}H\}$ NMR spectroscopy, eliminating the possibility of heating reaction mixtures to very high temperatures. In order to overcome this problem, a thermally more stable 1,4-diphosphabarrelene was chosen, and **17c** was used for the following desulfurisation attempts. While the reaction with neat tri-*n*-butylphosphite was repeated, reactions with the sterically much less demanding trimethylphosphane were also performed to prevent any kinetic hindrance due to repulsion of the *n*-propyl groups of **17c** (Scheme 33).

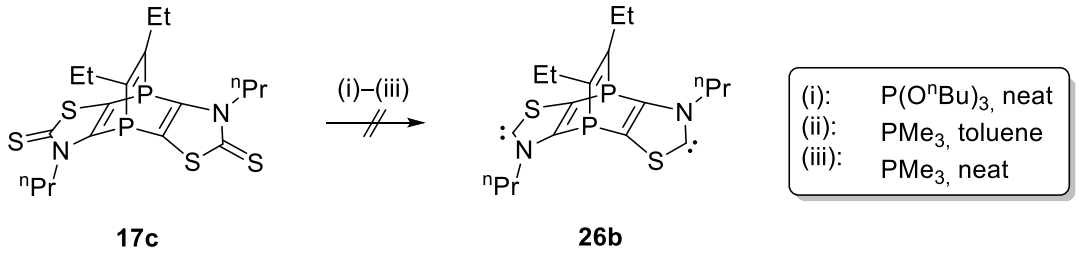


**17c** **26b**

*Scheme 33:* Targeted desulfurisations of **17c** to form **26b** using tri-*n*-butylphosphite or trimethylphosphane.

**17c** was stirred at 60 °C in neat tri-*n*-butylphosphite for 30 d. However, periodical $^{31}P\{^{1}H\}$ NMR spectroscopic monitoring of the reaction mixture showed that no reaction was taking place, and no signal for tri-*n*-butoxyphosphane sulfide could be detected. Thus, the focus was put on the reactions of **17c** with trimethylphosphane. As the boiling point of trimethylphosphane is very low at 38 °C,[135] both reactions were carried out in sealed high-pressure vessels and heated to 80 °C. After two weeks, $^{31}P\{^{1}H\}$ NMR experiments revealed very similar spectra for the two reaction mixtures (Figure 39, reagent signals are vertically clipped). Like for all previously discussed reactions with phosphanes, the main signal in the $^{31}P\{^{1}H\}$ NMR spectra (apart from trimethylphosphane) remained the starting material **17c**. Three products had formed close to 0 ppm, the main compound appearing at about 27 ppm with a content of 25% (top) and 2% (bottom), respectively. Yet again, a signal at 59.1 ppm, corresponding to trimethylphosphane sulfide,[133] was absent in both spectra, showing that no desulfurisation was taking place in either of the reaction mixtures. In the case of neat trimethylphosphane, the reaction was continued for another two weeks without a significant change in the $^{31}P\{^{1}H\}$ NMR spectrum, indicating that a desulfurisation of **17c** with trimethylphosphane was not feasible.

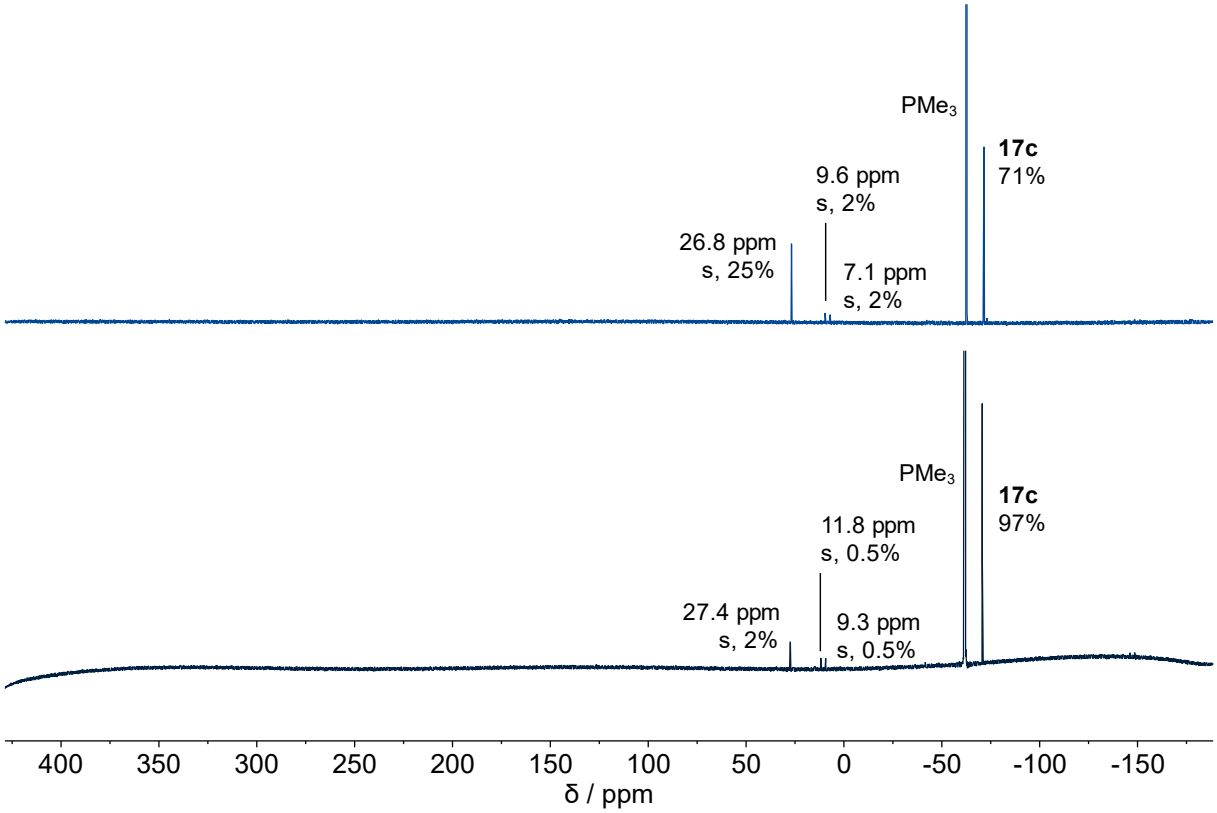


*Figure 39:* $^{31}P\{^{1}H\}$ NMR spectra of the reaction mixtures of **26a** using trimethylphosphane in toluene (top) and neat (bottom). Reagent signals are vertically clipped.

### 3.5.3 Reductive desulfurisations using low-valent molecular species

As phosphanes seemed to a desulfurisation potential too weak to furnish bis-NHCs **26a,b**, investigations into the use of low-valent species such as carbenes were carried out. Since desulfurisations using NHCs, affording the respective imidazole-2-thiones, have been reported,[136] first studies were done by adding 1,3-dimethylimidazole-2-ylidene ($IMe_2$) or TMS-diazomethane to 3-hexyne-based **17c** (Scheme 34). The reactions were started at −70 °C and ambient temperature, respectively, and the latter was heated to 70 °C to liberate dinitrogen.

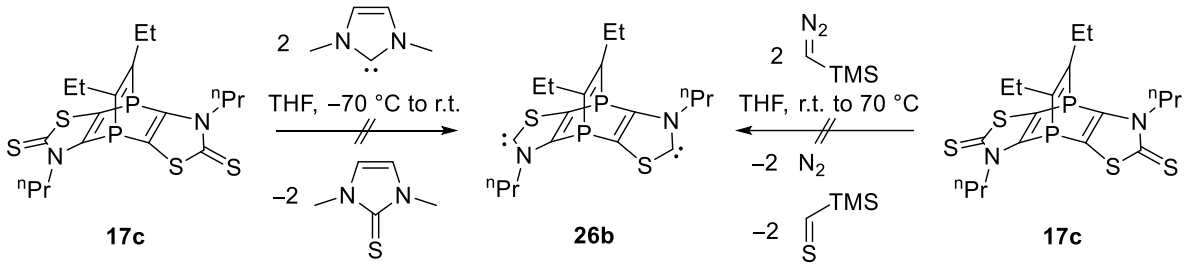


*Scheme 34:* Targeted desulfurisations of **17c** to form **26b** using different carbenes.

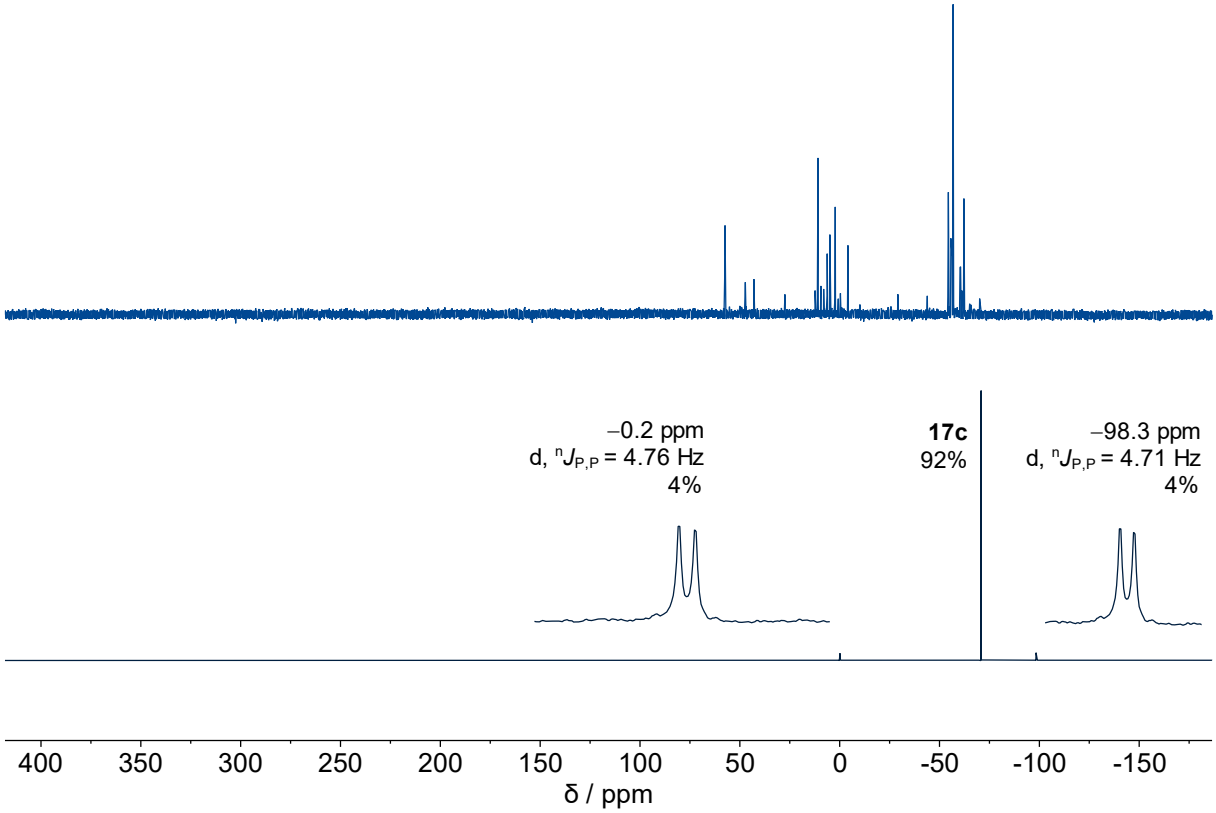


*Figure 40:* $^{31}P\{^{1}H\}$ NMR spectra of desulfurisation reactions of **17c** with $IMe_2$ (top) and TMS-diazomethane (bottom).

The addition of $IMe_2$ to **17c** led to an immediate colour change from yellow to orange. After slowly warming up the reaction mixture to ambient temperature, $^{31}P\{^{1}H\}$ NMR spectroscopic measurements were carried out, showing that **17c** had been almost fully consumed (Figure 40, top). However, the spectrum also revealed a very unselective reaction as more than 20 resonances were visible, most of which displayed P,P-couplings. With very few of the signals in a region of the spectrum which would fit to the expected product **26b**, the NHC $IMe_2$ seemed to primarily react at the phosphorus atoms, leading to the observed asymmetric products. This outcome did not promise a feasible desulfurisation of **17c**, so a reaction with TMS-diazomethane was investigated more closely. While initially, no reaction was observed, heating to 70 °C for 1 d led to the partial (content of 8%) formation of an AB-spin system in the $^{31}P\{^{1}H\}$ NMR spectrum, having a small P,P-coupling constant of only about 4.7 Hz. (Figure 40, bottom). The asymmetric nature of this product can suggest the desulfurisation of only one thione giving a compound like **27b** (compare Scheme 31). This would however contradict the previously proposed assignment of **27b** to an AB-spin system at −73.5 and −68.1 ppm, with $^{n}J_{P,P}$ = 20.5 Hz, being much more in line with $^{3}J_{P,P}$-couplings in asymmetric 1,4-diphosphabarrelenes (compare Table 3). Additionally, $^{13}C\{^{1}H\}$ experiments only showed the thione-carbon atoms of **17c**, rendering the possibility of the formation of **27b** even more

doubtful. Consequently, the nature of the formed product in the reaction with TMS-diazomethane remains elusive, as it was not possible to further characterise this product.

Apart from the formation of 7-aluma-1,4-diphosphanorbornadienes, the low-valent aluminine NacNacAl is able to desulfurise cyclic urea derivatives by forming aluminium sulfide-NHC complexes.[46] This reactivity was probed in the context of desulfurisations of **17c** in a reaction with two equivalents of NacNacAl (Scheme 35). The reaction was initially carried out at ambient temperature before heating the mixture to 70 °C.

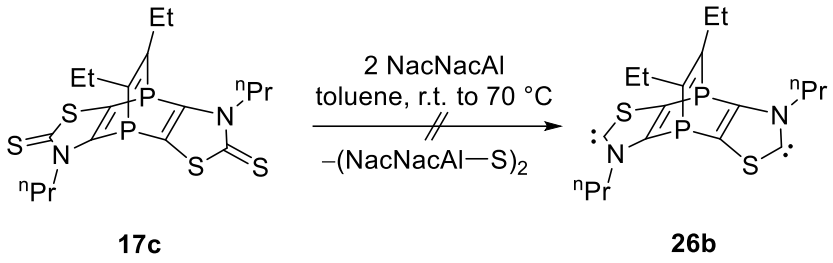


**17c** **26b**

*Scheme 35:* Targeted desulfurisation of **18c** to form **26b** using NacNacAl.

Monitoring the reaction mixture using $^{31}P\{^{1}H\}$ NMR spectroscopy suggested that no reaction had taken place even after 7 d as the signal of **17c** did not change and no other resonances could be detected in the $^{31}P\{^{1}H\}$ NMR spectra. Conversely, looking into $^{1}H$ NMR spectra revealed a different picture (Figure 41).

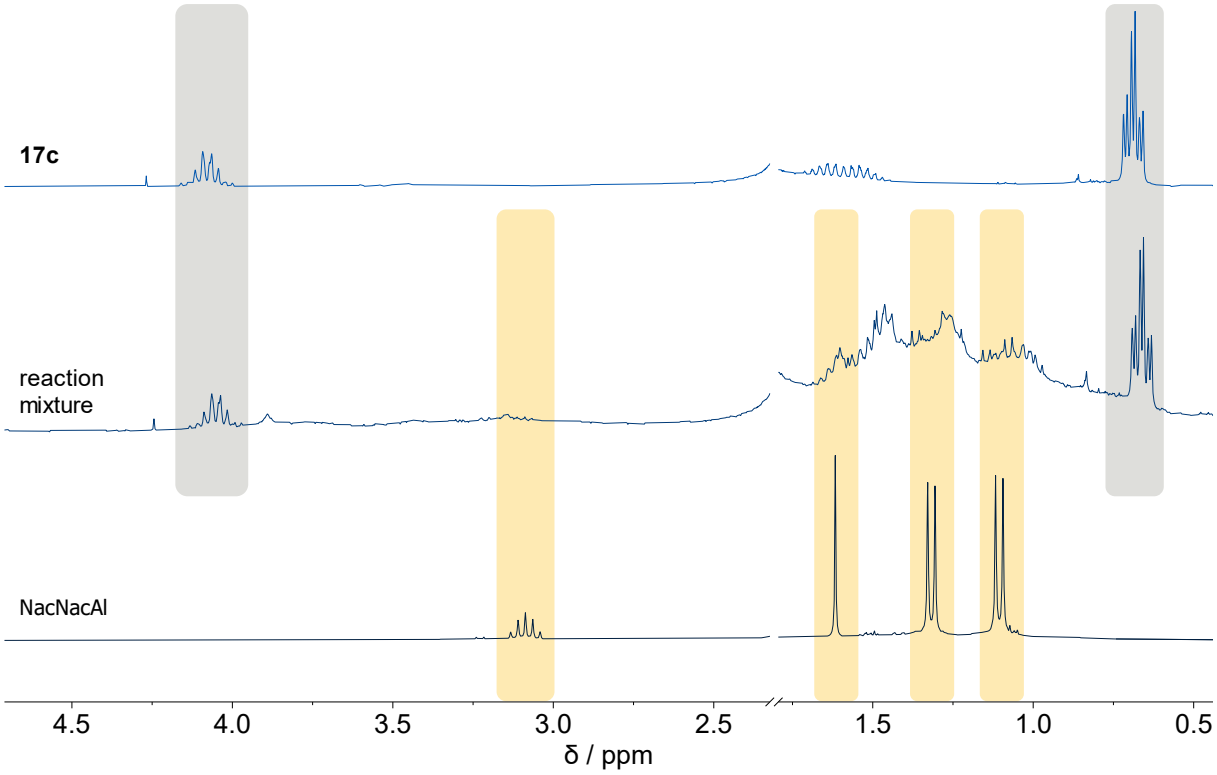


*Figure 41:* Excerpts of $^{1}H$ NMR spectra of **17c** (top), NacNacAl (bottom) and the reaction mixture of **17c** and NacNacAl (centre).

In the mixture, the $^{1}$H NMR signals of the alkyl groups in **17c** remained virtually unchanged (Figure 41, grey), while the sharp signals of the alkyl groups in NacNacAl had vanished, giving way for broad, complex multiplets in the same general region of the spectrum (Figure 41, yellow). Despite this being a definitive proof that NacNacAl had indeed reacted and largely been consumed, the desired product **26b** could not be detected since, again, $^{13}$C{$^{1}$H} NMR spectra did not show any signal expected for carbenes but only those present for the thiones of **17c**. Hence, while **26b** can be ruled out, the product of this reaction continues to be unknown as further conclusive evidence for its composition could be not obtained.

### 3.5.4 Theoretical study comparing desulfurisation potentials

After obtaining partially ambiguous results in the previously discussed desulfurisation attempts, a theoretical study was carried out comparing different desulfurisation potentials in a way analogous to a desulfurisation study by Espinosa Ferao and Streubel, published in 2020.[131] While sulfur-atom transfer potentials in the literature are usually computed relative to the $S_8/S_7$ couple, the couple of 3-hexyne-based **17c$^{Me}$/26b$^{Me}$** was chosen for reference in this study as **26b** is the experimental goal in direct desulfurisation reactions (Scheme 36). This couple was compared to other couples which were already discussed in the literature, such as CS/$CS_2$, an alkyl- and aminophosphane as well as a phosphite, and the $S_8/S_7$ couple itself (Figure 42). Moreover, the study was tailored to the employed systems by adding the desulfurisation potentials of the thiazole-2-ylidene-based 1,4-diphosphinine **28$^{Me}$** (Scheme 37), NacNacAl, the methyl-substituted imidazole-2-ylidene ($IMe_2$), thiazole-2-ylidene and dithiole-2-ylidene, as well as TMS-ylidene. With the reference of **17c$^{Me}$/26b$^{Me}$**, couples having a negative potential are thermodynamically able to desulfurise **17c$^{Me}$**, while a positive potential makes this thermodynamically infeasible.

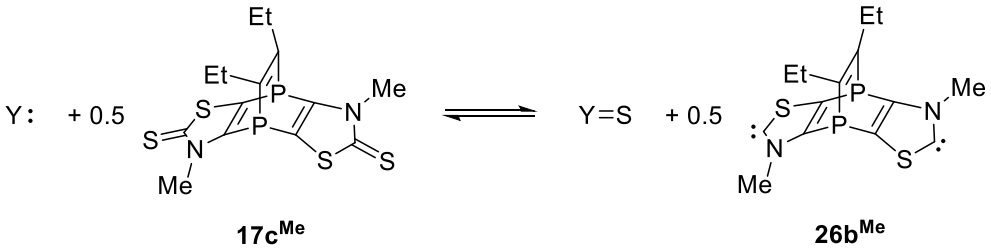


*Scheme 36:* Conceptual desulfurisation of **17c$^{Me}$** by reagent Y forming bis-carbene **26b$^{Me}$** and Y=S.

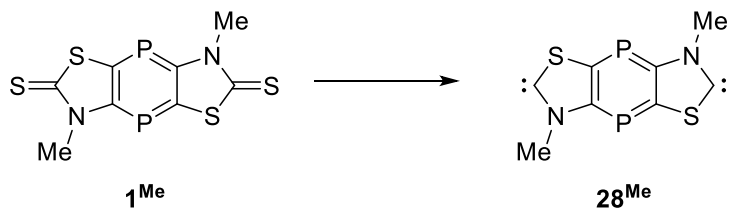


*Scheme 37:* Conceptual desulfurisation of **1$^{Me}$** to form diphosphinine-bis-carbene **28$^{Me}$**.

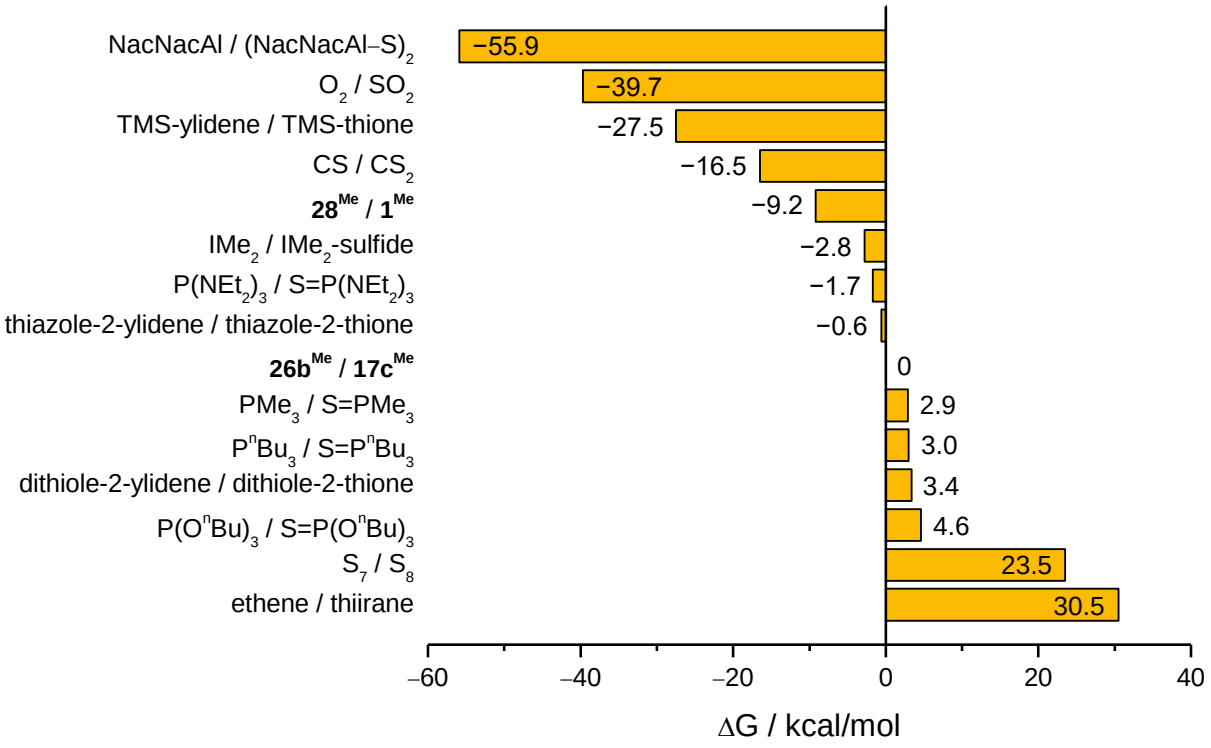


*Figure 42:* Relative thermodynamic desulfurisation potentials relative to the desulfurisation of **17c$^{Me}$**.

Compared to the literature-used reference couple of $S_8/S_7$, **17c$^{Me}$/26b$^{Me}$** has a desulfurisation potential which of −23.5 kcal/mol, indicating a stronger S-atom acceptor character for **26b$^{Me}$**. This effect is even stronger for the hypothetical 1,4-diphosphinine-based **28$^{Me}$** at −9.2 kcal/mol relative to **17c$^{Me}$/26b$^{Me}$**. Gauging the desulfurisation potentials of experimentally used reagents, both tri-*n*-butylphosphite and the two alkylphosphanes trimethylphosphane and tri-*n*-butylphosphane are weaker S-acceptors than **26b$^{Me}$**, explaining the absence of phosphane sulfides during the desulfurisation attempts. On the other hand, the desulfurisation potential of tris(diethylamino)phosphane at −1.7 kcal/mol should make the formation of **26b** possible. However, due to the very small difference in potentials, other factors influencing the reaction, such as kinetics, can easily prevent the desulfurisation of **17c**. The picture is very similar for the different heterocyclic carbenes, *i.e.* $IMe_2$, *N*-methylthiazole-2-ylidene and dithiol-2-ylidene. As expected, the potential of the thiazole-2-ylidene is very close to that of the thiazole-based couple of **17c$^{Me}$/26b$^{Me}$**. $IMe_2$/$IMe_2$-sulfide lies at −2.8 kcal/mol, having a very similar situation to that of tris(diethylamino)phosphane, and dithiole-2-ylidene has a desulfurisation potential that is weaker than the one of **26b$^{Me}$**, albeit also displaying only a small difference. The only two experimentally applied reagents having a significantly more negative desulfurisation potential than **17c$^{Me}$/26b$^{Me}$** are TMS-ylidene and NacNacAl. With values of −27.5 and −55.9 kcal/mol, respectively, they should be able to desulfurise **17c$^{Me}$** from a thermodynamic point of view, yet, a definitive statement about the general feasibility of this desulfurisation remains challenging as no mechanistic factors were taken into consideration in this study.

## 3.6 DESULFURISATION ATTEMPTS OF DOUBLY METHYLATED 1,4-DIPHOSPHABARRELENE SALTS

Apart from a “direct” desulfurisation, imidazole- and thiazole-ylidenes can be achieved from thiones or selones via a stepwise desulfurisation by first synthesising the imidazolium or thiazolium salts which can then be deprotonated affording the respective carbene.[65,68,70–73] This method has been used by Streubel and co-workers for the synthesis of rigid bis-NHCs from tricyclic, imidazole-2-thione based 1,4-dihydro-1,4-diphosphinines.[59,60,64] In this pathway, imidazole-2-selones **LXV** were first methylated using methyl trifluoromethane sulfonate (in the following: methyl triflate, MeOTf) and the furnished doubly methylated salts **LXVI** were deselenised in a reaction with sodium borohydrate, affording bis-imidazolium salts **LXVII** (Scheme 38). These were then deprotonated using KHMDS to achieve the synthesis of P-bridged bis-NHCs **LXVIII**. As the direct desulfurisation of 1,4-diphosphabarrelenes **17c,18c** did not furnish the desired bis-NHCs **26a,b** this pathway was chosen for a further and more detailed exploration.

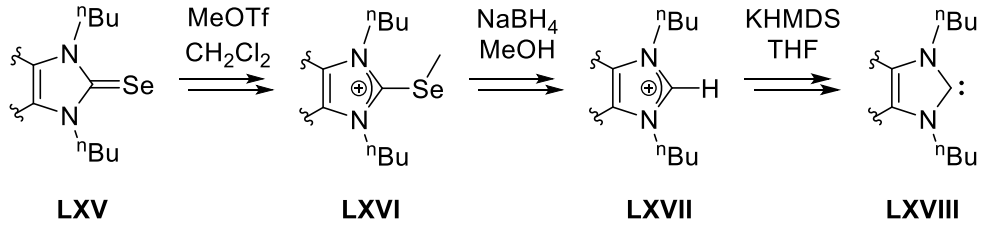


*Scheme 38:* General synthetic route to imidazole-2-ylidenes **LXVIII** from imidazole-2-selones **LXV**

### 3.6.1 S-Methylation reactions of 1,4-diphosphabarrelenes

In order to access this reductive desulfurisation reactivity, doubly methylated salts of 1,4-diphosphabarrelenes containing an unsaturated (**17b,c**) as well as a saturated (**18a,c**) bridge were synthesised using an excess of methyl triflate affording doubly methylated salts **39a–d** (Scheme 39). For both bridge types, an ester-substituted and an alkyl-substituted derivative were chosen to assess the effects of both the substituent and the nature of the bridge.

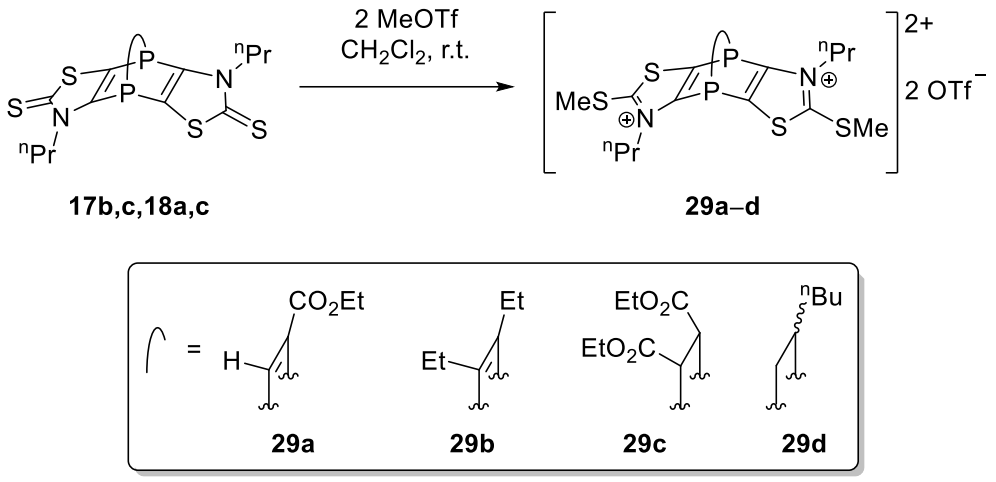


*Scheme 39:* Methylation reactions of 1,4-diphosphabarrelenes **17b,c** and **18a,c** to form doubly methylated salts **29a–d**.

All reactions were carried out using an excess of 0.1–1.5 eq. of methyl triflate at ambient temperature and a fast reaction was observed in all four cases. $^{31}P\{^{1}H\}$ NMR spectra showed the selective formation of a single product each. The resonances of these products lay very close to the ones of the respective starting materials (Table 6). Additionally, these signals revealed the same multiplicity and very similar P,P-coupling constants as the 1,4-diphosphabarrelenes. These striking similarities are in line with the expected S-methylation reactivity and the thione moieties not influencing the chemical and magnetic properties of the phosphorus atoms a lot as the chemical surroundings of the latter remain virtually unchanged in **29a–d** compared to **17b,c** and **18a,c**. All four products **29a–d** could be isolated in good yields and were fully characterised. Interestingly, although $^{31}P\{^{1}H\}$ chemical shifts had changed only little after the S-methylations, a distinct trend was observed: the chemical shifts of **29a,b** were highfield-shifted by about 2 ppm respective to **17b,c**, while **29c,d** displayed resonances which were generally slightly lowfield-shifted compared to **18a,c**.

*Table 6:* $^{31}P\{^{1}H\}$ NMR data of **17b,c** and **18a,c** as well as doubly methylated salts **29a–d** (if not specified the spectra were measured in $CDCl_3$).

| 2π-system | 1,4-diphosphabarrelene | | doubly methylated salt | |
|---|---|---|---|---|
| | $\delta(^{31}P\{^{1}H\})$ / ppm | $^{3}J_{P,P}$ / Hz | $\delta(^{31}P\{^{1}H\})$ / ppm | $^{3}J_{P,P}$ / Hz |
| ethyl propiolate | −87.1/−84.0 | 26.0 | −89.3/−84.6 | 25.4 |
| 3-hexyne | −71.2 | — | −73.9 | — |
| diethyl maleate | −75.8/−73.3 | 28.8 | −75.4/−75.2 | 28.2 |
| 1-hexene | −77.0/−73.6 | 24.2 | −74.3/−71.8[a] | 22.8[a] |
| | −77.7/−72.6 | 24.8 | −74.6/−71.4[a] | 23.1[a] |

[a]spectrum was measured in $CD_2Cl_2$

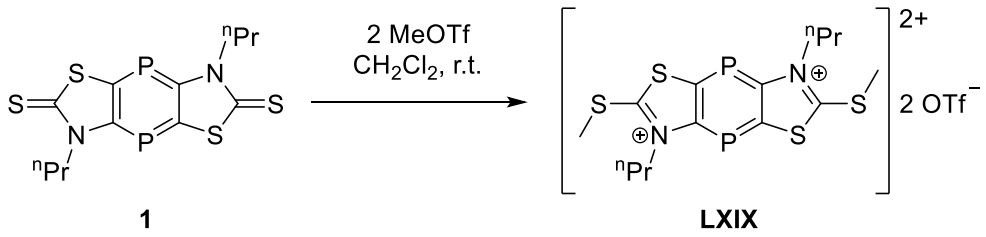


**1** **LXIX**

*Scheme 40:* Methylation of **1** to form doubly methylated 1,4-diphosphinine salt **LXIX**.

Although very similar (if present), the $^{3}J_{P,P}$-couplings of all derivatives had slightly smaller coupling constants than the ones of the respective starting materials, however, they remain in the region of 20–30 Hz. The difference in the $^{31}P\{^{1}H\}$ NMR data of **29a–d** to **17b,c** and **18a,c** is very small compared to the previously reported doubly methylated salt **LXIX** of 1,4-diphosphinine **1** (Scheme 40), in which case a Δ(δ(31P{1H})) of 30 ppm was observed.[110] However, as the conjugated π-system of **1** is retained upon methylation, its effect—and, thus, the creation of a dicationic molecule—has a much bigger impact on the chemical shift than in case of **29a–d**, which can be better described as classical bis-phosphanes. A similar, albeit inverse, effect was noticed after $^{1}H$ and $^{13}C\{^{1}H\}$ NMR spectroscopic investigations revealed a much larger change in chemical shift of the thione carbons for **29a–d** (ca. 11 ppm) compared to **LXIX** (3.3 ppm), as well as 2.8 ppm more highfield-shifted resonances for the S-methyl groups. This inverse trend can also be explained by the delocalised aromatic system of the 1,4-diphosphinine as its absence in **29a–d** leads to an increased π-donating effect of the nitrogen atoms and, to some extent, the endocyclic sulfur atoms, thus shielding the former thione-carbon and S-methyl groups of **29a–d** more than the ones of **LXIX**.

### 3.6.2 Reductive desulfurisations of doubly methylated salts

#### *3.6.2.1 Boron-based reductants*

After their synthesis, the doubly methylated 1,4-diphosphabarrelene salts **29a–d** were the subject of desulfurisation studies in order to furnish bis-thiazolium salts like **30** (Scheme 41). In order to have the highest tolerance of the 1,4-diposphabarrelene bridge towards harsh reaction conditions, **29b** was chosen as the focus for these studies, as its bridge was found to be the most inert out of the synthesised derivatives, both chemically and thermally. First, the literature-known reaction pathway using sodium borohydride in methanol was chosen (Scheme 41).[59,60] An excess of 5–10 eq. of sodium borohydride was added as a solid to **29b** in methanol at −40 °C, since sodium borohydride is known to react with methanol itself under formation of sodium methoxide and dihydrogen.

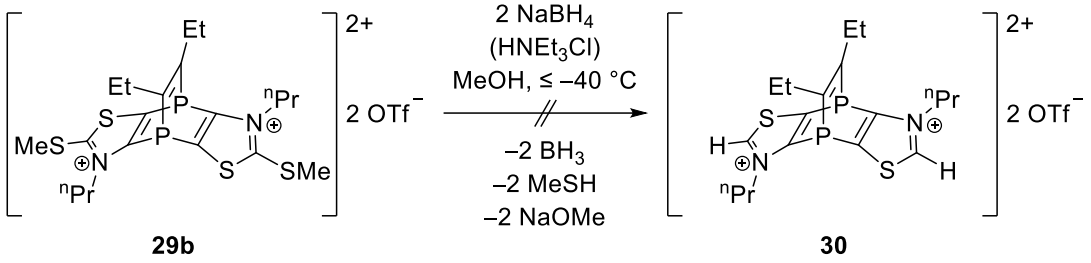


*Scheme 41:* Targeted reductive desulfurisation of **29b** using sodium borohydride (and triethylammonium chloride).

$^{31}P\{^{1}H\}$ NMR spectroscopic monitoring of the reaction mixture revealed the formation of several products (Figure 43, top). While the main signal was a singlet at −43.6 ppm with a content of 46% in the spectrum, two prominent AB-type spin systems were visible. One of these AB-spin systems (with a content of 24%) lay close to the main signal at −48.6 and −36.8 ppm, with a coupling constant of 30.8 Hz. The second AB-spin system (with a content of 14%) was comparatively far lowfield-shifted, appearing at chemical shifts of 136.8 and 199.5 ppm with a P,P-coupling of 35.5 Hz.

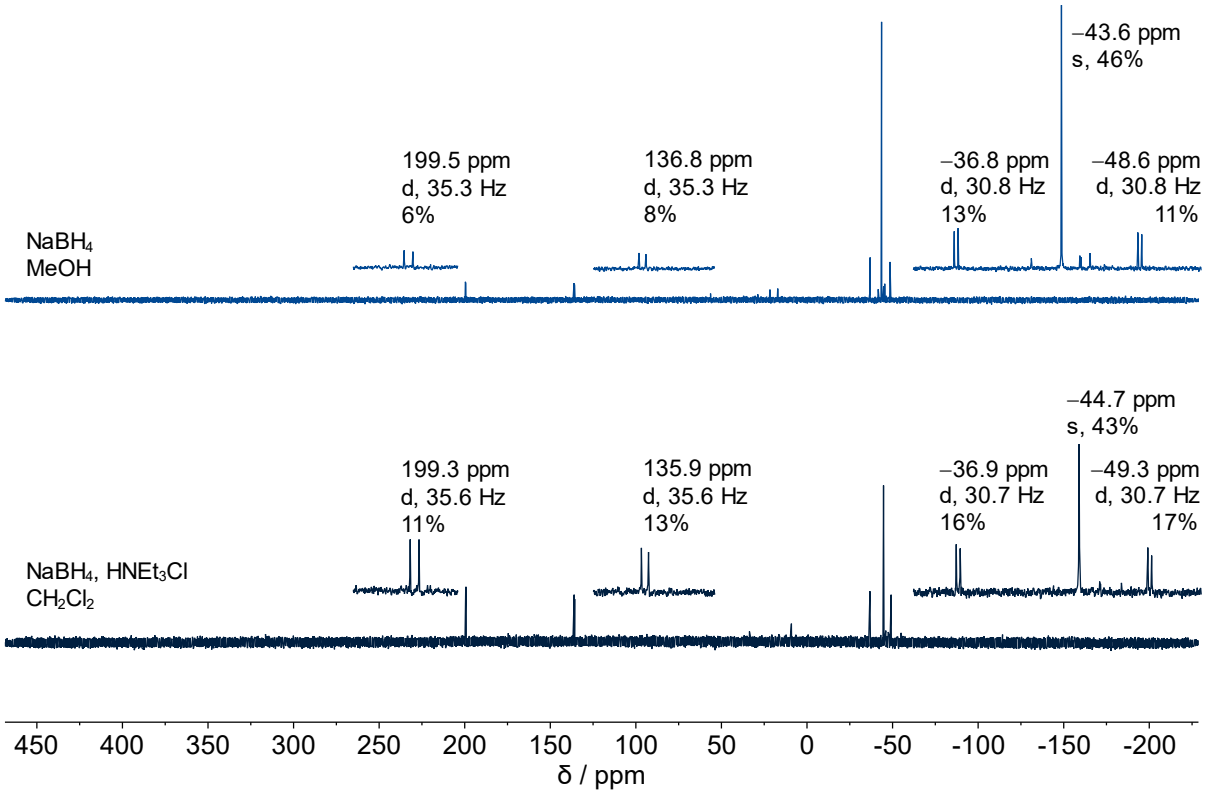


*Figure 43:* $^{31}P\{^{1}H\}$ NMR spectra of the reaction mixtures of **30** without (top, in MeOH) and with the addition of triethylammonium chloride (bottom, in $CH_2Cl_2$).

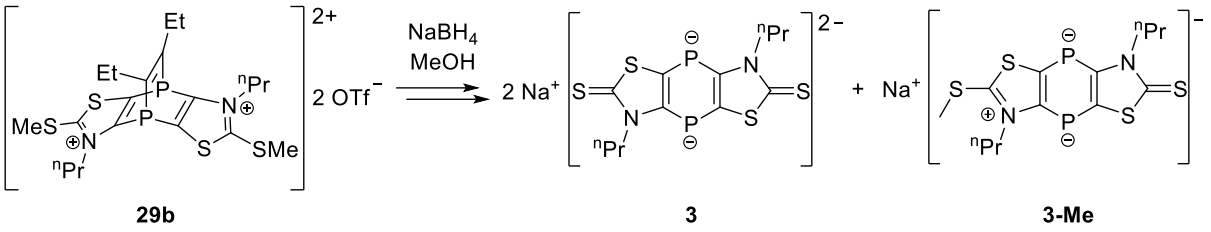


*Scheme 42:* Possible reaction products of a reaction of **29b** with sodium borohydride in methanol.

In analogy to the reaction of **1** with magnesium or potassium graphite (see section 3.1.1), the resonance at −43.6 ppm was recognised as compound **3**, the literature-known dianion of **1** (Scheme 42).[110] The absence of a second isomer of **3** can stem from the *syn* conformation of the central ring in **29b** due to the presence of the 1,4-diphosphabarrelene bridge. Remarkably, the formation of this product not only implies a reductive cleavage of the 1,4-diphosphabarrelene bridge, but also the elimination of the two S-methyl groups, forming back the thione moieties. Yet, a nucleophilic attack of either hydride or methoxide anions, both of which are present in the reaction mixture, can explain both reactivities, eliminating the bridge as an alkene and the methyl groups as either methane or dimethyl ether. Unfortunately, no signal for either product could be detected in $^{1}$H NMR spectra, nor a signal in the lowfield region which could fit to thiazolium protons. Hence, the formation of the desired product **30** remains questionable.

In addition to the main $^{31}$P[$^{1}$H} resonance at −43.6 ppm, the observed AB-spin system near this chemical shift also closely resembled the signals obtained with potassium graphite and TMS-Cl (Figure 9, bottom). Hence, it was assigned to the monomethylated dianionic **3-Me**, mirroring the partial formation of **3-TMS** in section 3.1.1 (compare Figure 10). While these findings explain the formation of signals in the highfield-region of the $^{31}$P{$^{1}$H} NMR spectrum, the asymmetric product creating the AB-spin system at low fields cannot be determined in a straight-forward fashion. An attack of methoxide at one phosphorus centre could be feasible, but chemical shifts of the resulting product **31** would be expected at significantly different chemical shifts, similar known examples displaying values close to 0 and beyond −60 ppm (Figure 44, left).[59]

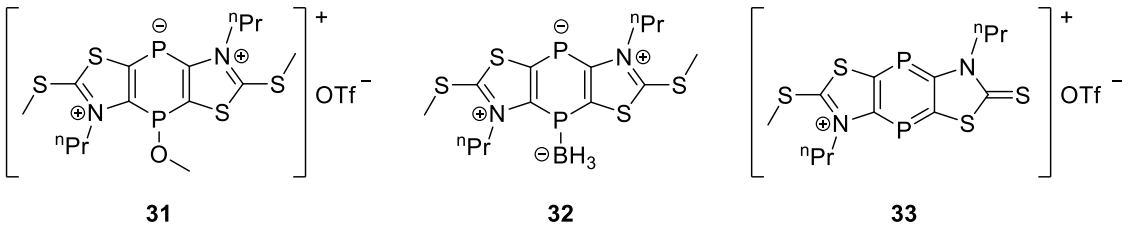


*Figure 44:* Possible side products of a reaction of **30** with sodium borohydride.

Another possible product could be **32**, carrying a phosphido-borane moiety (Figure 44, centre). However, literature-known phosphide-boranes also display chemical shifts below 10 ppm,[137] and **32** would show a characteristic pseudo-quartet splitting to the boron atom in $^{31}$P NMR spectra. Assuming a clean [4+2]-cycloreversion, the formation of mono-methylated 1,4-diphosphinine **33** can also seem viable (Figure 44, right). Yet, **33** is an observed (albeit unpublished) intermediate in the formation of **LXIX** and was found to have $^{31}$P chemical shifts of 137.4 and 148.7 ppm with a coupling constant of 69.8 Hz. As of yet, the AB-spin system in the highfield region of the $^{31}$P{$^{1}$H} NMR spectrum could not be assigned to a feasible structure. As no $^{1}$H NMR resonance of thiazolium-protons could be found, the reaction of **29b** with sodium borohydride in methanol was repeated, this time with the inclusion of triethylammonium chloride (Scheme 41). This addition aimed to suppress the formation of methoxide anions, increasing the selectivity and favouring the desulfurisation over nucleophilic attacks of methoxide. Interestingly, even adding 4 eq. of triethylammonium chloride at −60 °C only 2 min after the addition of sodium borohydride did not significantly change the outcome of the reaction as $^{31}$P{$^{1}$H} NMR spectra looked almost identical (Figure 43, bottom). While the number of small side products was decreased, the relative content of the three main products remained very similar, the major resonance at −44.7 ppm being somewhat diminished while the two AB-spin systems appeared slightly more prominent in the spectrum. Again, parallel monitoring using $^{1}$H NMR spectroscopy did not indicate the formation of thiazolium salts or thiomethanol.

The general lack of formation of the desired product **30** could be a result of the harsh reaction conditions associated with using a high excess of sodium borohydride in a protic solvent like methanol. For this reason, the desulfurisation of **29b** was attempted in THF, employing a different borohydride, *i.e.* lithium tri-*s*-butyl(hydrido)borate (in the following: L-selectride) at temperatures below −40 °C (Scheme 43). The usage of L-selectride allowed for an easier control of hydride stoichiometry compared to sodium borohydride as well as the formation of a bulkier and, thus, kinetically hindered borane. In addition, the salt elimination of lithium thiomethoxide was deemed more promising than the formation of thiomethanol, as it was expected to precipitate, eliminating it from the reaction equilibrium.

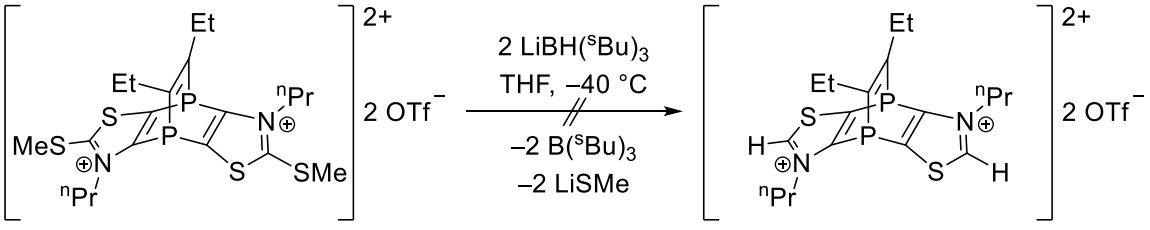


**29b** **30**

*Scheme 43:* Targeted reductive desulfurisation of **29b** using L-selectride.

An initial colour change of the reaction mixture from off-white to red and then to yellow was observed and $^{31}P\{^{1}H\}$ NMR studies initially showed the formation of a major product, appearing as a singlet at −62.5 ppm, together with two AB-spin systems between −60 and −25 ppm with coupling constants of 23 and 28 Hz. However, upon stirring the reaction for more than 2 h, the lowfield-shifted AB-spin system at 135.6 and 199.2 ppm, which had already been observed in the reactions of **29b** with sodium borohydride became visible (Figure 45, top). With a content of 74% by integration, this unknown compound was now the main product of the reaction, while the singlet at −62.5 ppm had decreased to a content of 26% as opposed to the initial 44%. Stirring the reaction mixture for a longer time led to a decrease of intensity for all resonances.

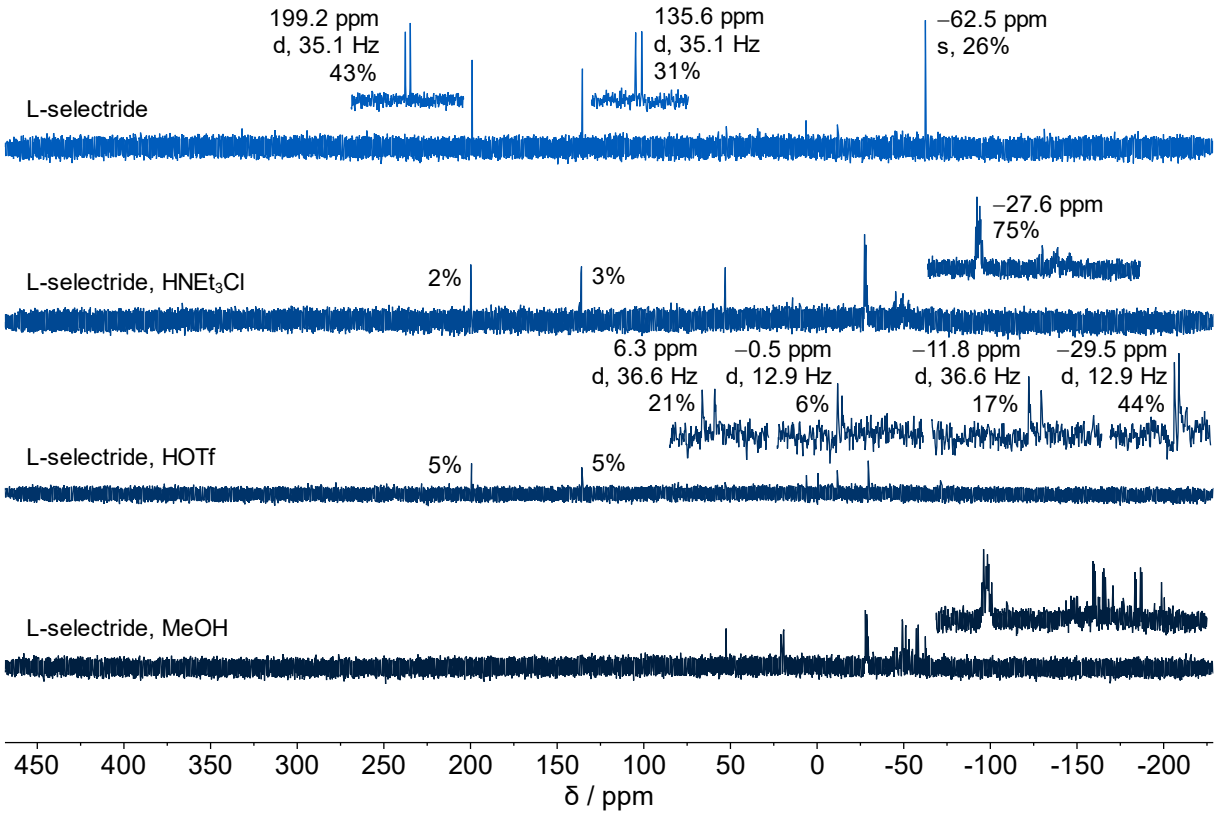


*Figure 45:* $^{31}P\{^{1}H\}$ NMR spectra of reaction mixtures of different desulfurisation attempts of **29b** using L-selectride.

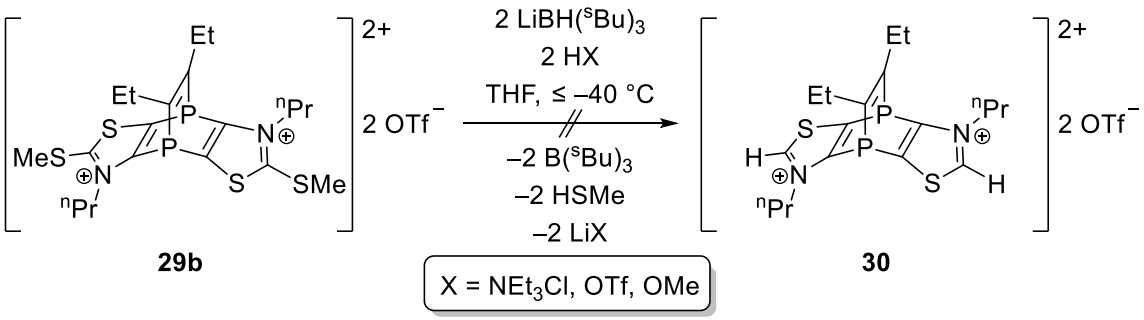


*Scheme 44:* Targeted reductive desulfurisation of **29b** using L-selectride and an additional proton source HX.

As access to the desired bis-thiazolium salt **30** could not be gained via this route, and **29b** was treated with L-selectride and different acidic compounds, *i.e.*, triethylammonium chloride, triflic acid and methanol, in order to promote the elimination of different lithium salts (Scheme 44). The additions of the proton sources were carried out at temperatures below −40 °C after initially adding L-selectride to **29b** at the same temperatures. While still present in small quantities, the formation of the AB-type spin system in the lowfield region of the $^{31}P\{^{1}H\}$ NMR spectra was successfully decreased by the addition of triethylammonium chloride and triflic acid (Figure 45, second from top, third from top), and was fully suppressed by adding methanol to the reaction mixture (Figure 45, bottom). Yet, all three $^{31}P\{^{1}H\}$ NMR spectra showed otherwise unselective reaction mixtures with multiple products in the highfield region. The addition of triethylammonium chloride led to the appearance of a plethora of signals around −27.6 ppm, making up the majority of visible signals in the spectrum, while two AB-spin systems between −30 and 10 ppm were formed upon addition of triflic acid. In the case of adding a drop of methanol, the $^{31}P\{^{1}H\}$ NMR spectra became very complex with more than ten signals appearing in a range between −65 and 55 ppm, most of which showed the doublet splitting of AB-type spin systems. Consequently, no product could be isolated from these reaction mixtures and the proposal of a reaction mechanism to explain the formation of these products is not possible.

### *3.6.2.2 Metallic reductants*

In addition to boron-based reductants targeting bis-thiazolium salt **30**, **29b** was treated with potassium metal and potassium graphite aiming to directly reduce the doubly methylated salt to the bis-NHC **26b** under elimination of potassium thiomethoxide and potassium triflate (Scheme 45). The reactions were carried out by adding THF to a potassium mirror or potassium graphite and **29b** at −196 °C and warming the mixture up until the solvent liquefied. The reaction was then stirred while slowly warming up to ambient temperature as a way to ensure the mildest possible reaction conditions for the desulfurisation reactions. For both cases, $^{31}P\{^{1}H\}$ NMR spectroscopic experiments were carried out after stirring the mixture for 18 h (Figure 46).

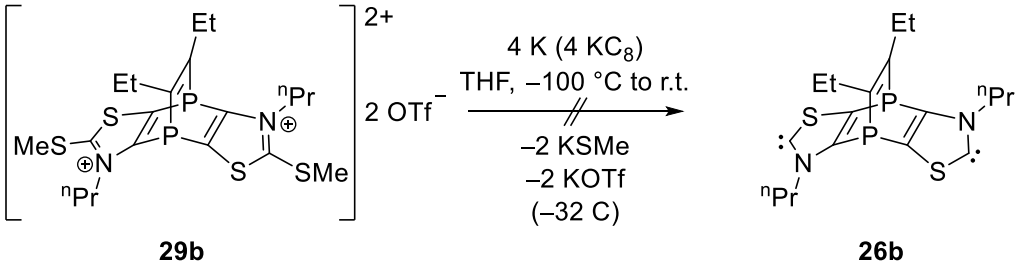


**29b** **26b**

*Scheme 45:* Targeted reductive desulfurisations of **29b** using potassium (or potassium graphite).

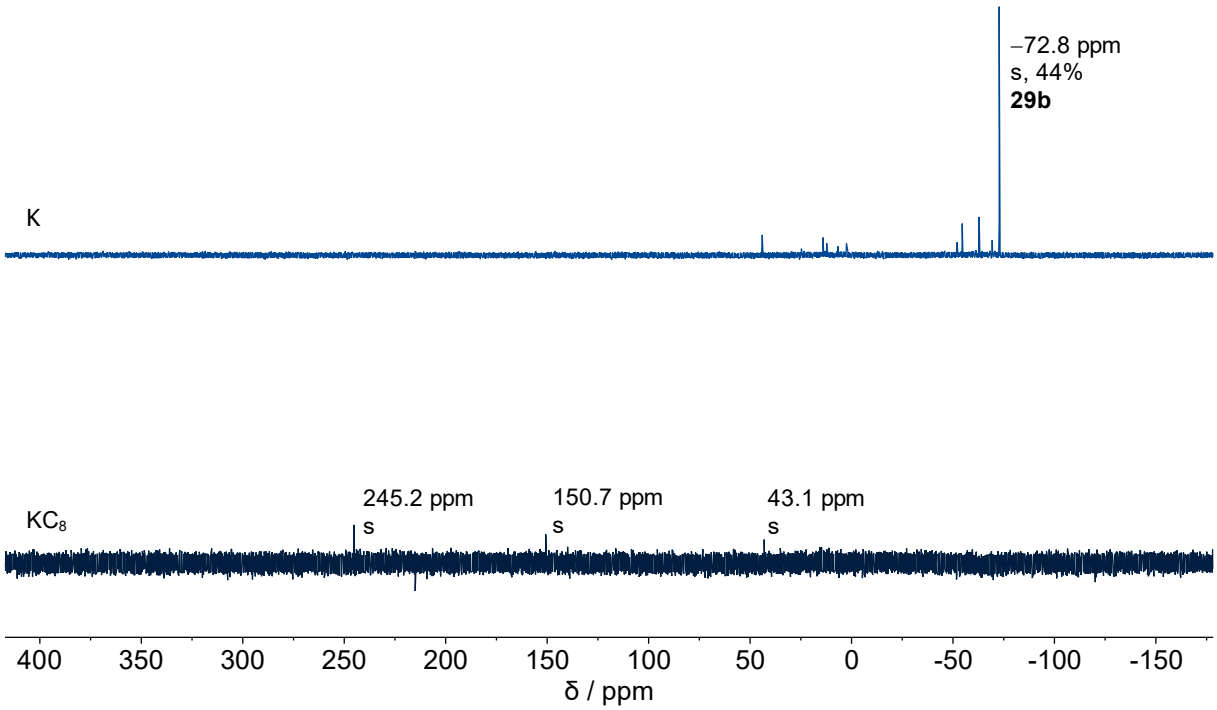


*Figure 46:* $^{31}P\{^{1}H\}$ NMR spectra of desulfurisations of **29b** using potassium (top) and potassium graphite (bottom).

Remarkably, in the reaction of **29b** with potassium metal, even after 18 h almost half of the starting material remained present in the reaction solution (Figure 46, top). Apart from this main signal at −72.8 ppm, ten small resonances were visible, including two AB-spin systems having P,P-coupling constants of about 20 Hz. Since none of the observed signals was present in the $^{31}P\{^{1}H\}$ NMR spectrum with a content of more than 10%, no further investigations into the nature of the formed products were conducted.

On the contrary, the $^{31}P\{^{1}H\}$ NMR spectrum of the reaction mixture of **29b** with potassium graphite showed only three singlets at 43.1, 150.7 and 245.2 ppm (Figure 46, bottom). Though, these resonances were only visible in a very low intensity, making integration and further analysis impossible. Likewise, the interpretation and assignment of the resonances to structural features is challenging. Yet, the formation of the desired product is very unlikely given the lowfield-nature of all observed $^{31}P\{^{1}H\}$ resonances and the synthesis of thiazole-based 1,4-diphosphabarrelene bis-NHCs was not possible.

In addition to the discussed desulfurisation attempts of both 1,4-diphosphabarrelenes (discussed in section 3.5) and doubly methylated 1,4-diphosphabarrelene salts (discussed in section 3.6.2), several more desulfurisation attempts were carried out, which will not be discussed in detail. However, they are described in Table 12 (section 7.2).

## 3.7 DIMERISATION ATTEMPTS OF THIAZOLIUM SALTS

After direct desulfurisation reactions of 1,4-diphosphabarrelenes as well as desulfurisations of doubly methylated 1,4-diphosphabarrelene salts did not result in the formation of the expected bis-carbenes and bis-thiazolium salts, the synthetic strategy was altered. With the di- or oligomerisation of thiazole-based bis-carbenes in mind, a direct coupling of the $C^2$-centres of thiazole-2-carbenes and further functionalisations of the resulting dithiadiazafulvalenes (DTDAF) was targeted. A similar approach is known for tetrathiafulvalenes (TTF) and the respective TTF-based 1,4-diphosphinine has indirectly been confirmed.[102] The conceptual synthetic method for thiazole-based analogues involves the dimerisation of thiazolium salts like **35** to form DTDAF **36** (Scheme 46). The subsequent backbone-phosphanylation and further functionalisations according to the well-established synthetic protocol for 1,4-diphosphinine **1**[100] would then lead to the synthesis of oligo- or poly-1,4-diphosphinine **38**.

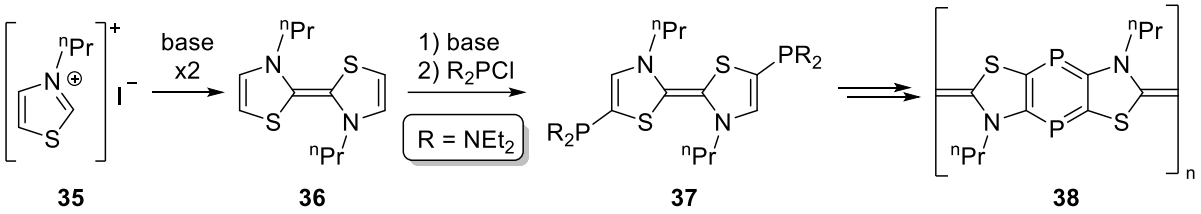


*Scheme 46:* Conceptual synthetic approach to oligo-1,4-diphosphinine **38** via the dimerisation of **35**.

### 3.7.1 Dimerisation studies of 3-*n*-propylthiazolium iodide

Several procedures for the synthesis and dimerisation of thiazolium salts are known to literature.[65,72,138] While thiazole-2-thiones and -selones can be used as precursors,[68,73] the most simple protocol for synthesising thiazolium salts starts from thiazole itself and proceeds via a reaction with an iodoalkane.[71] This reactivity was exploited when thiazole **34** was reacted in neat 1-iodopropane at 70 °C (Scheme 47). $^1$H NMR spectroscopy showed the clean formation of **35** in solution, with signature resonances for the thiazolium proton at 11.02 ppm as a doublet ($^4J_{H,H}$ = 1.75 Hz) and the two backbone protons at 8.21 and 8.29 ppm, both appearing as doublets of doublets with small coupling constants between 1.4 and 3.8 Hz.

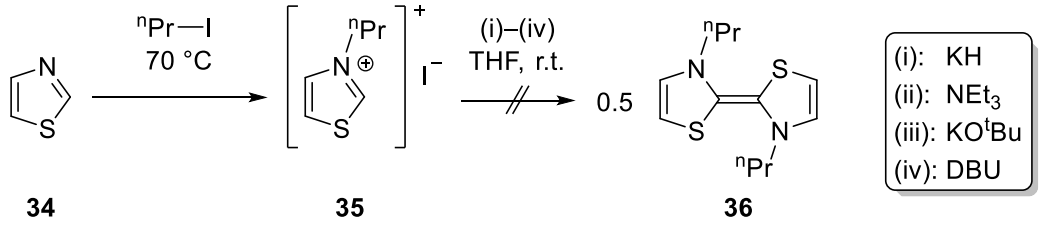


*Scheme 47:* Synthesis of thiazolium salt **35** and targeted dimerisation.

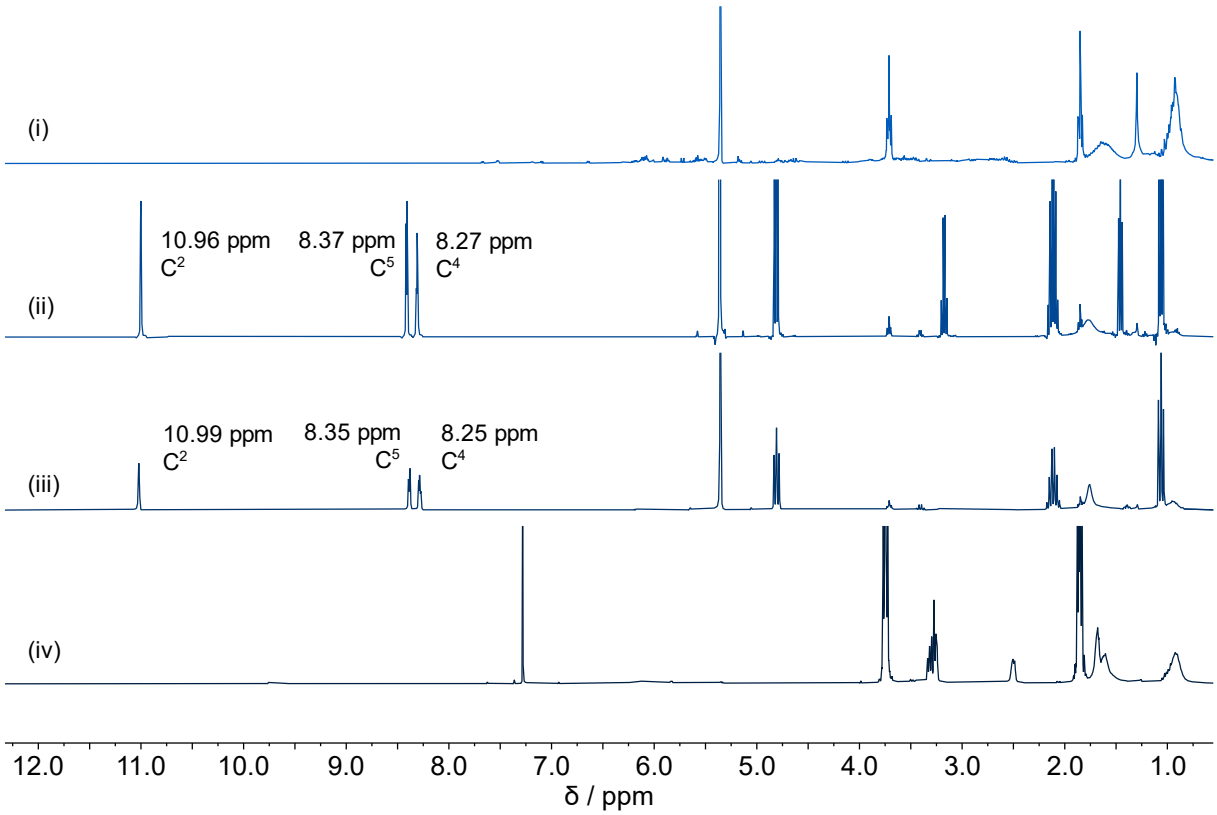


*Figure 47:* $^{1}$H NMR spectra in $CD_2Cl_2$ ((i)–(iii) or $CDCl_3$ (iv) of different deprotonation attempts of 3**5**.

In a second step, **35** was subjected to different bases in THF in order to deprotonate the $C^2$ position and dimerise the resulting carbene, as was shown in the literature for small substituents at nitrogen.[65] Four different bases were used for the deprotonation, *i.e.*, potassium hydride (i), triethylamine (ii), potassium *t*-butoxide (iii) and 1,8-diazabicyclo(5.4.0)undec-7-ene (DBU, iv). Monitoring the reactions with $^{1}$H NMR spectroscopy revealed two distinctly different behaviours: $NEt_3$ and KO$^{t}$Bu did not react with **35** at all and the $^{1}$H NMR signals for both $C^4$/$C^5$ and the $C^2$ proton remained unchanged in the spectrum, indicating no deprotonation had taken place. Conversely, all three resonances vanished upon treatment with KH and DBU. This disappearance, together with the generally much broader $^{1}$H NMR resonances, strongly suggests an unselective deprotonation and follow-up reactions of the formed carbenes. Indeed, abnormal NHCs carrying the carbene-functionality at a backbone-carbon atom as opposed to the $C^2$-atom are well-known when working with backbone-unprotected imidazoles.[50,51] Analogous abnormal thiazole-based carbenes would be feasible in the performed reaction, preventing the formation of the desired DTDAF **36**. Noteworthily, all literature-known examples of DTDAF carry at least one alkyl-group in the backbone, protecting it from deprotonation during the dimerisation step.[65,68,71–73,138]

### 3.7.2 Backbone-protection studies of thiazole and thiazolium salts

As no backbone-unsubstituted DTDAF is known to the literature, investigations into the protection of the thiazole-backbone were carried out. With the goal of synthesising backbone-phosphanylated DTDAF **37** in mind (Scheme 46), these studies were first focused on the protection using chlorobis(diethylamino)phosphane, $(Et_2N)_2PCl$. The reaction was carried in an analogous fashion to the backbone-phosphanylation of thiazole-2-thiones,[139] *i.e.*, by deprotonation using $^n$BuLi in THF at −80 °C, before the addition of $(Et_2N)_2PCl$ (Scheme 48, top).

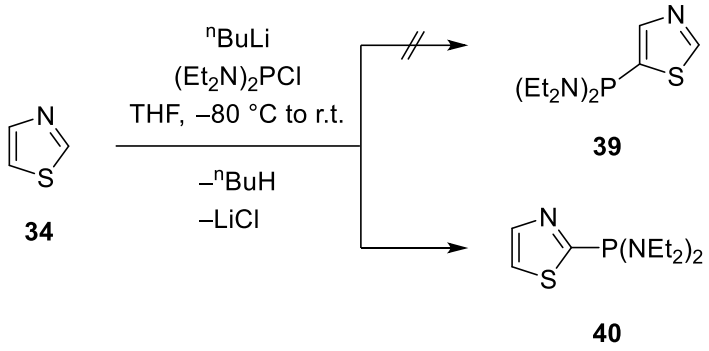


*Scheme 48:* Backbone- (top) and $C^2$-phosphanylation (bottom) of thiazole using $(Et_2N)_2PCl$.

The reaction was monitored using both $^1H$ and $^{31}P\{^1H\}$ NMR spectroscopy. The $^{31}P\{^1H\}$ NMR spectrum of the reaction mixture showed a selective reaction with a major resonance at 86.6 ppm, fitting well to similar, previously reported compounds.[110,139] However, comparing $^1H$ NMR spectra of the reaction mixture and **34** paints a different picture (Figure 48).

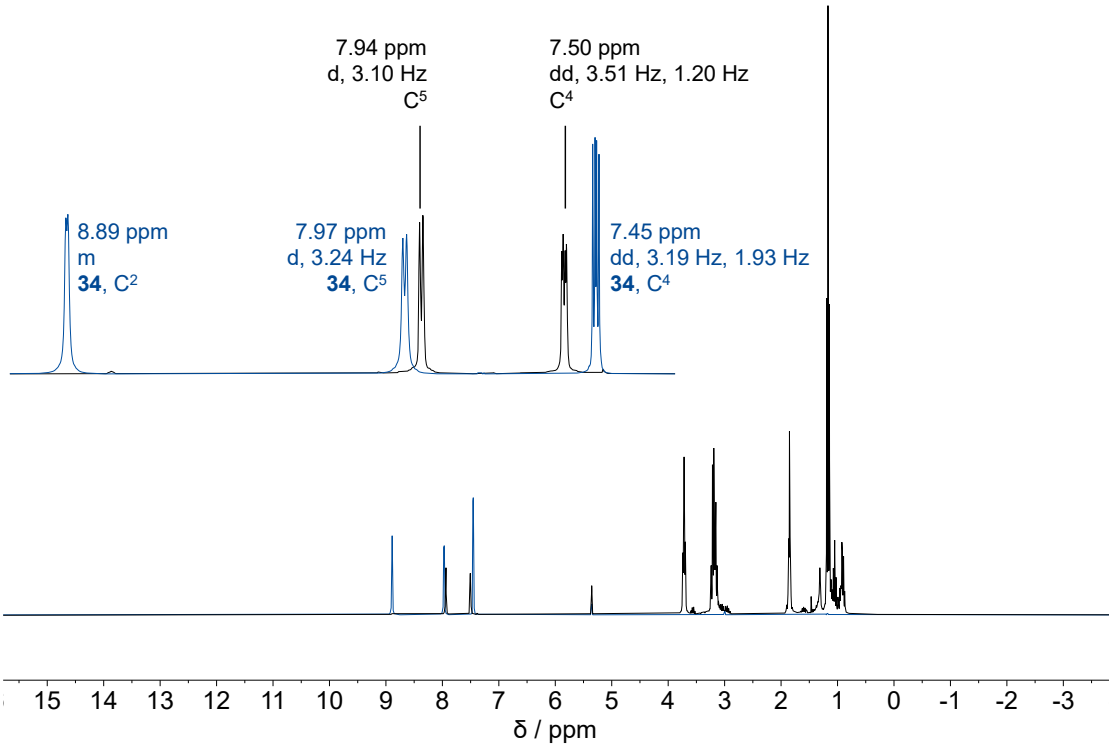


*Figure 48:* $^1H$ NMR spectra of thiazole (**34**, blue) and the reaction mixture of **39** (black).

A comparison of the protons at the $C^2$-, $C^4$- and $C^5$-positions of **34** (Figure 48, blue) and the reaction mixture (Figure 48, black) shows the unaltered presence of both backbone-protons in the reaction mixture and thus reveals a clean reaction at the $C^2$-position, forming **40** instead of the desired $C^5$-phosphanylated **39** (Scheme 48, bottom). This behaviour has previously been reported when protecting thiazole with $SiMe_3$ or $SnMe_3$ groups and was explained to be the result of the higher acidity of protons in $C^2$-position compared to $C^5$-position.[140] However, this report also discusses a rearrangement of the formed 2-trimethylsilyl- and 2-trimethylstannyl-thiazoles **41a,b** to the respective 5-silyl- and 5-stannyl-derivatives when stirring the reaction for a longer time. The mechanism of this rearrangement was proposed to proceed via the respective thiazole-5- and thiazole-2-anions **41'a,b** and **42'a,b** (Scheme 49).[140] Their interconversion is achieved by a nucleophilic attack of **41'a,b** on the 2,5-disubstituted thiazoles **43a,b**, which are assumed to be formed in small amounts due to a slight excess of base and tetrel chloride. The formed thiazole-2-anion **42'a,b** can then be reprotonated by **41a,b**, completing the conversion into the desired $C^5$-substituted **42a,b**. This acid/base equilibrium between **41a,b**, **42a,b** and their respective anions was proposed to be possible due to the similar p$K_a$ values of the $C^2$- and $C^5$-positions in thiazole.[141]

While the rearrangement of $C^2$-subsituted thiazoles is well understood for the case of silyl- and stannyl-substitution, no precedent of the same happening for phosphanyl-substituted thiazoles can be found in the literature and, in fact, a similar rearrangement was not observed in the case of **40**. Stirring the reaction mixture for several days did not lead to any change of signals in both the $^1H$ and $^{31}P\{^1H\}$ NMR spectra and, thus, the desired $C^5$-phosphanylated **39** could not be detected.

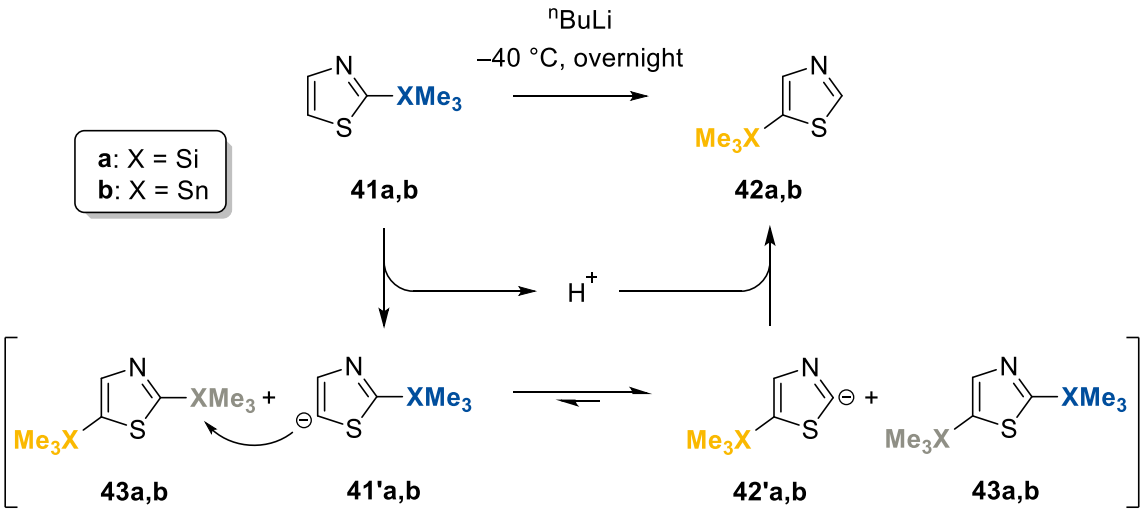


*Scheme 49:* Proposed rearrangement mechanism of $SiMe_3$/$SnMe_3$-substituted thiazoles.[140]

Since a direct phosphanylation of thiazole had led to a $C^2$-substitution instead of the desired backbone-protection, **34** was reacted with TMS-Cl according to a procedure found in the literature in order to form the known silylated thiazole **42a**,[140] with the goal of substituting the TMS group for a bis(diethylamino)phosphanyl group in a second step (Scheme 50). **34** was first treated with $^n$BuLi at −70 °C before adding TMS-Cl at −80 °C after 1 h.

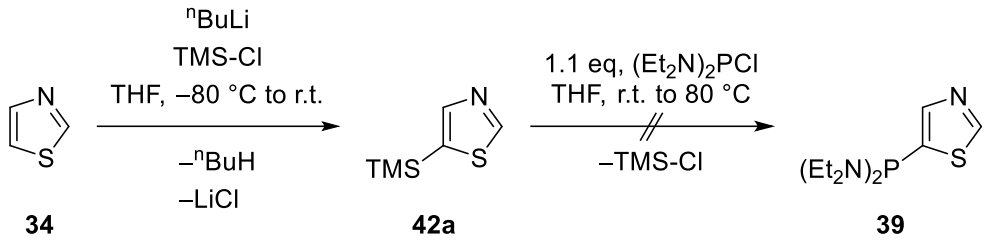


*Scheme 50:* Silylation reaction of **34** to form **42a** and targeted subsequent substitution to afford **39**.

After work-up, the formation **42a** could be confirmed by $^1$H NMR spectroscopy, with resonances fitting to the literature-known data (Figure 49, black).[140] In the spectrum, one signal for the backbone-protons had disappeared while the $C^2$-proton remained unchanged, confirming the rearrangement of **41a** to **42a**. The latter could be obtained with a yield of 68% and was employed in substitution reactions using $(Et_2N)_2PCl$ in THF (Scheme 50, right).

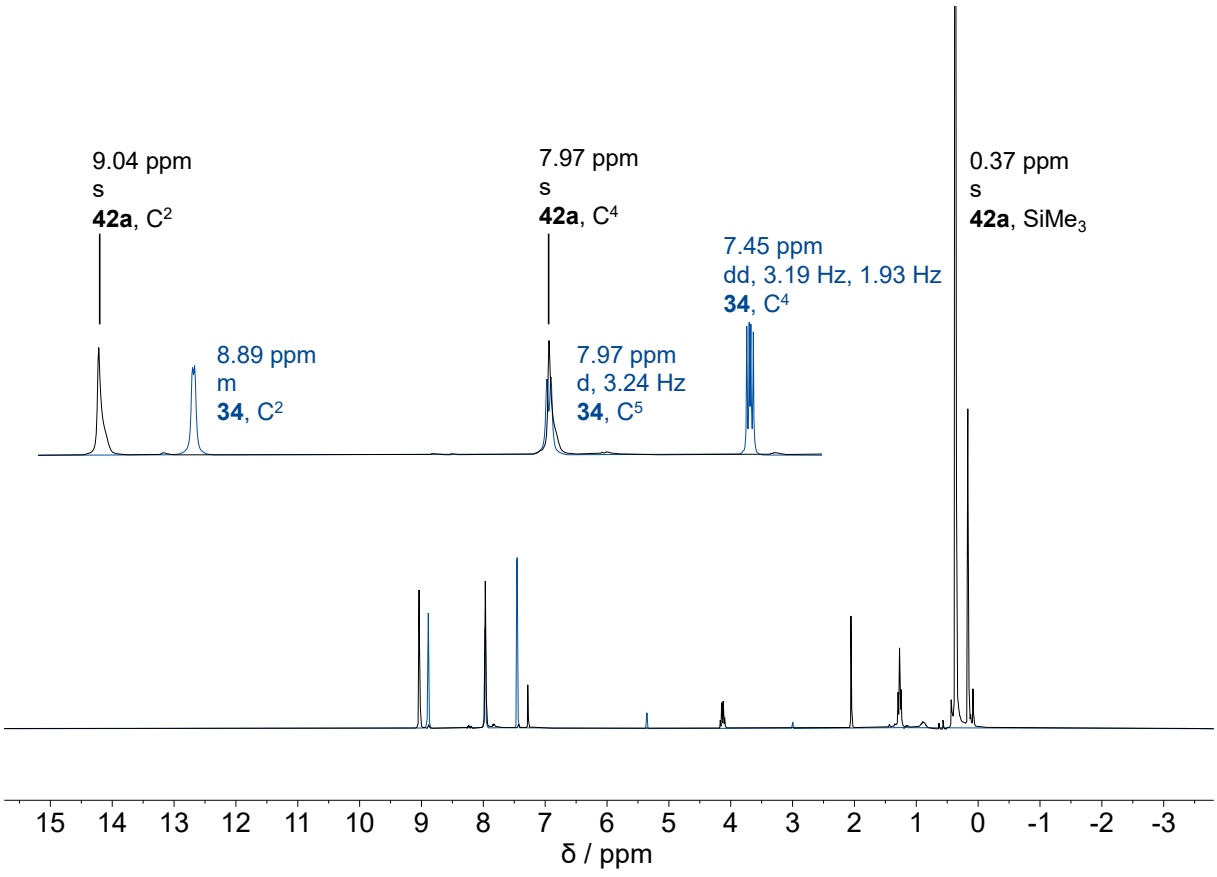


*Figure 49:* $^1$H NMR spectra of thiazole (**34**, blue) and **42a** after work-up (black).

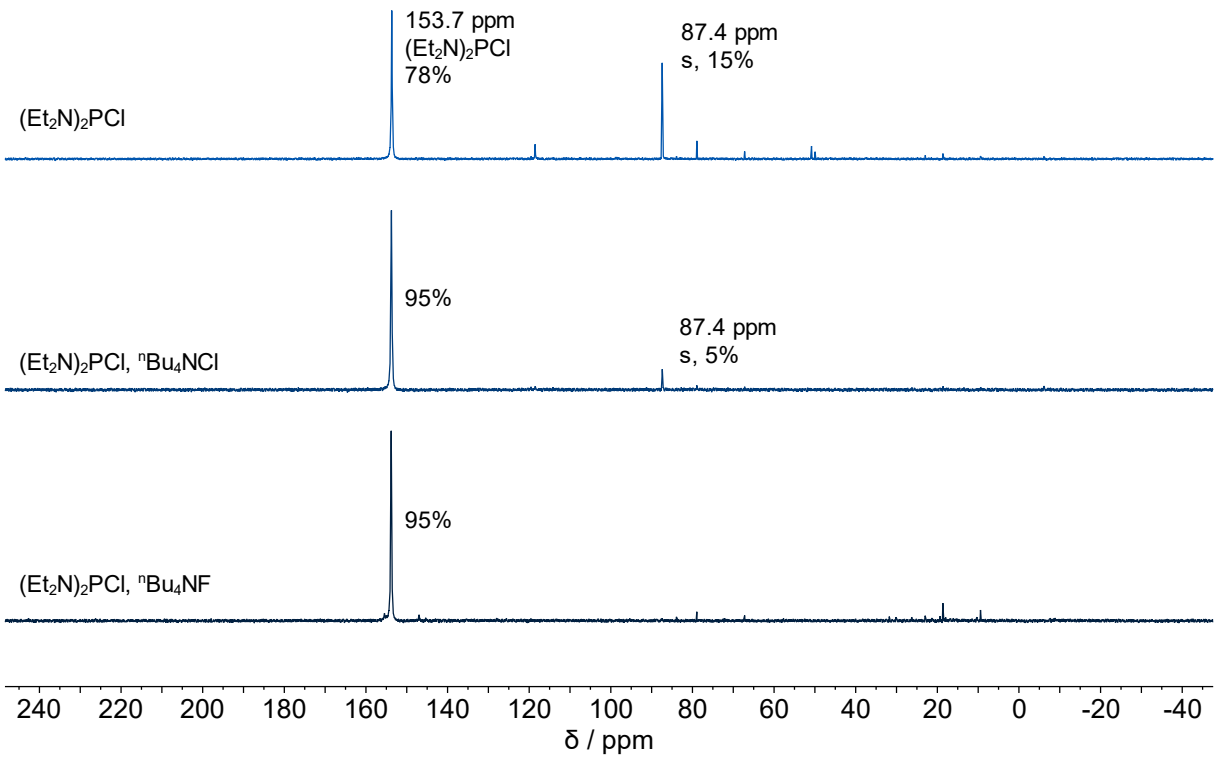


*Figure 50:* $^{31}P\{^{1}H\}$ NMR spectra of the reaction mixtures of reactions of **42a** with $(Et_2N)_2PCl$ (top) and while adding $^{n}Bu_4NCl$ (centre) or $^{n}Bu_4NF$ (bottom).

The synthetic approach for achieving the formation of **39** involved the addition of $(Et_2N)_2PCl$ in order to substitute the TMS group, eliminating TMS-Cl. $^{31}P\{^{1}H\}$ NMR spectra of the reaction mixture showed the partial formation of a singlet at 87.4 ppm with a content of 15% by integration (Figure 50, top). This signal fits well to the $^{31}P$ NMR shifts of known phosphanylated 1,3-thiazole-2-thiones.[110] However, in addition to the content in the $^{31}P\{^{1}H\}$ NMR spectrum not rising above 15%, even after heating the mixture to 70 °C for 8 d, $^{1}H$ NMR spectra showed—apart from almost unchanged signals of **42a**—the appearance of multiple resonances beyond 7 ppm, indicating a slow and unselective reaction of **42a** with the phosphane. In order to enhance the reactivity and promote the elimination of TMS halogenides, the reaction was repeated while adding tetra-*n*-butylammonium chloride ($^{n}Bu_4NCl$) or fluoride ($^{n}Bu_4NF$) to the mixture to eliminate TMS-Cl or TMS-F. Surprisingly, while these additions seemed to suppress the formation of several side products, the formation of **39** was not promoted by the addition of the ammonium salts, but decreased to a point where 95% of $(Et_2N)_2PCl$ was still present in the reaction mixtures even after heating to 80 °C for 1 d (Figure 50, centre/bottom).

A simple substitution reaction did not yield the desired phosphanylated thiazole **39**, hence, different synthetic pathways to the targeted DTDAF **37** were probed (Scheme 51). These pathways avoided the direct phosphanylation of **42a** by first converting the latter to the silylated thiazolium salt **44** before either dimerising and then phosphanylating, giving **37** via DTDAF **45**, or phosphanylating and then dimerising, proceeding via the intermediate thiazolium salt **46**.

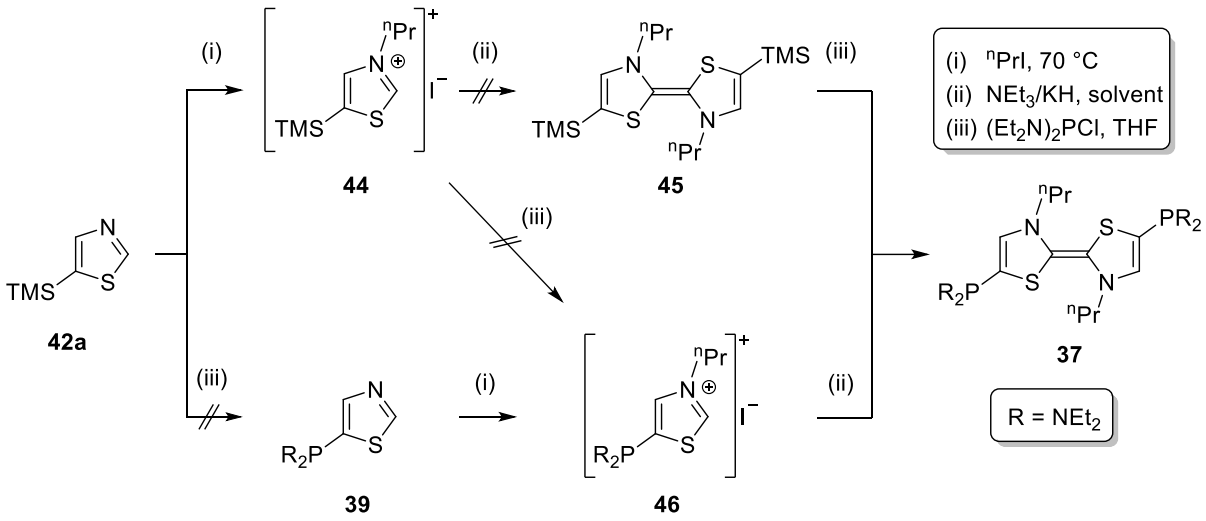


*Scheme 51:* Synthetic pathways from silylated **42a** to phosphanylated DTDAF **37**.

In order to afford thiazolium salt **44** from **42a**, the same synthetic procedure as for parent-thiazole **34** was applied (Scheme 51, top left), *i.e.*, a reaction in neat 1-iodopropane at elevated temperature (see section 3.7.1). After stirring the mixture for 21 h at 70 °C, **44** was selectively formed. The signature $C^2$- and $C^4$-protons were observed in the $^1$H NMR spectrum at 8.70 and 10.42 ppm, respectively, displaying a $^4J_{H,H}$ coupling constant of 1.16 Hz (Figure 51, top). As the reaction had resulted in the clean formation of thiazolium salt **44**, it was subjected *in situ* to different bases in DMSO-d6 or THF-d8.

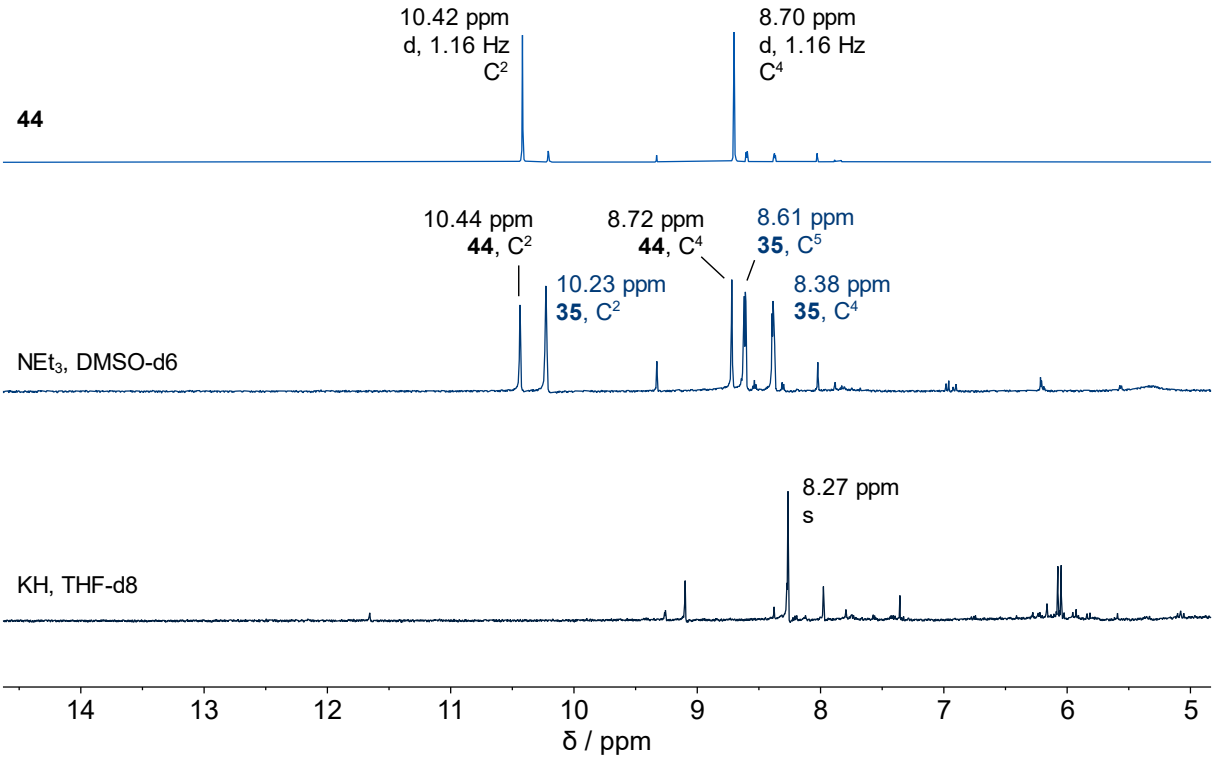


*Figure 51:* $^1$H NMR spectra of **44** (top) and the reaction mixtures of reactions with triethylamine (centre) or potassium hydride (bottom).

Triethylamine and potassium hydride were used as bases and showed very different reactivities in $^1$H NMR spectroscopic monitoring. The addition of triethylamine in DMSO-d6 led to a rather slow reaction with **44** still prominently present in the mixture after stirring the reaction mixture for 5 h (Figure 51, centre). Surprisingly, the second major product in the mixture was found to be thiazolium salt **35**, indicating that the addition of triethylamine led to the deprotection of the C$^5$ position in **44**, cleaving off the TMS group. The mechanism of formation of **35** could not be determined, but trace amounts of water in the solvent may be able to facilitate the substitution of TMS by a proton through the formation of TMS-OH.
When the deprotonation of **44** was attempted using potassium hydride, the $^1$H NMR spectrum revealed a significantly different outcome (Figure 51, bottom). The backbone signals of **44** had completely disappeared and instead, several singlets were visible in the lowfield region above 7 ppm, the most prominent being visible at 8.27 ppm. While this chemical shift may fit to the expected value for the C$^4$-proton of **45**, several broad resonances at higher field were observed as well as multiple signals for TMS groups, indicating an overall unselective reaction and making the isolation of **45** impossible.

With an unsuccessful direct dimerisation of silylated thiazolium salt **44**, another possible pathway is the phosphanylation of **44**, substituting the TMS group, and the following dimerisation of the formed thiazolium salt **46** (Scheme 51). This alternative route was probed by a reaction of **44** with $(Et_2N)_2PCl$, aiming for the C$^5$-phosphanylated salt **46** (Scheme 52, top). Previous substitutions of TMS by $(Et_2N)_2P$ had been found to proceed very slowly and the reaction was carried out at 80 °C.

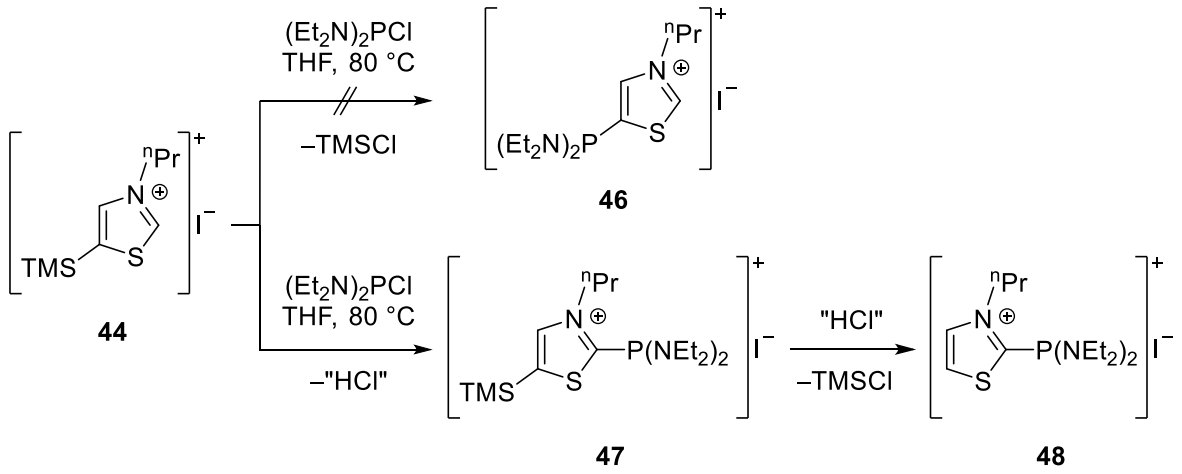


*Scheme 52:* Phosphanylation reactions of **44** at the C$^5$- (top) and C$^2$-positions (bottom) and follow-up reactivity.

The progress of the reaction was monitored using both $^{1}H$ and $^{31}P\{^{1}H\}$ NMR spectroscopy. In the $^{1}H$ NMR spectra, the slow consumption of **44** can observed by the decrease in content of its $C^{2}$- and $C^{4}$-protons at 9.33 and 11.45 ppm (Figure 52). Some small impurities of the unsubstituted thiazolium salt **35** can be seen in all spectra and do not take part in the reaction (Figure 52, grey). Already after 1 h of stirring at ambient temperature, the formation of a product was observed by the appearance of a doublet at 9.85 ppm, having a P,H-coupling constant of 1.10 Hz (Figure 52, blue). Interestingly, only one signal for this product is visible in the region of ring protons, speaking for a higher degree of substitution at the thiazolium ring. A likely explanation for this observation is the formation of **47** (Scheme 52, bottom), as the selective attack of $(Et_2N)_2PCl$ at the $C^{2}$ position of the ring has been found during the phosphanylation of thiazole. Hence, the $^{1}H$ NMR resonance was tentatively assigned to the $C^{4}$-proton of **47**.
When stirring the reaction mixture for a longer time at room temperature, a second product was formed, appearing in the $^{1}H$ NMR spectrum as two doublets of doublets at 8.76 and 9.50 ppm, with a H,H-coupling constant of 3.67 Hz and two P,H-couplings of 1.00 and 1.50 Hz. While two signals in this region of the spectrum are expected for **46**, the chemical shifts below 10 ppm strongly suggest two backbone protons in the $C^{4}$ and $C^{5}$ positions. As both resonances show small P,H-couplings, the signals were assigned to thiazolium salt **48**, carrying the phosphane moiety in $C^{2}$ position while the two backbone positions are both unprotected (Scheme 52, bottom).

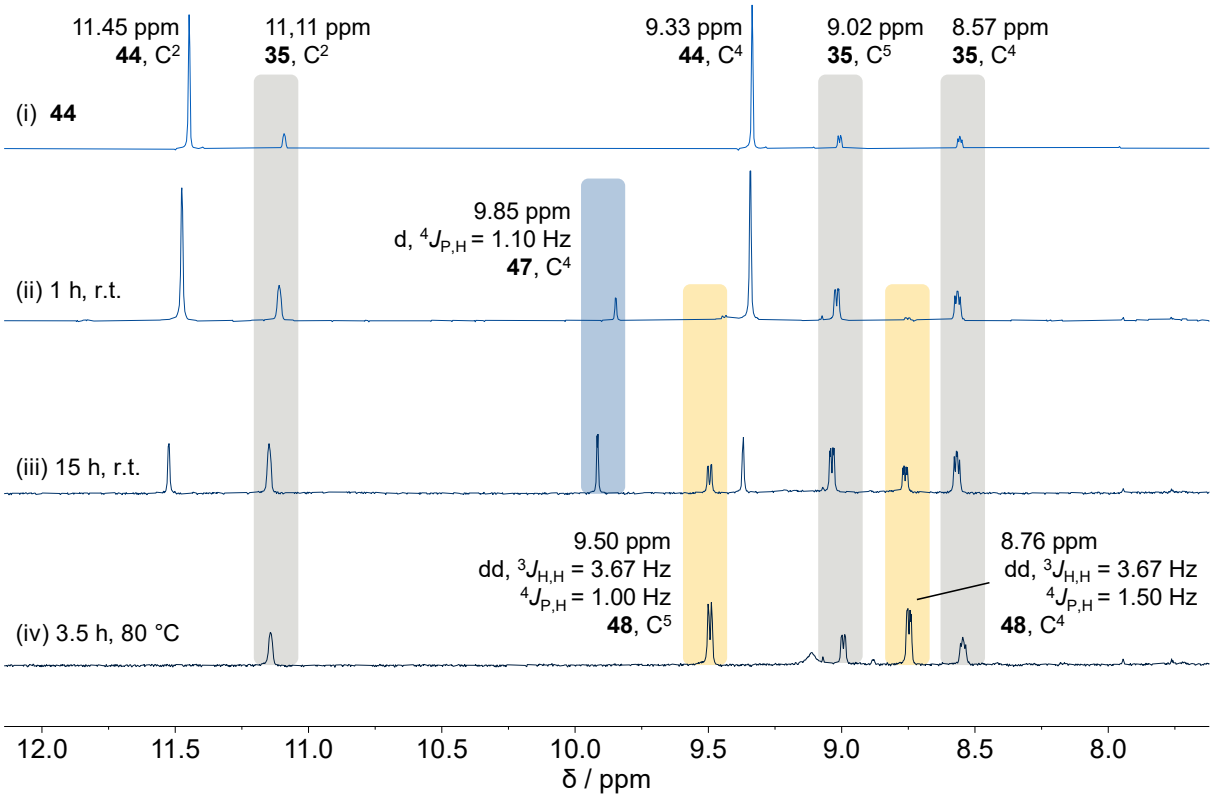


*Figure 52:* $^{1}H$ NMR spectra of **44** (i) and the reaction mixture of **46** after stirring for 1 h at r.t. (ii), 15 h at r.t. (iii) and additional 3.5 h at 80 °C (iv).

A possible formation mechanism of **48** goes via the previously discussed **47** as an intermediate. In the formation of **47**, HCl is formally eliminated during the attack of $(Et_2N)_2PCl$ to **44**, which can now substitute the silyl functionality, affording TMS-Cl and the $C^2$-functionalised **48**. The fact that upon heating the reaction mixture to 80 °C for 3.5 h the signal of **47** disappeared while the two resonances of **48** increased in intensity corroborates this proposed mechanism. Additionally, a look into $^{31}P\{^1H\}$ NMR spectroscopic monitoring pointed in the same direction (Figure 53): stirring the mixture for 1 h at room temperature led to the formation of a singlet at 79.2 ppm with a content of 72% by integration (Figure 53, top) and the ratio of contents shifted towards a second resonance at 78.9 ppm when stirring for 15 h (Figure 53, centre). Heating to 80 °C selectively formed the more highfield-shifted resonance (Figure 53, bottom), aligning well with the emergence of signals in the $^1H$ NMR spectra. Moreover, the close proximity of the two observed signals in the $^{31}P\{^1H\}$ NMR spectra speaks for a close chemical resemblance, further supporting the proposed structures of **47** and **48**.

As the phosphanylation of **44** proceeded at the $C^2$ instead of the desired $C^5$ position, a possible rearrangement of the phosphane moiety to form **46** was attempted. This reactivity was probed in the same way as for **40**, following the literature-known procedure for silyl-substituted thiazoles,[140] *i.e.*, by adding a drop of $^n$BuLi. However, this addition led to a very complex mixture in $^{31}P\{^1H\}$ NMR spectra, eliminating the possibility of a phosphane rearrangement to form **46**.

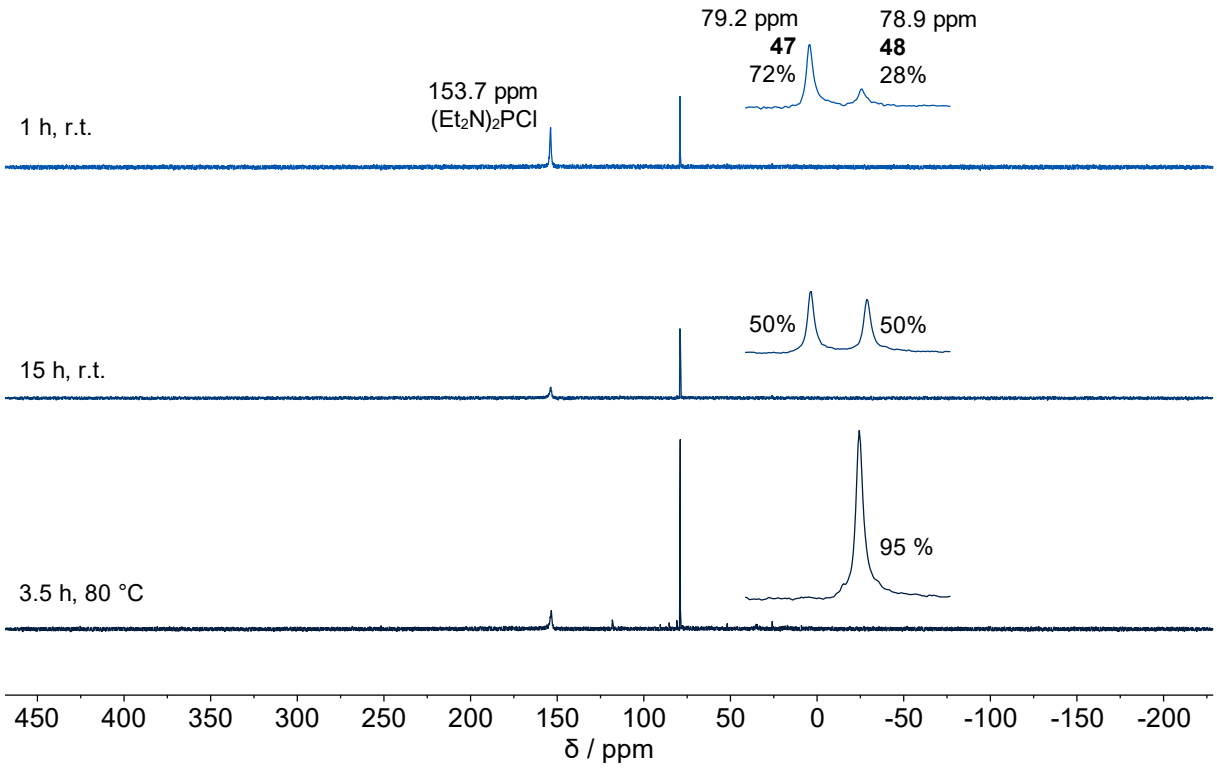


*Figure 53:* $^{31}P\{^1H\}$ NMR spectra of the reaction mixture of **46** after stirring for 1 h at r.t. (top), 15 h at r.t. (centre) and additional 3.5 h at 80 °C (bottom).

With neither the dimerisation of silyl-substituted thiazolium salts nor their phosphanylation yielding the desired products, the feasibility of the synthesis of DTDAF **37** was considered low as all attempted synthetic pathways to **37** proved unsuccessful. Hence, this approach to oligomerised thiazole-based 1,4-diphosphinines **38** was not further investigated.

## 3.8 THEORETICAL STUDY ON THE AROMATICITY OF DIPHOSPHININES AND RELATED COMPOUNDS

The previously discussed reactivity studies at both the phosphorus as well as the thione moieties of 1,4-diphosphinine **1** and 1,4-diphosphabarrelenes **17,18** led to several surprising results and unexpected problems. Due to the strong difference in reactivity of **1** compared to derivatives such as **LVI**, a distinct electronic difference between the different 1,4-diphosphinines was suspected. Therefore, a broader, systematic theoretical study was carried out to assess the aromaticity in these 1,4-diphosphinines and related compounds and to gauge the effect of fused heterocycles (in order to accommodate literature-known, previously discussed and unknown structures in a concise manner, the nomenclature of compounds was changed to all-Latin letters). All discussed structures can be seen in Figure 54.

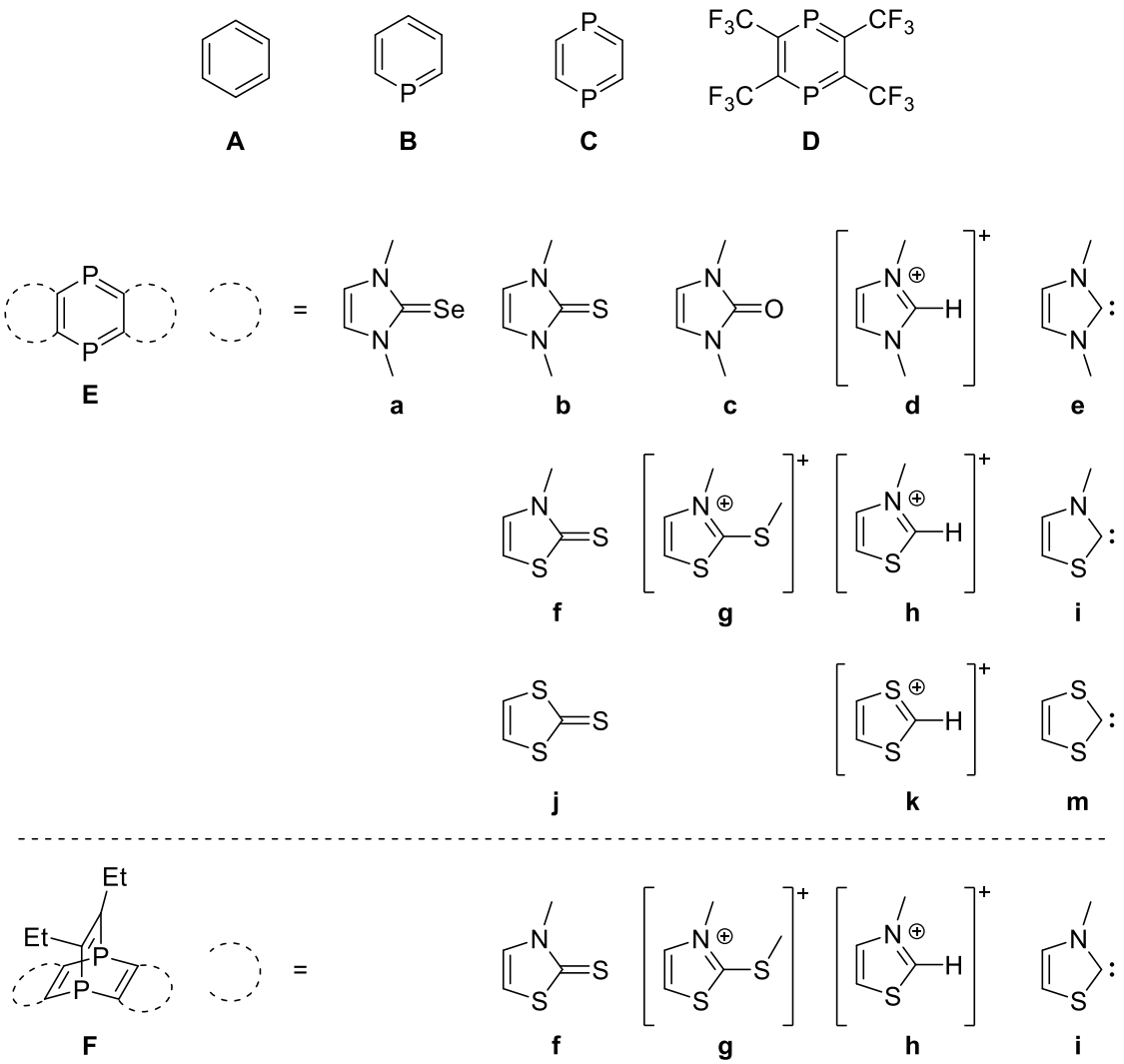


*Figure 54:* Lewis structures of benzene **A**, phosphinine **B**, mono- and tricyclic 1,4-diphosphinines **C,D,Ea–m**, and 1,4-diphosphabarrelenes **Ff–i**.

The study focused mainly on state of the art $\int NICS^{SOM}_{\pi,zz}$ and 2D XY-$NICS^{SOM}_{\pi,zz}$ calculations, although other aromatic indices, namely, HOMA and $ELF_{\pi}$, were also taken into account. While a detailed report on applied theoretical methods can be found in section 5.5, structures were optimised at the TPSS-D3BJ/def2-TZVP($CPCM_{THF}$) level of theory and single point energies were computed at PW6B95-D3BJ/def2-QZVP($CPCM_{THF}$). NICS values were calculated at B3LYP-D3/def2-TZVPP. In accordance to the methodology reported by Stanger,[28,29] a minimum distance of dummy atoms to the ring plane was determined due to the absence of so-called off-centre effects at this distance when performing XZ and YZ scans for parent-diphosphinine **C** (section 7.2, Figure 69). This distance was found to be 2 Å, thus, $NICS^{SOM}_{\pi,zz}$ scans in Z direction were done at distances of 2–6 Å to the ring plane(s) and then integrated from 0 to infinity. For a better comparability, all $\int NICS^{SOM}_{\pi,zz}$ values are discussed relative to benzene **A**. The absolute values as well as correlation coefficients are given in section 7.2.

### 3.8.1 Z-$NICS^{SOM}_{\pi,zz}$ scans

Although the aromaticity of reported 1,4-diphosphinines has been studied in terms of NICS by Nyulászi and Streubel,[59,99,100,104] all studied structures (Figure 54) were reinvestigated to ensure a systematic study. Firstly, $\int NICS^{SOM}_{\pi,zz}$ values of monocyclic **A–D** and the experimentally accessed tricyclic **Ea,b,f,j** were calculated (Figure 55; section 7.2, Table 13). While the three parent-systems of benzene **A**, phosphinine **B** and 1,4-diphosphinine **C** show very similar $\int NICS^{SOM}_{\pi,zz}$ values (>97%), all experimentally confirmed 1,4-diphosphinines possess lower aromaticity. Both monocyclic **D** and the imidazole-based tricyclic **Ea,b** display $\int NICS^{SOM}_{\pi,zz}$ values of close to 90%.

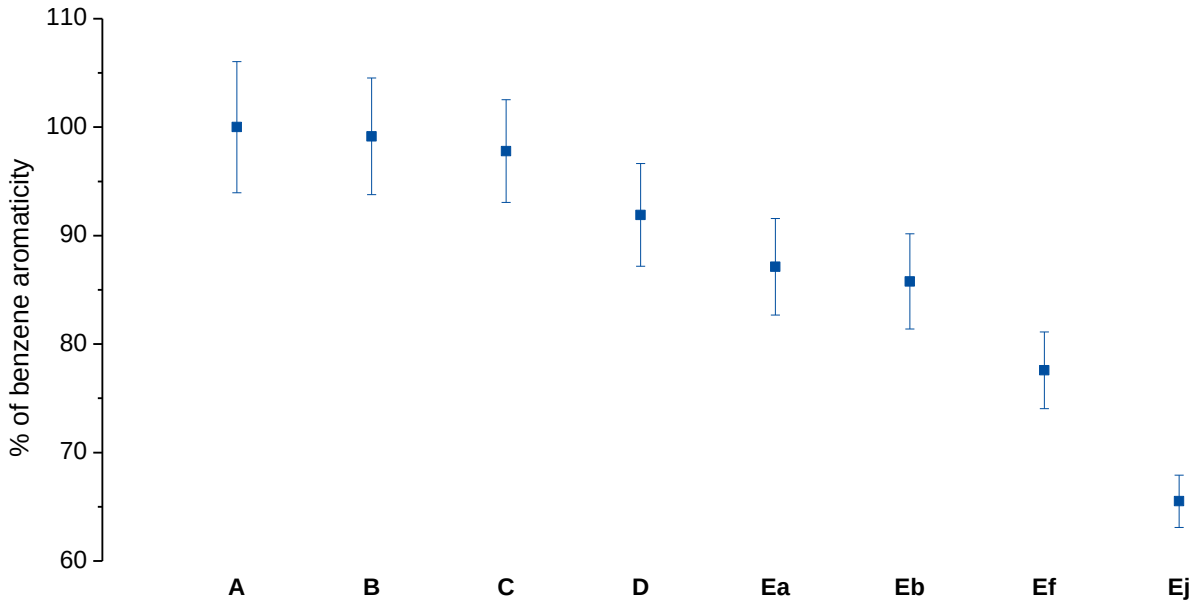


*Figure 55:* $\int NICS^{SOM}_{\pi,zz}$ values of monocyclic **A–D** and tricyclic **Ea,b,f,j**.

An increase in sulfur content in the fused five-membered rings leads to a significant drop in aromaticity, **Ef** showing a value of 77.6% relative to benzene, while only 65.5% was found for the dithiol-based **Ej**. This finding points towards a significant effect of the adjacent heterocycles on the aromaticity of the central 1,4-diphosphinine rings, hence, these five-membered rings were studied in more detail. In addition to the central rings, $NICS^{SOM}_{\pi,zz}$ scans were done for the fused five-membered rings of **Ea,b,f,j** as well as the free heterocycles **a,b,f,j**. Again, all $\int NICS^{SOM}_{\pi,zz}$ values were compared to the value of benzene (Table 7). Notably, the correlation coefficients of the exponential fits of these five-membered rings had significantly lower values (0.658–0.946) than the ones obtained during fitting for the 1,4-diphosphinine rings (≥0.996) and in the case of thiazole-based **Ef** the exponential fitting failed completely. Comparing the other three tricyclic systems, free and fused five-membered rings display similar $\int NICS^{SOM}_{\pi,zz}$ values for a given system, the only significant deviation between the two being found for **Ej**, where fusing the dithiole-2-thione to a central 1,4-diphosphinine leads to an increase in antiaromatic behaviour, *i.e.*, positive $\int NICS^{SOM}_{\pi,zz}$ values. In general, all values of the fused heterocycles lie close to zero, indicating only small (anti-) aromatic or non-aromatic properties. Yet, the trend of more positive values for a higher sulfur content which was found for the central rings is mirrored in the five-membered rings, both fused and free.

*Table 7:* $\int NICS^{SOM}_{\pi,zz}$ values for fused and free five-membered rings of **Ea,b,f,i**.

| | Fused | | Free | |
|---|---|---|---|---|
| | $\int NICS^{SOM}_{\pi,zz}$ / ppm·Å | % of benzene aromaticity | $\int NICS^{SOM}_{\pi,zz}$ / ppm·Å | % of benzene aromaticity |
| **A** | — | — | −78.7 ± 4.8 | 100 |
| **Ea** | −9.9 ± 1.0 | 12.6 | −11.2 ± 2.0 | 14.2 |
| **Eb** | −9.8 ± 1.6 | 12.4 | −9.1 ± 1.8 | 11.5 |
| **Ef** | —[a] | —[a] | 3.7 ± 0.4 | −4.7 |
| **Ej** | 18.5 ± 5.7 | −23.6 | 5.4 ± 0.4 | −6.9 |

[a]no exponential fit to the calculated values could be applied

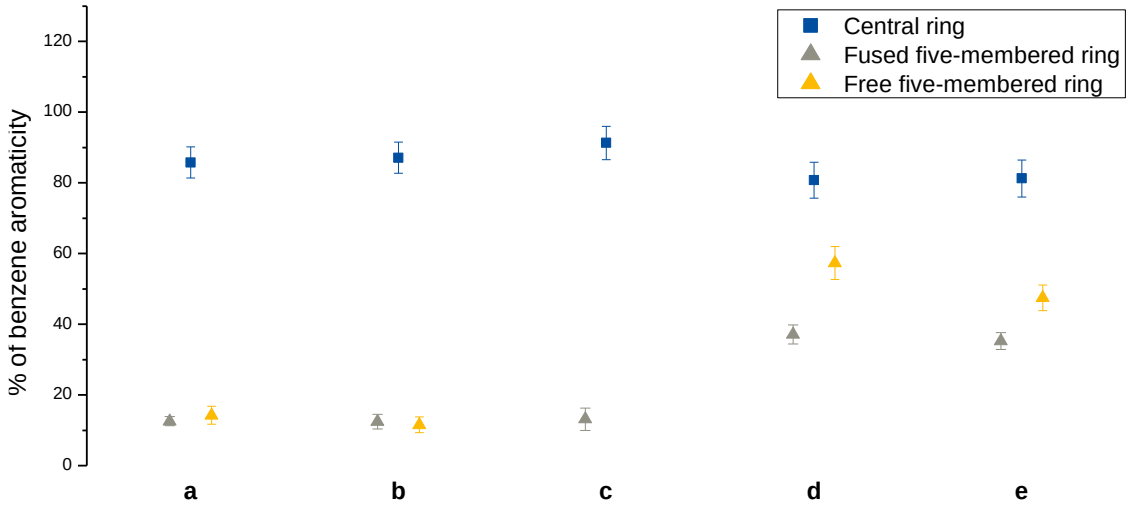


*Figure 56:* $\int NICS^{SOM}_{\pi,zz}$ values of central rings (blue) and fused five-membered rings (grey) of **Ea–e** as well as free **a–e** (yellow).

The differences in reactivity between systems like **Ea** and **Eb** prompted a study aimed at the effect of the $C^2$-substitution on the overall aromaticity of these tricyclic 1,4-diphosphinines. Consequently, the experimentally known **Ea,b** were supplemented by imidazole-2-ketone-based **Ec**, imidazolium-based **Ed** and NHC-based **Ee** (Figure 54). $\int NICS^{SOM}_{\pi,zz}$ values of the central 1,4-diphosphinine rings as well as the fused and free five-membered heterocycles were calculated for all systems (Figure 56; section 7.2, Table 14). Although the central rings of **Ea–e** display somewhat similar $\int NICS^{SOM}_{\pi,zz}$ values, the three chalcogen-substituted derivatives **Ea–c** are slightly more aromatic than **Ed,e** (86–91% compared to ~80% relative to benzene). A more distinct difference can be found between **Ea–c** and **Ed,e** in the fused cycles: **Ea–c** have almost non-aromatic fused five-membered rings with values below 20% relative to benzene, indicating that the double bonds in their backbones mostly contribute to the ring current of the 1,4-diphosphinine ring. In contrast, a significant degree of aromaticity of almost 40% of that of benzene can be found in the imidazolium- and NHC-rings of **Ed,e**. This behaviour can also be seen to an even larger extent in the free heterocycles (no exponential fit could be applied in the case of **c**). The $\int NICS^{SOM}_{\pi,zz}$ values of free **d** and **e** are—at 57% and 47%, respectively—even higher than those of their fused counterparts. This fact points towards the backbone-double bonds of the fused heterocycles contributing to both the central and the fused rings of **Ed,e**. The slightly reduced aromaticity of their 1,4-diphosphinine rings compared to the chalcogen-substituted **Ea–c** corroborates this theory as shared double bonds would reduce the ring current of both the central and the fused ring systems compared to their individual counterparts.

The largely different aromatic situation of **Ed,e** compared to **Ea–c** prompted an investigation into the effect of introducing sulfur into the outer rings of these carbenium- and carbene-containing systems. Hence, thiazole-based **Eh,i** and dithiole-based **Ek,m** were compared to **Ed,e** (Figure 57; section 7.2, Table 14). Interestingly, while the aromaticity of the central rings of **Ed,e** was previously discussed as being diminished compared to that of chalcogen-substituted derivatives, the $\int NICS^{SOM}_{\pi,zz}$ values of thiazole-based **Eh,i** are similar to the one of the thione **Ef** and those of dithiole-based **Ek,m** are higher than the $\int NICS^{SOM}_{\pi,zz}$ value of the thione **Ej**, indicating a similar or even enhanced central aromaticity of thiazolium-, dithiolium- or carbene-based **Eh,i,k,m** compared to the respective thiones **Ef,j**. On the other hand, all six fused five-membered heterocycles display a decrease in aromaticity compared to their free analogues, being in line with a shared ring current between all three individual cycles. The previously reported remarkably high degree of aromaticity of dithiolium **k** could be reproduced in this study.[142] Its fused counterpart, **Ek**, possesses a $\int NICS^{SOM}_{\pi,zz}$ value which is in line with the other examined derivatives. Unsurprisingly, in general the dithiole-carbene based **Em** is the system with the overall smallest ring current out of all six studied cation- and carbene-based derivatives, agreeing well with the previously found diminished aromaticity for higher sulfur content of the fused five-membered heterocycles.

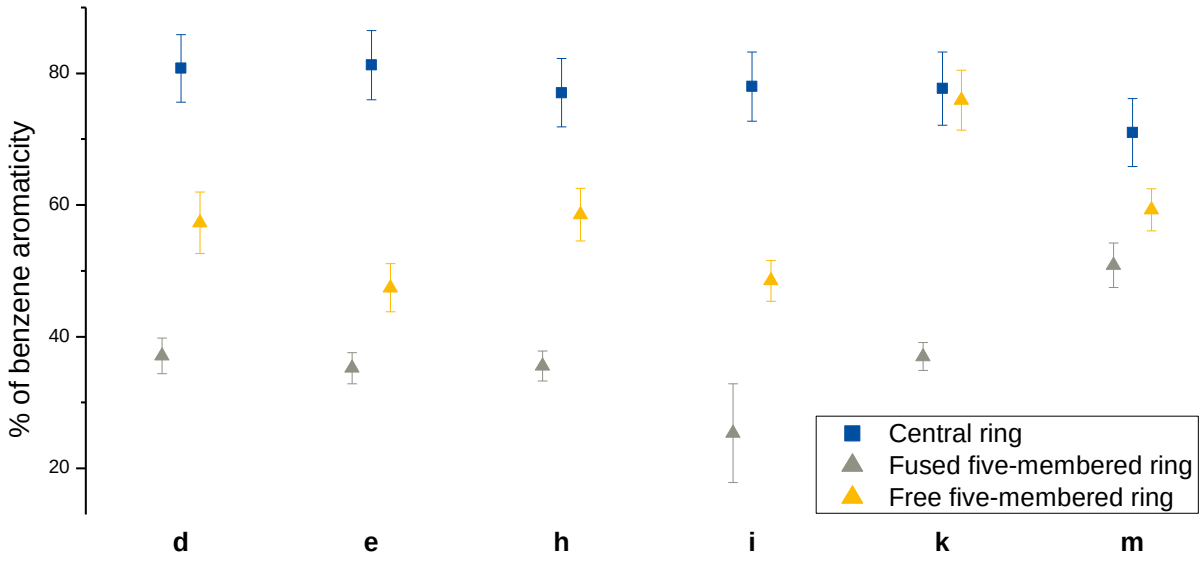


*Figure 57:* $\int NICS^{SOM}_{\pi,zz}$ values of central rings (blue), fused five-membered rings (grey) and free five-membered rings (yellow) of (**E**)**e,d,i,h,m,k**.

A general trend of cationic five-membered rings leading to global aromaticity was suspected, hence, a closer look was taken on the consequence of methylated and desulfurised 1,4-diphosphinines **Ef–i** and 1,4-diphosphabarrelenes **Ff–i** for the aromaticity of the central rings (of **Ef–i**) and the thiazole-rings in particular (Figure 58; section 7.2, Table 15, Table 16). With the previously discussed $\int NICS^{SOM}_{\pi,zz}$ values of both central and fused heterocycles of **Ef,h,i** being similar and in the expected range for these systems (Figure 58, blue, yellow), a large discrepancy to this range was found for the 1,4-diphosphinine of **Eg**. The central ring revealed a $\int NICS^{SOM}_{\pi,zz}$ value of 119.9% compared to benzene, making it significantly more aromatic than the latter. Conversely, the aromaticity in the fused heterocycle is low at only 16.2%, showing that—similar to the previously discussed situation in **Ea–c**—the backbone-double bond of the methylated thiazole-2-thione contributes mostly to the central ring's ring current, increasing its aromaticity and decreasing the one in the fused ring. This explanation is substantiated when comparing the fused heterocycles in **Ef–i** (Figure 58, yellow) to their free analogues (Figure 58, light blue). Again, more negative $\int NICS^{SOM}_{\pi,zz}$ values were obtained for the free thiazoles compared to the fused cycles in **Ef–i**, yet, the difference is considerably smaller in the case of methylated **g** than in the thiazolium **h** and carbene derivatives **i** (no exponential fit could be applied in the case of **Ef**). The values for thiazole rings fused to 1,4-diphosphabarrelenes in **Ff–i** (Figure 58, grey) generally lie in between those of the free heterocycles and the fused rings in **Ef–i**, albeit closer to **f–i**. Overall, the situation in **Ff–i** closely resembles the one of the free **f–i**. Understandably, this stems from the rather classical phosphane moiety in **Ff–i** compared to the low-valent phosphorus atoms in **Ef–i**, enabling a much higher contribution of the backbone-double bonds to the central rings of the latter, while isolating the five-membered heterocycles in the former.

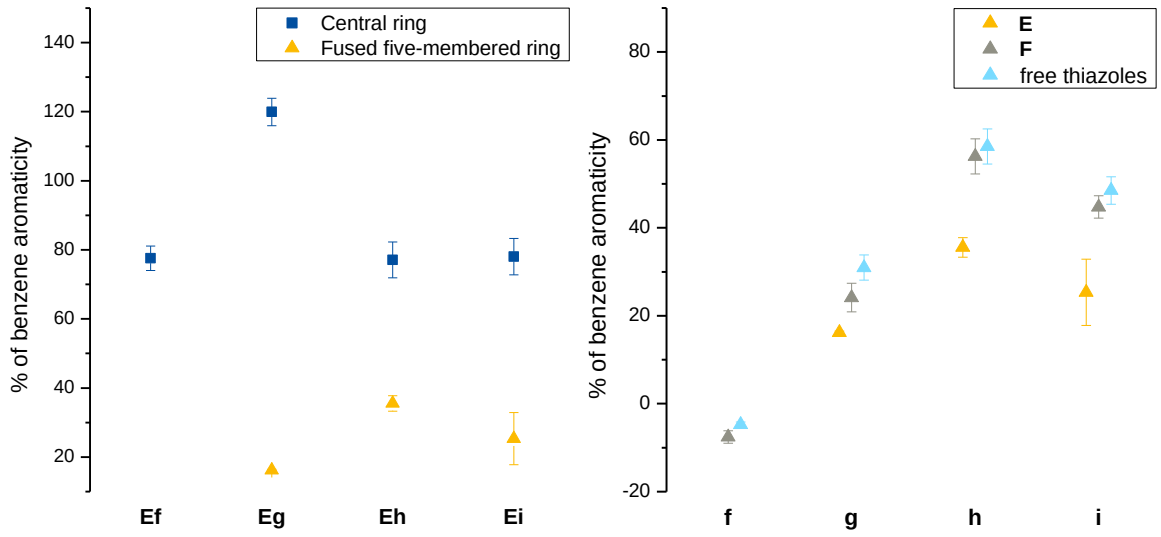


*Figure 58:* $\int NICS^{SOM}_{\pi,zz}$ values of central (blue) and fused (yellow) rings of **Ef–i** (left) and $\int NICS^{SOM}_{\pi,zz}$ values of fused and free five-membered heterocycles of **Ef–i** (yellow), **Ff–i** (grey) and **f–l** (light blue, right).

### 3.8.2 XY-NICS$^{SOM}_{\pi,zz}$ scans

$\int$ NICS$^{SOM}_{\pi,zz}$ values derived from Z-NICS$^{SOM}_{\pi,zz}$ scans give a good gauge for the aromaticity of a given ring in a molecule. However, when dealing with polycyclic systems, the concept of global aromaticity has to be taken into account, which is ill described by local Z-NICS$^{SOM}_{\pi,zz}$ scans along a single axis. Therefore, NICS$^{SOM}_{\pi,zz}$ scans were performed in both X and Y direction in order to get an understanding of the aromatic situation in the different polycyclic systems as a whole. While a similar procedure has been used for carbon-based monocyclic systems,[32] no two-dimensional study on NICS in phosphorus-containing heterocycles has been reported. Recently, 2D isochemical shielding contour plots (ISCP) of several main group three-membered heterocycles were published with the goal of evaluating ring strain energies in these heterocycles.[143] As previously discussed, a distance of 2 Å to the ring plane was determined to be able to obtain off-centre free NICS$^{SOM}_{\pi,zz}$ (section 7.2, Figure 69). Thus, this distance was chosen for all following XY-NICS$^{SOM}_{\pi,zz}$ scans (for a detailed description of theoretical methods see section 5.5).

The monocycles **A–D** were examined first (Figure 59). When compared to benzene **A**, all three P-containing systems correlate well on both a qualitative and quantitative level. A comparison of XY-NICS$^{SOM}_{\pi,zz}$ scans with $\int$ NICS$^{SOM}_{\pi,zz}$ values confirms the comparatively high degree of aromaticity in **A–C** and the somewhat weaker ring current of **D**, which can be deduced from the XY-NICS$^{SOM}_{\pi,zz}$ scans by a shallower minimum in the case of **D**, having a minimal value of −11.9 ppm as opposed to values below −13 ppm for **A–C**. Notably, even though a graphical interpretation of the minima of **B,C** suggests a higher degree of aromaticity than benzene, $\int$ NICS$^{SOM}_{\pi,zz}$ show a steeper curve for the latter, owing to the smaller ring size compared to **B,C**. Thus, the smaller but steeper minimum in **A** can lead to the interpretation of a weaker aromaticity even though **A–C** were shown to behave very similar to each other.

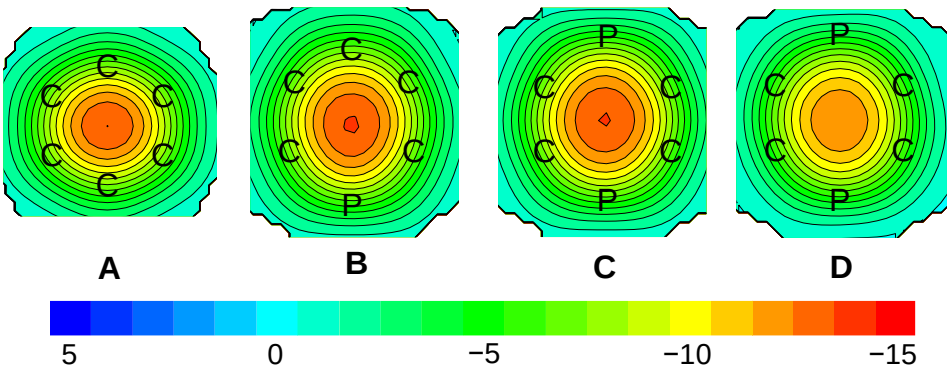


*Figure 59:* XY-NICS$^{SOM}_{\pi,zz}$ scans of benzene **A**, phosphinine **B**, as well as monocyclic 1,4-diphosphinines **C,D** (values in ppm).

XY- $NICS^{SOM}_{\pi,zz}$ scans were also performed for all other investigated systems, *i.e.*, 1,4-diphosphinines **Ea–m** (Figure 60), five-membered heterocycles **a–m** (Figure 61) and 1,4-diphosphabarrelenes **Ff–i** (Figure 62). Examination of the central 1,4-diphosphinine rings of **Ea–m** corroborates the trends found in the $\int NICS^{SOM}_{\pi,zz}$ studies. A higher sulfur content in the fused heterocycles leads to a shallower minimum for all experimentally confirmed systems **Ea,b,f,j** (Figure 60). This trend is broken for imidazolium-, thiazolium-, dithiolium- and carbene based **Ed,e,h,l,k,m**, in which case very similar behaviours in the central ring were observed. The only exception to this is the previously discussed **Em**, possessing a minimum of −10.0 ppm as opposed to around −11 ppm for the other derivatives. Interestingly, all systems possessing a $\pi$ bond in the $C^2$ position, show a paratropic contribution around the $C^2$ atom. This effect is particularly prominent for the thiazole- and dithiole-based thiones **Ef,j**, where a strong paratropic current is not only located around $C^2$ but also spread out to the two heteroatoms. The presence of two nitrogen atoms in the five-membered ring (**Ea–c**) seems to suppress this paratropic current to some extent. In agreement with $\int NICS^{SOM}_{\pi,zz}$ values, this contribution also affects the central rings, decreasing their aromaticity. On the other hand, the involvement of the backbone-double bonds of the fused heterocycles into the central delocalisation, the 1,4-diphosphinine rings also influences the outer rings.

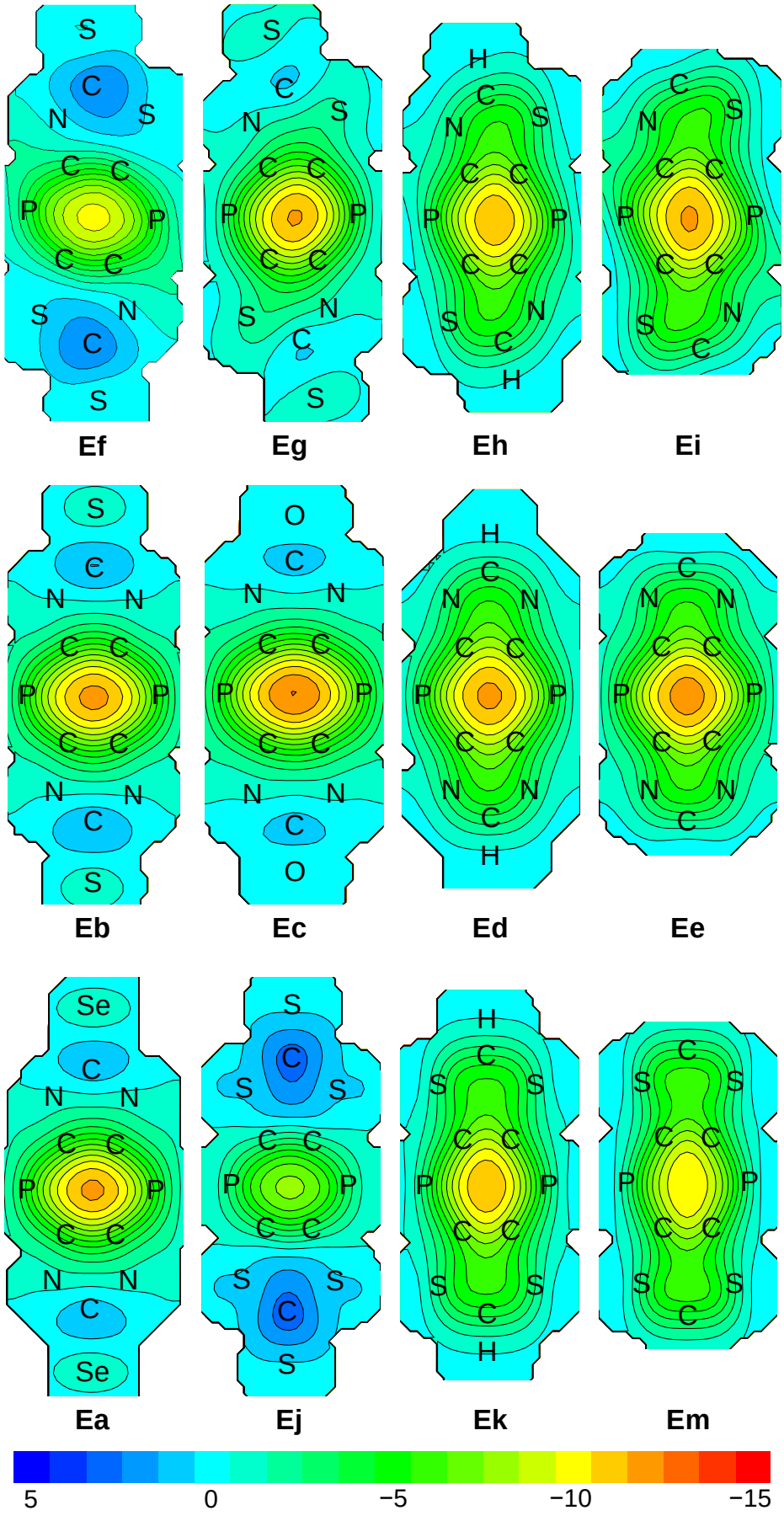


*Figure 60:* XY-NICS$^{SOM}_{\pi,zz}$ scans of tricyclic 1,4-diphosphinines **Ea–m** (values in ppm).

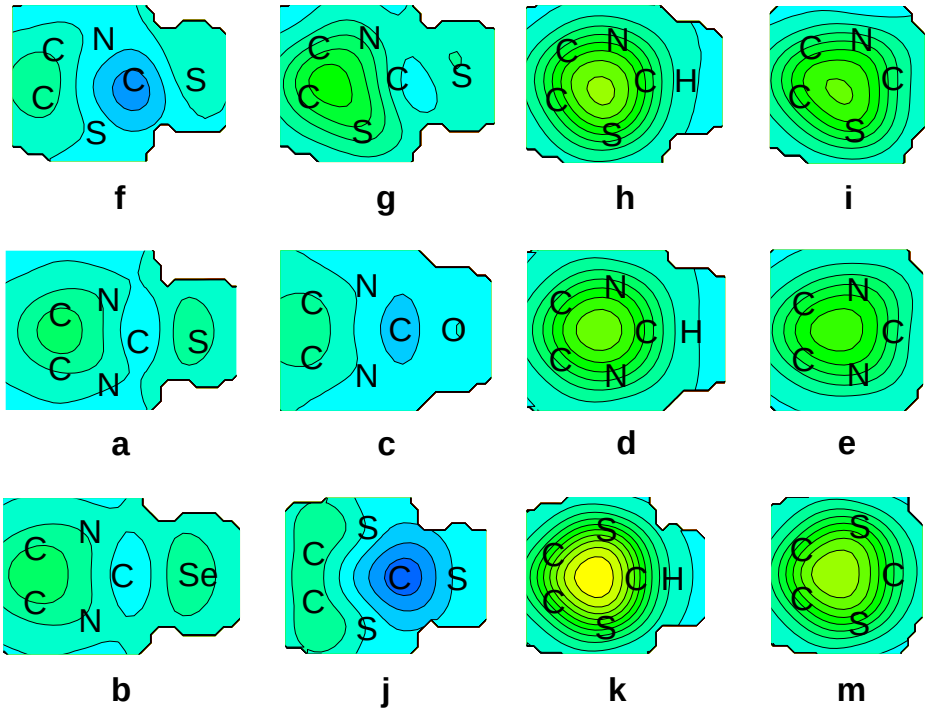


*Figure 61:* XY-NICS$^{SOM}_{\pi,zz}$ scans of five-membered heterocycles **a–m** (values in ppm).

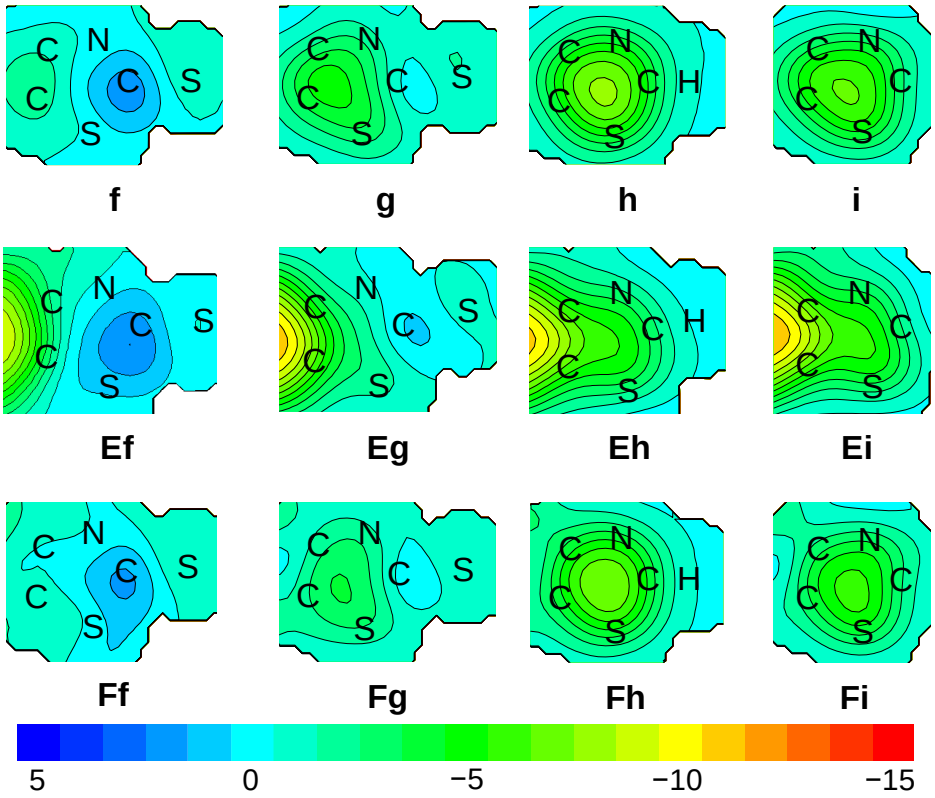


*Figure 62:* XY-NICS$^{SOM}_{\pi,zz}$ scans five-membered heterocycles **f–i**: free (top) and fused (to a 1,4-diphosphinine: **E**, centre; to a 1,4-diphosphabarrelene: **F** bottom; values in ppm).

As a result, the central well is much less extended towards the five-membered heterocycles for a higher sulfur content, resulting in a further increase in $NICS^{SOM}_{\pi,zz}$ values above the outer rings. Notably, the doubly methylated thiazole-based system **Eg** closely resembles the imidazole-based **Ea–c** with a very small paratropic contribution at $C^2$. Yet, the central aromatic well is even more diffuse in this case, reaching out into parts of the outer heterocycles and partially resembling a global aromaticity across the whole molecule. True global aromaticity is only observed for the carbenium- and carbene-based derivatives **Ed,e,h,l,k,m**, which all show negative $NICS^{SOM}_{\pi,zz}$ values throughout all three heterocycles, thus possessing a global ring current. A similar trend was recently observed in anisotropy of the current density (AICD) and $NICS(1)_{z,z}$ investigations on 2-aryl-substituted imidazolium-based 1,4-diphosphinines.[103] These findings allow the conclusion of a global aromaticity only occurring on carbenium- and carbene-fused 1,4-diphosphinines, while chalcogen-substitution at $C^2$ suppresses a global ring current and only leads to a local current in the central 1,4-diphosphinine.

For a more complete picture, tricyclic **Ea–m** were also compared to the free five-membered rings **a–m** using XY-$NICS^{SOM}_{\pi,zz}$ scans (Figure 61). In general, free **a–m** show the same trends as the fused heterocycles in **Ea–m**. The carbenes **e,i,m** and their related cations **d,h,k** show an aromatic minimum, with **k** having the most negative $NICS^{SOM}_{\pi,zz}$ values and agreeing well with the results from $\int NICS^{SOM}_{\pi,zz}$ studies. On the other hand, heterocycles bearing a $\pi$ bond at $C^2$ show a non-aromatic behaviour, with high paratropic contributions around the $C^2$ atom for a higher endocyclic sulfur content. This paratropic current may be the result of so-called Y-aromaticity, a phenomenon observed in Y-shaped molecules which show greater stability than was initially expected.[144] However, the obtained data are not sufficient to conclusively verify this effect in the examined systems. Interestingly, while **Eg** largely possessed local aromaticity in the central ring, free **g** shows a minimum inside the ring, indicating some degree of aromaticity, although a small paratropic current around the $C^2$ position can be seen. This speaks for at least some double bond character in the exocyclic $C^2$-S bond, approaching the situation in **f**. A state between non-aromatic **f** and aromatic **h** corresponds well with tricyclic **Eg**, which can also be seen as an intermediate between **f** and **h**. In the non-aromatic chalcogen-substituted **Ea–c,f,j**, the lowest $NICS^{SOM}_{\pi,zz}$ values can be found off-centre towards the respective backbone-double bond. Yet, even though these values are negative, they do not indicate ring currents but rather the local $\pi$-electron density of said double bonds. Coupled with the paratropic contributions around $C^2$ for higher S-content in the ring, it becomes apparent through XY-$NICS^{SOM}_{\pi,zz}$ scans that the overall positive values found in $\int NICS^{SOM}_{\pi,zz}$ investigations for these systems do not suggest antiaromatic behaviour, but rather a combination of the two different local effects. An additional trend can be found when examining

the imidazole-based chalcogen-substituted **a–c**, since the diamagnetic current around the backbone-double bonds is shifted more towards the centre of the ring for heavier chalcogens. This leads to negative $NICS^{SOM}_{\pi,zz}$ values throughout most of the ring in the case of **a**, while **c** is likely better described by a cyclic urea derivative with a localised and isolated backbone-double bond. Compared to the tricyclic **Ea–c**, the difference between the free five-membered heterocycles is much larger, as the annelation to the 1,4-diphosphinine leads to a delocalisation of the backbone double bonds into the central ring in all three cases.

As for the Z-$NICS^{SOM}_{\pi,zz}$ scans, the outer, fused heterocycles of 1,4-diphosphabarrelenes **Ff–i** were also investigated by XY-$NICS^{SOM}_{\pi,zz}$ scans (Figure 62). $\int NICS^{SOM}_{\pi,zz}$ values suggested very similar ring currents between **Ff–i** and the free analogues, while the outer rings of 1,4-diphosphinines **Ef–i** showed much lower $\int NICS^{SOM}_{\pi,zz}$ values. This is reflected in the XY-$NICS^{SOM}_{\pi,zz}$ scans, with very similar pictures of **Ff–i** and **f–i**, almost on a quantitative level. The 1,4-diphosphabarrelenes generally show a higher distortion than the free heterocycles, which is a result of the highly complex structure beyond the backbone of the five-membered rings of **Ff–i** as opposed to the hydrogen substitution in **f–i**. **Ef** and **Eg** possess higher paratropic contributions around C2, thus, yielding higher $\int NICS^{SOM}_{\pi,zz}$ values than **f,g** and **Ff,g**. As previously discussed, the comparatively diminished aromaticity of the outer rings of the two globally aromatic derivatives **Eh,i** is a result of the backbone-double bond being shared between the central and fused cycles, reducing the strength of the individual ring currents but allowing a global one. All in all, the performed XY-$NICS^{SOM}_{\pi,zz}$ scans of **Ff–i** in comparison to **Ef–i** and **f–i** correspond closely with the obtained $\int NICS^{SOM}_{\pi,zz}$ values of these compounds.

### 3.8.3 Structural (HOMA) and electronic ($ELF_\pi$) parameters

As the use of a single criterion can be misleading when gauging the aromaticity of a given molecule, the scope of this study was expanded beyond the magnetics-based NICS and two different parameters were also taken into account: the geometry-based HOMA and the electronics-based $ELF_\pi$. For a better visualisation, the latter was split into $ELF_\pi$ bifurcation values for each ring of the investigated systems, obtained by the average of all individual bonds, as well as $ELF_\pi$ plots. These plots were generated at a distance of 1 Å above the plane as XZ and YZ plots for **C** showed enough contribution of the 2p-orbitals of carbon with the 3p-orbitals of phosphorus.

Expectedly, the monocyclic systems **A–D** were found to be close to each other both in HOMA and $ELF_\pi$ analyses (section 7.2, Table 17, Table 18). Yet, although the $ELF_\pi$ bifurcation values of parent phosphinine **B**, parent 1,4-diphosphinine **C** and $CF_3$-substituted **D** all show a higher aromaticity than benzene, having values of 101% relative to **A**, especially the HOMA value of

**D** drops significantly to 77.8%, indicating a considerable structural change of the ring compared to **A**. Interestingly, when comparing the different tricyclic 1,4-diphosphinines **Ea–m**, both HOMA and $ELF_\pi$ become less sensitive, giving HOMA values between 72 and 80% and $ELF_\pi$ bifurcation values between 85 and 93% for all 12 investigated systems. In the case of $ELF_\pi$. While mostly very similar, 2D- $ELF_\pi$ plots of **Ea–e** show an interesting deviation of imidazolium-based **Ed** from the derivatives with different $C^2$-substitutions (Figure 63), as a comparatively high contribution can be found around the $C^2$-atom. A similar situation is found in the carbene-based **Ee**, albeit less pronounced. Yet, this effect can explain the global aromaticity found for **Ed,e** in XY-$NICS^{SOM}_{\pi,zz}$ studies, as a high $\pi$-contribution across the whole molecule promotes $\pi$-delocalisation.

When comparing the different carbenium- and carbene-based **Ed,e,h,i,k,m**, HOMA, $ELF_\pi$ and $\int NICS^{SOM}_{\pi,zz}$ are very similar to each other, with $ELF_\pi$ showing the highest values relative to benzene (Table 8). Although a decreasing trend with further incorporation of sulfur into the fused heterocycles is found in $\int NICS^{SOM}_{\pi,zz}$, while a small increase was found in HOMA calculations, all three methods give results in the same magnitude between 70 and 95%.

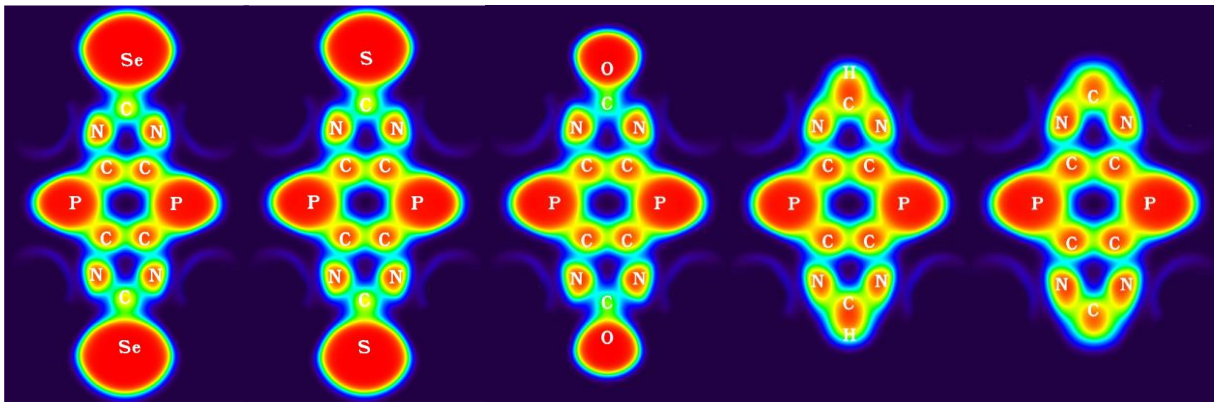


*Figure 63:* 2D-$ELF_\pi$ plots of **Ea–e** (arbitrary units; for better visibility, methyl groups are omitted).

*Table 8:* HOMA, $ELF_\pi$ bifurcation and $\int NICS^{SOM}_{\pi,zz}$ values of carbenium ions **Ed,h,k** and carbenes **Ee,i,m**.

| | HOMA<br>% of $C_6H_6$ | $ELF_\pi$<br>% of $C_6H_6$ | $\int NICS^{SOM}_{\pi,zz}$<br>% of $C_6H_6$ |
|---|---|---|---|
| **Ed** | 73.7 | 94.0 | 80.8 |
| **Ee** | 74.3 | 88.0 | 81.2 |
| **Eh** | 76.3 | 91.0 | 77.1 |
| **Ei** | 77.5 | 92.1 | 78.0 |
| **Ek** | 80.4 | 92.5 | 77.7 |
| **Em** | 74.4 | 93.3 | 71.0 |

Examining the four experimentally accessed tricyclic 1,4-diphosphinines **Ea,b,f,j**, HOMA and $ELF_\pi$ bifurcation values go against $\int NICS^{SOM}_{\pi,zz}$ as they show an almost unaltered and slightly increasing delocalisation in the central ring for a higher sulfur content, $\int NICS^{SOM}_{\pi,zz}$ showing the opposite trend of a significantly decreasing ring current (Figure 64). The increase in aromaticity shown by HOMA and $ELF_\pi$ likely is a result of the smaller orbital overlap of the lone pairs of sulfur compared to nitrogen, isolating the central ring and, thus increasing delocalisation in this ring (Figure 65). A possible explanation for $\int NICS^{SOM}_{\pi,zz}$ decreasing upon introduction of sulfur atoms in the outer rings can be the previously discussed effect of paratropic currents around the $C^2$ position, arbitrarily changing $NICS^{SOM}_{\pi,zz}$ to more positive values in their vicinity.

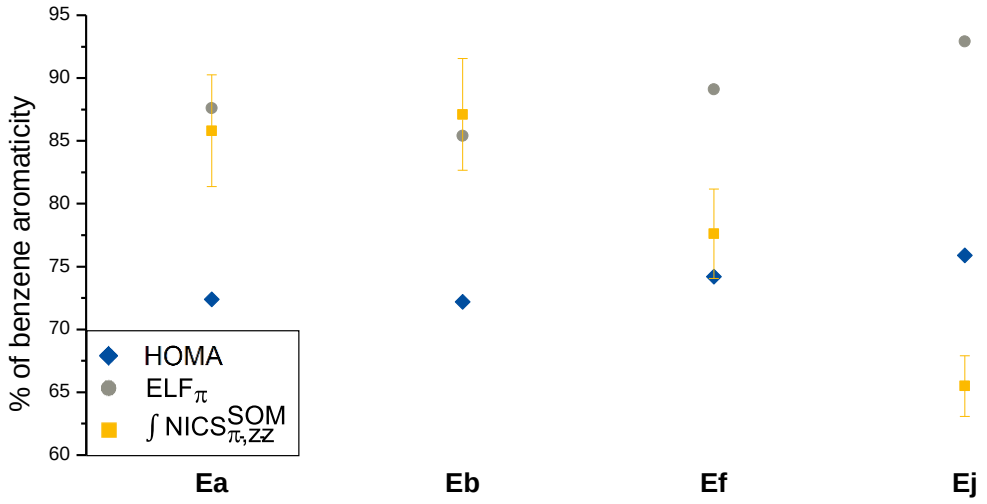


*Figure 64:* HOMA (blue), $ELF_\pi$ (grey) and $\int NICS^{SOM}_{\pi,zz}$ (yellow) values of the central rings of tricyclic 1,4-diphosphinines **Ea,b,f,j**.

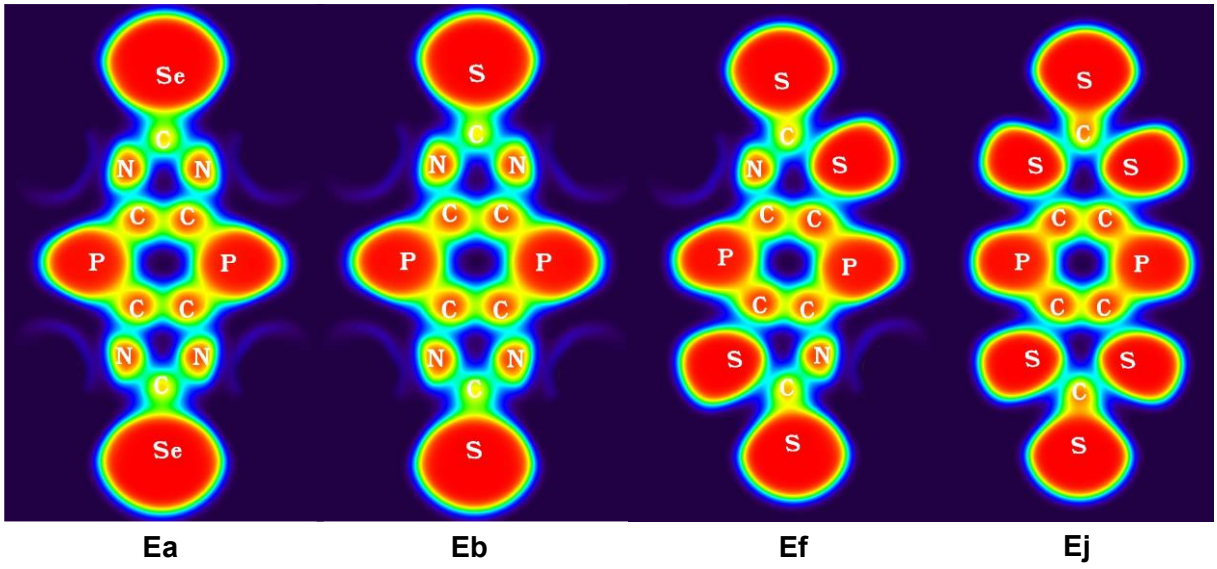


*Figure 65:* 2D-$ELF_\pi$ plots of **Ea,b,f,j** (arbitrary units; for better visibility, methyl groups are omitted).

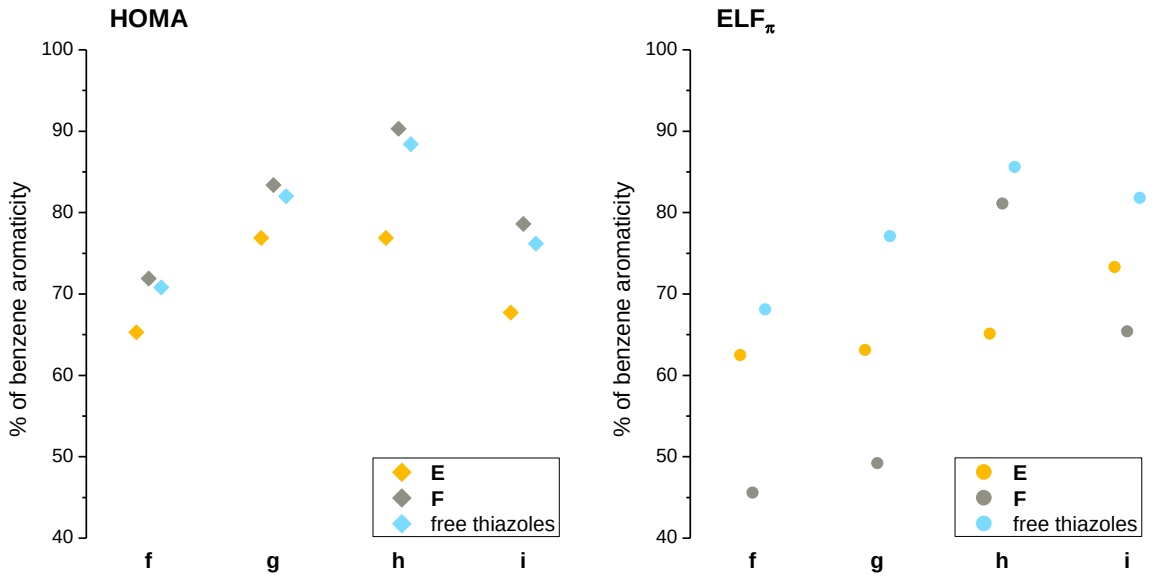


*Figure 66:* HOMA (left) and ELF$_\pi$ bifurcation values (right) of **Ef–i** (yellow), **Ff–i** (grey) and free **f–i** (light blue).

When studying HOMA and ELF$_\pi$ values of 1,4-diphosphabarrelenes **Ff–i** in relation to 1,4-diphosphinines **Ef–i** and free **f–i**, a different picture was observed: HOMA and ELF$_\pi$ differed considerably for all three structural motifs (HOMA: Figure 66, left; ELF$_\pi$: Figure 66, right). Although generally giving smaller values, $\int$ NICS$^{SOM}_{\pi,zz}$ studies largely agreed with the trend in HOMA values of the most aromatic compounds being the thiazolium systems **Eh**, **Fh** and **h** (compare Figure 58, right). ELF$_\pi$ did not show any clear trends between **E**, **F** and the free heterocycles. Even though bifurcation values of free **f–i** seem to follow the trend observed in $\int$ NICS$^{SOM}_{\pi,zz}$ and HOMA, **Ef–i** should increase in aromaticity from **Ef** to **Ei** according to ELF$_\pi$. The values of **Ff–i** do not show any pattern, a likely cause for this being the huge deviation from planarity in the 1,4-diphosphabarrelenes. This leads to highly complex molecular orbitals and a clean dissection between $\sigma$- and $\pi$-symmetric orbitals is almost impossible. Thus, the validity of ELF$_\pi$ remains highly questionable and HOMA and $\int$ NICS$^{SOM}_{\pi,zz}$ seem to be the more reliable methods in this case.

In general, both Z- and XY-NICS$^{SOM}_{\pi,zz}$ studies seem to be more sensitive towards changes in the ring current than HOMA and ELF$_\pi$ analyses. All in all, the three methods agree reasonably well with each other, showing a local aromaticity in the 1,4-diphosphinine rings of the experimentally confirmed **Ea,b,f,j**, as well as the hypothetical **Ec**. Conversely, the carbenium- and carbene-based **Ed,e,h,l,k,m** display a global aromaticity across the whole tricyclic system. The doubly methylated **Eg** is a borderline case, where the C$^2$-sulfur atoms appear to suppress global aromaticity to some extent. When it comes to 1,4-diphosphabarrelens **Ff–i**, the outer fused heterocycles may be seen as independent systems that closely resemble the situation in their free analogues **f–i**.

# 4 SUMMARY

Although known since the 1970s,[97] 1,4-diphosphinines remain a scarcely explored field of research. With only five isolated, tricyclic derivatives based on nitrogen- and/or sulfur-containing heterocycles,[59,99–101,103] studies on their reactivity as a whole and their relation to differently substituted derivatives go a long way in understanding the properties of both the heteroaromatic 1,4-diphosphinine ring as well as the effect of the outer, fused heterocycles.

The work of this Ph.D. thesis focused on P- and S-centred reactivity studies of a thiazole-2-thione based 1,4-diphosphinine, exploring both (cyclo-)addition and oxidation reactions at the two phosphorus centres as well as the quest for P-bridged, thiazole-based bis-carbenes and the oligomerisation of these tricyclic scaffolds.

The studies were divided into three parts. The first part concentrated on P-centred reactivity. 1,4-diphosphinine **1** was treated with different reagents to achieve the formation of 1,4-dihydro-1,4-diphosphinines **2,4a** (Scheme 53). Significant differences to the synthetically more explored imidazole-2-thione based 1,4-diphosphinine **LVI** were found as **1** reacted more readily with diphenyl disulfane, allowing a reaction at much lower temperatures, while the silylation using trimethylsilyl chloride showed signs of the formation of **4a**, but scaling up the reaction to allow isolation likely resulted in a very different reactivity at the thione moieties. A control experiment using the imidazole-based **LVI** led to the expected formation of the respective 1,4-addition product, giving a first hint on the significance and influence of sulfur atoms in the fused five-membered rings of **1** compared to **LVI**.

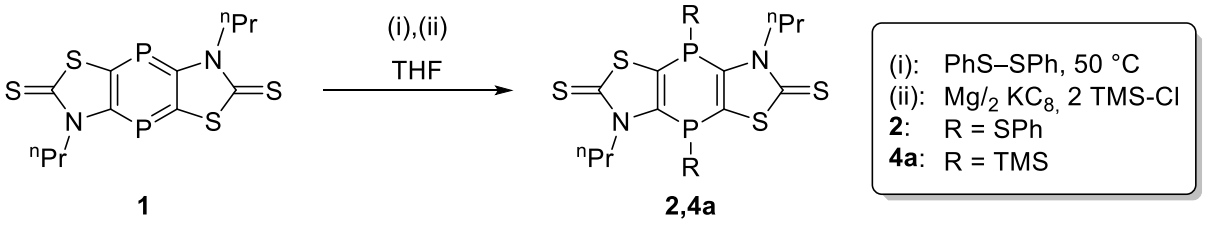


*Scheme 53:* Synchronous 1,4-additions to 1,4-diphosphinine **1**.

Apart from synchronous 1,4-addition reactions, **1** was reacted with different nucleophiles to form the zwitterionic and anionic 1,4-dihydro-1,4-diphosphinines **5a–e**, expanding the scope of these mono anions beyond the only previously known derivative **5c** (Scheme 54). In a second step, methyl iodide and trimethylsilyl chloride were added to **5a–e** to furnish **6a–e** and **9a–e**, respectively. Interestingly, while the carbene-substituted **5a,b** showed a remarkable proneness to form back 1,4-diphosphinine **1**, which was energetically confirmed by theoretical studies.

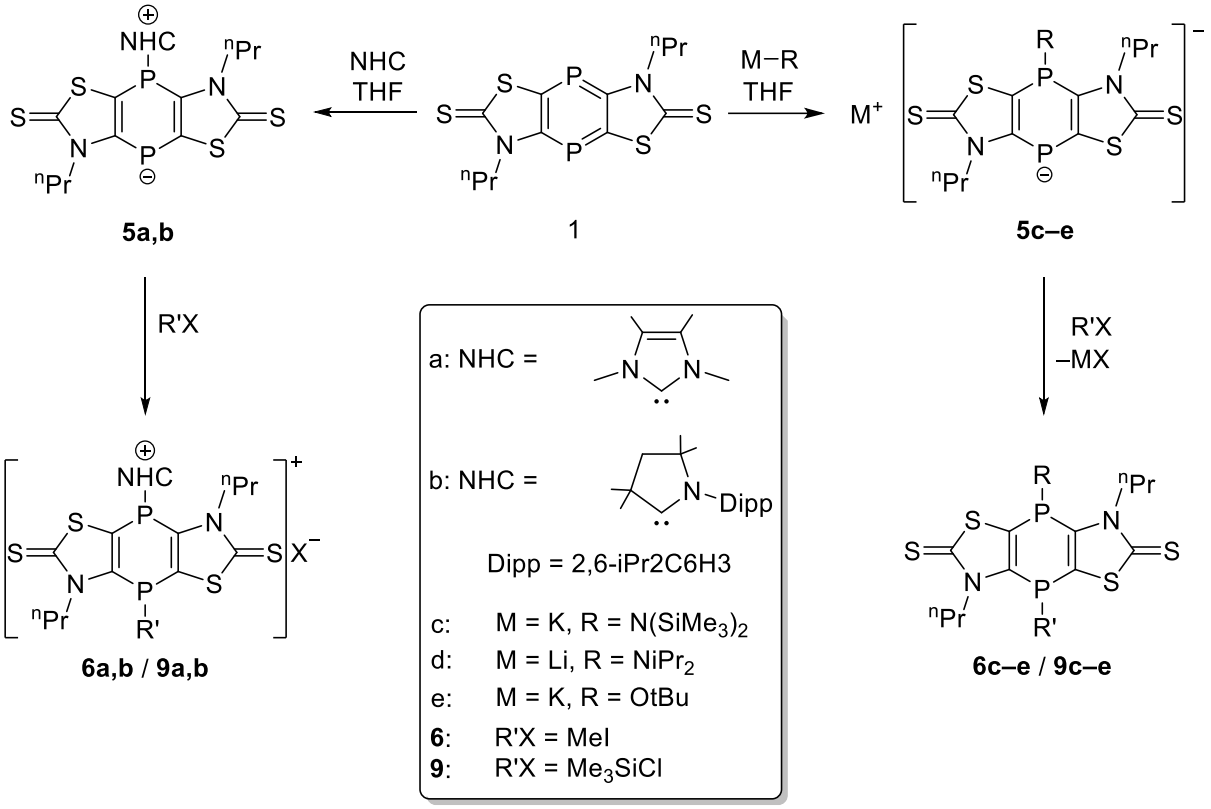


*Scheme 54:* Sequential 1,4-additions of 1,4-diphosphinine **1** via the synthesis of anionic **5a–f** followed by methylation and silylation

Nevertheless, **6a,c,e** were detected in solution and **6c** could be isolated and fully characterised. In contrast, the formation of **9a–e** could not be confirmed.

Performing an analogous sequential addition using lithium hydroxide led to the formation of the remarkable P(III)/P(IV) mixed-valent product **5f'**, which was found to react with acids, forming back **1**. Theoretical investigations allowed the proposal of the structure of **5f'** and a reaction mechanism of the reaction with HCl, forming **1** via **7b** and **8b** (Scheme 55).

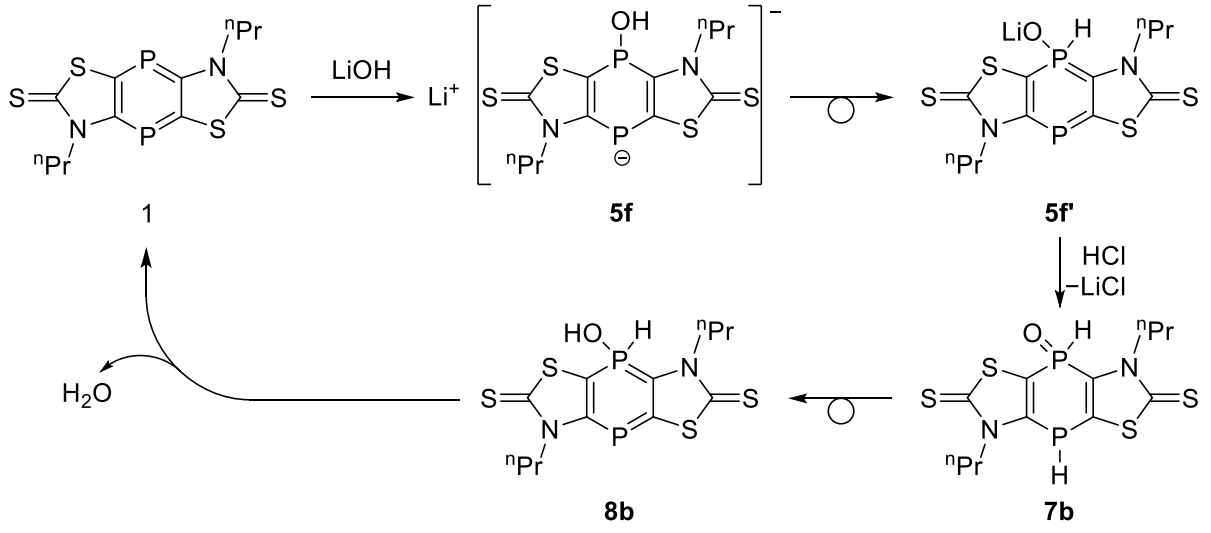


*Scheme 55:* Proposed mechanism of the formation of **5f'** and its reaction with HCl.

Apart from 1,4-additions, [4+1]-cycloaddition reactions of **1** were investigated (Scheme 56). Interestingly, the addition of carbon tetrachloride did not yield the expected 1,4-diphosphanorbornadiene **12** but the product of a C-Cl bond activation, *i.e.*, a 1,4-addition product analogous to **6**. While the addition of silylenes, germylenes and sulfur did not furnish **13**, **15** or **16**, the 7-metalla-1,4-diphosphanorbornadiene **14a** (M = Ga) could be isolated. Conversely, NacNacAl appeared to react with both the central ring as well as the thione moieties, leading to unknown asymmetric products.

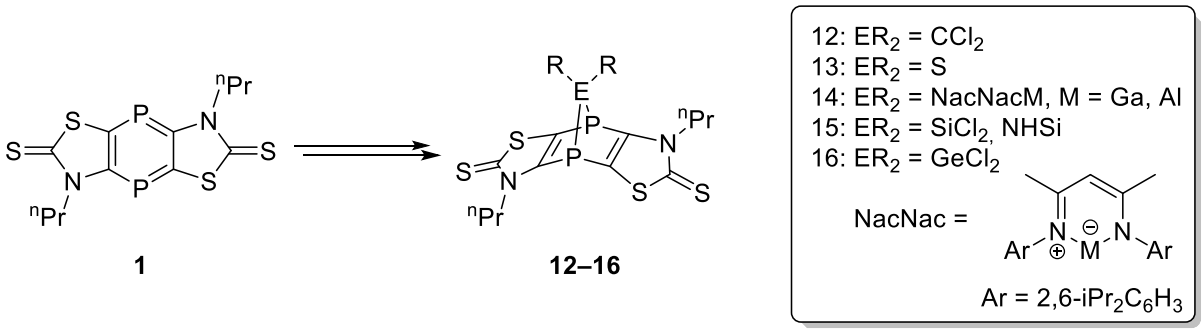


**1** **12–16**

*Scheme 56:* [4+1]-cycloaddition reactions of **1** forming 1,4-norbornadienes **12–16**.

In addition to 1,4-diphosphanorbornadiene **14a**, 1,4-diphosphabarrelenes **17a–c** and 7,8-dihydro-1,4-diphosphabarrelenes **18a–f** could be achieved in [4+2]-cycloaddition reactions, exploring the scope of possible substitution patterns on the bridge atoms (Scheme 57). The molecular structures of **17c** and **18f** could be confirmed by single crystal X-ray diffraction analyses, showing a close resemblance with known derivatives of both thiazole- and imidazole-based 1,4-diphosphabarrelenes (Figure 67).

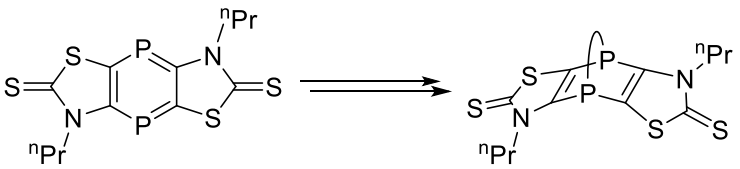

**1** **17,18**

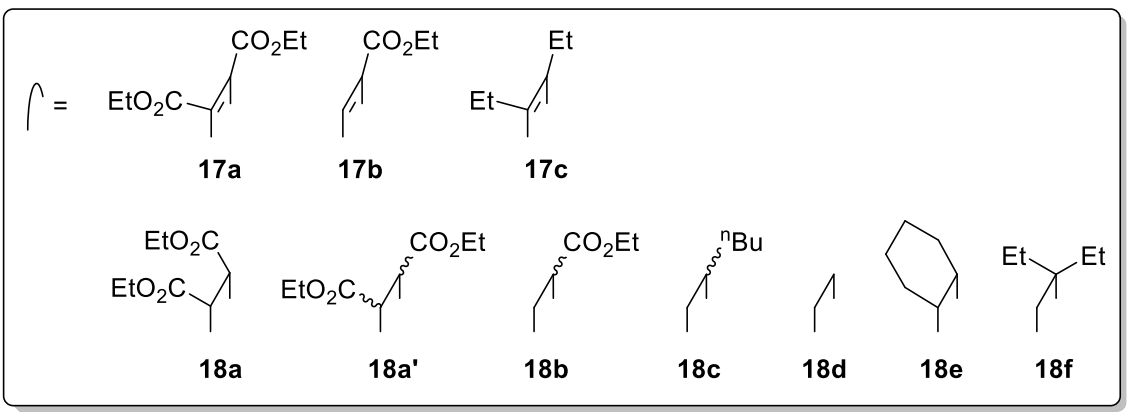

**17a** **17b** **17c**

**18a** **18a'** **18b** **18c** **18d** **18e** **18f**

*Scheme 57:* [4+2]-cycloaddition reactions of **1** forming (7,8-dihydro-)1,4-diphosphabarrelenes **17,18**.

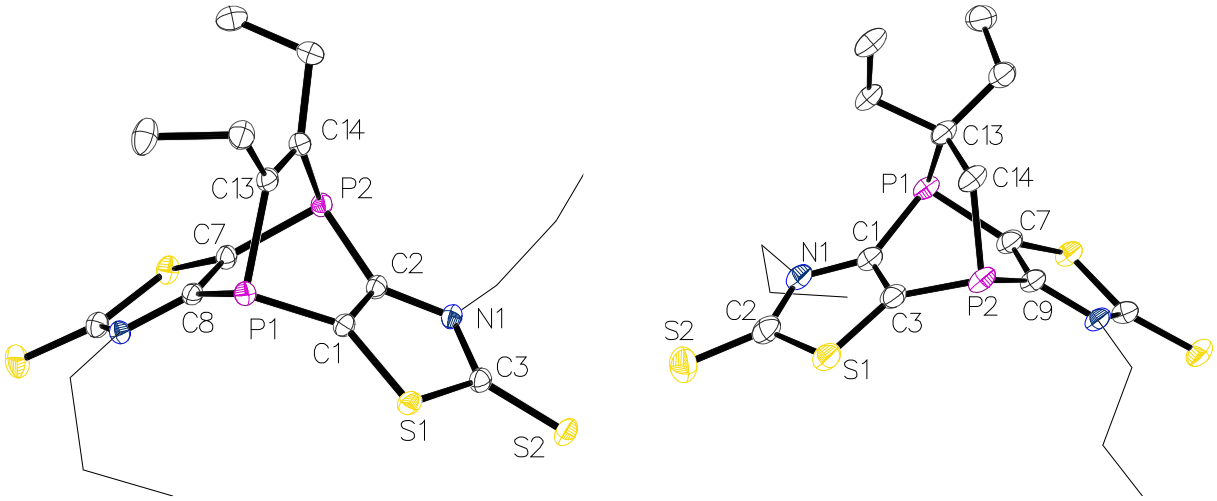


**17c** **18f**

*Figure 67:* Molecular structures of **17c** and **18f** in the single crystal lattice. Hydrogen atoms were omitted and *n*-propyl groups are shown as wire-frames for clarity.

A combined experimental and theoretical thermal decomposition study of **17,18** revealed an interesting trend of 7,8-dihydro-1,4-diphosphinines **18** being more prone to [4+2]-cycloreversion upon heating than **17**. The scope of 1,4-diphosphabarrelenes of **1** could be extended to heteroatom-containing bridges with the synthesis of the photochemically labile **20**[129] as well as the mixed-valent P(III)/P(V) 1,4-diphosphabarrelene oxide **19** (Scheme 58). The chemistry of P(V) 1,4-diphosphabarrelenes was further explored by the synthesis of **22a** and **24a** (Scheme 59), which could be isolated and characterised.

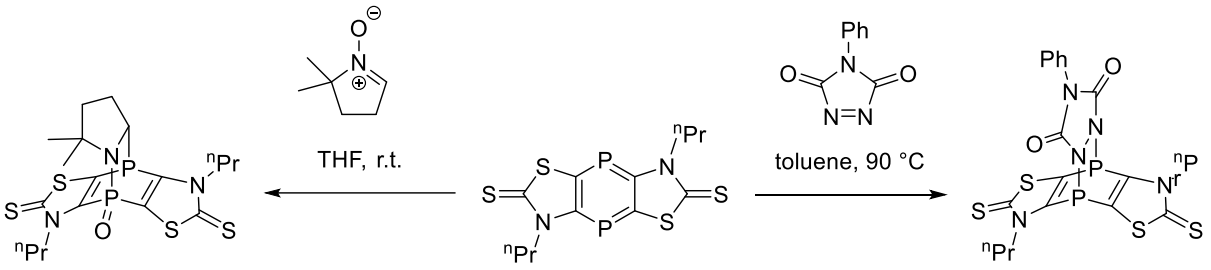


**19** **1** **20**

*Scheme 58:* [4+2]-cycloaddition reactions of **1** with DMPO and 5-phenyl-1,2,5-triazoline-3,5-dione.[129]

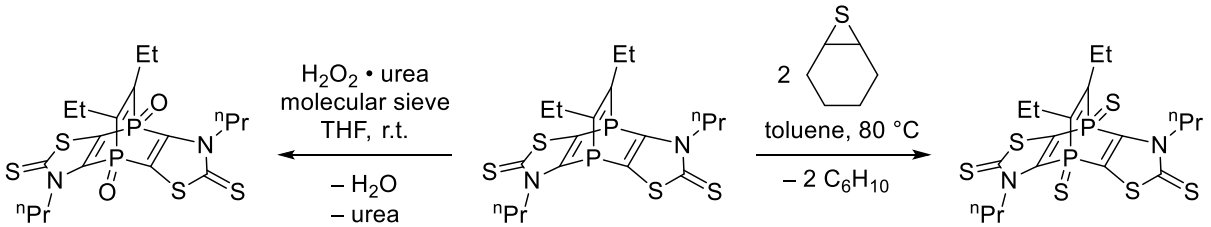


**22b** **17c** **24a**

*Scheme 59:* Oxidation of **17c** using hydrogen peroxide urea adduct (left) and cyclohexene sulfide (right).

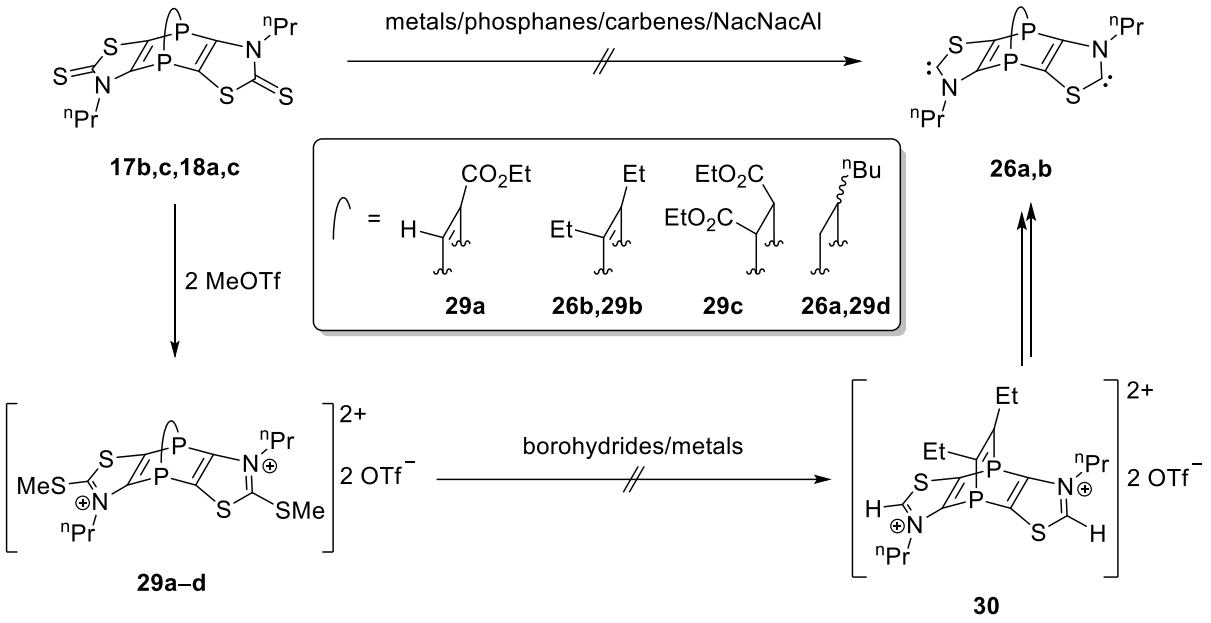


*Scheme 60:* Methylation reactions of **17b,c** and **18a,c** and desulfurisation attempts of **17b,c**, **18a,c** and **29a–d**.

The second part of this thesis focused on the reactivity of the thione moieties at the thiazole-rings, targeting bis-carbenes and C-C coupled oligomers. In this vein, desulfurisation attempts of 1,4-diphosphabarrelenes **17c,18c** were conducted using multiple approaches such as reactions with metals, phosphanes or carbenes (Scheme 60). Yet, all attempts, including a reaction with NacNacAl, did not yield the desired bis-carbenes **26a,b**. In accordance to these findings, a theoretical desulfurisation study showed the comparatively high stability of **17c** towards many known desulfurisation agents such as tri-*n*-butylphosphane.

In addition to the direct desulfurisation of 1,4-diphosphabarrelenes, an indirect route via doubly methylated salts **29a–d** and bis-thiazolium salt **30** was attempted. Four different 1,4-diphosphabarrelenes were methylated, forming the first doubly methylated thiazole-2-thione-based 1,4-diphosphabarrelene salts **29a–d**. However, attempts to desulfurise the derivative **29b** proved unsuccessful and **30** could not be detected in any desulfurisation attempt.

In order to introduce C-C double bonds in an earlier synthetic step, multiple synthetic procedures to furnish dithiadiazafulvalene **37** from thiazole **34** were attempted (Scheme 61). While first steps of the approaches showed promising results, the phosphanylation and dimerisation of thiazoles and thiazolium iodides was challenging, owing to the close chemical resemblance of the $C^2$- and $C^5$-position in thiazoles and, thus, leading to undesired or unselective substitutions and deprotonations.

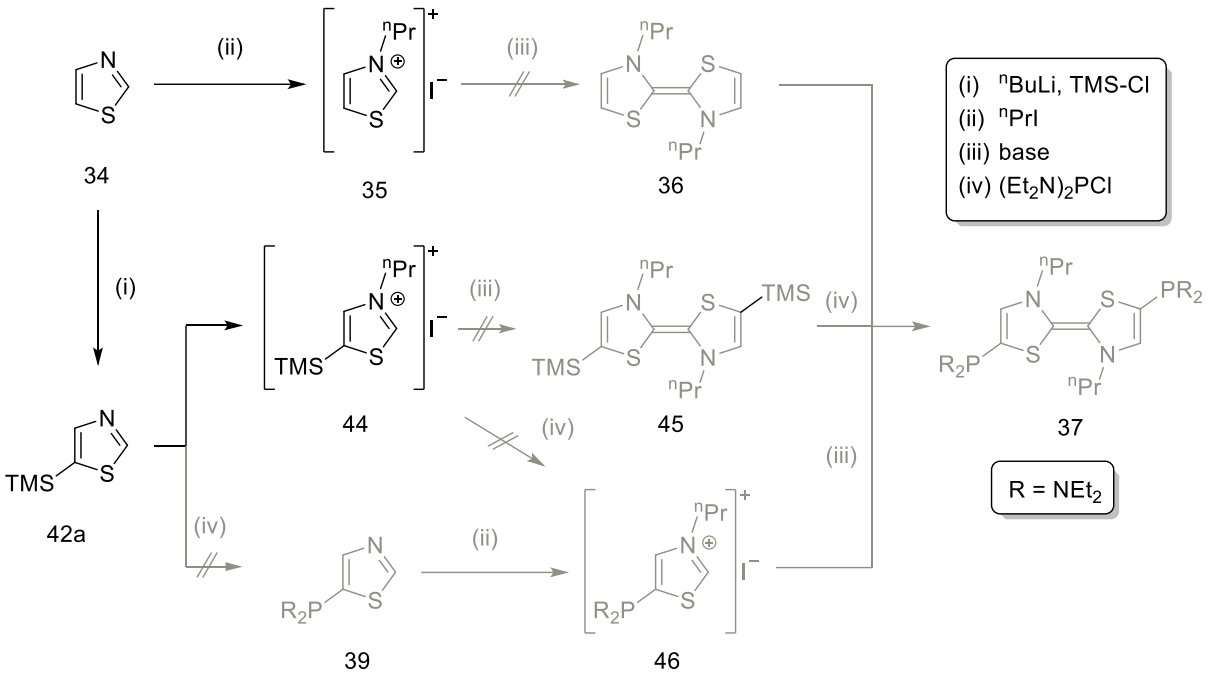


*Scheme 61:* Different synthetic approaches to DTDAF **37** from thiazole **34**.

As the experimental results showed an interesting deviation of the reactivity of **1** and related compounds to the respective imidazole-based analogues, the third part of the work was comprised of a theoretical study on the aromatic properties of all experimentally accessed neutral 1,4-diphosphinines as well as several similar structures using state of the art $\int NICS^{SOM}_{\pi,zz}$ and XY-$NICS^{SOM}_{\pi,zz}$ scans as well as HOMA and $ELF_{\pi}$ analyses. These methods revealed the $C^2$-chalcogen substituted 1,4-diphosphinines to be only locally aromatic in the central ring, while carbene- and carbenium-based derivatives showed global aromaticity across all three rings of the respective tricyclic system. Comparison to free five-membered heterocycles displayed a similarity between the free and fused rings, the 1,4-diphosphinine having only a small impact on the overall situation in the outer ring. Investigations into a 1,4-diphosphabarrelene thione and its methylated, thiazolium- and carbene- analogues revealed an even smaller influence of the scaffold on the outer rings, the latter showing a very close resemblance to their free counterparts and, thus, suggesting highly aromatic properties of barrelene-based bis-NHCs.

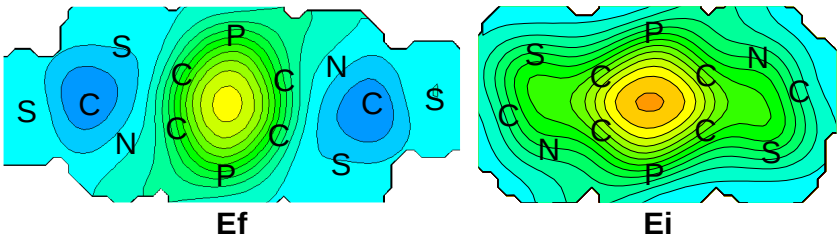


*Figure 68:* XY-$NICS^{SOM}_{\pi,zz}$ scans of thiazole-2-thione-based **Ef** and thiazole-2-ylidene-based **Ei**.

# 5 EXPERIMENTAL SECTION

## 5.1 GENERAL WORKING TECHNIQUES

If not specified, all reactions were performed in a dried and deoxygenated argon atmosphere using Schlenk or glovebox techniques. The used argon (>99.998%) was purified by a system of three columns (deoxygenation by a BTS copper catalyst (BASF PuriStar® R3-155) at ca. 100 °C, drying with silica gel, phosphorus pentoxide desiccant with indicator (Sicapent®) and calcium chloride). Glassware, spatulas, cannulas and filter papers were dried in a compartment drier at 110 °C for at least 1 h. Additionally, glassware was heated with a heat gun (up to 550 °C) under active vacuum ($10^{-2}$ mbar) and kept under vacuum for 5–10 min. Sterile syringes were purged with argon three times before use. The used solvents were dried using standard procedures[145] by refluxing over proper desiccants (*n*-pentane, petroleum ether 40/65 and toluene over sodium wire (Ø = 2 mm); diethyl ether stabilized with 3,5-di-tert-butyl-4-hydroxytoluene (BHT) and tetrahydrofuran over benzophenone and sodium wire; dichloromethane over calcium hydride) in an argon atmosphere for several days and distilled before use. Alternatively, diethyl ether and toluene were dried using a Mbraun SPS-800 solvent purification system. For filtration Schlenk frits or stainless steel cannulas (Ø = 1–2 mm) with Whatman® glass microfiber filters (grade GF/B) were used. After use, stainless steel cannulas were cleaned with diluted hydrochloric acid, water and acetone, while glassware was stored in a concentrated solution of potassium hydroxide in *i*-propanol for at least 2 d (only overnight for glass frits) and in diluted hydrochloric acid for at least several hours. Afterwards, the glassware was washed with demineralised water and acetone. All glass joints were greased with either OKS 1112 grease of PTFE paste (Carl Roth).

## 5.2 METHODS AND DEVICES

### 5.2.1 NMR spectroscopy

NMR spectra were recorded on a Bruker Avance I 300 MHz, Bruker Avance I 400 MHz, Bruker Avance I 500 Mhz, Bruker Avance III HD Ascend 500 MHz or a Bruker Avance III HD Ascend 700 MHz spectrometer at the NMR department of the University of Bonn and subsequently analysed using the program Mestrenova 14.2 by *Mestrelab Research S.L*. Obtained $^{1}H$ and $^{13}C\{^{1}H\}$ NMR spectra were calibrated using the residual proton/carbon signal of the used deuterated solvents relative to tetramethylsilane[146] (residual peaks given in ppm, $C_6D_6$: $\delta(^{1}H) = 7.160$, $\delta(^{13}C) = 128.060$, $CDCl_3$: $\delta(^{1}H) = 7.260$, $\delta(^{13}C) = 77.160$, $CD_2Cl_2$: $\delta(^{1}H) = 5.320$, $\delta(^{13}C) = 53.840$, THF-d8: $\delta(^{1}H) = 1.730/3.580$, $\delta(^{13}C) = 25.370/67.570$, toluene-d8:

δ($^{1}$H) = 2.090, δ($^{13}$C) = 20.400). For heteronuclear NMR spectra the IUPAC recommended method was used, which specifies the chemical shift δ of a compound as

$$\delta = 10^{6} \cdot \frac{\Xi_{sample} - \Xi_{reference}}{\Xi_{reference}}$$

in which $\Xi_{sample}$ denotes the frequency of the respective nucleus relative to the frequency of $^{1}$H. The values of Ξ and the natural abundance for all measured nuclei are given in Table 9. Deuterated solvents were stored over 10w% molecular sieve (3 Å) for at least 2 d before use. All chemical shifts δ are given in parts per million (ppm) and scalar coupling constants $^{n}J_{X,Y}$ in Hertz (Hz), with n being the number of covalent bonds between the nuclei X and Y. The multiplicity of a given signal is described as follows: s = singlet, d = doublet, t = triplet, q = quartet, quint = quintet, sext = sextet, hept = heptet, m = multiplet and combinations of these. Broad signals were denotet with “br.”. In $^{1}$H NMR data, the number of nuclei in a respective signal is given according to integration. Complex NMR spectra were analysed by a combination of 1D and 2D NMR experiments (*i.e.*, COSY, HSQC, HMBC). All NMR measurements were carried out at 298 K if not stated otherwise.

*Table 9:* Natural abundance *N*. frequency factor Ξ and references of measured nuclei.

| Isotope | *N* / % | Ξ / % | reference |
|---|---|---|---|
| $^{1}$H | 99.989 | 100.0000 | 1% $SiMe_4$ ($CDCl_3$) |
| $^{13}$C | 1.07 | 25.1450 | 1% $SiMe_4$ ($CDCl_3$) |
| $^{31}$P | 100 | 40.4807 | 85% $H_3PO_4$ ($H_2O$) |

### 5.2.2 Mass spectrometry

All samples were measured by the analytical department of the University of Bonn. Electron impact ionisation (EI) experiments were performed on a Thermo Finnigan MAT 95 XL sector field instrument using an ionisation energy of 70 eV, calibration and referencing were done using perfluorokerosene (PKF). Electrospray injection (ESI) and atomospheric pressure chemical ionisation (APCI) measurements were done on a Thermo Fisher Scientific Orbitrap XL spectrometer using acetonitrile or dichloromethane as solvents. Air sensitive samples were submitted in sealed glass vials after preparation in a glovebox and only opened shortly before measuring. For all samples, selected data is given, reducing isotopic patterns to the mass-to-charge ratio (m/z) of the isotopomer with the highest relative abundance, which is given in parentheses. As high-resolution mass spectra (HRMS) using ESI or APCI were recorded in a single measurement, no standard deviations were obtained.

### 5.2.3 Infrared spectroscopy

ATR-IR spectra of solids were recorded inside a glovebox at ambient temperature in a spectral range from 400–4000 $cm^{-1}$ using a Bruker Alpha FTIR spectrometer with a single-reflection ATR unit (Platinum-ATR Diamond) or a Shimadzu IRSpirit FTIR spectrometer with a single-reflection ATR unit (QATR-S). Apodisation was done using the Happ-Genzel function. The data sets were analysed with the software *EZ Omnic 7.3* from *Fisher Scientific* and *LabSolutions IR 2.26* from *Shimadzu*. Peak intensities are given as very strong (vs), strong (s), medium (m) or weak (w). Only selected peaks at wave numbers >1500 $cm^{-1}$ are given.

### 5.2.4 Elemental analysis

All elemental analyses were performed by the technical staff of the University of Bonn on a Elementar Vario Micro analysis device in triplicate or more. The samples were prepared in a glovebox by weighing in a tin or silver sample container using a micro-analytical balance. The given values for C, H, N (and S) content are given as the average of the obtained data.

### 5.2.5 Melting point determination

Samples for melting point determination were filled into glass capillaries (Ø = 0.1 mm) up to height of approximately 0.2 mm under glovebox conditions. The capillaries were sealed with grease. Melting points were determined with a MPmeter from Toledo or a melting point determination apparatus after Dr. Tottoli. No internal or external temperature corrections were applied.

### 5.2.6 Single crystal X-ray diffraction analysis

Singly crystal X-ray diffraction studies were performed on a Bruker D8 Venture or a STOE Stadivari diffractometer, equipped with a low-temperature device (Bruker Kryoflex or Oxford Cryostream 800 series), at 100(2) K by using graphite monochromated Mo-Kα radiation (λ = 0.71073 Å) or Cu-Kα radiation (λ = 1.54186 Å). Bond parameter analyses were done using the software *Olex2 1.5*.[147]

### 5.2.7 UV/vis spectroscopy

UV/vis spectra were recorded on a UV-1650PC spectrometer from *Shimadzu* with a double-beam optics photometric system in a maximal range of wavelengths of 190–1100 nm having a spectral band width of 2 nm and a wavelength accuracy of ±0.5 nm with an automatic wavelength correction. All spectra were recorded in a range of 280–700 nm using quartz glass (Suprasil® quartz, Heraeus) cuvettes (Hellma precision cells 110-QS). Due to the presence of air-sensitive compounds in the measurements, extinction coefficients could not be detmined.

## 5.3 WASTE DISPOSAL

Laboratory chemical waste was disposed according to the 'Gefahrstoffverordnung' (GefStoffV). Reactive chemical waste was quenched and solvents, solids, filter/filtration waste and heavy metal-containing waste, as well as syringes and cannulas, were separated into individual containers. The waste containers were submitted to the department *4.2 Arbeits- und Umweltschutz* of the University of Bonn.

## 5.4 USED CHEMICALS

*Table 10:* List of used commercially available chemicals.

| Chemical | CAS | Producer |
|---|---|---|
| (η2-Bis(trimethylsilyl)-ethyne)bis(η5-cyclopenta-dienyl)titanium | 56-34-8 | TCI |
| 1,4,7,10-tetraoxacyclodecane | 294-93-9 | Acros |
| 1,8-Diazabicyclo(5.4.0)undec-7-ene | 6674-22-2 | Sigma-Aldrich |
| 1-hexene | 592-41-6 | Sigma-Aldrich |
| 1-iodopropane | 107-08-4 | Sigma-Aldrich |
| 2-ethyl-1,butene | 760-21-4 | abcr |
| 3-hexyne | 928-49-4 | Acros |
| 5,5-dimethyl-1-pyrrolidine-*N*-oxide | 3317-61-1 | Sigma-Aldrich |
| 9-borabicyclo(3.3.1)nonane, 0.5 M in THF | 280-64-8 | Sigma-Aldrich |
| Acetone | 67-64-1 | Julius Hoesch |
| benzene-d6 | 1076-43-3 | Deutero GmbH |
| carbonic dichloride, 15% in toluene | 75-44-5 | Sigma-Aldrich |
| chloro(trimethyl)silane | 75-77-4 | Acros |
| chloroform-d | 865-49-6 | Deutero GmbH |
| Cyclohexene | 110-83-8 | Merck |
| cyclohexene sulfide | 286-28-2 | Sigma-Aldrich |
| Dichloromethane | 75-09-2 | Fisher |
| dichloromethane-d2 | 1665-00-5 | Deutero GmbH |
| diethyl acetylene dicarboxylate | 762-42-5 | Sigma-Aldrich |
| diethyl ether | 60-29-7 | VWR |
| diethyl fumarate | 623-91-6 | Thermo Scientific |
| diethyl maleate | 141-05-9 | TCI |
| diethylzinc, ca. 15% in hexene | 557-20-0 | TCI |
| Dimethylsulfoxide | 67-68-5 | Riedel-de-Haën |
| dimethylsulfoxide-D6 | 2206-27-1 | Deutero GmbH |

| | | |
|---|---|---|
| Diphenyldisulfane | 882-33-7 | TCI |
| Ethanol | 64-17-5 | Julius Hoesch |
| Ethene | 74-85-1 | Sigma-Aldrich |
| Ethyl acrylate | 140-88-5 | TCI |
| Ethyl propiolate | 623-47-2 | Merck |
| Germanium dichloride dioxane complex | 28595-67-7 | Sigma-Aldrich |
| Hydrochloric acid, 35–37% | 7647-01-0 | VWR |
| Hydrogen chloride, 4 M in dioxane | 7647-01-0 | abcr |
| Hydrogen peroxide urea adduct | 124-43-6 | Fluka |
| Iodomethane | 74-88-4 | Merck |
| Lithium bis(trimethylsilyl)amide | 4039-32-1 | Sigma-Aldrich |
| Lithium hydroxide | 1310-65-2 | Alfa Aesar |
| Lithium tri-*s*-butyl(hydrido)borate, 1 M in THF | 38721-52-7 | Acros |
| Magnesium | 7439-95-4 | Carl Roth |
| Magnesium sulfate | 7487-88-9 | VWR |
| Methanol | 67-56-1 | Alfa Aesar |
| Methanol-d4 | 811-98-3 | euriso-top |
| Methyl trifluoromethanesulfunate | 333-27-7 | fluorochem |
| Methyllithium, 1.6 M in $Et_2O$ | 917-54-4 | Sigma-Aldrich |
| Molecular sieves, 3 Å, 1.7–2.4 mm | — | Alfa Aesar |
| *n*-butyllithium, 1.6 M in hexane | 109-72-8 | Acros |
| *n*-pentane | 109-66-0 | Fisher |
| Petroleum ether 40/65 | 64742-49-0 | Julius Hoesch |
| Potassium | 7440-09-7 | Riedel-de-Haën |
| Potassium bis(trimethylsilyl)amide | 40949-94-8 | Sigma-Aldrich |
| Potassium hydride | 7693-26-7 | Sigma-Aldrich |
| Potassium hydroxide | 1310-58-3 | Sigma-Aldrich |
| Potassium *t*-butoxide | 865-47-4 | Alfa Aesar |
| Pyridine-*N*-oxide | 694-59-7 | Merck |
| Silica gel 60 (63–200 mesh) | 7631-86-9 | Merck |
| Sodium borohydride | 16940-66-2 | Sigma-Aldrich |
| Sulfur | 7704-34-9 | abcr |
| Tetrachloromethane | 56-23-5 | Acros |
| Tetrahydrofurane | 109-99-9 | Fisher |
| Tetrahydrofurane-d8 | 1693-74-9 | Carl Roth |
| Tetra-*n*-butylammonium chloride | 1112-67-0 | Sigma-Aldrich |
| Tetra-*n*-butylammonium fluoride | 429-41-4 | Alfa Aesar |

| | | |
|---|---|---|
| Thiazole | 288-47-1 | fluorochem |
| Toluene | 108-88-3 | VWR |
| Toluene-d8 | 2037-26-5 | euriso-top |
| Tri-*n*-butylphosphite | 102-85-2 | Fluka |
| Triethylamine | 121-44-8 | Sigma-Aldrich |
| Triethylammonium chloride | 3327-22-8 | Merck |
| Trifluoromethanesulfonic acid | 1493-13-6 | fluorochem |
| Trifluoromethanesulfonic anhydride | 358-23-6 | abcr |
| Trimethylsilyl diazomethane | 18107-18-1 | Acros |
| Tri-*n*-butylphosphane | 998-40-3 | Alfa Aesar |
| Zinc dichloride | 7646-85-7 | Alfa Aesar |

*Table 11:* Syntheses of starting materials according to literature-known procedures.

| Chemical | CAS | Producer |
|---|---|---|
| [1,3-bis(2,6-di-*i*-proplyphenyl)-1*H*-imidazolium-2-yl]dichlorosilylene[122] | 1187680-47-2 | — |
| 1-(2,6-di-i-propylphenyl)-3,3,5,5-tetramethylazolidine-2-ylidene[148] | 869085-70-1 | D. Biskup |
| 1,2-dihydro-1,3-bis(2,6-di-i-propylphenyl)-4,6-dimethyl-1,3,3-diazaaluminine[149] | 325465-25-6 | B. M. Gabidullin |
| 1,2-dihydro-1,3-bis(2,6-di-*i*-propylphenyl)-4,6-dimethyl-1,3,3-diazagallinine[150] | 317322-17-1 | R. Zakarina |
| 1,3,4,5-tetramethylimidazole-2-ylidene[151] | 141556-40-3 | T. Kalisch |
| 1,3,5,7-tetra-*n*-butyl-di(1,3-imidazole-2(3H)-thione)[2,3-d:5,6-d']-4,8-diphosphinine[99] | 2102393-27-9 | M. R. K. Ramachandran |
| 1,3-bis(2,2-dimethylpropyl)-1,3-dihydro-2*H*-1,3,2-benzodiazasilol-2-ylidene[124] | 172295-83-9 | — |
| 1,3-dimethylimidazole-2-ylidene[151] | 52356-52-2 | T. Kalisch |
| 3,7-di-*n*-propyl-di(1,3-thiazole-2(3H)-thione)[2,3-d:5,6-d']-4,8-diphosphinine[100] | 2252457-16-0 | T. Kalisch |
| 4-phenyl-1,2,4-triazoline-3,5-dione[152] | 4233-33-4 | — |
| Chlorobis(diethylamino)phosphane[153] | 685-83-6 | T. Kalisch |
| Lithium di-*i*-proplyamide[154] | 79060-88-1 | S. Kermanshahian |
| Potassium graphite[155] | 12081-88-8 | P. Brehm |
| Sodium disperson in sodium chloride | | P. Brehm |
| Sodium naphthalide[156] | 4111-54-0 | T. Kalisch |
| Sodium tetrakis(3,5-bis(trifluoromethyl)phenyl)borate[157] | 79060-88-1 | F. Gleim |
| Trimethylphosphane[158] | 594-09-2 | T. Kalisch, P. Brehm |
| Tris(diethylamino)phosphane[159] | 2283-11-6 | — |

## 5.5 THEORETICAL METHODS

### 5.5.1 General methods

All structures were built with the open-source software *Avogadro 1.2.0*.[160] Structures were optimised using the *ORCA*[161] 4.0.1.2 program package at the TPSS-D3BJ/def2-TZVP(CPCM$_{THF}$) level of theory, a combination of the mega-GGA density functional TPSS[162] with BJ-damped DFT-D3[163] dispersion correction and the def2-TZVP[164] basis set, including the conductor-like polarisable continuum model (CPCM)[165] as a solvent model for THF. In order to accelerate the optimisations and following harmonic frequency calculations, the density-fitting RI-J (def2/J) approach was used.[166] The DFT grid was set to 4, with the grid for the final energy being set to 5. Optimised structures were characterised by frequency analyses in order to identify the nature of the respective located stationary point (no imaginary frequency below −30 cm$^{-1}$ for minima and only one imaginary frequency for transition states) and to get access to thermal corrections (for 298.15 K and 1 atm) according to the modified ideal gas-rigid rotor-harmonic oscillator model. Transition states were obtained via relaxed potential energy surface scans along the important bond in *ORCA* 4.0.1.2 or by nudged elastic band calculations[167] using *ORCA* 5.0.4. The transition state vibration was taken from the respective highest energy structure and the structure was optimised, keeping the imaginary frequency. Final single point energies were calculated with *ORCA* 4.0.1.2 on the RI-PW6B95-D3BJ/def2-QZVP(CPCM$_{THF}$)[164,168] level of theory using the density-fitting RI-JK (def2/JK)[169] approach. The final Gibbs free energies G were obtained from the sum of the electronic single point energies and the thermal corrections accessed from the frequency analyses. Calculated structures were visualised using the software *UCSF Chimera 1.17.2*.[170]

### 5.5.2 Aromaticity studies

NICS values were calculated at the B3LYP-D3BJ/def2-TZVP[171] level of theory as this functional is commonly used for NICS calculations and allows easier comparisons to other calculations. These calculations were done with *ORCA* 5.0.4 using standard procedures for setting up dummy atoms. NICS$^{SOM}_{\pi,zz}$ values were obtained by first rotating the optimised structures into the XY plane. σ-contribution free components were calculated using the so-called σ-only model (SOM) developed by Stanger.[28] This was done by artificially saturating ring-atoms by adding H-atoms and calculating NICS$_{\pi,zz}$ values. This data was subtracted from the NICS$_{\pi,zz}$ values of the original system, thus giving NICS$^{SOM}_{\pi,zz}$. In order to obtain off-centre effect free values, XZ- and YZ-scans were performed on parent 1,4-diphosphinine to determine a reasonable distance to the molecular plane. 0.1 Å steps were used in Z-direction, while 0.2 Å steps were employed in the respective X- or Y-direction across the ring system (Figure 69). As a result of

this study, Z-scans were done at distances from 2–6 Å above the ring plane in increments of 0.2 Å. $\int NICS^{SOM}_{\pi,zz}$ were accomplished by fitting an exponential function to the calculated data using the software *OriginPro 8G*[172] and integrating the function from 0 to infinity. XY-NICS scans were realised by creating a grid of dummy atoms 2 Å above the ring system in increments of 0.2 Å. The 2D-grid was truncated at distances above 1.6 Å to the closest atom of the ring system in order to reduce computational resources. HOMA values were obtained from optimised minimum structures using the open-source software *MultiWFN* with default parameters.[173] $ELF_\pi$ plots and $ELF_\pi$ bifurcation values were accessed using *MultiWFN*. $ELF_\pi$ bifurcation values are given as the average of bifurcation values of all bonds in a given cycle.

## 5.6 SYNTHESES AND CHARACTERISATIONS

### 5.6.1 Synthesis of 3,7-di-*n*-propyl-di(1,3-thiazole-2(3*H*)-thione)[2,3-d:5,6-d']-4,8-bis-(thiophenoxy)-4,8-dihydro-4,8-diphosphinine (2)

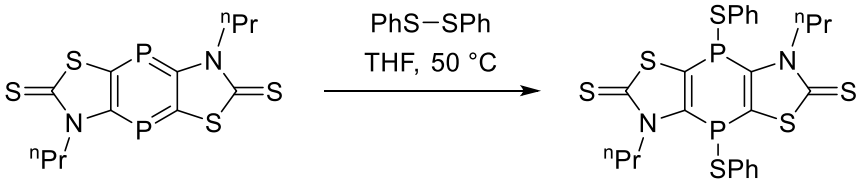


**1** **2**

In a 10 mL Schlenk tube 21.9 mg (0.100 mmol, 1.02 eq.) of diphenyl disulfane were added to a suspension of 37.0 mg (0.098 mmol, 1.00 eq.) of **1** in 4 mL THF at ambient temperature. The mixture was heated to 50 °C and stirred for 3 h before removing solvent *in vacuo* ($10^{-2}$ mbar) and washing the residue three times with 1.5 mL of *n*-pentane each. After drying *in vacuo* ($10^{-2}$ mbar) **2** was obtained as a yellow solid.

**Reaction code:** TK-221 (05p5a034.21)

**Molecular formula:** $C_{24}H_{24}N_2P_2S_6$

**Molecular weight:** 594.78 g/mol

**Yield:** 19.2 mg (0.032 mmol, 33%)

**Melting point:** 248 °C (dec.)

| | | | | |
|---|---|---|---|---|
| **Elemental analysis:** | calculated / % | C 48.47 | H 4.07 | N 4.71 |
| | found / % | C 46.04 | H 4.39 | N 4.08 |

**MS** (EI, 70 eV, selected data): m/z (%): 626.0 (3) $[M+2\ O]^{+\bullet}$, 610.0 (2) $[M+O]^{+\bullet}$, 594.1 (5) $[M]^{+\bullet}$, 376.0 (87) $[M-2\ PhS]^+$, 333.9 (33) $[M-2\ PhS-C_3H_7+H]^+$, 291.9 (84) $[M-2\ PhS-2\ C_3H_7+2\ H]^+$, 218 (100) $[PhS\text{-}SPh]^+$, 110.0 (72) $[Ph\text{-}SH]^+$.

**IR** (ATR Diamond, selected data): $\tilde{\nu}$ / $cm^{-1}$ = 2869 (w, *v*(CH)), 2968 (w, *v*(CH)).

**$^{1}$H NMR** (500.0 MHz, 298.0 K, $CD_2Cl_2$): δ / ppm = 1.00 (t, 6H, $^{3}J_{H,H}$ = 7.38 Hz, $CH_2CH_2CH_3$), 1.53–1.65 (m, 2H, $CH_2CH_2CH_3$), 1.83–1.98 (m, 2H, $CH_2CH_2CH_3$), 4.05 (m, 2H, $CH_2CH_2CH_3$), 4.60 (m, 2H, $CH_2CH_2CH_3$), 6.64 (dt, 4H, $^{3}J_{H,H}$ = 7.00 Hz, $^{3}J_{H,H}$ = 1.46 Hz, *m*-$C_6H_5$), 7.22 (m, 4H, *o*-$C_6H_5$), 7.40 (tt, 2H, $^{3}J_{H,H}$ = 7.56 Hz, $^{3}J_{H,H}$ = 1.20 Hz, *p*-$C_6H_5$).

**$^{13}$C{$^{1}$H} NMR** (125.8 MHz, 298.0 K, $CD_2Cl_2$): δ / ppm = 11.5 (s, $CH_2CH_2CH_3$), 22.3 (t, $^{4}J_{P,C}$ = 2.46 Hz, $CH_2CH_2CH_3$), 51.5 (t, $^{3}J_{P,C}$ = 5.54 Hz, $CH_2CH_2CH_3$), 124.9 (d, $^{1}J_{P,C}$ = 33.9 Hz, P*C*S), 129.9 (s, *p*-$C_6H_5$), 130.5 (s, *o*-$C_6H_5$), 135.4 (s, *m*-$C_6H_5$), 140.3 (d, $^{1}J_{P,C}$ = 31.0 Hz, P*C*N), 190.3 (t, $^{3}J_{P,C}$ = 3.51 Hz, *C*=S).

**$^{31}$P{$^{1}$H} NMR** (202.4 MHz, 298.0 K, $CD_2Cl_2$): δ / ppm = –20.8 (s).

**$^{31}$P NMR** (202.4 MHz, 298.0 K, $CD_2Cl_2$): δ / ppm = –20.8 (s).

### 5.6.2 Attempted synthesis of 3,7-di-*n*-propyl-di(1,3-thiazole-2(3*H*)-thione)[2,3-d:5,6-d']-4,8-bis(trimethylsilyl)-4,8-dihydro-4,8-diphosphinine (4a)

#### *5.6.2.1 Magnesium, trimethylsilyl chloride*

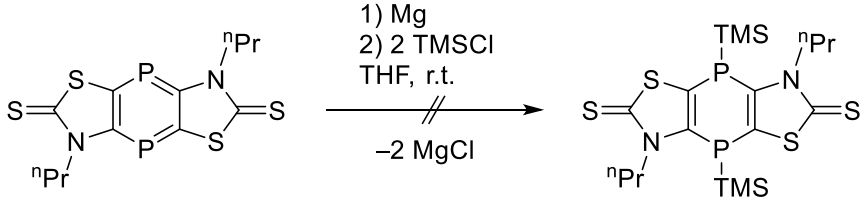


**1** **4a**

In a 10 mL Schlenk tube 52.6 mg (2.164 mmol, 25.9 eq.) Mg was added to a suspension of 31.5 mg (0.084 mmol, 1.00 eq.) of **1** in 2.5 mL of THF at ambient temperature. The reaction mixture was stirred for 15 min before adding 0.03 mL (0.236 mmol, 2.82 eq.) of TMS-Cl. After stirring for 24 h $^{31}$P{$^{1}$H} NMR spectroscopic investigations were performed before stirring for another 26 h and the subsequent addition of 0.05 mL (0.393 mmol, .4.70 eq.) of TMS-Cl.

**Reaction code:** TK-510 (TIM230517m3a045)

**$^{31}$P{$^{1}$H} NMR** (121.5 MHz, 298.0 K, THF): δ / ppm = –59.8 (d, $^{3}J_{P,P}$ = 7.85 Hz), −24.5 (d, $^{3}J_{P,P}$ = 7.85 Hz).

*5.6.2.2 Potassium graphite, trimethylsilyl chloride*

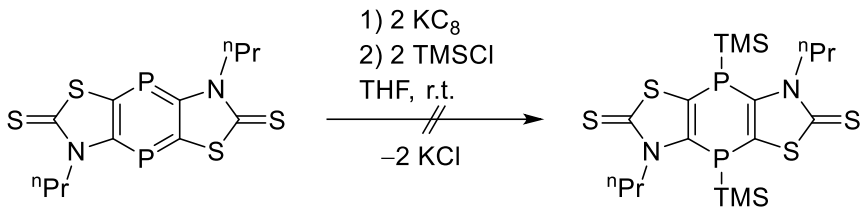


**1** **4a**

$KC_8$ was added to a suspension of **1** in THF (amounts given below). The black-violet reaction mixture was stirred for 10 min at ambient temperature before addition of TMS-Cl. After stirring for further 10 min at ambient temperature an aliquot was taken for $^{31}P\{^1H\}$ NMR spectroscopic measurements.

**Reaction code:** TK-518 (TIM230530t4a030)

m(**1**) = 7.2 mg (0.019 mmol, 1.00 eq.)
m($KC_8$) = 5.6 mg (0.041 mmol, 2.17 eq.)
V(TMS-Cl) = 5 µl (0.039 mmol, 2.06 eq.)
V(THF) = 0.7 mL

**$^{31}P\{^1H\}$ NMR** (162.0 MHz, 298.0 K, THF): δ / ppm = –92.1 (s).

**Reaction code:** TK-519 (TIM230531p5a014)

m(**1**) = 41.4 mg (0.110 mmol, 1.00 eq.)
m($KC_8$) = 32.2 mg (0.238 mmol, 2.17 eq.)
V(TMS-Cl) = 29 µl (0.228 mmol, 2.07 eq.)
V(THF) = 4 mL

**$^{31}P\{^1H\}$ NMR** (202.4 MHz, 298.0 K, THF): δ / ppm = –43.7 (s), –37.6 (s), –31.9 (s).

### 5.6.3 Synthesis of 1,3,5,7-tetra-*n*-butyl-di(1,3-imidazole-2(3*H*)-thione)[2,3-d:5,6-d']-4,8-bis(trimethylsilyl)-4,8-dihydro-4,8-diphosphinine (4b)

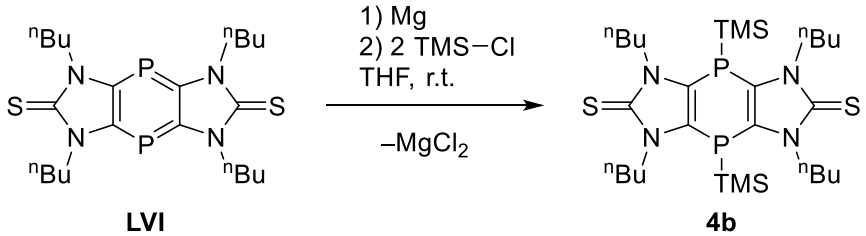


**LVI** **4b**

To a solution of 9.7 mg (0.020 mmol, 1.00 eq.) of **LVI** in 2 mL THF 14.1 mg (0.593 mmol, 29.6 eq.) of Mg were added at ambient temperature in a 10 mL Schlenk tube. After stirring for 15 min, 6.5 µL (0.051 mmol, 2.55 eq.) of TMS-Cl were added and the mixture was stirred for further 2 h.

**Reaction code:** TK-513 (TIM230515m3a015)

**$^{31}P\{^{1}H\}$ NMR** (121.5 MHz, 298.0 K, THF): δ / ppm = −114.9 (s).

### 5.6.4 Synthesis of 3,7-di-*n*-propyl-di(1,3-thiazole-2(3*H*)-thione)[2,3-d:5,6-d']-4-(1',3',4',5'-tetramethyl-imidazolium)-4,8-dihydro-4,8-diphosphinino-8-phosphan-1-ide (5a)

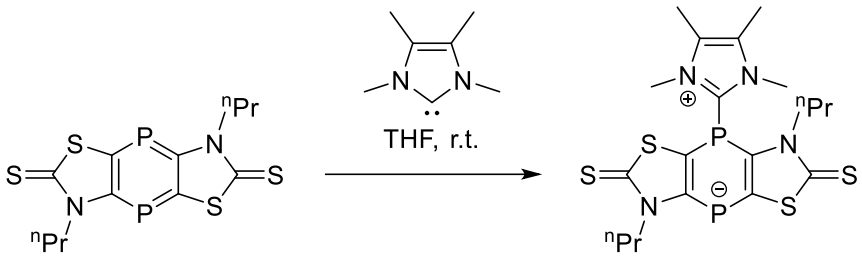


**1** **5a**

In a 10 mL Schlenk tube, a solution of 22.6 mg (0.182 mmol, 1.20 eq.) of $IMe_4$ in 1.25 mL of toluene were added to a solution of 62.3 mg (0.165 mmol, 1.00 eq.) of **1** in 1.75 mL toluene at ambient temperature. The mixture was stirred for 2 h before removing solvent *in vacuo* ($10^{-2}$ mbar) at 50 °C. 1 mL of solvent (see below) was added to the brown residue.

**Solvent: DCM**

**Reaction code:** TK-90 ((17t4a038.19, 17p5a016.19)

**$^{31}P\{^{1}H\}$ NMR** (202.48 MHz, 298.0 K): δ / ppm = −55.7 (s, $P^{-}$), −24.2 (s, P-$IMe^{4}$).

**Solvent: methanol-d4**

**Reaction code:** TK-92 (17m3a049.19)

1H NMR (300.1 MHz, 298.0 K, methanol-d4): δ / ppm = 0.96–1.10 (m, 6H, $CH_2CH_2CH_3$), 1.80–1.96 (m, 4H, $CH_2CH_2CH_3$), 2.25 (s, 6H, $NCH_3$), 3.74 (s, 6H, $=C(CH_3)N$), 3.90–4.05 (m, 1H, $CH_2CH_2CH_3$), 4.12–4.38 (m, 2H, $CH_2CH_2CH_3$), 4.50–4.66 (m, 1H, $CH_2CH_2CH_3$).

### 5.6.5 Attempted synthesis of 3,7-di-*n*-propyl-di(1,3-thiazole-2(3*H*)-thione)[2,3-d:5,6-d']-4-(1'-(2',6'-di-*i*-propylphenyl)-3',3',5',5'-tetramethyl-azolidinium)-4,8-dihydro-4,8-diphosphinino-8-phosphan-1-ide (5b)

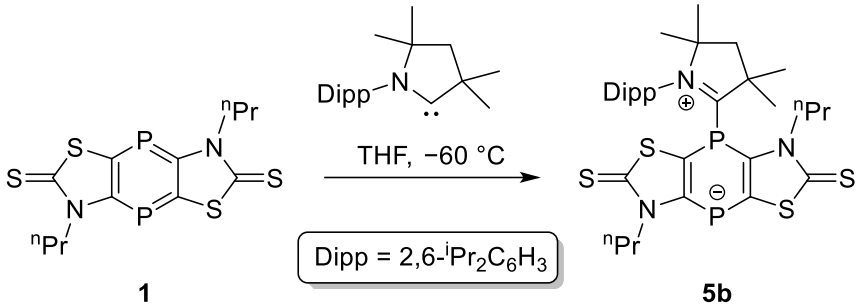


**1** **5b**

In a 10 mL Schlenk tube, 3 mL of THF were added to a mixture of 33.5 mg (0.222 mmol, 1.00 eq.) of **1** and 63.8 mg (0.223 mmol, 1.00 eq.) of 1-(2,6-di-*i*-propylphenyl)-3,3,5,5-tetramethyl-azolidine-2-ylidene ($CAAC^{Pr,Me}$) at −60 °C. The mixture was stirred for 1 h.

**Reaction code:** TK-556 (TIM230918m3a008)

**$^{31}P\{^{1}H\}$ NMR** (121.5 MHz, 298.0 K, THF): δ / ppm = −57.0 (br. s, $P^-$), −9.05 (br. s, P-$CAAC^{Pr,Me}$).

### 5.6.6 Attempted synthesis of potassium 3,7-di-*n*-propyl-di(1,3-thiazole-2(3*H*)-thione)-[2,3-d:5,6-d']-4-bis(trimethylsilyl)amino-4,8-dihydro-4,8-diphosphinino-8-phosphan-1-ide (5c)

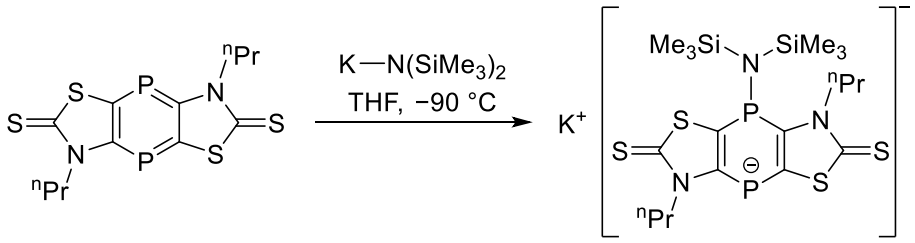


**1** **5c**

In a 10 mL Schlenk tube, a solution of 55.9 mg (0.280 mmol, 1.00 eq.) of KHMDS in 1mL THF was added to a suspension of 105.6 mg (0.281 mmol, 1.00 eq.) of **1** in 3.5 mL THF at −90 °C. The mixture was stirred for 1 h while slowly warming up.

**Reaction code:** TK-557 (TIM230920m3a017)

**$^{31}P\{^{1}H\}$ NMR** (121.5 MHz, 298.0 K, THF): δ / ppm = −29.1 (br. s, $P^-$), 8.78 (br. s, P-$N(SiMe_3)_2$).

### 5.6.7 Attempted synthesis of lithium 3,7-di-*n*-propyl-di(1,3-thiazole-2(3*H*)-thione)[2,3-d:5,6-d']-4-(di-*i*-propylamino)-4,8-dihydro-4,8-diphosphinino-8-phosphan-1-ide (5d)

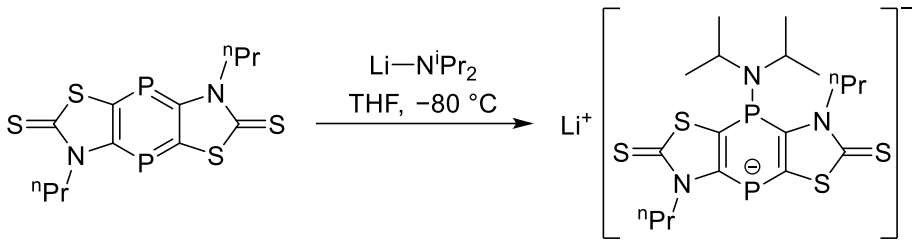


**1** **5d**

In a 10 mL Schlenk tube, 3 mL of THF were added to a mixture of 70.2 mg (0.186 mmol, 1.00 eq.) of **1** and 20.7 mg (0.193 mmol, 1.04 eq.) of LDA at −80 °C. The mixture was stirred for 1.5 h while slowly warming up.

**Reaction code:** TK-572 (TIM231026p5a051)

**$^{31}P\{^{1}H\}$ NMR** (121.5 MHz, 298.0 K, THF): δ / ppm = −34.8 (br. s, $P^-$), 5.19 (br. s, P-N$^i$Pr$_2$).

### 5.6.8 Synthesis of potassium 3,7-di-*n*-propyl-di(1,3-thiazole-2(3*H*)-thione)[2,3-d:5,6-d']-4-(*t*-butoxy)-4,8-dihydro-4,8-diphosphinino-8-phosphan-1-ide (5e)

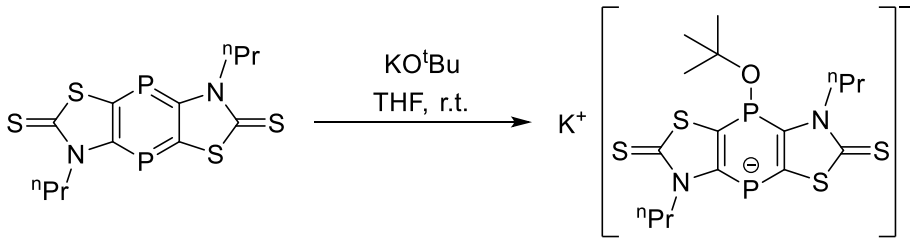


**1** **5e**

In a 20 mL Schlenk vessel, 5 mL of THF were added to a mixture of 108.5 mg (0.288 mmol, 1.00 eq.) of **1** and 35.9 mg (0.294 mmol, 1.02 eq.) of potassium *t*-butoxide at ambient temperature. Solvent was removed *in vacuo* ($10^{-2}$ mbar) after stirring the mixture for 1.5 h and the residue was washed three times with 3 mL of *n*-pentane each to give **5e** as a brown powder.

**Reaction code:** TK-567 (TIM231025p9a032)

**Molecular formula:** $C_{16}H_{23}KN_2OP_2S_4$

**Molecular weight:** 488.66 g/mol

**Yield:** 126.3 mg (0.259 mmol, 90%)

**Melting point:** 178 °C (dec.)

**MS** (neg. ESI, selected data): m/z (%): 497.002 (100) $[M+3O]^{-\bullet}$, 468.971 (40) $[M+3O-C_2H_4]^{-\bullet}$, 424,945 (33) $[M+O-2C_2H_4]^{-\bullet}$.

**HRMS** (neg. ESI) for $C_{12}H_{14}N_2OP_2S_4O_2H$ theor./exp. 424.9446 /424.9451 $[M+2O-2C_2H_4]^{-\bullet}$.

**IR** (ATR Diamond, selected data): $\tilde{\nu}$ / $cm^{-1}$ = 2872 (w, *v*(CH)), 2930 (w, *v*(CH)), 2968 (w, *v*(CH)).

**$^1$H NMR** (500.1 MHz, 298.0 K, THF-d8): δ / ppm = 0.89–1.00 (m, 6H, $CH_2CH_2CH_3$), 1.10 (s, 9H, *$^t$Bu*), 1.81–1.90 (m, 4H, $CH_2CH_2CH_3$), 4.12–4.23 (m, 3H, $CH_2CH_2CH_3$), 4.64–4.74 (m, 1H, $CH_2CH_2CH_3$).

**$^{13}$C{$^1$H} NMR** (125.8 MHz, 298.0 K, THF-d8): δ / ppm = 11.6 (s, $CH_2CH_2CH_3$), 11.7 (s, $CH_2CH_2CH_3$), 20.4 (d, $^4J_{P,C}$ = 4.52 Hz, $CH_2CH_2CH_3$), 22.0 (d, $^4J_{P,C}$ = 6.81 Hz, $CH_2CH_2CH_3$), 31.0 (d, $^3J_{P,C}$ = 7.22 Hz, $OC(CH_3)_3$), 49.9 (d, $^3J_{P,C}$ = 46.4 Hz, $CH_2CH_2CH_3$), 50.3 (d, $^3J_{P,C}$ = 20.8 Hz, $CH_2CH_2CH_3$), 74.2 (s, $OC(CH_3)_3$) 107.6 (dd, $^1J_{P,C}$ = 19.7 Hz, $^2J_{P,C}$ = 8.88 Hz, P*C*S) 131.1 (dd, $^1J_{P,C}$ = 9.30 Hz, $^2J_{P,C}$ = 2.75 Hz, P*C*N), 149.2 (dd, $^1J_{P,C}$ = 55.2 Hz, $^2J_{P,C}$ = 7.73 Hz, P*C*S), 164.3 (dd, $^1J_{P,C}$ = 52.6 Hz, $^2J_{P,C}$ = 5.14 Hz, P*C*N), 185.4 (dd, $^3J_{P,C}$ = 5.49 Hz, $^3J_{P,C}$ = 1.65 Hz, *C*=S), 189.8 (d, $^3J_{P,C}$ =f 10.4 Hz, *C*=S).

**$^{31}$P{$^1$H} NMR** (202.5 MHz, 298.0 K, THF-d8): δ / ppm = −15.5 (d, $^3J_{P,P}$ = 3.81 Hz, $P^-$), 31.4 (m, $^3J_{P,P}$ = 3.81 Hz P-O$^t$Bu).

**$^{31}$P NMR** (202.5 MHz, 298.0 K, THF-d8): δ / ppm = −15.5 (m, $P^-$), 31.4 (m, P-O$^t$Bu).

### 5.6.9 Synthesis of Lithium 3,7-di-*n*-propyl-di(1,3-thiazole-2(3*H*)-thione)[2,3-d:5,6-d']-4-oxo-4σ$^4$λ$^5$,8σ$^2$λ$^3$-diphosphinino-8-phosphan-4-ide (5f')

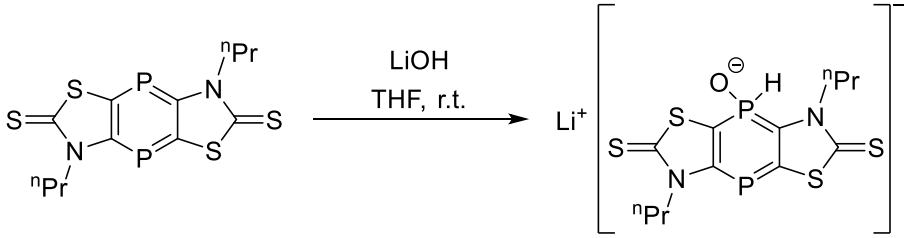


**1** **5f'**

In a 10 mL Schlenk tube, 2 mL of THF were added to a mixture of 42.0 mg (0.112 mmol, 1.00 eq.) of **1** and 3.0 mg (0.125 mmol, 1.12 eq.) of LiOH at ambient temperature. The mixture was stirred for 21 h before removing solvent *in vacuo* ($10^{-2}$ mbar). The residue was extracted twice with 0.5 mL of toluene each, before washing with 2 mL of *n*-pentane.

**Reaction code:** TK-197 (48p5a007.20)

**Molecular formula:** $LiC_{12}H_{15}N_2OP_2S_4$

**Molecular weight:** 400.39 g/mol

**Yield:** —

**MS** (neg. ESI, selected data): m/z (%): 424.945 (100) $[M+2O]^{-\bullet}$.

**IR** (ATR Diamond, selected data): $\tilde{\nu}$ / $cm^{-1}$ = 2439 (w, PH), 2871 (m, CH), 2961 (m, CH).

**$^{1}$H NMR** (500.1 MHz, 298.0 K, THF-d8): δ / ppm = 0.97 (t, 3H, $^{3}J_{H,H}$ = 7.47 Hz, $CH_2CH_2\mathit{CH_3}$), 1.00 (t, 3H, $^{3}J_{H,H}$ = 7.55 Hz, $CH_2CH_2\mathit{CH_3}$), 1.80–1.88 (m, 2H, $CH_2\mathit{CH_2}CH_3$), 1.93–2.02 (m, 2H, $CH_2\mathit{CH_2}CH_3$), 4.01–4.09 (m, 1H, $\mathit{CH_2}CH_2CH_3$), 4.10–4.17 (m ,1H, $\mathit{CH_2}CH_2CH_3$), 4.18–4.26 (m, 1H, $\mathit{CH_2}CH_2CH_3$), 4.60–4.68 (m, 1H, $\mathit{CH_2}CH_2CH_3$), 9.06 (dd, 1H, $^{4}J_{P,H}$ = 1.50 Hz, $^{1}J_{P,H}$ = 544.8 Hz, P*H*).

**$^{13}$C{$^{1}$H} NMR** (125.8 MHz, 298.0 K, THF-d8): δ / ppm = 11.6 (s, $CH_2CH_2\mathit{CH_3}$), 11.6 (s, $CH_2CH_2\mathit{CH_3}$), 20.5 (d, $^{4}J_{P,C}$ = 4.66 Hz, $CH_2\mathit{CH_2}CH_3$), 22.5 (s, $CH_2\mathit{CH_2}CH_3$), 50.3 (d, $^{3}J_{P,C}$ = 2.04 Hz, $\mathit{CH_2}CH_2CH_3$), 50.4 (d, $^{3}J_{P,C}$ = 21.0 Hz, $\mathit{CH_2}CH_2CH_3$), 95.8 (dd, $^{1}J_{P,C}$ = 140.3 Hz, $^{2}J_{P,C}$ = 11.0 Hz, S*C*PH-O$^{-}$), 122.5 (dd, $^{1}J_{P,C}$ = 134.3 Hz, $^{2}J_{P,C}$ = 11.2 Hz, N*C*PH-O$^{-}$), 153.8 ($^{1}J_{P,C}$ = 61.9 Hz, $^{2}J_{P,C}$ = 17.3 Hz, S*C*P), 168.7 ($^{1}J_{P,C}$ = 58.5 Hz, $^{2}J_{P,C}$ = 13.4 Hz, N*C*P), 187.3 (dd, $^{3}J_{P,C}$ = 9.37 Hz, $^{3}J_{P,C}$ = 5.39 Hz, *C*=S), 190.8 (d, $^{3}J_{P,C}$ = 7.33 Hz, *C*=S).

**$^{31}$P{$^{1}$H} NMR** (202.5 MHz, 298.0 K, THF-d8): δ / ppm = −18.9 (s, PH-O$^{-}$), −16.0 (s, $PR_2$).

**$^{31}$P NMR** (202.5 MHz, 298.0 K, THF-d8): δ / ppm = −18.9 (d, $^{1}J_{P,H}$ = 544.9 Hz, PH-O$^{-}$), −16.0 (s, $PR_2$).

### 5.6.10 Synthesis of 3,7-di-*n*-propyl-di(1,3-thiazole-2(3*H*)-thione)[2,3-d:5,6-d']- 8-methyl-4-(1',3',4',5'-tetramethyl-imidazolium)-4,8-dihydro-4,8-diphosphinine iodide (6a)

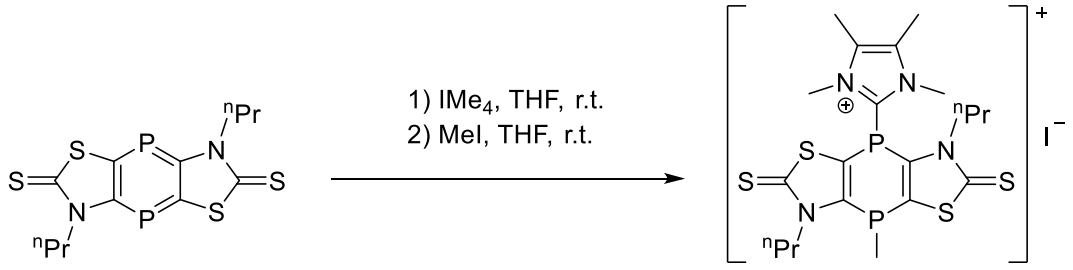


**1** **6a**

In a 10 mL Schlenk vessel, 6 ml THF were added to a mixture of 101.7 mg (0.270 mmol, 1.00 eq.) of **1** and 33.5 mg (0.270 mmol, 1.00 eq.) of $IMe_4$ at ambient temperature. The mixture was stirred for 15 min before the addition of 0.02 mL (0.321 mmol, 1.19 eq.) of MeI. The reaction was stirred for 1.5 h and then filtered. The residue was washed with 3 mL of THF and dried *in vacuo* ($10^{-2}$ mbar) to give a beige solid.

**Reaction code:** TK-554 (TIM230908m3a013, TIM230912m3a049)

**$^{31}P\{^{1}H\}$ NMR** (121.5 MHz, 297.9 K, $CH_2Cl_2$): δ / ppm = −68.1 (d, $^{3}J_{P,P}$ = 18.2 Hz, P-IMe$^4$), −64.9 (d, $^{3}J_{P,P}$ = 24.6 Hz, P-IMe$^4$ *isomer*), −50.4 (d, $^{3}J_{P,P}$ = 18.2 Hz, P-$CH_3$), −46.2 (d, $^{3}J_{P,P}$ = 24.0 Hz, P-$CH_3$ *isomer*), 134.3 (s, **1**).

**$^{31}P$ NMR** (202.5 MHz, 298.0 K, THF-d8): δ / ppm = −68.1 (d, $^{3}J_{P,P}$ = 18.5 Hz, P-IMe$^4$), −64.9 (d, $^{3}J_{P,P}$ = 24.1 Hz, P-IMe$^4$ *isomer*), −50.4 (dq, $^{3}J_{P,P}$ = 18.2 Hz, $^{2}J_{P,H}$ = 5.37 Hz, P-$CH_3$), −46.2 (m, P-$CH_3$ *isomer*), 134.3 (s, **1**).

### 5.6.11 Attempted synthesis of 3,7-di-*n*-propyl-di(1,3-thiazole-2(3*H*)-thione)[2,3-d:5,6-d']-8-methyl-4-(1'-(2',6'-di-*i*-propylphenyl)-3',3',5',5'-tetramethyl-azolidinium)-4,8-dihydro-4,8-diphosphinine iodide (6b)

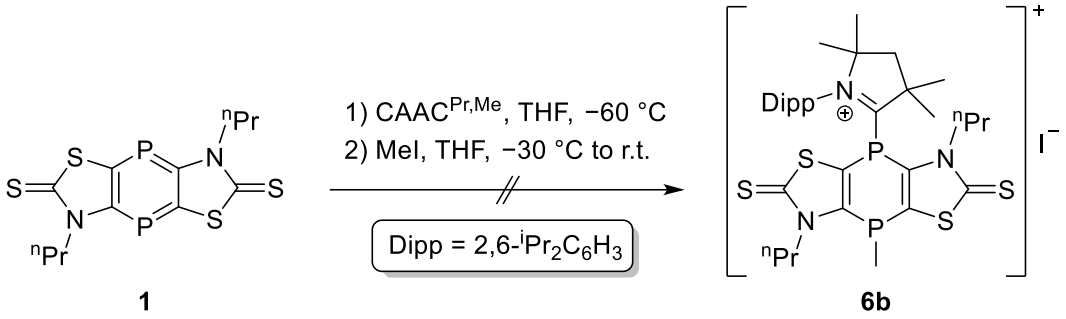


**1** **6b**

In a 10 mL Schlenk vessel, 3 ml THF were added to a mixture of 33.5 mg (0.222 mmol, 1.00eq.) of **1** and 63.8 mg (0.223 mmol, 1.00 eq.) of CAAC$^{Pr,Me}$ at −60 °C. After stirring the reaction mixture for 2 h, 0.02 mL (0.321 mmol, 1.45 eq.) of MeI were added at −30 °C before stirring for a further 30 min. Solvent was removed *in vacuo* ($10^{-2}$ mbar) and $CH_2Cl_2$ was added at room temperature.

**Reaction code:** TK-556 (TIM230918m3a008, TIM230918m3a010)

### 5.6.12 Synthesis of 3,7-di-*n*-propyl-di(1,3-thiazole-2(3*H*)-thione)[2,3-d:5,6-d']- 8-methyl-4-bis(trimethylsilyl)amino-4,8-dihydro-4,8-diphosphinine (6c)

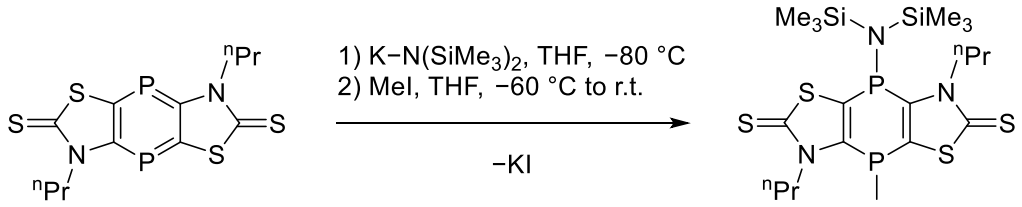


**1** **6c**

In a 10 mL Schlenk vessel, 5 mL THF were added to a mixture of 171.9 mg (0.457 mmol, 1.00 eq.) of **1** and 91.3 mg (0.458 mmol, 1.00 eq.) of KHMDS at −80 °C. After stirring for 1 h, 0.03 mL (0.482 mmol, 1.05 eq.) MeI were added at −60 °C. The mixture was stirred for 3 h before filtering off the solvent. the brown residue was washed three times with 6 mL *n*-pentane each and then dried *in vacuo* ($10^{-2}$ mbar). **6d** was obtained as an orange solid.

**Reaction code:** TK-559 (TIM230927p5a022)

**Molecular formula:** $C_{19}H_{35}N_3P_2S_4Si_2$

**Molecular weight:** 551.87 g/mol

**Yield:** 135.8 mg (0.246 mmol, 54%)

**Melting point:** 192 °C (dec. to **1**)

**MS** (APCI, selected data): m/z (%): 552.081 (100) $[M+H]^{+\bullet}$.

**HRMS** (neg. ESI) for $C_{19}H_{35}N_3P_2S_4Si_2H$ theor./exp. 552.0800/552.0803 $[M+H]^{+\bullet}$.

**IR** (ATR Diamond, selected data): $\tilde{\nu}$ / $cm^{-1}$ = 2962 (w, *ν*(CH)).

**$^1$H NMR** (500.1 MHz, 298.0 K, THF-d8): δ / ppm = 0.01 (s, Si(*CH*$_3$)$_3$), 0.97–1.03 (m, 6H, $CH_2CH_2CH_3$), 1.54 (d, 1H, $^1J_{P,H}$ = 4.98 Hz, P*CH*$_3$) 1.80–1.96 (m, 3H, $CH_2CH_2CH_3$), 1.97-2.09 (m, 1H, $CH_2CH_2CH_3$), 3.83 (ddd, 1H $^XJ_{H,H}$ = 13.7 Hz, $^XJ_{H,H}$ = 10.3 Hz, $^XJ_{H,H}$ = 5.70 Hz, $CH_2CH_2CH_3$), 4.08 (ddd, 1H $^XJ_{H,H}$ = 13.4 Hz, $^XJ_{H,H}$ = 10.8 Hz, $^XJ_{H,H}$ = 5.85 Hz, $CH_2CH_2CH_3$), 4.52 (ddd, 1H $^XJ_{H,H}$ = 13.5 Hz, $^XJ_{H,H}$ = 10.3 Hz, $^XJ_{H,H}$ = 5.39 Hz, $CH_2CH_2CH_3$), 4.64 (ddd, 1H $^XJ_{H,H}$ = 13.4 Hz, $^XJ_{H,H}$ = 10.9 Hz, $^XJ_{H,H}$ = 4.81 Hz, $CH_2CH_2CH_3$).

**$^{13}$C{$^1$H} NMR** (125.8 MHz, 298.0 K, THF-d8): δ / ppm = 3.23 (d, $^3J_{P,C}$ = 14.8 Hz, Si(*CH*$_3$)$_3$), 10.2 (s, $CH_2CH_2CH_3$), 10.2 (s, $CH_2CH_2CH_3$), 16.7 (dd, $^1J_{P,C}$ = 17.5 Hz, $^4J_{P,C}$ = 11.3 Hz), 20.2 (d, $^4J_{P,C}$ = 4.52 Hz, $CH_2CH_2CH_3$), 20.8 (d, $^4J_{P,C}$ = 3.88 Hz, $CH_2CH_2CH_3$), 50.7 (d, $^3J_{P,C}$ = 6.81 Hz, $CH_2CH_2CH_3$), 51.0 (d, $^3J_{P,C}$ = 13.0 Hz, $CH_2CH_2CH_3$), 123.0 (d, $^1J_{P,C}$ = 17.8 Hz, P*C*S), 130.5 (dd, $^1J_{P,C}$ = 33.3 Hz, $^2J_{P,C}$ = 4.61 Hz, P*C*S), 138.9 (dd, $^1J_{P,C}$ = 13.2 Hz, $^2J_{P,C}$ = 3.64 Hz, P*C*N), 144.2 (dd, $^1J_{P,C}$ = 36.9 Hz, $^2J_{P,C}$ = 3.53 Hz, P*C*N), 189.5 (d, $^3J_{P,C}$ = 5.39 Hz, *C*=S), 189.8 (d, $^3J_{P,C}$ = 7.36 Hz, *C*=S).

**$^{31}$P{$^1$H} NMR** (202.5 MHz, 298.0 K, THF-d8): δ / ppm = –51.4 (d, $^3J_{P,P}$ = 18.5 Hz), 13.4 (d, $^3J_{P,P}$ = 18.5 Hz).

**$^{31}$P NMR** (202.5 MHz, 298.0 K, THF-d8): δ / ppm = –51.4 (dq, $^3J_{P,P}$ = 18.5 Hz, $^2J_{P,H}$ = 5.08 Hz), 13.4 (d, $^3J_{P,P}$ = 18.5 Hz).

### 5.6.13 Attempted synthesis of 3,7-di-*n*-propyl-di(1,3-thiazole-2(3*H*)-thione)[2,3-d:5,6-d']-8-methyl-4-(di-*i*-propylamino)-4,8-dihydro-4,8-diphosphinine (6d)

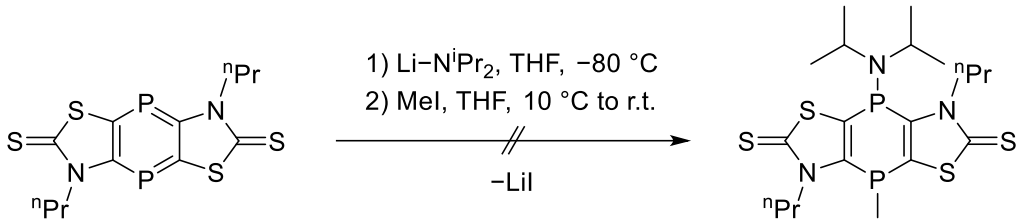


**1** **6d**

A solution of 9.8 mg (0.091 mmol, 1.00 eq.) of LDA in 1 mL THF was added to a suspension of 34.3 mg (0.091 mmol, 1.00 eq.) of **1** in 2 mL THF at −80 °C in a 10 mL Schlenk vessel. After stirring for 5 h while slowly warming up, 0.01 mL (0.161 mmol, 1.46 eq.) of MeI were added at 10 °C. The mixture was stirred for 5 min.

**Reaction code:** TK-551 (TIM230906m3a021)

### 5.6.14 Attempted synthesis of 3,7-di-*n*-propyl-di(1,3-thiazole-2(3*H*)-thione)[2,3-d:5,6-d']-8-methyl-4-(*t*-butoxy)-4,8-dihydro-4,8-diphosphinine (6e)

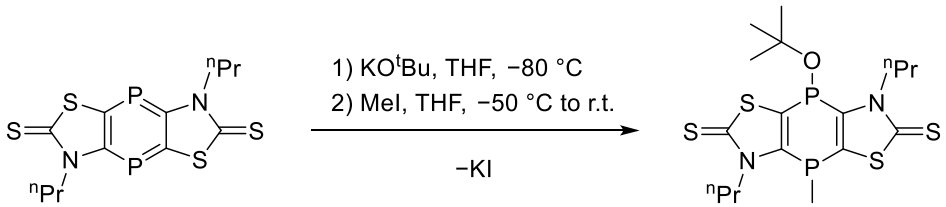


**1** **6e**

In a 10 mL Schlenk vessel, 5 mL THF were added to a mixture of 52.8 mg (0.140 mmol, 1.00 eq.) of **1** and 17.1 mg (0.140 mmol, 1.00 eq.) of KO$^{t}$Bu at −80 °C. The reaction was stirred for 3 h while slowly warming up and 0.01 mL (0.161 mmol, 1.15 eq.) of MeI were added at −50 °C. The mixture was stirred for 23 h before removing solvent *in vacuo* ($10^{-2}$ mbar) and re-adding 3 mL of THF.

**Reaction code:** TK-562 (TIM231005m3a015, TIM231006m3a043)

**$^{31}$P{$^{1}$H} NMR** (121.5 MHz, 298.0 K, THF): δ / ppm = –53.4 (d, $^{3}J_{P,P}$ = 11.5 Hz, P-CH$_3$), −50.3 (d, $^{3}J_{P,P}$ = 14.6 Hz), −47.2 (d, $^{3}J_{P,P}$ = 10.5 Hz), 45.1 (d, $^{3}J_{P,P}$ = 11.5 Hz, P-O$^{t}$Bu), 50.3 (d, $^{3}J_{P,P}$ = 14.2 Hz), 52.7 (d, $^{3}J_{P,P}$ = 10.5 Hz).

**$^{31}$P NMR** (121.5 MHz, 298.0 K, THF): δ / ppm = –53.3 (dq, $^{3}J_{P,P}$ = 10.3 Hz, $^{2}J_{P,H}$ = 5.11 Hz, P-CH$_3$), 45.2 (d, $^{3}J_{P,P}$ = 11.4 Hz, P-O$^{t}$Bu).

### 5.6.15 Attempted synthesis of 3,7-di-*n*-propyl-di(1,3-thiazole-2(3*H*)-thione)[2,3-d:5,6-d']-8-methyl-4-oxo-4,8-dihydro-4σ⁴λ⁵,8σ³λ³-diphosphinine (7a)

*5.6.15.1 Methyl iodide/triflate*

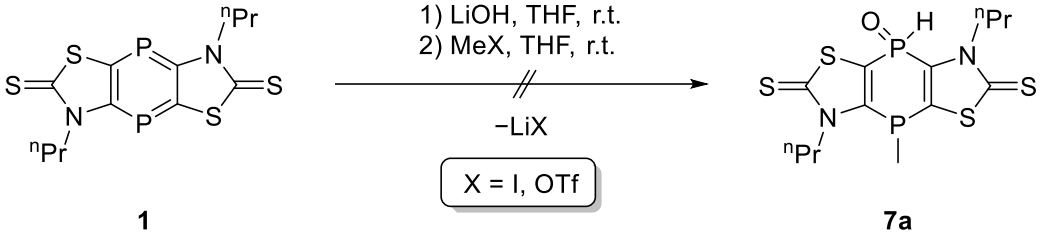


**1** **7a**

In a 10 mL Schlenk vessel, 5 mL THF were added to a mixture of 46.5 mg (0.124 mmol, 1.00 eq.) of **1** and 3.0 mg (0.125 mmol, 1.01 eq.) of LiOH at ambient temperature. The mixture was stirred for 28 h before the addition of 1.56 mL (0.125 mmol, 1.01 eq.) of a 0.0803 M solution of MeI in THF at ambient temperature. The reaction mixture was stirred further for 1 h.

**Reaction code:** TK-198 (48t4a049.20)

**$^{31}P\{^{1}H\}$ NMR** (162.0 MHz, 298.0 K, THF): δ / ppm = −18.7 (s, PH-O⁻), −15.7 (s, $PR_2$).

**$^{31}P$ NMR** (162.5 MHz, 298.0 K, THF): δ / ppm = −18.7 (d, $^{1}J_{P,H}$ = 544.8 Hz, PH-O⁻), −15.7 (s, $PR_2$).

In a 10 mL Schlenk vessel, 3 mL THF were added to a mixture of 33.5 mg (0.089 mmol, 1.00 eq.) of **1** and 2.1 mg (0.088 mmol, 0.99 eq.) of LiOH at ambient temperature. The mixture was stirred for 4 h before the addition of 0.39 mL (0.089 mmol, 1.00 eq.) of a 0.2285 M solution of MeOTf in THF at ambient temperature. The reaction mixture was stirred further for 30 min.

**Reaction code:** TK-199 (48t4a016.20)

**$^{31}P\{^{1}H\}$ NMR** (162.0 MHz, 298.0 K, THF): δ / ppm = −18.7 (s, PH-O⁻), −15.7 (s, $PR_2$).

*5.6.15.2 Methyl iodide/triflate, 12-crown-4*

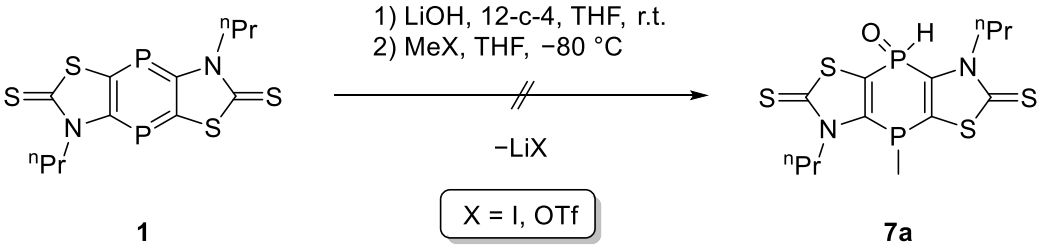


**1** **7a**

In a 10 mL Schlenk vessel, a solution of 14 µL (0.087 mmol, 1.00 eq.) of 12-crown-4 in 3 mL THF were added to a mixture of 32.8 mg (0.087 mmol, 1.00 eq.) of **1** and 2.1 mg (0.088 mmol, 1.01 eq.) of LiOH at ambient temperature. The mixture was stirred for 2 h before the addition

of 0.11 mL (0.088 mmol, 1.01 eq.) of a 0.803 M solution of MeI in THF at −80 °C. The reaction mixture was stirred further for 1 h while slowly warming up.

**Reaction code:** TK-202 (49t4a093.20)

In a 10 mL Schlenk vessel, a solution of 19 µL (0.118 mmol, 0.99 eq.) of 12-crown-4 in 3 mL THF were added to a mixture of 44.7 mg (0.119 mmol, 1.00 eq.) of **1** and 2.8 mg (0.117 mmol, 0.99 eq.) of LiOH at ambient temperature. The mixture was stirred for 4 h before the addition of 0.52 mL (0.119 mmol, 1.00 eq.) of a 0.229 M solution of MeOTf in THF at −80 °C. The reaction mixture was stirred further for 30 min while slowly warming up.

**Reaction code:** TK-200 (48t4a066.20)

### 5.6.16 Attempted synthesis of 3,7-di-*n*-propyl-di(1,3-thiazole-2(3*H*)-thione)[2,3-d:5,6-d']--4-oxo-4,8-dihydro-4σ⁴λ⁵,8σ³λ³-diphosphinine (7b)

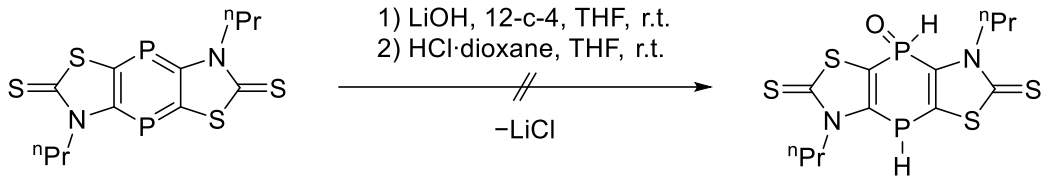


**1** **7b**

In a 10 mL Schlenk tube, a solution of 12 µL (0.074 mmol, 1.00 eq.) of 12-crown-4 in 4 mL THF is added to a mixture of 27.8 mg (0.074 mmol, 1.00 eq.) **1** and 1.7 mg (0.071 mmol, 0.96 eq.) LiOH at ambient temperature. The mixture was stirred 28 h before the addition of 0.02 mL (0.080 mmol, 1.08 eq. of a 4 M solution of HCl in dioxane. The orange suspension was stirred for another 10 min.

**Reaction code:** TK-203

**$^{31}P\{^{1}H\}$ NMR** (121.5 MHz, 298.0 K, THF): δ / ppm = 53.3 (s), 133.0 (s).

### 5.6.17 Attempted synthesis of 3,7-di-*n*-propyl-di(1,3-thiazole-2(3*H*)-thione)[2,3-d:5,6-d']-8-trimethylsilyl-4-(1',3',4',5'-tetramethyl-imidazolium)-4,8-dihydro-4,8-diphosphinine chloride (9a)

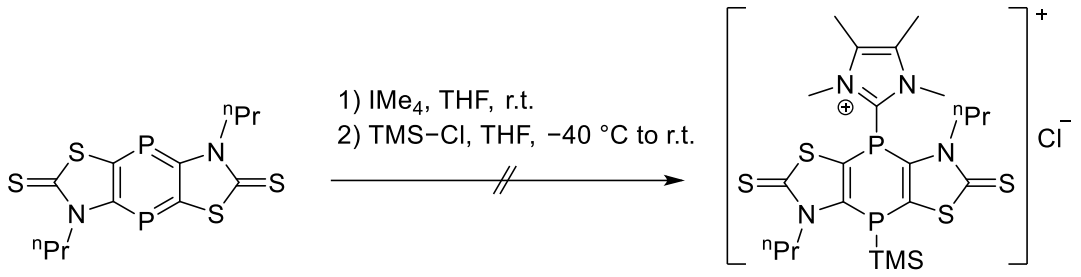


**1** **9a**

In a 10 mL Schlenk vessel, 5 ml THF were added to a mixture of 107.4 mg (0.285 mmol, 1.00 eq.) of **1** and 35.2 mg (0.283 mmol, 0.99 eq.) of $IMe_4$ at ambient temperature. The mixture was stirred for 1.5 h before the addition of 0.04 mL (0.313 mmol, 1.10 eq.) of TMS-Cl at −40 °C and further stirring for 1.5 h.

**Reaction code:** TK-565 (TIM231020m3a013)

**$^{31}P\{^{1}H\}$ NMR** (121.5 MHz, 298.0 K, THF): δ / ppm = −95.9 (s), 133.0 (s).

### 5.6.18 Attempted synthesis of 3,7-di-*n*-propyl-di(1,3-thiazole-2(3*H*)-thione)[2,3-d:5,6-d']-8-trimethylsilyl-4-(1'-(2',6'-di-*i*-propylphenyl)-3',3',5',5'-tetramethyl-azolidinium)-4,8-dihydro-4,8-diphosphinine chloride (9b)

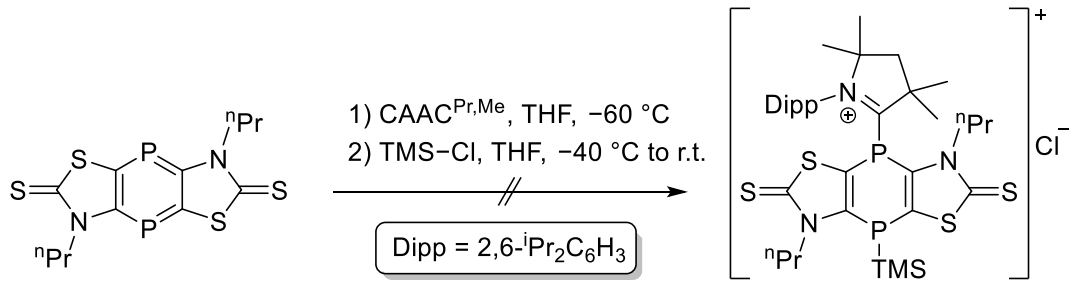


**1** **9b**

In a 10 mL Schlenk vessel, 5 ml THF were added to a mixture of 68.0 mg (0.181 mmol, 1.00eq.) of **1** and 52.0 mg (0.182 mmol, 1.01 eq.) of $CAAC^{Pr,Me}$ at −60 °C. After stirring the reaction mixture for 1.5 h, 0.03 mL (0.235 mmol, 1.30 eq.) of TMS-Cl were added at −40 °C before stirring for a further 1.5 h.

**Reaction code:** TK-566 (TIM231020m3a015)

**$^{31}P\{^{1}H\}$ NMR** (121.5 MHz, 298.0 K, THF): δ / ppm = 65.9 (s), 136.4 (s).

### 5.6.19 Attempted synthesis of 3,7-di-*n*-propyl-di(1,3-thiazole-2(3*H*)-thione)[2,3-d:5,6-d']-8-trimethylsilyl-4-bis(trimethylsilyl)amino-4,8-dihydro-4,8-diphosphinine (9c)

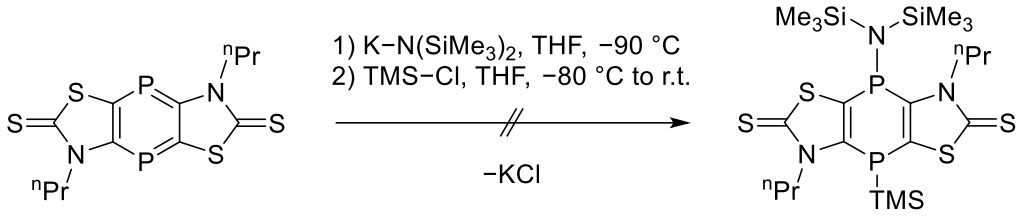


**1** **9c**

In a 10 mL Schlenk vessel, 2 mL THF were added to a mixture of 47.1 mg (0.125 mmol, 1.00 eq.) of **1** and 24.9 mg (0.125 mmol, 1.00 eq.) of KHMDS at −90 °C. After stirring for 3 h, 0.02 mL (0.156 mmol, 1.25 eq.) TMS-Cl were added at −80 °C. The mixture was stirred for 1.5 h while slowly warming up.

**Reaction code:** TK-558 (TIM230920m3a025)

**$^{31}P\{^{1}H\}$ NMR** (121.5 MHz, 298.0 K, THF): δ / ppm = −36.6 (t, $^{n}J_{P,P}$ = 20.1 Hz), 21.9 (t, $^{n}J_{P,P}$ = 20.7 Hz).

### 5.6.20 Attempted synthesis of 3,7-di-*n*-propyl-di(1,3-thiazole-2(3*H*)-thione)[2,3-d:5,6-d']-8-trimethylsilyl-4-(di-*i*-propylamino)-4,8-dihydro-4,8-diphosphinine (9d)

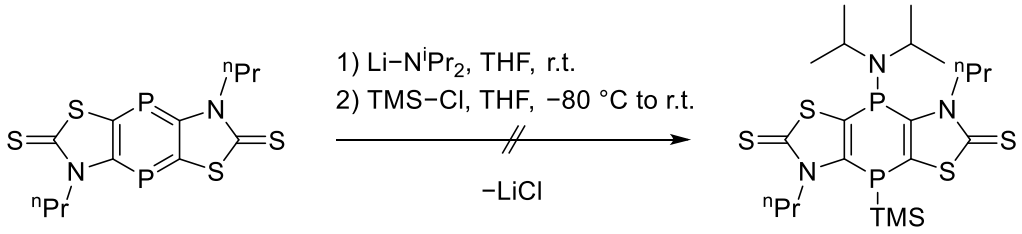


**1** **9d**

A solution of 12.1 mg (0.113 mmol, 1.06 eq.) of LDA in 1 mL THF was added to a suspension of 40.0 mg (0.107 mmol, 1.00 eq.) of **1** in 2 mL THF at r.t. in a 10 mL Schlenk vessel. After stirring for 30 min, 0.02 mL (0.156 mmol, 1.46 eq.) of TMS-Cl were added at −80 °C. The mixture was stirred for 17.5 h while slowly warming up.

**Reaction code:** TK-553 (TIM230908t4a002)

### 5.6.21 Attempted synthesis of 3,7-di-*n*-propyl-di(1,3-thiazole-2(3*H*)-thione)[2,3-d:5,6-d']-8-trimethylsilyl-4-(*t*-butoxy)-4,8-dihydro-4,8-diphosphinine (9e)

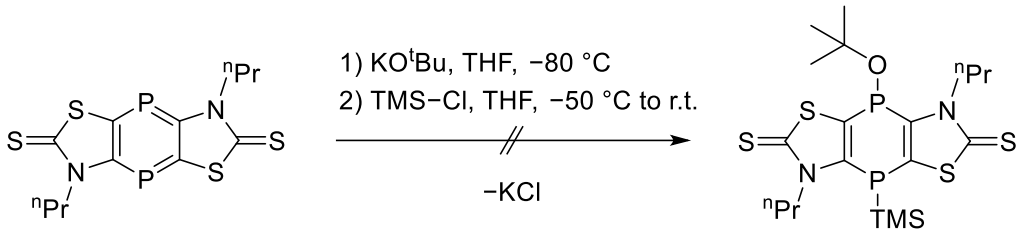


**1** **9e**

In a 10 mL Schlenk vessel, 2 mL THF were added to a mixture of 35.2 mg (0.094 mmol, 1.00 eq.) of **1** and 11.4 mg (0.093 mmol, 0.99 eq.) of KO$^t$Bu at −80 °C. The reaction was stirred for 3 h while slowly warming up and 0.02 mL (0.156 mmol, 1.67 eq.) of TMS-Cl were added at −50 °C.

**Reaction code:** TK-563 (TIM231005m3a013)

**$^{31}$P{$^1$H} NMR** (121.5 MHz, 298.0 K, THF): δ / ppm = 49.6 (s), 133.4 (s).

### 5.6.22 Synthesis of 3,7-di-*n*-propyl-di(1,3-thiazole-2(3*H*)-thione)[2,3-d:5,6-d']-4-chloro-8-trichloromethyl-4,8-dihydro-4,8-diphosphinine (12)

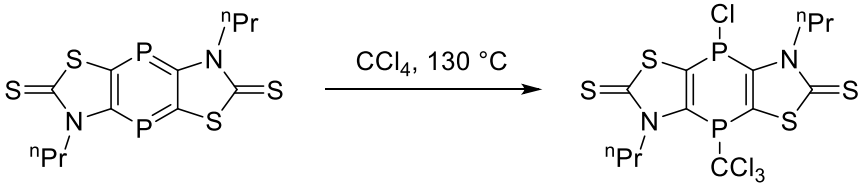


**1** **12**

In a 10 mL Schlenk tube 39.7 mg (0.105 mmol, 1.00 eq.) of **1** were dissolved in 5 mL of carbon tetrachloride. The mixture was stirred for 2 h at 130 °C. The solvent was removed at 80 °C *in vacuo* ($10^{-2}$ mbar) and the yellow residue was washed three times with 2 mL *n*-pentane each. The product **5** was obtained as a yellow solid.

**Reaction code:** TK-146 (33m3a022.19, 33c5a021.19, 33m3b049.19)

**Molecular formula:** $C_{13}H_{14}Cl_4N_2P_2S_4$

**Molecular weight:** 530.26 g/mol

**Yield:** 44.5 mg (0.084 mmol, 80%)

**Melting point:** 144 °C

**MS** (EI, 70 eV, selected data): m/z (%): 527.9 (100) $[M]^{+\bullet}$, 408.9 (13) $[M-2\ C_3H_6-Cl]^{+\bullet}$.

**IR** (ATR Diamond, selected data): $\tilde{\nu}$ / $cm^{-1}$ = 2869 (w, *v*(CH)), 2928 (w, *v*(CH)), 2960 (w, *v*(CH)).

**$^{1}$H NMR** (499.1 MHz, 298.0 K, toluene-d8): δ / ppm = 0.71 (t, 6H, $^{3}J_{H,H}$ = 7.39 Hz, $CH_2CH_2\mathit{CH_3}$), 0.76 (td, $^{3}J_{H,H}$ = 7.39 Hz, $^{3}J_{H,H}$ = 3.45 Hz, $CH_2CH_2\mathit{CH_3}$, *2nd isomer*), 1.42-1.50 (m 1H, $CH_2\mathit{CH_2}CH_3$), 1.53-1.63 (m, 1H, $CH_2\mathit{CH_2}CH_3$), 1.66-1.74 (m, 1H, $CH_2\mathit{CH_2}CH_3$), 1.84-1.97 (m, 1H, $CH_2\mathit{CH_2}CH_3$), 3.92-3.99 (m, 1H, $\mathit{CH_2}CH_2CH_3$), 4.02-4.10 (m, 1H, $\mathit{CH_2}CH_2CH_3$), 4.25-4.34 (m, 1H, $\mathit{CH_2}CH_2CH_3$), 4.58-4.66 (m, 1H, $\mathit{CH_2}CH_2CH_3$).

**$^{13}$C{$^{1}$H} NMR** (125.5 MHz, 298.0 K, toluene-d8): δ / ppm = 11.2 (d, $^{5}J_{P,C}$ = 1.44 Hz, $CH_2CH_2\mathit{CH_3}$), 11.3 (d, $^{5}J_{P,C}$ = 0.96 Hz, $CH_2CH_2\mathit{CH_3}$), 20.6 (d, $^{4}J_{P,C}$ = 3.38 Hz, $CH_2\mathit{CH_2}CH_3$), 20.9 (d, $^{4}J_{P,C}$ = 3.12 Hz, $CH_2\mathit{CH_2}CH_3$), 51.6 (d, $^{3}J_{P,C}$ = 7.54 Hz, $\mathit{CH_2}CH_2CH_3$), 51.8 (d, $^{3}J_{P,C}$ = 11.4 Hz, $\mathit{CH_2}CH_2CH_3$), 116.3 (d, $^{1}J_{P,C}$ = 23.6 Hz, P$\mathit{CCl_3}$), 133.6 (dd, $^{1}J_{P,C}$ = 47.5 Hz, $^{2}J_{P,C}$ = 3.33 Hz, P*C*S), 135.4 (dd, $^{1}J_{P,C}$ = 15.8 Hz, $^{2}J_{P,C}$ = 3.91 Hz, P*C*N), 148.4 (dd, $^{1}J_{P,C}$ = 54.2 Hz, $^{2}J_{P,C}$ = 2.08 Hz, P*C*N), 190.0 (d, $^{3}J_{P,C}$ = 2.84 Hz, *C*=S), 191.3 (d, $^{3}J_{P,C}$ = 6.58 Hz, *C*=S).

**$^{31}$P{$^{1}$H} NMR** (202.1 MHz, 297.9 K, toluene-d8): δ / ppm = −10.1 (d, $^{3}J_{P,P}$ = 6.33 Hz, P-$CCl_3$), 0.82 (d, $^{3}J_{P,P}$ = 6.41 Hz, P-$CCl_3$, *2nd isomer*), 26.2 (d, $^{3}J_{P,P}$ = 6.41 Hz, P-Cl, *2nd isomer*), 29.6 (d, $^{3}J_{P,P}$ = 6.33 Hz, P-Cl).

**$^{31}$P NMR** (202.1 MHz, 297.9 K, toluene-d8): δ / ppm = −10.1 (dd, $^{3}J_{P,P}$ = 6.21 Hz, $^{4}J_{P,H}$ = 2.97 Hz, P-$CCl_3$), 0.82 (dd, $^{3}J_{P,P}$ = 5.75 Hz, $^{4}J_{P,H}$ = 3.42 Hz, P-$CCl_3$, *2nd isomer*), 26.2 (d, $^{3}J_{P,P}$ = 5.75 Hz, P-Cl, *2nd isomer*), 29.6 (d, $^{3}J_{P,P}$ = 6.21 Hz, P-Cl).

### 5.6.23 Attempted synthesis of 3,7-di-*n*-propyl-4,8-epithio[1,4]diphosphinino[2,3-d:5,6-d']bis[1,3]thiazole-2,6(3,7H)-dithione (13)

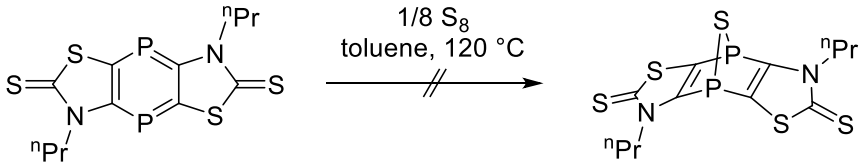


**1** **13**

4 mL of toluene were added to a mixture of 96.5 mg (0.256 mmol, 1.00 eq.) of **1** and 8.5 mg (0.265 mmol, 1.04 eq.) of $S_8$ in a 10 mL Schlenk tube. The suspension was heated to 120 °C and stirred for seven days while $^{31}$P{$^{1}$H} NMR spectroscopic monitoring was performed.

**Reaction code:** TK-103 (23m3b027.19, 24m3b006.19)

### 5.6.24 Synthesis of spiro[1',2'-dihydro-1',3'-bis(2',6'-di-*i*-propylphenyl)-4',6'-dimethyl-1',3',2'-diazagallinine-2,9'-[3,7]-di-*n*-propyl-[3,7]-dihydro-[4,8]-gallano[1,4]diphosphinino[2,3-d:5,6-d']bis[1,3]thiazole-[2,6]-dithione] (14a)

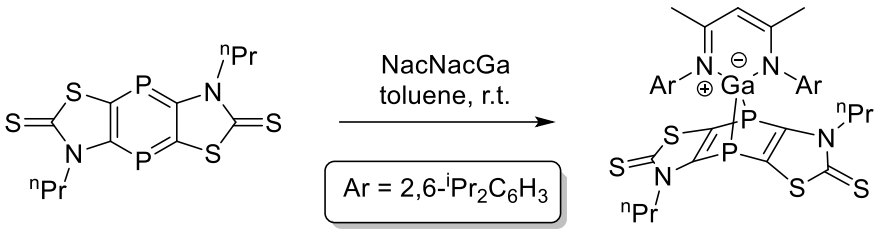


**1** **14a**

In a 10 mL vial a suspension of 51.3 mg (0.136 mmol, 1.00 eq.) **1** in 2 mL of toluene was added to a solution of 73.6 mg (0.151 mmol, 1.11 eq.) NacNacGa in 1 mL toluene. The mixture was stirred at ambient temperature for 20 h. The resulting suspension was decanted and the obtained solution was evaporated *in vacuo* ($10^{-2}$ mbar) before addition of diethyl ether. The suspension was cooled to −30 °C and decanted again. The solid residues were combined and dried *in vacuo* to give **7a** as an off-white powder.

**Reaction code:** TK-K-14 (TK-14-c)

**Molecular formula:** $C_{41}H_{55}GaN_4P_2S_4$

**Molecular weight:** 863.83 g/mol

**Yield:** 70 mg (0.081 mmol, 60%)

**MS** (EI, 70 eV, selected data): m/z (%): 928.2 $[M+3O+H_2O]^{+\bullet}$, 910.1 $[M+3O]^{+\bullet}$, 880.2 $[M+H_2O]^{+\bullet}$ 862.2 $[M]^{+\bullet}$, 486.1 $[C_{29}H_{41}GaN_2]^{+\bullet}$, 375.9 $[M-C_{29}H_{41}GaN_2]^{+\bullet}$, 333.8 $[M-C_{29}H_{41}GaN_2-C_3H_7+H]^{+\bullet}$, 291.9 $[M-C_{29}H_{41}GaN_2-2\ C_3H_7+2\ H]^{+\bullet}$.

**HRMS** (ESI) for $C_{41}H_{56}GaN_4P_2S_4O_3$ theor./exp. 911.1961/911.1964 $[M+3O+H]^{+\bullet}$.
for $C_{41}H_{56}GaN_4P_2S_4$ theor./exp. 863.211/863.206 $[M+H]^{+\bullet}$.

**IR** (ATR Diamond, selected data): $\tilde{\nu}$ / $cm^{-1}$ = 2867 (w, *v*(CH)), 2929 (m, *v*(CH)), 2959 (w, *v*(CH)).

**$^1$H NMR** (600.2 MHz, 298.1 K, $C_6D_6$): δ / ppm = 0.58 (t, 6H, $^3J_{H,H}$ = 7.39 Hz, $CH_2CH_2CH_3$), 0.87 (d, 6H, $^3J_{H,H}$ = 6.80 Hz, Ar-CH-$CH_3$), 0.88 (d, 6H, $^3J_{H,H}$ = 6.82 Hz, Ar-CH-$CH_3$), 1.40 (d, 6H, $^3J_{H,H}$ = 6.83 Hz, Ar-CH-$CH_3$), 1.47 (d, 6H, $^3J_{H,H}$ = 6.92 Hz, Ar-CH-$CH_3$), 1.48 (s, 6H, N-C-$CH_3$), 1.53−1.69 (m, 4H, $CH_2CH_2CH_3$), 2.84 (hept, 2H, $^3J_{H,H}$ = 6.81 Hz, Ar-$CH$-$CH_3$), 2.98 (hept, 2H, $^3J_{H,H}$ = 6.81 Hz, Ar-$CH$-$CH_3$), 3.82−3.89 (m, 2H, $CH_2CH_2CH_3$), 4.62−4.69 (m, 2H, $CH_2CH_2CH_3$), 4.77 (1H, s, N-C-$CH$), 6.95 (4H, dm, $^3J_{H,H}$ = 7.77 Hz, *m*-Dipp), 7.37 (2H, t, $^3J_{H,H}$ = 7.77 Hz, *p*-Dipp).

**$^{13}C\{^1H\}$ NMR** (150.9 MHz, 298.4 K, $C_6D_6$): δ / ppm = 11.3 (s, $CH_2CH_2\mathit{CH_3}$), 20.8 (s, $CH_2\mathit{CH_2}CH_3$), 23.8 (s, Ar-CH$\mathit{CH_3}$), 24.3 (s, Ar-CH$\mathit{CH_3}$), 24.3 (s, Ar-CH$\mathit{CH_3}$), 24.4 (s, Ar-CH$\mathit{CH_3}$), 24.4 (s, Ar-CH$\mathit{CH_3}$), 25.2 (s, N-C-$\mathit{CH_3}$), 25.6 (s, N-C-$\mathit{CH_3}$), 28.9 (s, Ar-$\mathit{CH}$-$CH_3$), 29.1 (s, Ar-$\mathit{CH}$-$CH_3$), 53.4 (dd, $^3J_{P,C}$ = 4.16 Hz, $^4J_{P,C}$ = 4.16 Hz, $\mathit{CH_2}CH_2CH_3$), 96.5 (s, N-C-$\mathit{CH}$), 125.1 (s, *m*-Ar), 126.0 (s, *m*-Ar), 128.2 (s, *p*-Ar), 132.7−133.s (s, P$\mathit{C}$S), 140.1 (s, *i*-Ar), 141.3 (s, *o*-Ar), 142.0 (s, *o*-Ar), 160.3−160.8 (m, P$\mathit{C}$N), 170.4 (s, N-$\mathit{C}$-$CH_3$), 190.8 (s, $\mathit{C}$=S).

**$^{31}P\{^1H\}$ NMR** (243.0 MHz, 298.0 K, $C_6D_6$): δ / ppm = −81.7 (s).

**$^{31}P$ NMR** (243.0 MHz, 298.0 K, $C_6D_6$): δ / ppm = −81.7 (s).

### 5.6.25 Synthesis of spiro[1',2'-dihydro-1',3'-bis(2',6'-di-*i*-propylphenyl)-4',6'-dimethyl-1',3',2'-diazaaluminine-2,9'-[3,7]-di-*n*-propyl-[3,7]-dihydro-[4,8]-alumano-[1,4]diphosphinino[2,3-d:5,6-d']bis[1,3]thiazole-[2,6]-dithione] (14b)

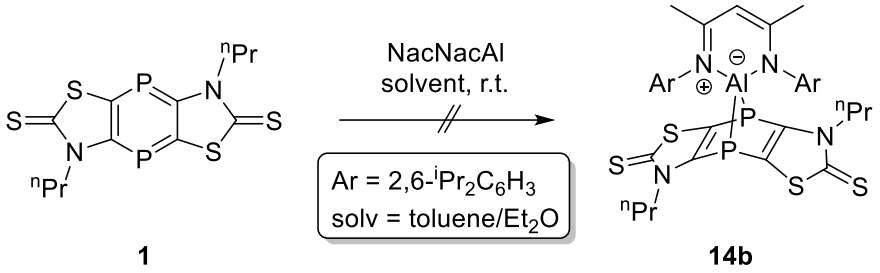


**1** **14b**

*5.6.25.1 Reaction in benzene*

In a 10 mL vial a solution of 7.7 mg (0.017 mmol, 0.99 eq.) of NacNacAl in 0.5 ml benzene was added dropwise to a suspension of 6.6 mg (0.018, 1.00 eq.) of **1** in 0.5 mL benzene. An immediate colour change from red to dark brown was observed. The reaction was stirred for 3.5 h before the addition of 8.5 mg (0.019 mmol, 1.09 eq.) of NacNacAl to the reaction mixture. After stirring for a further 19 h 5.5 mg (0.012 mmol, 0.71 eq.) of NacNacAl were added.

**Reaction code:** TK-K-21(TK-21-2, TK-21-3, TK-21-4)

**$^{31}P\{^1H\}$ NMR** (243.0 MHz, 299.1 K, $C_6D_6$): δ / ppm = −108.4 (d, $^3J_{P,P}$ = 22.3 Hz, ), −100.6 (s), −88.2 (d, $^3J_{P,P}$ = 22.3 Hz).

**$^{31}P$ NMR** (243.0 MHz, 298.0 K, $C_6D_6$): δ / ppm = −108.5 (dd, $^3J_{P,P}$ = 20.8 Hz, $^nJ_{P,H}$ = 6.25 Hz), −100.6 (s), −88.1 (d, $^3J_{P,P}$ = 20.8 Hz).

*5.6.25.2 Reaction in diethyl ether*

In a 10 mL vial, a suspension of 9.4 mg (0.025 mmol, 1.00 eq.) of **1** in 1 mL diethyl ether was added to a solution of 11.1 mg (0.250 mmol, 1.00 eq.) of NacNacAl in 1 mL diethyl ether and

the mixture was stirred for 7 h. Diethyl ether was removed and the residue was taken up in 2 mL of toluene.

**Reaction code:** TK-K-18 (TK-18-5)

**$^{31}P\{^{1}H\}$ NMR** (243.0 MHz, 299.1 K, $C_6D_6$): δ / ppm = −108.5 (d, $^{3}J_{P,P}$ = 22.0 Hz), −88.0 (d, $^{3}J_{P,P}$ = 21.4 Hz).

**$^{31}P$ NMR** (243.0 MHz, 298.0 K, $C_6D_6$): δ / ppm = −108.5 (dd, $^{3}J_{P,P}$ = 22.6 Hz, $^{n}J_{P,H}$ = 5.10 Hz), −88.0 (d, $^{3}J_{P,P}$ = 22.6 Hz).

### 5.6.26 Attempted synthesis of 3,7-di-*n*-propyl-4,8-dichlorosilano[1,4]diphosphinino[2,3-d:5,6-d']bis[1,3]thiazole-2,6(3,7*H*)-dithione (15a)

*5.6.26.1 NHC-stabilised $SiCl_2$*

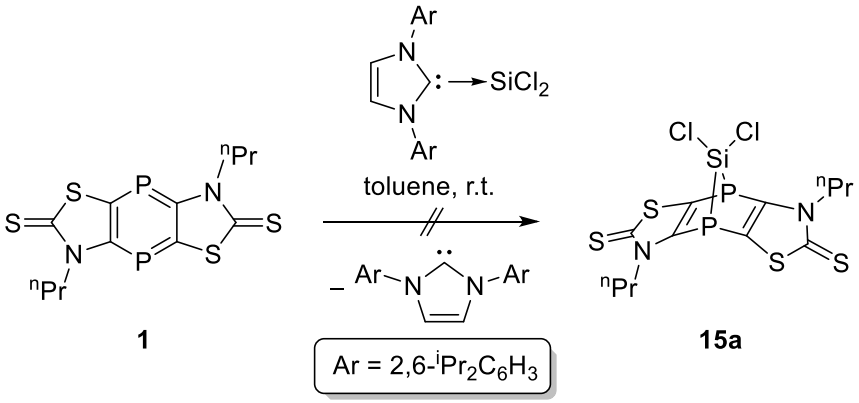


In a 10 mL vial 16.0 mg (0.043 mmol, 1.00 eq.) of **1** and 20.9 mg (0.043 mmol, 1.01 eq.) of [1,3-bis(2,6-di-*i*-proplyphenyl)-1*H*-imidazolium-2-yl]dichlorosilylene[122] were suspended in 1 mL toluene and stirred for 1 h at ambient temperature.

**Reaction code:** TK-K-19, TK-K-20 (TK-19-1, TK-20-1)

**$^{31}P\{^{1}H\}$ NMR** (243.0 MHz, 301.1 K, $C_6D_6$): δ / ppm = −91.3 (d, $^{3}J_{P,P}$ = 10.5 Hz), −85.8 (d, $^{3}J_{P,P}$ = 10.3 Hz), −71.9 (s), −39.3 (s), −38.1 (s), −37.1 (s), −35.6 (s), −13.6 (s), −2.88 (d, $^{3}J_{P,P}$ = 21.5 Hz), −2.27 (d, $^{3}J_{P,P}$ = 21.5 Hz).

*5.6.26.2 NHC-stabilised $SiCl_2$, $ZnCl_2$*

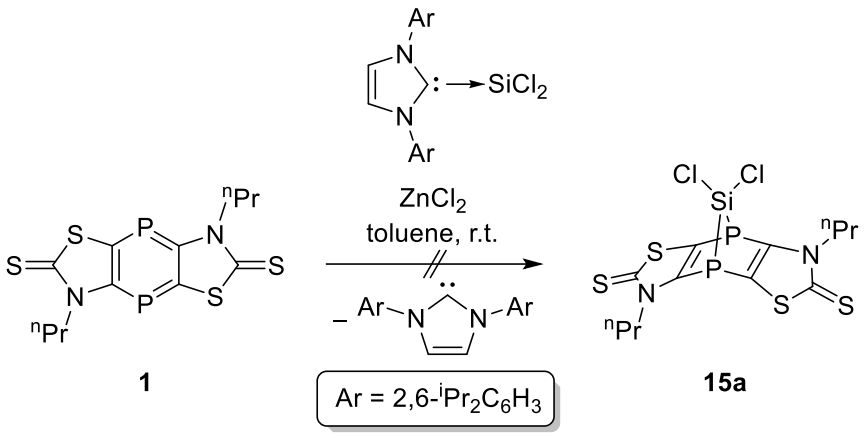


In a 10 mL Schlenk tube 11.3 mg (0.030 mmol, 1.00 eq.) of **1** and 5.1 mg (0.037 mmol, 1.25 eq.) of $ZnCl_2$ were suspended in 1 mL diethyl ether. A solution of 17.5 mg (0.030 mmol, 1.00 eq.) of [1,3-bis(2,6-di-*i*-proplyphenyl)-1*H*-imidazolium-2-yl]dichlorosilylene[122] in 3 mL diethyl ether were added at −90 °C. The solution was warmed up to ambient temperature while stirring for 19 h before removing the solvent *in vacuo* ($10^{-2}$ mbar) due to insolubility. 2 mL of toluene were added and the mixture was stirred for 2 h.

**Reaction code:** TK-486 (TIM230323m3b048)

**$^{31}P\{^1H\}$ NMR** (121.5 MHz, 298.0 K, toluene): δ / ppm = 133.1 (s).

### 5.6.27 Attempted synthesis of spiro[1,3-bis(2,2-dimethylpropyl)-1,3-dihydro-2*H*-1,3,2-benzodiazasilol-2-ylidene-2,9'-[3,7]-di-*n*-propyl-[3,7]-dihydro-[4,8]-silano-[1,4]diphosphinino[2,3-d:5,6-d']bis[1,3]thiazole-[2,6]-dithione] (15b)

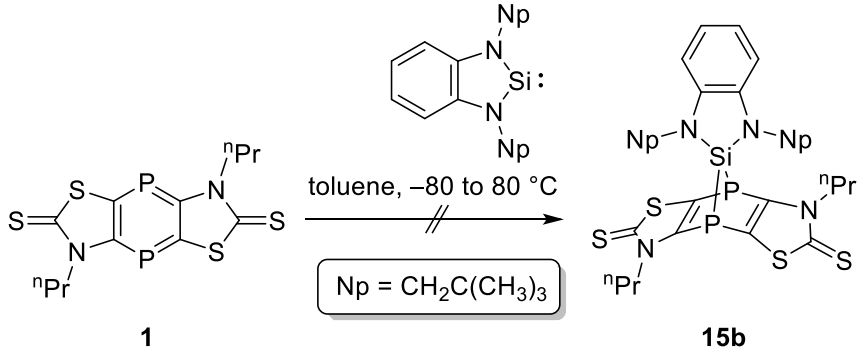


In a 10 mL Schlenk vessel 27.9 mg (0.074 mmol, 1.00 eq.) of **1** were dissolved in 1.5 mL toluene. A solution of 21.8 mg (0.079 mmol, 1.07 eq.) of 1,3-bis(2,2-dimethylpropyl)-1,3-dihydro-2*H*-1,3,2-benzodiazasilol-2-ylidene[124] in 1 mL toluene was added at −80 °C and the solution was stirred for 2.5 h while slowly warming up to ambient temperature. It was then further stirred for 21 h before heating the red suspension to 80 °C and stirring for 18 h.

**Reaction code:** TK-470/-476 (TIM230223m3a054, TIM230224m3a017, TIM230306p5a006)
**$^{31}P\{^{1}H\}$ NMR** (202.4 MHz, 298.0 K, $CDCl_3$): δ / ppm = −105.1 (s), −97.9 (s), 132.2 (s).

### 5.6.28 Attempted synthesis of 3,7-di-*n*-propyl-4,8-dichlorogermano[1,4]diphosphinine[2,3-d:5,6-d']bis[1,3]thiazole-2,6(3,7*H*)-dithione (16a)

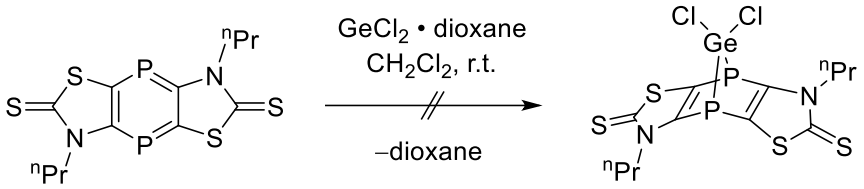


**1** **16a**

In a 10 mL vial, a solution of 5.3 mg (0.023 mmol, 1.00 eq.) of germanium dichloride dioxane complex in 0.2 mL $CH_2Cl_2$ were added to a solution of 8.6 mg (0.023 mmol, 1.00 eq.) of **1** in 0.5 mL $CH_2Cl_2$ at ambient temperature. The reaction mixture was stirred for 2 h.
**Reaction code:** TK-K-9 (TK-9-2)

**$^{31}P$ NMR** (162.0 MHz, 298.2 K, $CDCl_3$): δ / ppm = 138.5 (s).

### 5.6.29 Attempted synthesis of 3,7-di-*n*-propyl-4,8-dichlorogermano[1,4]diphosphinino[2,3-d:5,6-d']bis[1,3]thiazole-2,6(3,7*H*)-dithionium tetrakis(3,5-bis(trifluoromethyl)phenyl)borate (16b)

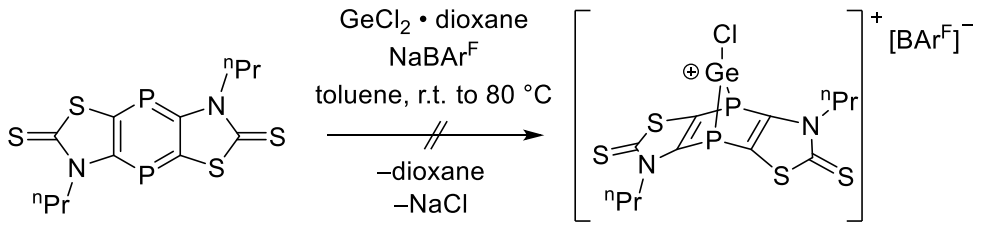


**1** **16b**

$BAr^F = [B(C_6H_3(CF_3)_2)_4]^-$

In a 10 mL vial, a solution of 2.2 mg (0.015 mmol, 1.53 eq.) of germanium dichloride dioxane complex in 1 mL toluene were added to 9.8 mg (0.011 mmol, 1.06 eq.) of $NaB(C_6H_3(CF_3)_2)_4$ at ambient temperature. After stirring for 10 min, 3.9 mg (0.010 mmol, 1.00 eq.) of **1** were added and the mixture was stirred for 30 h at ambient temperature before heating to 80 °C and holding the reaction mixture at this temperature for further 17 h.

**Reaction code:** TK-472 (TIM230301p5a007, TIM230302m3a050, TIM230306m3a007)

**$^{31}P\{^{1}H\}$ NMR** (121.5 MHz, 298.0 K, toluene): δ / ppm = −104.7 (s), −97.2 (s), 134.2 (s).

### 5.6.30 Synthesis of 9,10-bis(ethylcarboxy)-3,7-di-*n*-propyl-4,8-etheno[1,4]diphosphinino[2,3-d:5,6-d']bis[1,3]thiazole-2,6-dithione (17a)

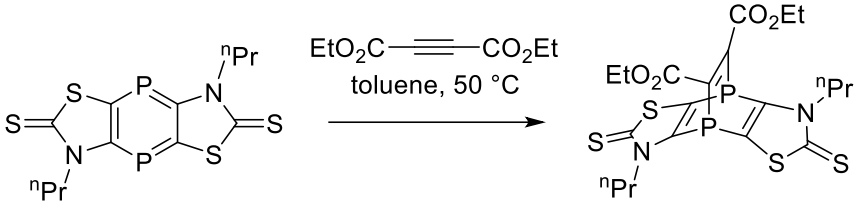


**1** **17a**

In a 20 mL Schlenk vessel, 0.07 mL (0.436 mmol, 1.17 eq.) of diethyl acetylene dicarboxylate were added to a suspension of 140 mg (0.371 mmol, 1.00 eq.) of **1** in 6 mL toluene. The mixture was heated to 50 °C and stirred at this temperature for 6.5 h before removing volatiles *in vacuo* ($10^{-2}$ mbar). The residue was washed three times with 4 mL *n*-pentane each before drying *in vacuo* ($10^{-2}$ mbar). The product was obtained as an orange solid.

**Reaction code:** TK-544 (TIM230828p5a009)

**Molecular formula:** $C_{20}H_{24}N_2O_4P_2S_4$

**Molecular weight:** 546.61 g/mol

**Yield:** 147.1 mg (0.269 mmol, 72%)

**Melting point:** 81 °C (dec. to **1**)

| **Elemental analysis:** | | | | |
|---|---|---|---|---|
| | calculated / % | C 43.95 | H 4.43 | N 5.13 |
| | found / % | C 42.20 | H 4.81 | N 4.31 |

**MS** (pos. ESI, selected data): m/z (%): 515.044 (100) $[M-2O+H]^{+\bullet}$.
(neg. ESI, selected data): m/z (%): 579.3 (100) $[M+O+OH]^{-\bullet}$.

**IR** (ATR Diamond, selected data): $\tilde{\nu}$ / $cm^{-1}$ = 1719 (s, *v*(CO)), 2872 (w, *v*(CH)), 2935 (w, *v*(CH)), 2966 (w, *v*(CH)).

**$^{1}H$ NMR** (500.0 MHz, 298.0 K, $CDCl_3$): δ / ppm = 1.00 (t, 6H, $^{3}J_{H,H}$ = 7.38 Hz, $CH_2CH_2CH_3$), 1.33 (t, 6H, $^{3}J_{H,H}$ = 7.15 Hz, $OCH_2CH_3$), 1.76–1.89 (m, 4H, $CH_2CH_2CH_3$), 4.26–4.38 (m, 6H, $OCH_2CH_3$, $CH_2CH_2CH_3$), 4.43–4.53 (m, 2H, $CH_2CH_2CH_3$).

**$^{13}C\{^{1}H\}$ NMR** (125.8 MHz, 298.0 K, $CDCl_3$): δ / ppm = 11.3 (s, $CH_2CH_2CH_3$), 14.1 (s, $OCH_2CH_3$), 22.5 (d, $^{4}J_{P,C}$ = 1.82 Hz, $CH_2CH_2CH_3$), 51.8 (dd, $^{3}J_{P,C}$ = 4.84 Hz, $^{4}J_{P,C}$ = 4.84 Hz,

*CH*$_2$CH$_2$CH$_3$), 63.2 (s, O*CH*$_2$CH$_3$), 131.4–132.0 (m, P*C*S), 157.4–157.9 (m, P*C*CO$_2$Et), 159.7–160.0 (m, P*C*N), 164.7–165.4 (m, C*C*O$_2$Et), 189.6 (s, *C*=S).

**$^{31}$P{$^{1}$H} NMR** (202.4 MHz, 298.0 K, $CDCl_3$): δ / ppm = −75.5 (s).

**$^{31}$P NMR** (202.4 MHz, 298.0 K, $CDCl_3$): δ / ppm = −75.5 (s).

### 5.6.31 Synthesis of 3,7-di-*n*-propyl-9-ethylcarboxy-4,8-etheno[1,4]diphosphinino[2,3-d:5,6-d']bis[1,3]thiazole-2,6-dithione (17b)

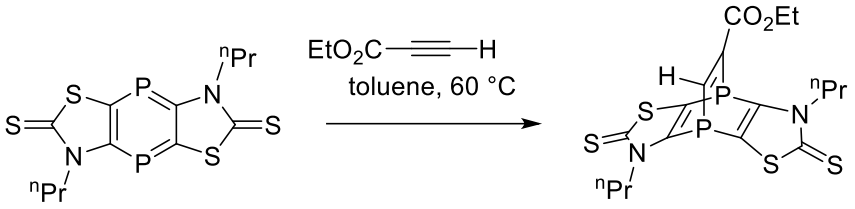


**1** **17b**

In a 20 mL Schlenk vessel, 292 mg (0.775 mmol, 1.00 eq.) **1** were dissolved in 12 mL toluene. After addition of 0.40 mL (3.95 mmol, 5.09 eq.) of ethyl propiolate the reaction mixture was stirred at 60 °C for 1.5 h. Volatiles were removed *in vacuo* ($10^{-2}$ mbar) at 50 °C and the dark orange residue was washed three times with 5 mL of *n*-pentane and three times with 5 mL of diethyl ether before drying the residue *in vacuo* ($10^{-2}$ mbar). The product was obtained as an orange solid.

**Reaction code:** TK-110 (25p5a025.19)

**Molecular formula:** $C_{17}H_{20}N_2O_2P_2S_4$

**Molecular weight:** 474.55 g/mol

**Yield:** 257 mg (0.542 mmol, 70%)

**Melting point:** 113 °C (dec. to **1**)

**MS** (pos. ESI, selected data): m/z (%): 474.995 (100) $[M+H]^{+\bullet}$.

**IR** (ATR Diamond, selected data): $\tilde{\nu}$ / cm$^{-1}$ = 1702 (s, *v*(CO)), 2870 (w, *v*(CH)), 2928 (w, *v*(CH)), 2958 (w, *v*(CH)).

**$^{1}$H NMR** (500.1 MHz, 298.0 K, $CDCl_3$): δ / ppm = 0.99 (t, 3H, $^{3}J_{H,H}$ = 7.44 Hz, CH$_2$CH$_2$*CH*$_3$), 0.99 (t, 3H, $^{3}J_{H,H}$ = 7.44 Hz, CH$_2$CH$_2$*CH*$_3$), 1.36 (t, 3H, $^{3}J_{H,H}$ = 7.13 Hz, OCH$_2$*CH*$_3$), 1.74–1.86 (m, 4H, CH$_2$*CH*$_2$CH$_3$), 4.29–4.41 (m, 4H, *CH*$_2$CH$_2$CH$_3$), 4.41–4.51 (m, 2H, O*CH*$_2$CH$_3$), 8.74 (dd, 1H, $^{2}J_{P,H}$ = 61.6 Hz, $^{3}J_{P,H}$ = 6.77 Hz, C*H*).

**$^{13}C\{^{1}H\}$ NMR** (125.8 MHz, 298.0 K, $CDCl_3$): δ / ppm = 11.2 (d, $^{5}J_{P,C}$ = 1.66 Hz, $CH_2CH_2\mathit{CH_3}$), 11.3 (d, $^{5}J_{P,C}$ = 1.66 Hz, $CH_2CH_2\mathit{CH_3}$), 14.2 (s, $OCH_2\mathit{CH_3}$), 22.4 (d, $^{4}J_{P,C}$ = 3.56 Hz, $CH_2\mathit{CH_2}CH_3$), 22.5 (d, $^{4}J_{P,C}$ = 3.40 Hz, $CH_2\mathit{CH_2}CH_3$), 51.4 (d, $^{3}J_{P,C}$ = 9.92 Hz, $\mathit{CH_2}CH_2CH_3$), 62.8 (d, $^{4}J_{P,C}$ = 1.50 Hz, $O\mathit{CH_2}CH_3$), 131.7 (dd, $^{1}J_{P,C}$ = 26.0 Hz, $^{2}J_{P,C}$ = 4.80 Hz, P*C*S), 133.3 (dd, $^{1}J_{P,C}$ = 28.2 Hz, $^{2}J_{P,C}$ = 5.51 Hz, P*C*S), 157.8 (dd, $^{1}J_{P,C}$ = 12.8 Hz, $^{2}J_{P,C}$ = 5.13 Hz, P*C*N), 158.6 (dd, $^{1}J_{P,C}$ = 24.0 Hz, $^{2}J_{P,C}$ = 4.27 Hz, P*C*H), 159.5 (dd, $^{1}J_{P,C}$ = 15.9 Hz, $^{2}J_{P,C}$ = 2.00 Hz, P*C*N), 161.4 (dd, $^{2}J_{P,C}$ = 3.58 Hz, $^{3}J_{P,C}$ = 19.6 Hz, C*C*$O_2$Et), 163.9 (dd, $^{1}J_{P,C}$ = 34.0 Hz, $^{2}J_{P,C}$ = 3.71 Hz, *C*$CO_2$Et), 189.0 (d, $^{3}J_{P,C}$ = 2.12 Hz, NS*C*=S), 189.1 (d, $^{3}J_{P,C}$ = 1.95 Hz, NS*C*=S).

**$^{31}P\{^{1}H\}$ NMR** (202.5 MHz, 298.0 K, $CDCl_3$): δ / ppm = −87.1 (d, $^{3}J_{P,P}$ = 25.97 Hz), −84.0 (d, $^{3}J_{P,P}$ = 25.97 Hz).

**$^{31}P$ NMR** (202.5 MHz, 298.0 K, $CDCl_3$): δ / ppm = −87.1 (dd, $^{3}J_{P,P}$ = 25.9 Hz, $^{3}J_{P,H}$ = 6.71 Hz), −84.0 (dd, $^{3}J_{P,P}$ = 25.9 Hz, $^{2}J_{P,H}$ = 61.6 Hz).

### 5.6.32 Synthesis of 9,10-diethyl-3,7-di-*n*-propyl-4,8-etheno[1,4]diphosphinino[2,3-d:5,6-d']bis[1,3]thiazole-2,6-dithione (17c)

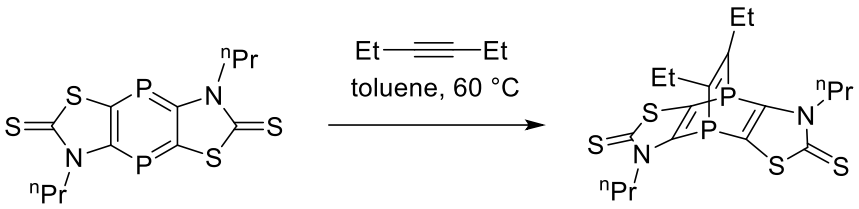


**1** **17c**

In a 10 mL Schlenk vessel, 0.05 mL (0.440 mmol, 5.5 eq.) 3-hexyne were added to a suspension of 30 mg (0.080 mmol, 1.00 eq.) of **1** in 2 mL toluene. The mixture was stirred at 60 °C for 22 d before removal of volatiles *in vacuo* ($10^{-2}$ mbar). The residue was washed three times with 2 mL of *n*-pentane each. After drying *in vacuo* ($10^{-2}$ mbar), the product was obtained as a yellow solid.

**Reaction code:** TK-297 (49p5a023.21)

**Molecular formula:** $C_{18}H_{24}N_2P_2S_4$

**Molecular weight:** 458.60 g/mol

**Yield:** 16.2 mg (0.035 mmol, 57%)

**Melting point:** 190 °C (dec. to **1**)

**X-ray diffraction analysis:** very good structure (A1, GSTR751, GXraymo_6824f)

**MS** (EI, 70 eV, selected data): m/z (%): 458.0 (100) $[M]^{+\bullet}$, 375.9 $[M-C_6H_{10}]^{+\bullet}$, 291.8 $[M-C_6H_{10}-2C_3H_7+2H]^{+\bullet}$.

**HRMS** (pos. ESI) for $C_{18}H_{24}N_2P_2S_4$ theor./exp. 458.0298/458.0296 $[M]^{+\bullet}$.

**IR** (ATR Diamond, selected data): $\tilde{\nu}$ / $cm^{-1}$ = 2869 (w, *v*(CH)), 2933 (m, *v*(CH)), 2963 (w, *v*(CH)).

**$^1$H NMR** (500.0 MHz, 298.0 K, $CDCl_3$): δ / ppm = 1.00 (t, 6H, $^3J_{H,H}$ = 7.40 Hz, $CH_2CH_2CH_3$), 1.08 (t, 6H, $^3J_{H,H}$ = 7.44 Hz, $CCH_2CH_3$), 1.73–1.90 (m, 4H, $CH_2CH_2CH_2$), 2.43–2.60 (m, 4H, $CCH_2CH_3$), 4.31–4.38 (m, 2H, $CH_2CH_2CH_3$) 4.40–4.47 (m, 2H, $CH_2CH_2CH_3$).

**$^{13}$C{$^1$H} NMR** (125.8 MHz, 298.0 K, $CDCl_3$): δ / ppm = 11.3 (s, $CH_2CH_2CH_3$), 13.6 (s, $CCH_2CH_3$), 22.4 (dd, $^4J_{P,C}$ = 1.67 Hz, $^4J_{P,C}$ = 1.67 Hz, $CH_2CH_2CH_3$) 28.1 (m, $CCH_2CH_3$) 31.1 (d, $^4J_{P,C}$ = 15.4 Hz, $CH_2CH_2CH_2CH_3$), 51.6 (dd, $^3J_{P,C}$ = 4.79 Hz, $^4J_{P,C}$ = 4.79 Hz, $CH_2CH_2CH_3$), 133.7 (dd, $^1J_{P,C}$ = 18.2 Hz, $^2J_{P,C}$ = 13.8 Hz, PCS), 156.8 (dd, $^1J_{P,C}$ = 9.49 Hz, $^2J_{P,C}$ = 8.51 Hz, $PCCH_2CH_3$), 160.8 (dd, $^1J_{P,C}$ = 12.6 Hz, $^2J_{P,C}$ = 9.08 Hz, PCN), 189.3 (s, C=S).

**$^{31}$P{$^1$H} NMR** (202.4 MHz, 298.0 K, $CDCl_3$): δ / ppm = −71.2 (s).

**$^{31}$P NMR** (202.4 MHz, 298.0 K, $CDCl_3$): δ / ppm = −71.2 (m).

### 5.6.33 Synthesis of *rel*-(9*S*,10*R*)-9,10-bis(ethylcarboxy)-3,7-di-*n*-propyl-4,8-ethano-[1,4]diphosphinino[2,3-d:5,6-d']bis[1,3]thiazole-2,6-dithione (18a)

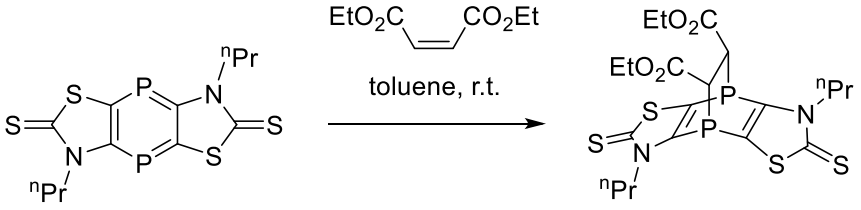


**1** **18a**

In a 10 mL Schlenk vessel, 0.09 mL (0.724 mmol, 5.07 eq.) diethyl maleate were added to a suspension of 53.8 g (0.143 mmol, 1.00 eq.) of **1** in 4 mL toluene. The mixture was stirred for 4 h at ambient temperature and volatiles were removed *in vacuo* ($10^{-2}$ mbar). The residue was washed three times with 1.5 mL of *n*-pentane each and dried *in vacuo* ($10^{-2}$ mbar). The product was obtained as a colourless solid.

**Reaction code:** TK-123 (27m3b052.19, 28p5a002.19)

**Molecular formula:** $C_{20}H_{26}N_2O_4P_2S_4$

**Molecular weight:** 548.63 g/mol

**Yield:** 49.4 mg (0.090 mmol, 63%)

**Melting point:** 140 °C (dec. to **1**)

| **Elemental analysis:** | | | | | |
|---|---|---|---|---|---|
| | calculated / % | C 43.79 | H 4.78 | N 5.11 | S 23.37 |
| | found / % | C 43.45 | H 4.74 | N 5.00 | S 23.30 |

**MS** (pos. ESI, selected data): m/z (%): 549.032 (68) $[M+H]^{+\bullet}$, 219.187 (100) $[M-C_8H_{12}O_4-2C_3H_7+2H]^{+\bullet}$.

**IR** (ATR Diamond, selected data): $\tilde{\nu}$ / $cm^{-1}$ = 1724 (s, *v*(CO)), 2871 (w, *v*(CH)), 2932 (w, *v*(CH)), 2959 (w, *v*(CH)).

**$^{1}$H NMR** (300.1 MHz, 298.0 K, $CDCl_3$): δ / ppm = 1.01 (t, 3H, $^{3}J_{H,H}$ = 7.37 Hz, $CH_2CH_2CH_3$), 1.02 (t, 3H, $^{3}J_{H,H}$ = 7.39 Hz, $CH_2CH_2CH_3$), 1.20 (t, 3H, $^{3}J_{H,H}$ = 7.16 Hz, $OCH_2CH_3$), 1.22 (t, 3H, $^{3}J_{H,H}$ = 7.16 Hz, $OCH_2CH_3$), 1.74–1.92 (m, 4H, $CH_2CH_2CH_3$), 3.37 (ddd, $^{2}J_{P,H}$ = 2.54 Hz, $^{3}J_{P,H}$ = 6.32 Hz, $^{3}J_{H,H}$ = 9.38 Hz, P*CH*), 3.47 (ddd, $^{2}J_{P,H}$ = 3.08 Hz, $^{3}J_{P,H}$ = 6.49 Hz, $^{3}J_{H,H}$ = 9.62 Hz, P*CH*), 3.99–4.14 (m, 4H, $OCH_2CH_3$), 4.22–4.32 (m, 1H, $CH_2CH_2CH_3$), 4.34–4.42 (m, 2H, $CH_2CH_2CH_3$), 4.49–4.57 (m, 1H, $CH_2CH_2CH_3$).

**$^{13}$C{$^{1}$H} NMR** (125.8 MHz, 298.0 K, $CDCl_3$): δ / ppm = 11.3 (d, $^{5}J_{P,C}$ = 1.16 Hz, $CH_2CH_2CH_3$), 11.3 (d, $^{5}J_{P,C}$ = 0.87 Hz, $CH_2CH_2CH_3$), 14.1 (s, $OCH_2CH_3$), 14.2 (s, $OCH_2CH_3$), 22.1 (d, $^{4}J_{P,C}$ = 3.22 Hz, $CH_2CH_2CH_3$), 22.5 (d, $^{4}J_{P,C}$ = 3.49 Hz, $CH_2CH_2CH_3$), 44.3 (dd, $^{1}J_{P,C}$ = 18.4 Hz, $^{2}J_{P,C}$ = 1.99 Hz, P*CH*), 45.2 dd, $^{1}J_{P,C}$ = 15.8 Hz, $^{2}J_{P,C}$ = 1.84 Hz, P*CH*), 51.1 (d, $^{3}J_{P,C}$ = 10.1 Hz, $CH_2CH_2CH_3$), 51.3 (d, $^{3}J_{P,C}$ = 10.7 Hz, $CH_2CH_2CH_3$), 62.8 (d, $^{4}J_{P,C}$ = 1.23 Hz, $OCH_2CH_3$), 62.9 (s, $OCH_2CH_3$), 127.0 (dd, $^{1}J_{P,C}$ = 26.0 Hz, $^{2}J_{P,C}$ = 4.63 Hz, P*C*S), 128.5 ($^{1}J_{P,C}$ = 23.4 Hz, $^{2}J_{P,C}$ = 4.32 Hz,, P*C*S), 152.0 ($^{1}J_{P,C}$ = 18.6 Hz, $^{2}J_{P,C}$ = 2.46 Hz, P*C*N), 152.6 ($^{1}J_{P,C}$ = 16.4 Hz, $^{2}J_{P,C}$ = 1.92 Hz, P*C*N), 168.6 (d, $^{2}J_{P,C}$ = 9.04 Hz, C*C*$O_2$Et), 169.4 (d, $^{2}J_{P,C}$ = 10.6 Hz, C*C*$O_2$Et), 190.4 (s, *C*=S), 190.8 (d, $^{3}J_{P,C}$ = 2.29 Hz, *C*=S).

**$^{31}$P{$^{1}$H} NMR** (202.5 MHz, 298.0 K, $CDCl_3$): δ / ppm = −75.8 (d, $^{3}J_{P,P}$ = 28.8 Hz), −73.3 (d, $^{3}J_{P,P}$ = 28.8 Hz).

**$^{31}$P NMR** (202.5 MHz, 298.0 K, $CDCl_3$): δ / ppm = −75.8 (ddd, $^{3}J_{P,P}$ = 28.8 Hz, $^{2}J_{P,H}$ = 2.53 Hz, $^{3}J_{P,H}$ = 6.06 Hz), −73.3 (dm $^{3}J_{P,P}$ = 25.4 Hz).

### 5.6.34 Synthesis of *rel*-(9*R*,10*R*)-9,10-bis(ethylcarboxy)-3,7-di-*n*-propyl-4,8-ethano-[1,4]diphosphinino[2,3-d:5,6-d']bis[1,3]thiazole-2,6-dithione (18a')

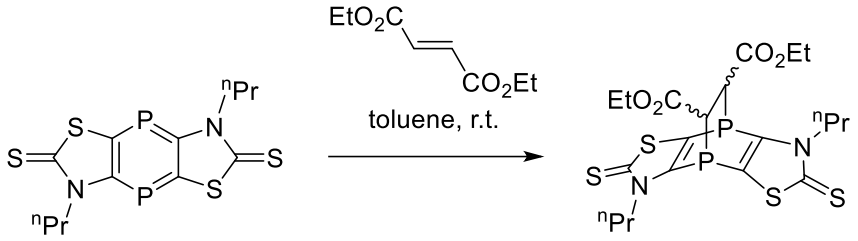


**1** **18a'**

In a 25 mL Schlenk vessel, 0.3 mL (1.83 mmol, 4.40 eq.) of diethyl fumarate were added to a suspension of 157 mg (0.417 mmol, 1.00 eq.) of **1** in 12 mL toluene. The mixture was stirred for 23 h and volatiles were removed *in vacuo* ($10^{-2}$ mbar). The residue was washed three times with 4 mL of *n*-pentane each and dried *in vacuo* ($10^{-2}$ mbar). The product was obtained as a colourless solid.

**Reaction code:** TK-347 (50p5a051.22)

**Molecular formula:** $C_{20}H_{26}N_2O_4P_2S_4$

**Molecular weight:** 548.63 g/mol

**Yield:** 154 mg (0.281 mmol, 67%)

**Melting point:** 118 °C (dec. to **1**)

| | | | | | |
|---|---|---|---|---|---|
| **Elemental analysis:** | calculated / % | C 43.79 | H 4.78 | N 5.11 | S 23.37 |
| | found / % | C 43.71 | H 4.74 | N 5.02 | S 23.33 |

**MS** (pos. ESI, selected data): m/z (%): 549.032 $[M+H]^{+\bullet}$, 517.060 $[M–2\ CH_3–H]^+$.

**IR** (ATR Diamond, selected data): $\tilde{\nu}$ / $cm^{-1}$ = 1714 (s, *v*(CO)), 2904 (w, *v*(CH)), 2941 (w, *v*(CH)), 2974 (w, *v*(CH)).

**$^1$H NMR** (500.0 MHz, 298.0 K, $CDCl_3$): δ / ppm = 0.99 (t, 6H, $^3J_{H,H}$ = 7.41 Hz, $CH_2CH_2CH_3$), 1.03 (t, 6H, $^3J_{H,H}$ = 7.42 Hz, $CH_2CH_2CH_3$ *isomer*), 1.26 (t, 6H, $^3J_{H,H}$ = 7.15 Hz, $OCH_2CH_3$), 1.28 (t, 6H, $^3J_{H,H}$ = 7.15 Hz, $OCH_2CH_3$ *isomer*), 1.65–1.88 (m, 4+4H, $CH_2CH_2CH_3$, $CH_2CH_2CH_3$ *isomer*), 3.61 (d, $^2J_{P,H}$ = 2.20 Hz, P*CH*), 3.82 (d, $^2J_{P,H}$ = 2.86 Hz, P*CH isomer*), 4.09–4.20 (m, 4+4H, $OCH_2CH_3$, $OCH_2CH_3$ *isomer*), 4.20–4.28 (m, 2H, $CH_2CH_2CH_3$, $CH_2CH_2CH_3$ *isomer*), 4.34–4.51 (m, 6H, $CH_2CH_2CH_3$, $CH_2CH_2CH_3$ *isomer*).

**$^{13}$C{$^1$H} NMR** (125.8 MHz, 298.0 K, $CDCl_3$): δ / ppm = 11.2 (s, $CH_2CH_2CH_3$ *isomer*), 11.2 (s, $CH_2CH_2CH_3$), 14.2 (s, $OCH_2CH_3$), 14.4 (s, $OCH_2CH_3$ *isomer*), 22.2 (dd, $^4J_{P,C}$ = 1.63 Hz, $^5J_{P,C}$ = 1.63 Hz, $CH_2CH_2CH_3$), 22.4 (dd, $^4J_{P,C}$ = 1.78 Hz, $^5J_{P,C}$ = 1.78 Hz, $CH_2CH_2CH_3$ isomer),

43.9 (dd, $^{1}J_{P,C}$ = 11.8 Hz, $^{2}J_{P,C}$ = 9.74 Hz, P*C*H *isomer*), 45.2 (dd, $^{1}J_{P,C}$ = 11.4 Hz, $^{2}J_{P,C}$ = 8.97 Hz, P*C*H), 51.1 (d, $^{3}J_{P,C}$ = 8.96 Hz, *C*H$_2$CH$_2$CH$_3$), 51.1 (d, $^{3}J_{P,C}$ = 9.27 Hz, *C*H$_2$CH$_2$CH$_3$ *isomer*), 63.1 (s, O*C*H$_2$CH$_3$), 63.2 (s, O*C*H$_2$CH$_3$ *isomer*), 127.6 (dd, $^{1}J_{P,C}$ = 13.5 Hz, $^{2}J_{P,C}$ = 1.22 Hz, P*C*S *isomer*), 127.7 (d, $^{1}J_{P,C}$ = 13.7 Hz, P*C*S), 152.1 (dd, $^{1}J_{P,C}$ = 12.4 Hz, $^{2}J_{P,C}$ = 9.29 Hz, P*C*N), 152.4 (dd, $^{1}J_{P,C}$ = 12.4 Hz, $^{2}J_{P,C}$ = 9.66 Hz, P*C*N *isomer*), 169.1 (dd, $^{2}J_{P,C}$ = 3.91 Hz, $^{3}J_{P,C}$ = 3.91 Hz, C*C*O$_2$Et *isomer*), 170.0 (dd, $^{2}J_{P,C}$ = 4.71 Hz, $^{3}J_{P,C}$ = 4.71 Hz, C*C*O$_2$Et), 190.5 (s, *C*=S *isomer*), 190.6 (d, $^{3}J_{P,C}$ = 2.29 Hz, *C*=S).

**$^{31}$P{$^{1}$H} NMR** (202.5 MHz, 298.0 K, $CDCl_3$): δ / ppm = −72.5 (s), −72.3 (s, *isomer*).

**$^{31}$P NMR** (202.5 MHz, 298.0 K, $CDCl_3$): δ / ppm = −72.5 (br. s), −72.3 (m, *isomer*); isomeric ratio 53:47.

### 5.6.35 Synthesis of 3,7-di-*n*-propyl-9-ethylcarboxy-4,8-ethano[1,4]diphosphinino[2,3-d:5,6-d']bis[1,3]thiazole-2,6-dithione (18b)

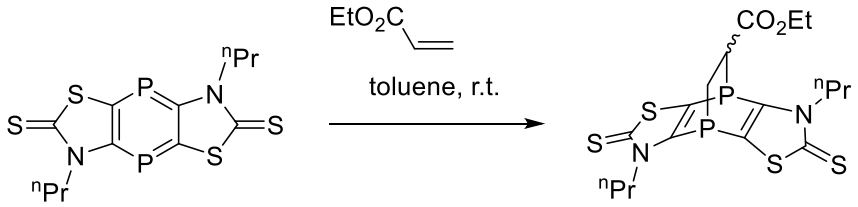


In a 20 mL Schlenk vessel, 0.1 mL (0.939 mmol, 2.99 eq.) of ethyl acrylate were added to a suspension of 118.1 mg (0.314 mmol, 1.00 eq.) of **1** in 6 mL toluene. The mixture was stirred for 30 min at ambient temperature and volatiles were removed *in vacuo* ($10^{-2}$ mbar) before washing the off-white residue three times with 1 mL of diethyl ether and three times with 2 mL of *n*-pentane each. After drying *in vacuo* ($10^{-2}$ mbar) the product was obtained as a pale-yellow solid.

**Reaction code:** TK-534 (TIM230810p5s008)

**Molecular formula:** $C_{17}H_{22}N_2O_2P_2S_4$

**Molecular weight:** 476.56 g/mol

**Yield:** 57.2 mg (0.120 mmol, 38%)

**Melting point:** 79 °C

| **Elemental analysis:** | | | | | |
|---|---|---|---|---|---|
| | calculated / % | C 42.85 | H 4.65 | N 5.88 | S 26.91 |
| | found / % | C 39.54 | H 4.95 | N 5.33 | S 24.53 |

**MS** (pos. ESI, selected data): m/z (%): 461.034 (25) $[M-CH_3]^{+\bullet}$, 445.039 (100) $[M-S+H]^{+\bullet}$, 344.986 (45) $[M-CO_2Et-2C_2H_5]^{+\bullet}$.

**HRMS** (pos. ESI) for $C_{17}H_{22}N_2O_2P_2S_4H$ theor./exp. 477.0112/477.0112 $[M+H]^{+\bullet}$.

**IR** (ATR Diamond, selected data): $\tilde{\nu}$ / $cm^{-1}$ = 1725 (m, *v*(CO), 2870 (w, *v*(CH)), 2934 (w, *v*(CH)), 2962 (w, *v*(CH)).

**$^1$H NMR** (500.0 MHz, 298.0 K, $CDCl_3$): δ / ppm = 0.96–1.03 (m, 6H, $CH_2CH_2\mathit{CH_3}$), 1.17–1.32 (m, 3H, $CO_2CH_2\mathit{CH_3}$), 1.63–1.87 (m, 4H, $CH_2\mathit{CH_2}CH_3$), 2.05–2.35 (m, 2H, P$\mathit{CH_2}$), 3.13–3.21 (m, 1H, P$\mathit{CH}CO_2Et$),z 4.07–4.28 (m, 2H, $CO_2\mathit{CH_2}CH_3$), 4.30–4.49 (m, 4H, $\mathit{CH_2}CH_2CH_3$).

**$^{13}$C{$^1$H} NMR** (125.73 MHz, 298.0 K, $CDCl_3$): δ / ppm = 11.1 (d,$^5J_{P,C}$ = 1.45 Hz $CH_2CH_2\mathit{CH_3}$ *isomer*), 11.2 (m, $CH_2CH_2\mathit{CH_3}$), 14.2 (s, $CO_2CH_2\mathit{CH_3}$ *isomer*), 14.4 (s, $CO_2CH_2\mathit{CH_3}$), 22.1 (d, $^4J_{P,C}$ = 3.53 Hz, $CH_2\mathit{CH_2}CH_3$ *isomer*), 22.3 (d, $^4J_{P,C}$ = 3.52 Hz, $CH_2\mathit{CH_2}CH_3$), 22.4 (d, $^4J_{P,C}$ = 3.53 Hz, $CH_2\mathit{CH_2}CH_3$ *isomer*), 22.4 (d, $^4J_{P,C}$ = 3.53 Hz, $CH_2\mathit{CH_2}CH_3$), 24.0 (dd, $^2J_{P,C}$ = 15.3 Hz, $^3J_{P,C}$ = 2.07 Hz, P$\mathit{CH_2}$), 24.4 (dd, $^2J_{P,C}$ = 15.4 Hz, $^3J_{P,C}$ = 2.11 Hz, P$\mathit{CH_2}$ *isomer*), 40.4 (dd, $^2J_{P,C}$ = 16.9 Hz, $^3J_{P,C}$ = 1.51 Hz, P*CH*), 41.0 (dd $^2J_{P,C}$ = 15.8 Hz, $^3J_{P,C}$ = 1.35 Hz, P*CH* *isomer*), 51.0 (m, $\mathit{CH_2}CH_2CH_3$), 62.7 (s, $CO_2\mathit{CH_2}CH_3$ *isomer*), 62.8 (s, $CO_2\mathit{CH_2}CH_3$), 125.6 (dd, $^1J_{P,C}$ = 27.6 Hz, $^2J_{P,C}$ = 5.22 Hz, P*C*S), 127.0 (dd, $^1J_{P,C}$ = 24.6 Hz, $^2J_{P,C}$ = 5.85 Hz, P*C*S *isomer*), 128.8 (dd, $^1J_{P,C}$ = 23.8 Hz, $^2J_{P,C}$ = 4.74 Hz, P*C*S *isomer*), 129.5 (dd, $^1J_{P,C}$ = 24.3 Hz, $^2J_{P,C}$ = 4.12 Hz, P*C*S), 150.8 (dd, $^1J_{P,C}$ = 19.6 Hz, $^2J_{P,C}$ = 3.27 Hz P*C*N *isomer*), 152.1 (dd, $^1J_{P,C}$ = 17.7 Hz, $^2J_{P,C}$ = 3.64 Hz P*C*N), 153.5 (dd, $^1J_{P,C}$ = 16.9 Hz, $^2J_{P,C}$ = 2.46 Hz P*C*N), 153.9 (dd, $^1J_{P,C}$ = 17.0 Hz, $^2J_{P,C}$ = 2.05 Hz, P*C*N *isomer*), 170.2 (d, $^2J_{P,C}$ = 8.04 Hz, *C*$O_2$Et), 171.1 (d, $^2J_{P,C}$ = 8.72 Hz, *C*$O_2$Et *isomer*), 190.3 (m, *C*=S).

**$^{31}$P{$^1$H} NMR** (202.4 MHz, 298.0 K, $CDCl_3$): δ / ppm = −80.0 (d, $^3J_{P,P}$ = 29.3 Hz, $PCH_2$ *isomer*), −79.7 (d, $^3J_{P,P}$ = 28.8 Hz, $PCH_2$), −75.4 (d, $^3J_{P,P}$ = 29.3 Hz, $PCHCO_2Et$ *isomer*), −74.1 (d, $^3J_{P,P}$ = 29.0 Hz, $PCHCO_2Et$).

**$^{31}$P NMR** (202.4 MHz, 298.0 K, $CDCl_3$): δ / ppm = −79.8 (m, $PCH_2$, $PCH_2$ *isomer*), −75.4 (dm, $^3J_{P,P}$ = 29.4 Hz, $PCHCO_2Et$ *isomer*), −74.1 (dm, $^3J_{P,H}$ = 29.0 Hz, $PCHCO_2Et$).

### 5.6.36 Synthesis of 3,7-di-*n*-propyl-9-*n*-butyl-4,8-ethano[1,4]diphosphinino[2,3-d:5,6-d']bis[1,3]thiazole-2,6-dithione (18c)

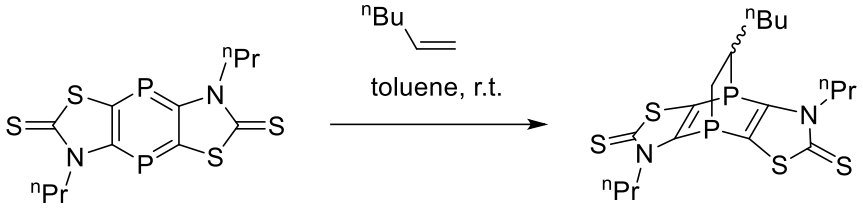


**1** **18c**

In a 20 mL Schlenk vessel, 0.1 mL (0.796 mmol, 2.08 eq.) of 1-hexene was added to a suspension of 143.8 mg (0.382 mmol, 1.00 eq.) of **1** in 10 mL toluene. The mixture was stirred for 4 h before removing volatiles *in vacuo* ($10^{-2}$ mbar). The residue was washed four times with 5 mL of *n*-pentane each and dried *in vacuo* ($10^{-2}$ mbar). The product was obtained as a colourless solid.

**Reaction code:** TK-212 (02s7b016.21)

**Molecular formula:** $C_{18}H_{26}N_2P_2S_4$

**Molecular weight:** 460.60 g/mol

**Yield:** 99.5 mg (0.216 mmol, 57%)

**Melting point:** 130 °C (dec. to **1**)

| | | | | | |
|---|---|---|---|---|---|
| **Elemental analysis:** | calculated / % | C 46.94 | H 5.69 | N 6.08 | S 27.84 |
| | found / % | C 41.54 | H 5.20 | N 5.24 | S 23.18 |

**MS** (EI, 70 eV, selected data): m/z (%): m/z = 460.0 $[M]^{+\bullet}$, 375.9 $[M-C_6H_{12}]^{+\bullet}$, 333.8 $[M-C_6H_{12}-C_3H_7+H]^{+\bullet}$, 291.8 $[M-C_6H_{12}-2\ C_3H_7+2\ H]^{+\bullet}$, 84.0 $[C_6H_{12}]^{+\bullet}$.

**IR** (ATR Diamond, selected data): $\tilde{\nu}$ / $cm^{-1}$ = 2868 (w, *v*(CH)), 2921 (m, *v*(CH)), 2955 (w, *v*(CH)).

**$^1$H NMR** (700.4 MHz, 298.0 K, $CDCl_3$): δ / ppm = 0.92 (td, 6H, $^3J_{H,H}$ = 7.34 Hz, $^4J_{H,H}$ = 3.74 Hz, $CH_2CH_2CH_2CH_3$), 1.01 (td, 6H, $^3J_{H,H}$ = 7.40 Hz, $^4J_{H,H}$ = 2.74 Hz, $CH_2CH_2CH_3$), 1.03 (q, 6H, $^3J_{H,H}$ = 7.74 Hz, $CH_2CH_2CH_3$), 1.18–1.26 (m, 1H, $CH_2CH_2CH_2CH_3$), 1.28–1.38 (m, $PCH_2$ (2H), $CH_2CH_2CH_2CH_3$ (4H), $CH_2CH_2CH_2CH_3$ (1H)), 1.41–1.54 (m, 6H, $CH_2CH_2CH_2CH_3$ (4H), $CH_2CH_2CH_2CH_3$ (2H)) 1.70–1.94 (m, 8H, $CH_2CH_2CH_3$), 2.04–2.13 (m, 2H, PCHⁿBu, PCHⁿBu *isomer*), 2.20–2.28 (m, 2H, $PCH_2$) 4.28–4.33 (m, 1H, $CH_2CH_2CH_3$), 4.36–4.46 (m, 7H, $CH_2CH_2CH_3$).

**$^{13}$C{$^1$H} NMR** (125.73 MHz, 298.0 K, $CDCl_3$): δ / ppm = (176.1 MHz, 298.0 K, $CDCl_3$): δ / ppm = 11.3 (d, $^5J_{P,C}$ = 1.21 Hz, $CH_2CH_2CH_3$), 11.3 (d, $^5J_{P,C}$ = 1.40 Hz, $CH_2CH_2CH_3$ *isomer*),

14.0 (s, $CH_2CH_2CH_2\mathit{CH_3}$), 14.0 (s, $CH_2CH_2CH_2\mathit{CH_3}$ *isomer*), 22.3 (d, $^4J_{P,C}$ = 3.00 Hz, $CH_2\mathit{CH_2}CH_3$), 22.4 (d, $^4J_{P,C}$ = 3.46 Hz, $CH_2\mathit{CH_2}CH_3$ *isomer*), 22.4 (d, $^4J_{P,C}$ = 3.48 Hz, $CH_2\mathit{CH_2}CH_3$, $CH_2\mathit{CH_2}CH_3$ *isomer*), 22.5 (s, $CH_2CH_2\mathit{CH_2}CH_3$ *isomer*), 22.6 (s, $CH_2CH_2\mathit{CH_2}CH_3$), 27.4 (dd, $^1J_{P,C}$ = 12.3 Hz, $^2J_{P,C}$ = 3.62 Hz, P$\mathit{CH_2}$, isomer), 27.7 (dd, $^1J_{P,C}$ = 12.4 Hz, $^2J_{P,C}$ = 3.60 Hz, P$\mathit{CH_2}$), 31.1 (d, $^4J_{P,C}$ = 15.4 Hz, $CH_2\mathit{CH_2}CH_2CH_3$), 31.3 (d, $^4J_{P,C}$ = 15.4 Hz, $CH_2\mathit{CH_2}CH_2CH_3$ *isomer*), 34.9 (dd, $^4J_{P,C}$ = 17.3 Hz, $^4J_{P,C}$ = 1.09 Hz, P$\mathit{CH}$$^n$Bu), 35.2 (dd, $^4J_{P,C}$ = 10.1 Hz, $^4J_{P,C}$ = 1.79 Hz, $\mathit{CH_2}CH_2CH_2CH_3$), 35.4 (dd, $^4J_{P,C}$ = 16.1 Hz, $^4J_{P,C}$ = 1.14 Hz, P$\mathit{CH}$$^n$Bu *isomer*), 35.7 (dd, $^4J_{P,C}$ = 10.6 Hz, $^4J_{P,C}$ = 1.89 Hz, $\mathit{CH_2}CH_2CH_2CH_3$ *isomer*), 50.9 (d, $^3J_{P,C}$ = 10.7 Hz, $\mathit{CH_2}CH_2CH_3$ *isomer*), 51.0 (d, $^3J_{P,C}$ = 10.7 Hz, $\mathit{CH_2}CH_2CH_3$), 51.1 (d, $^3J_{P,C}$ = 10.5 Hz, $\mathit{CH_2}CH_2CH_3$ *isomer*), 126.2 (dd, $^1J_{P,C}$ = 28.7 Hz, $^2J_{P,C}$ = 5.67 Hz, P*C*S), 127.2 (dd, $^1J_{P,C}$ = 23.8 Hz, $^2J_{P,C}$ = 5.30 Hz, P*C*S), 128.9 (dd, $^1J_{P,C}$ = 23.5 Hz, $^2J_{P,C}$ = 5.40 Hz, P*C*S *isomer*), 129.6 (dd, $^1J_{P,C}$ = 24.0 Hz, $^2J_{P,C}$ = 6.21 Hz, P*C*S *isomer*), 151.6 (dd, $^1J_{P,C}$ = 22.0 Hz, $^2J_{P,C}$ = 3.50 Hz, P*C*N *isomer*), 152.6 (dd, $^1J_{P,C}$ = 16.8 Hz, $^2J_{P,C}$ = 3.24 Hz, P*C*N *isomer*), 153.7 (dd, $^1J_{P,C}$ = 16.1 Hz, $^2J_{P,C}$ = 3.25 Hz, P*C*N), 154.9 (dd, $^1J_{P,C}$ = 16.9 Hz, $^2J_{P,C}$ = 3.97 Hz, P*C*N), 190.2 (d, $^3J_{P,C}$ = 1.98 Hz, *C*=S *isomer*), 190.3 (d, $^3J_{P,C}$ = 2.07 Hz, *C*=S), 190.4 (d, $^3J_{P,C}$ = 1.86 Hz, *C*=S *isomer*), 190.5 (d, $^3J_{P,C}$ = 2.00 Hz, *C*=S).

**$^{31}$P{$^1$H} NMR** (121.5 MHz, 298.0 K, $CDCl_3$): δ / ppm = −77.7 (d, $^3J_{P,P}$ = 24.5 Hz, *P*$CH_2$, *isomer*), −77.0 (d, $^3J_{P,P}$ = 24.2 Hz, *P*$CH_2$), −73.6 (d, $^3J_{P,P}$ = 24.2 Hz, *P*CH$^n$Bu), −72.6 (d, $^3J_{P,P}$ = 24.5 Hz, *P*CH$^n$Bu, *isomer*).

**$^{31}$P NMR** (121.5 MHz, 298.0 K, $CDCl_3$): δ / ppm = −77.7 (dt, $^3J_{P,P}$ = 24.5 Hz, $^2J_{P,H}$ = 7.90 Hz, *P*$CH_2$, *isomer*), −77.0 (dt, $^3J_{P,P}$ = 24.2 Hz, $^2J_{P,H}$ = 8.15 Hz, *P*$CH_2$), −73.6 (m, *P*CH$^n$Bu), −72.6 (m, *P*CH$^n$Bu, *isomer*).

### 5.6.37 Synthesis of 3,7-di-*n*-propyl-4,8-ethano[1,4]diphosphinino[2,3-d:5,6-d']bis-[1,3]thiazole-2,6-dithione (18d)

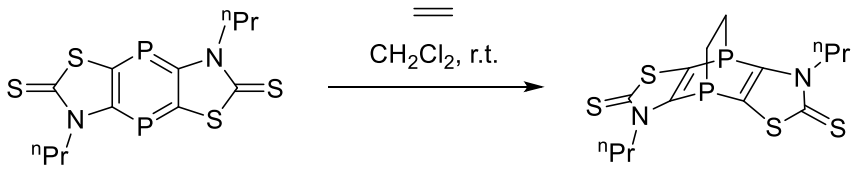


**1** **18d**

In a 10 mL Schlenk vessel, 7.0 mg (0.0186 mmol) of **1** was stirred in dichloromethane under an atmosphere of ethene. After 2 h, volatiles were removed *in vacuo* ($10^{-2}$ mbar) and the product was obtained as a colourless solid.

**Reaction code:** TK-K-5 (TK-5-c)

**Molecular formula:** $C_{14}H_{18}N_2P_2S_4$

**Molecular weight:** 404.50 g/mol

**Yield:** 7.5 mg (0.0185 mmol, 100%)

**Melting point:** 183 °C (dec. to **1**)

| **Elemental analysis:** | calculated / % | C 41.57 | H 4.49 | N 6.93 | S 31.70 |
|---|---|---|---|---|---|
| | found / % | C 41.36 | H 4.56 | N 6.82 | S 32.48 |

**MS** (pos. ESI, selected data): m/z (%): 403.9 $[M]^{+\bullet}$, 376.0 $[M–C_2H_4]^{+\bullet}$, 333.8 $[M–C_2H_4–C_3H_7+H]^{+\bullet}$, 291.9 $[M–C_2H_4–2\ C_3H_7+2\ H]^{+\bullet}$.

**IR** (ATR Diamond, selected data): $\tilde{\nu}$ / $cm^{-1}$ = 2869 (w, *v*(CH)), 2927 (w, *v*(CH)), 2957 (w, *v*(CH)).

**$^1$H NMR** (400.3 MHz, 298.1 K, $CDCl_3$): δ / ppm = 1.00 (t, 6H, $^3J_{H,H}$ = 7.39 Hz, $CH_2CH_2CH_3$), 1.69–1.95 (m, 4H, $CH_2CH_2CH_3$), 1.87–1.92 (m, 4H, $PCH_2$), 4.31-4.44 (m, 4H, $CH_2CH_2CH_3$).

**$^{13}$C{$^1$H} NMR** (100.7 MHz, 298.2 K, $CDCl_3$): δ / ppm = 11.3 (s, $CH_2CH_2CH_3$), 19.6 (t, $^{1/2}J_{P,C}$ = 7.09 Hz, $PCH_2$), 22.4 (t, $^{4/5}J_{P,C}$ = 1.89 Hz, $CH_2CH_2CH_3$), 50.9 (t, $^{3/4}J_{P,C}$ = 5.07 Hz, $CH_2CH_2CH_3$), 127.8 (dd, $^1J_{P,C}$ = 16.3 Hz, $^2J_{P,C}$ = 13.4 Hz, PCS), 153.0 (dd, $^1J_{P,C}$ = 11.0 Hz, $^2J_{P,C}$ = 9.07 Hz, PCN), 190.2 (s, C=S).

**$^{31}$P{$^1$H} NMR** (162.0 MHz, 298.1 K, $CDCl_3$): δ / ppm = −82.1 (s).

**$^{31}$P NMR** (121.5 MHz, 298.1 K, $CDCl_3$): δ / ppm = −82.1 (m).

### 5.6.38 Synthesis of *rel*-(9*S*,10*R*)-3,7-di-*n*-propyl-4,8-[1',2']-cyclohexano[1,4]diphosphinino[2,3-d:5,6-d']bis[1,3]thiazole-2,6-dithione (18e)

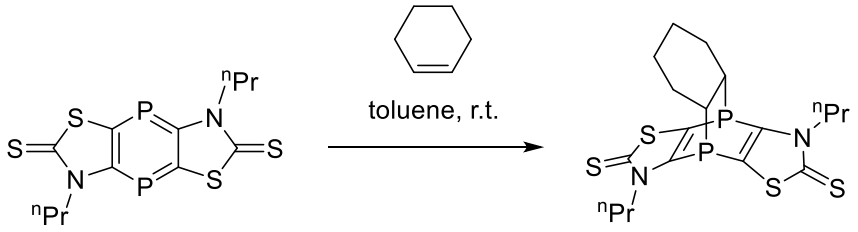


**1** **18e**

In a 25 mL Schlenk vessel, 0.25 mL (2.47 mmol, 11.12 eq.) of cyclohexene were added to a suspension of 83.4 mg (0.222 mmol, 1.00 eq) of **1** in 10 mL toluene. The mixture was stirred for 24 h at ambient temperature and volatiles were removed *in vacuo* ($10^{-2}$ mbar). The residue was washed three times with 3 mL of *n*-pentane each and dried *in vacuo* ($10^{-2}$ mbar). The product was obtained as a colourless solid.

**Reaction code:** TK-502 (TIM230502t4a043, TIM230503s7a021)

**Molecular formula:** $C_{18}H_{24}N_2P_2S_4$

**Molecular weight:** 458.60 g/mol

**Yield:** 75.1 mg (0.164 mmol, 74%)

**Melting point:** 79 °C

**Elemental analysis:** calculated / % C 47.14 H 5.28 N 6.11
found / % C 42.34 H 5.59 N 5.30

**MS** (EI, 70 eV, selected data): m/z (%): 475.0 (2) $[M+OH]^{+\bullet}$, 459.0 (1) $[M+H]^{+\bullet}$, 458.0 (1) $[M]^{+\bullet}$, 443.0 (2) $[M-CH_3]^{+\bullet}$, 427.1 (9) $[M-2CH_3-H]^{+\bullet}$, 219.2 (100) $[M-2CS_2-C_3H_7-H]^{+\bullet}$.

**HRMS** (pos. ESI) for $C_{18}H_{24}N_2P_2S_4$ theor./exp. 459.0370/459.0370 $[M+H]^{+\bullet}$.

**IR** (ATR Diamond, selected data): $\tilde{\nu}$ / $cm^{-1}$ = 2871 (w, *v*(CH)), 2929 (m, *v*(CH)).

**$^1$H NMR** (700.4 MHz, 298.0 K, $CDCl_3$): δ / ppm = 0.77–0.90 (m, 2H, $PCHCH_2C\mathit{H}_2$), 1.00 (t, 3H, $^3J_{H,H}$ = 7.36 Hz, $CH_2CH_2C\mathit{H}_3$), 1.02 (t, 3H, $^3J_{H,H}$ = 7.40 Hz, $CH_2CH_2C\mathit{H}_3$), 0.94–1.08 (m, 2H, $PCHCH_2C\mathit{H}_2$) 1.67–1.78 (m, 4H, $PCHC\mathit{H}_2$), 1.78–1.92 (m, 4H, $CH_2C\mathit{H}_2CH_2$), 2.08–2.20 (m, 2H, PC*H*), 4.26–4.45 (m, 4H, $C\mathit{H}_2CH_2CH_3$).

**$^{13}$C{$^1$H} NMR** (176.1 MHz, 298.0 K, $CDCl_3$): δ / ppm = 11.3 (s, $CH_2CH_2\mathit{CH}_3$), 21.4 (d, $^2J_{P,H}$ = 17.7 Hz, $PCH\mathit{CH}_2$), 21.6 (d, $^2J_{P,H}$ = 17.4 Hz, $PCH\mathit{CH}_2$), 22.3 (d, $^4J_{P,C}$ = 3.18 Hz, $CH_2\mathit{CH}_2CH_3$), 22.4 (d, $^4J_{P,C}$ = 3.43 Hz, $CH_2\mathit{CH}_2CH_3$), 25.0 (d, $^3J_{P,H}$ = 19.9 Hz, $PCHCH_2\mathit{CH}_2$), 25.4 (d, $^3J_{P,H}$ = 17.6 Hz, $PCHCH_2\mathit{CH}_2$), 34.8 (dd, $^1J_{P,H}$ = 10.3 Hz, $^2J_{P,H}$ = 3.67 Hz, P*CH*), 35.3 (dd, $^1J_{P,H}$ = 10.9 Hz, $^2J_{P,H}$ = 3.65 Hz, P*CH*), 51.0 (d, $^3J_{P,C}$ = 10.2 Hz, $\mathit{CH}_2CH_2CH_3$), 51.1 (d, $^3J_{P,C}$ = 10.4 Hz, $\mathit{CH}_2CH_2CH_3$), 127.3 (dd, $^1J_{P,C}$ = 27.4 Hz, $^2J_{P,C}$ = 5.67 Hz, P*C*S), 127.6 (dd, $^1J_{P,C}$ = 23.9 Hz, $^2J_{P,C}$ = 5.93 Hz, P*C*S), 152.4 (dd, $^1J_{P,C}$ = 17.0 Hz, $^2J_{P,C}$ = 3.60 Hz P*C*N), 153.3 (dd, $^1J_{P,C}$ = 20.3 Hz, $^2J_{P,C}$ = 3.25 Hz, P*C*N), 190.3 (s, *C*=S), 190.6 (s, *C*=S).

**$^{31}$P{$^1$H} NMR** (162.0 MHz, 298.0 K, $CDCl_3$): δ / ppm = −69.5 (d, $^3J_{P,H}$ = 20.4 Hz), −68.3 (d, $^3J_{P,H}$ = 20.4 Hz).

**$^{31}$P NMR** (202.4 MHz, 298.0 K, $CDCl_3$): δ / ppm = (162.0 MHz, 298.0 K, $CDCl_3$): δ / ppm = −69.5 (m), −68.3 (m).

### 5.6.39 Synthesis of 9,9-diethyl-3,7-di-*n*-propyl-4,8-ethano[1,4]diphosphinino[2,3-d:5,6-d']bis[1,3]thiazole-2,6-dithione (18f)

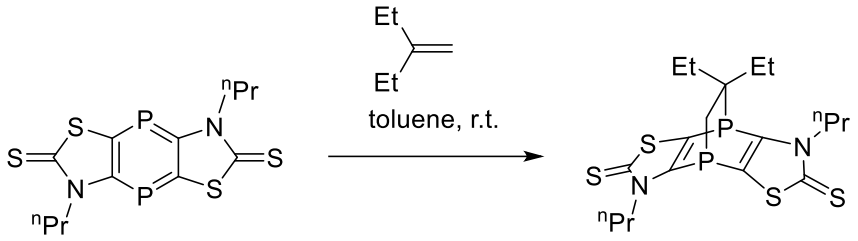


**1** **18f**

In a 10 mL Schlenk vessel, 0.05 mL (0.409 mmol, 2.42 eq.) of 2-ethyl-1-butene were added to a suspension of 63.7 mg (0.169 mmol, 1.00 eq.) of **1** in 4 mL toluene. The mixture was stirred for 48 h at ambient temperature and volatiles were removed *in vacuo* ($10^{-2}$ mbar). The residue was washed three times with 2 mL of *n*-pentane each and dried *in vacuo* ($10^{-2}$ mbar). The product was obtained as a colourless solid.

**Reaction code:** TK-374 (20p5a037.22)

**Molecular formula:** $C_{18}H_{26}N_2P_2S_4$

**Molecular weight:** 460.61 g/mol

**Yield:** 39 mg (0.085 mmol, 80%)

**Melting point:** 150 °C (dec. to **1**)

**X-ray diffraction analysis:** very good structure (B1, GSTR797, GXray7140)

| | | | | |
|---|---|---|---|---|
| **Elemental analysis:** | calculated / % | C 46.94 | H 5.69 | N 6.08 |
| | found / % | C 47.88 | H 6.09 | N 5.90 |

**MS** (EI, 70 eV, selected data): m/z (%): 460.1 (2) $[M]^{+\bullet}$, 376.0 (71) $[M-C_6H_{12}]^{+\bullet}$, 334.0 (35) $[M-C_6H_{12}-C_3H_7+H]^{+\bullet}$, 291.9 (100) $[M-C_6H_{12}-2\ C_3H_7+2\ H]^{+\bullet}$.

**HRMS** (neg. ESI) for $C_{18}H_{26}N_2P_2S_4OH$ theor./exp. 477.0476/477.0479 $[M+OH]^{+\bullet}$.
for $C_{12}H_{15}N_2P_2S_4OH$ theor./exp. 392.9537/392.9535 $[M-C_6H_{12}+OH]^{+\bullet}$.
(pos. ESI) for $C_{18}H_{26}N_2P_2S_4H$ theor./exp. 461.0527/461.0531 $[M+H]^{+\bullet}$.
for $C_{12}H_{15}N_2P_2S_4H$ theor./exp. 376.9588/376.9586 $[M-C_6H_{12}+H]^{+\bullet}$.

**$^1$H NMR** (500.0 MHz, 298.0 K, $CDCl_3$): δ / ppm = 0.92–1.02 (m, 12H, $CH_2CH_2$, $CCH_2CH_3$), 1.16–1.50 (m, 4H, $CCH_2CH_3$), 1.56 (ddd, 1H, $^2J_{H,H}$ = 14.4 Hz, $^2J_{P,H}$ = 8.01 Hz, $^3J_{P,H}$ = 2.22 Hz $PCH_2$), 1.67 (ddd, 1H, $^2J_{H,H}$ = 14.4 Hz, $^2J_{P,H}$ = 7.19 Hz, $^3J_{P,H}$ = 2.18 Hz $PCH_2$), 1.70–1.92 (m, 4H, $CH_2CH_2CH_3$), 4.18 (dddd, 1H, $^2J_{H,H}$ = 13.1 Hz, $^3J_{H,H}$ = 9.91 Hz, $^3J_{H,H}$ = 6.17 Hz,

$^{4}J_{P,H}$ = 1.93 Hz, *CH*$_2$CH$_2$CH$_3$), 4.38 (td, 2H, $^{3}J_{H,H}$ = 7.53 Hz, $^{4}J_{P,H}$ = 1.15 Hz, *CH*$_2$CH$_2$CH$_3$) 4.50 (ddd, 1H, $^{2}J_{H,H}$ = 13.1 Hz, $^{3}J_{H,H}$ = 10.0 Hz, $^{3}J_{H,H}$ = 5.18 Hz, *CH*$_2$CH$_2$CH$_3$).

**$^{13}$C{$^{1}$H} NMR** (125.8 MHz, 298.0 K, $CDCl_3$): δ / ppm = 9.21 (d, $^{3}J_{P,C}$ = 6.27 Hz, C(CH$_2$*CH$_3$*)$_2$), 9.33 (d, $^{3}J_{P,C}$ = 7.96 Hz, C(CH$_2$*CH$_3$*)$_2$), 11.2 (d, $^{5}J_{P,C}$ = 1.47 Hz, CH$_2$CH$_2$*CH$_3$*), 11.3 (s, CH$_2$CH$_2$*CH$_3$*), 22.1 (d, $^{4}J_{P,C}$ = 2.75 Hz, CH$_2$*CH$_2$*CH$_3$), , 22.3 (d, $^{4}J_{P,C}$ = 3.39 Hz, CH$_2$*CH$_2$*CH$_3$), 29.9 (d, $^{2}J_{P,C}$ = 19.8 Hz, C(*CH$_2$*CH$_3$)$_2$), 30.3 (d, $^{2}J_{P,C}$ = 20.5 Hz, C*CH$_2$*CH$_3$), 34.1 (dd, $^{1}J_{P,C}$ = 12.8 Hz, $^{2}J_{P,C}$ = 4.25 Hz, P*CH$_2$*), 46.3 (dd, $^{1}J_{P,C}$ = 9.56 Hz, $^{2}J_{P,C}$ = 2.16 Hz, *C*(CH$_2$CH$_3$)$_2$), 51.1 (dd, $^{3}J_{P,C}$ = 10.7 Hz, *CH$_2$*CH$_2$CH$_3$), 51.1 (dd, $^{3}J_{P,C}$ = 10.1 Hz, *CH$_2$*CH$_2$CH$_3$), 128.2 (dd, $^{3}J_{P,C}$ = 23.1 Hz, $^{2}J_{P,C}$ = 4.90 Hz, P*C*S), 128.9 (dd, $^{3}J_{P,C}$ = 27.6 Hz, $^{2}J_{P,C}$ = 6.03 Hz, P*C*S), 153.0 (dd, $^{1}J_{P,C}$ = 16.3 Hz, $^{2}J_{P,C}$ = 2.86 Hz, P*C*N), 154.2 (dd, $^{1}J_{P,C}$ = 21.1 Hz, $^{2}J_{P,C}$ = 3.84 Hz, P*C*N), 190.4 (d, $^{3}J_{P,C}$ = 2.03 Hz, *C*=S), 190.5 (d, $^{3}J_{P,C}$ = 1.99 Hz, *C*=S).

**$^{31}$P{$^{1}$H} NMR** (202.4 MHz, 298.0 K, $CDCl_3$): δ / ppm = −73.4 (d, $^{3}J_{P,P}$ = 23.4 Hz, *P*CH$_2$), −63.4 (d, $^{3}J_{P,P}$ = 23.4 Hz, *P*Et$_2$.

**$^{31}$P NMR** (202.4 MHz, 298.0 K, $CDCl_3$): δ / ppm = −73.4 (dt, $^{3}J_{P,P}$ = 23.4 Hz, $^{2}J_{P,H}$ = 7.52 Hz, *P*CH$_2$), −63.4 (m, *P*Et$_2$).

### 5.6.40 Synthesis of 3,7-di-*n*-propyl-4,8-[1',2']-5',5'-dimethyl-1'-pyrroline-4-oxo-[1σ$^{4}$λ$^{5}$,4σ$^{3}$λ$^{3}$]diphosphinino[2,3-d:5,6-d']bis[1,3]thiazole-2,6-dithione (19)

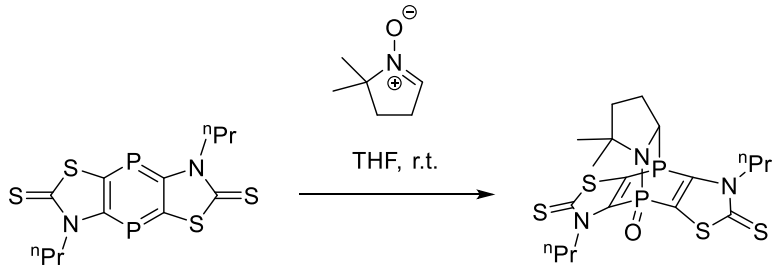


**1** **19**

A solution 13.8 mg 5,5-dimethyl-1-pyrrolidine-*N*-oxide (DMPO) in 2 mL THF was added to a suspension of 46.0 mg of **1** in 2 mL THF. The mixture was stirred for 20 h before removing the solvent at room temperature *in vacuo* ($10^{-2}$ mbar). The crude product was purified *via* column chromatography (Ø = 2 cm, 2 cm $SiO_2$, 20 mL DCM). Volatiles were removed at ambient temperature *in vacuo* ($10^{-2}$ mbar) and the residue was washed twice with 2 mL of *n*-pentane each before drying *in vacuo* ($10^{-2}$ mbar). The product was obtained as a pale-yellow powder (7.8 mg; 0.0159 mmol; 13 %) with an isomeric ratio of 1:2.

**Reaction code:** TK-282 (24p5a055.21, 24s7c004.21)

**Molecular formula:** $C_{18}H_{25}N_3OP_2S_4$

**Molecular weight:** 489.61 g/mol

**Yield:** 7.8 mg; (0.016 mmol; 13%)

**Melting point:** 190 °C (dec.)

**MS** (EI, 70 eV, selected data): m/z (%): 505.0 (2) $[M+O]^+$, 489.0 (2) $[M]^{+\bullet}$, 463.0 (0.4) $[M-C_2H_4+2H]^+$, 420.9 (0.2) $[M-C_5H_8]^+$, 407.9 (0.6) $[M-C_6H_{11}N+O]^+$, 391.9 (2) $[M-C_6H_{11}N]$, 375.9 (2) $[M-C_6H_{11}N-O]^+$, 349.9 (1) $[M-C_6H_{11}N-C_3H_7+H]^+$, 333.9 (0.4) $[M-C_6H_{11}N-O-C_3H_7+H]^+$, 112.1 (10) $[C_6H_{11}NO-H]^+$, 98.0 (64) $[C_6H_{11}NO-O+H]^+$, 82.0 (100) $[C_6H_{11}NO-2CH_3-H]^+$, 69.0 (70) $[C_6H_{11}NO-O-C_2H_4]^+$.
(LIFDI, selected data): m/z (%) = 489.3 (100) $[M]^{+\bullet}$.

**IR** (ATR Diamond, selected data): $\tilde{\nu}$ / $cm^{-1}$ = 2855 (w, *v*(CH)), 2924 (m, *v*(CH)), 2961 (w, *v*(CH)).

**$^1$H NMR** (700.4 MHz, 298.0 K, THF-d8): δ / ppm = 0.93–1.00 (m, 6H, $CH_2CH_2CH_3$), 1.18 (s, 1.8H, $NC(CH_3)_2$), 1.30 (s, 0.8H, $NC(CH_3)_2$ *isomer*), 1.31 (s, 1.2H, $NC(CH_3)_2$), 1.33–1.45 (m, 1.5H, $PCHCH_2CH_2$), 1.56 (s, 1H, $NC(CH_3)_2$ *isomer*), 1.56 (s, 2H, $NC(CH_3)_2$), 1.75–1.88 (m, 4.3H, $CH_2CH_2CH_2$, $PCHCH_2$ *isomer*), 1.95–2.01 (m, 1H, $PCHCH_2$), 2.04–2.11 (m, 1H, $PCHCH_2CH_2$), 4.23–4.33 (m, 2.4H, $CH_2CH_2CH_3$, PCH), 4.34–4.39 (m, 0.3H, $CH_2CH_2CH_3$ *isomer*), 4.45–4.50 (m, 0.6H, $CH_2CH_2CH_3$ *isomer*), 4.58–4.62 (m, 1.2H, $CH_2CH_2CH_3$).

**$^{13}$C{$^1$H} NMR** (176.1 MHz, 298.0 K, THF-d8): δ / ppm = 11.3 (s, $CH_2CH_2CH_3$ *isomer*), 11.3 (s, $CH_2CH_2CH_3$), 11.5 (s, $CH_2CH_2CH_3$), 11.5 (s, $CH_2CH_2CH_3$ *isomer*), 22.7 (s, $CH_2CH_2CH_3$), 22.8 (s, $CH_2CH_2CH_3$ *isomer*), 23.0 (d, $^4J_{P,C}$ = 3.00 Hz, $CH_2CH_2CH_3$), 23.2 (d, $^4J_{P,C}$ = 3.46 Hz, $CH_2CH_2CH_3$ *isomer*), 26.8 (d, $^3J_{P,C}$ = 5.11 Hz, $NC(CH_3)_2$), 27.9 (d, $^3J_{P,C}$ = 4.69 Hz, $NC(CH_3)_2$), 29.6 (dd, $^3J_{P,C}$ = 12.8 Hz, $^3J_{P,C}$ = 3.96Hz, $PCHCH_2CH_2$), 29.8 (dd, $^3J_{P,C}$ = 8.44 Hz, $^3J_{P,C}$ = 2.12 Hz, $PCHCH_2CH_2$ *isomer*), 31.9 (s, $NC(CH_3)_2$), 32.0 (s, $NC(CH_3)_2$ *isomer*), 44.2 (dd, $^2J_{P,C}$ = 12.0 Hz, $^3J_{P,C}$ = 6.99 Hz, $PCHCH_2$), 44.3 (dd, $^2J_{P,C}$ = 9.76 Hz, $^3J_{P,C}$ = 6.02 Hz, $PCHCH_2$ *isomer*), 50.4 (s, $CH_2CH_2CH_3$ *isomer*), 50.6 (s, $CH_2CH_2CH_3$), 50.8 (d, $^3J_{P,C}$ = 9.71 Hz, $CH_2CH_2CH_3$, *isomer*), 51.2 (d, $^3J_{P,C}$ = 8.45 Hz, $CH_2CH_2CH_3$), 63.7 (dd, $^1J_{P,C}$ = 18.1 Hz, $^2J_{P,C}$ = 3.34 Hz, PCH), 64.9 (dd, $^1J_{P,C}$ = 19.9 Hz, $^2J_{P,C}$ = 2.66 Hz, PCH, *isomer*), 65.8 (s (br.), $PNCMe_2$), 66.6 (s (br.), $PNCMe_2$ *isomer*), 122.7 (dd, $^1J_{P,C}$ = 33.0 Hz, $^2J_{P,C}$ = 12.2 Hz, PCS), 123.4 (dd, $^1J_{P,C}$ = 160.8 Hz, $^2J_{P,C}$ = 5.85 Hz, PCS), 128.8 (d, $^1J_{P,C}$ = 128 Hz, PCS *isomer*), 151.2 (d, $^1J_{P,C}$ = 119.8 Hz, PCN), 157.6 (dd, $^1J_{P,C}$ = 16.5 Hz, $^2J_{P,C}$ = 11.7 Hz, PCN), 190.6 (d, $^3J_{P,C}$ = 4.41 Hz, C=S *isomer*), 190.7 (d, $^3J_{P,C}$ = 4.78 Hz, C=S *isomer*), 190.9 (d, $^3J_{P,C}$ = 5.50 Hz, C=S), 191.1 (dd, $^3J_{P,C}$ = 9.11 Hz, $^3J_{P,C}$ = 2.62 Hz, C=S).

**$^{31}P\{^{1}H\}$ NMR** (202.4 MHz, 298.0 K, THF-d8): δ / ppm = −86.9 (d, $^{3}J_{P,P}$ = 4.20 Hz, *P*CH, *isomer*), −81.8 (d, $^{3}J_{P,P}$ = 3.99 Hz, *P*CH), −1.08 (d, $^{3}J_{P,P}$ = 4.20 Hz, *P*(N)=O, *isomer*), −0.89 (d, $^{3}J_{P,P}$ = 4.99 Hz, *P*(N)=O).

**$^{31}P$ NMR** (202.4 MHz, 298.0 K, THF-d8): δ / ppm = −86.9 (d, $^{3}J_{P,P}$ = 4.20 Hz, *P*CH, *isomer*), −81.8 (d, $^{3}J_{P,P}$ = 3.99 Hz, *P*CH), −1.08 (d, $^{3}J_{P,P}$ = 4.20 Hz, *P*(N)=O, *isomer*), −0.89 (d, $^{3}J_{P,P}$ = 4.99 Hz, *P*(N)=O).

### 5.6.41 Synthesis of 3,7-di-*n*-propyl-4,8-[1',2']-4'-phenyl-1',2',4'-triazoline-3',5'-diono-[1,4]diphosphinino[2,3-d:5,6-d']bis[1,3]thiazole-2,6-dithione (20)

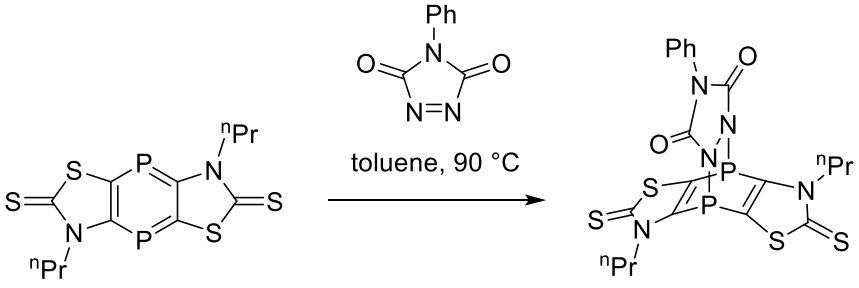


**1** **20**

A solution of 23.8 mg (0.136 mmol, 2.05 eq.) 4-phenyl-1,2,4-triazoline-3,5-dione in 4 ml toluene was added to a suspension of 48.8 mg (0.130 mmol, 1.00 eq.) **1** in 2 ml toluene at ambient temperature. The mixture was stirred at 90 °C for 30 min and filtered. The yellow residue was washed twice with 1 mL *n*-pentane each. After drying *in vacuo* ($10^{-2}$ mbar) the product was obtained as a yellow solid.

**Reaction code:** TK-133 (30p5b001.19, 50t4b031.19, 17m3a012.20)

**Molecular formula:** $C_{20}H_{19}N_5O_2P_2S_4$

**Molecular weight:** 551.59 g/mol

**Yield:** 48 mg; (0.087 mmol; 67%)

**MS** (EI, 70 eV, selected data): m/z (%): 551.0 (40) $[M]^{+\bullet}$, 376 (85 %) $[C_{12}H_{14}N_2P_2S_4]^{+\bullet}$, 334.0 (35%) $[M-C_{12}H_{14}N_2P_2S_4\text{-nPr}]^{+\bullet}$, 177.1 (40%) $[C_8H_5N_3O_2]^{+\bullet}$.[110]

**HRMS** (neg. ESI) for $C_{20}H_{19}N_5O_2P_2S_4$ theor./exp. 550.9897/550.9893 $[M]^{+\bullet}$.[110]

**IR** (ATR Diamond, selected data): $\tilde{\nu}$ / $cm^{-1}$ = 1699 (s, *v*(CO)), 1748 (s, *v*(CO)), 2873 (w, *v*(CH)), 2932 (w, *v*(CH)), 2961 (w, *v*(CH)).

**$^{1}$H NMR** (500.1 MHz, 298.0 K, $CDCl_3$): δ / ppm = 1.03 (t, 6H, $^{3}J_{H,H}$ = 7.33 Hz, $CH_2CH_2CH_3$), 1.80–1.92 (m, 4H, $CH_2CH_2CH_3$), 4.35–4.43 (m, 2H, $CH_2CH_2CH_3$), 4.45–4.52 (m, 2H, $CH_2CH_2CH_3$), 7.41–7.45 (m, 2H, $C_6H_5$), 7.46–7.49 (m, 1H, $pC_6H_5$), 7.49–7.51 (m, 2H, $C_6H_5$).

**$^{13}$C{$^{1}$H} NMR** (125.8 MHz, 298.0 K, $CDCl_3$): δ / ppm = 11.4 (s, $CH_2CH_2CH_3$), 22.7 (s, $CH_2CH_2CH_3$), 51.1 (s, $CH_2CH_2CH_3$), 125.7 (s, $p$-$C_6H_5$), 125.9 (s, $C_6H_5$), 128.9 (s, $i$-$C_6H_5$) 129.2 (d, $^{2}J_{P,C}$ = 2.42 Hz, N(*C*O)N), 129.5 ($C_6H_5$), 130.7 (d, $^{1}J_{P,C}$ = 6.55 Hz, P*C*S), 155.2 (s, P*C*N), 189.4 (s, *C*=S).

**$^{31}$P{$^{1}$H} NMR** (202.5 MHz, 298.0 K, $CDCl_3$): δ / ppm = −45.8 (s).

**$^{31}$P NMR** (202.5 MHz, 298.0 K, $CDCl_3$): δ / ppm = −45.8 (s).

### 5.6.42 Attempted synthesis of 9-*n*-butyl-3,7-di-*n*-propyl-4,8-ethano-4-λ$^{5}$-phosphanono [1,4]diphosphinino[2,3-d:5,6-d']bis[1,3]thiazole-2,6-dithione (21a)

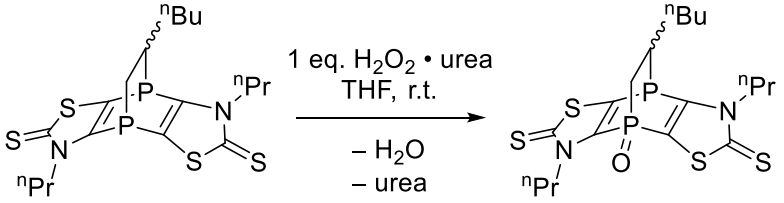


**18c** **21a**

*5.6.42.1 DMPO*

In a 10 mL Schlenk vessel, 3 mL THF were added to a mixture of 30.6 mg (0.066 mmol, 1.00 eq.) **18c** and 7.1 mg (0.063 mmol, 0.94 eq.) DMPO at ambient temperature. The mixture was stirred for 1 h at this temperature.

**Reaction code:** TK-233 (08m3a005.21)

*5.6.42.2 Pyridine-N-oxide*

In a 10 mL Schlenk vessel, 7.7 mg (0.081 mmol, 1.22 eq.) of pyridine-N-oxide were added to a solution of 30.6 mg (0.066 mmol, 1.00 eq.) **18c** in 3 mL THF at ambient temperature. The mixture was stirred for 1 h at this temperature.

**Reaction code:** TK-233 (08m3a011.21)

*5.6.42.3 DMSO*

In a 10 mL Schlenk vessel, 2.5 µL (0.035 mmol, 1.04 eq.) of DMSO were added to solution of 15.6 mg (0.034 mmol, 1.00 eq.) **18c** in 2 mL THF at ambient temperature. The mixture was stirred for 2.8 h.

**Reaction code:** TK-283 (25m3a034.21)

*5.6.42.4 Hydrogen peroxide-urea adduct*

In a 10 mL Schlenk vessel, 6.1 mg (0.065 mmol, 1.03 eq.) hydrogen peroxide-urea were added to a solution of 29.0 mg (0.063 mmol, 1.00 eq.) **18c** in 2 mL THF at ambient temperature. The mixture was stirred for 1h before heating to 40 °C for 24 h.

**Reaction code:** TK-315 (02m3a037.22, 02m3a060.22)

### 5.6.43 Synthesis of 9,10-diethyl-3,7-di-*n*-propyl-4,8-etheno-4,8-di-λ⁵-phosphanono[1,4]-diphosphinino[2,3-d:5,6-d']bis[1,3]thiazole-2,6-dithione (22b)

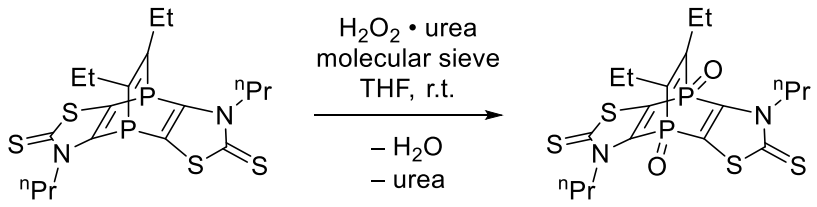


**17c** **22b**

In a 20 mL Schlenk vessel, 232.2 mg (2,468 mmol, 10.03 eq.) of hydrogen peroxide - urea were added to a suspension of 113.0 mg (0.246 mmol, 1.00 eq.) **17c** and some molecular sieves (3 Å) in 10 mL THF. The mixture was stirred for 24 h at ambient temperature and extracted with THF. Volatiles were removed *in vacuo* ($10^{-2}$ mbar) and the residue was washed three times with 3 mL *n*-pentane each. After drying *in vacuo* ($10^{-2}$ mbar) the product was obtained as a yellow solid.

**Reaction code:** TK-458 (TIM230203p5b025, TIM230207s7a008)

**Molecular formula:** $C_{18}H_{24}N_2O_2P_2S_4$

**Molecular weight:** 490.59 g/mol

**Yield:** 40 mg; (0.082 mmol; 33%)

**Melting point:** 146 °C (dec.)

**MS** (APCI, selected data): m/z (%): 491.026 (30) $[M+H]^{+\bullet}$.

**HRMS** (pos. ESI) for $C_{18}H_{24}N_2O_2P_2S_4H$ theor./exp. 491.0269/491.0267 $[M+H]^{+\bullet}$.

**IR** (ATR Diamond, selected data): $\tilde{\nu}$ / $cm^{-1}$ = 2972 (w, *v*(CH)).

**$^1$H NMR** (500.0 MHz, 298.0 K, THF-d8): δ / ppm = 0.97 (t, 6H, $^3J_{H,H}$ = 7.39 Hz, $CH_2CH_2\mathit{CH_3}$), 1.18 (t, 6H, $^3J_{H,H}$ = 7.47 Hz, $CCH_2\mathit{CH_3}$), 1.75–1.87 (m, 4H, $CH_2\mathit{CH_2}CH_2$), 2.71–2.84 (m, 4H, $C\mathit{CH_2}CH_3$), 4.38–4.52 (m, 4H, $\mathit{CH_2}CH_2CH_3$).

**$^{13}$C{$^1$H} NMR** (125.8 MHz, 298.0 K, THF-d8): δ / ppm = 11.2 (s, $CH_2CH_2\mathit{CH_3}$), 14.1 (s, $CCH_2\mathit{CH_3}$), 22.9 (s, $CH_2\mathit{CH_2}CH_3$), 23.2 (t, $^2J_{P,C}$ = 10.9 Hz, $C\mathit{CH_2}CH_3$), 51.1 (s, $\mathit{CH_2}CH_2CH_3$), 129.5 (dd, $^1J_{P,C}$ = 18.2 Hz, $^2J_{P,C}$ = 13.8 Hz, P*C*S), 154.0 (dd, $^1J_{P,C}$ = 9.49 Hz, $^2J_{P,C}$ = 8.51 Hz, P*C*N), 158.0 (dd, $^1J_{P,C}$ = 12.6 Hz, $^2J_{P,C}$ = 9.08 Hz, P*C*$CH_2CH_3$), 190.5 (t, $^3J_{P,C}$ = 7.35 Hz, *C*=S).

**$^{31}$P{$^1$H} NMR** (202.4 MHz, 298.0 K, THF-d8): δ / ppm = −12.6 (s).

**$^{31}$P NMR** (202.4 MHz, 298.0 K, THF-d8): δ / ppm = −12.6 (tt, $^3J_{P,H}$ = 10.0 Hz, $^4J_{P,H}$ = 7.57 Hz).

### 5.6.44 Synthesis of 9,10-diethyl-3,7-di-*n*-propyl-4,8-etheno-4,8-di-λ$^5$-phosphanethiono-[1,4]diphosphinino[2,3-d:5,6-d']bis[1,3]thiazole-2,6-dithione (24a)

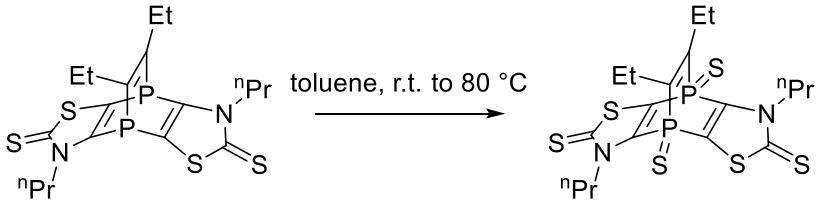


**17c** **24a**

*5.6.44.1 Sulfur*

In a 10 mL Schlenk vessel, 5 mg (0.156 mmol, 3.47 eq.) of sulfur were added to a suspension of 20.6 mg (0.045 mmol, 1.00 eq.) **17c** in 2 mL toluene. The reaction was stirred for 30 min at ambient temperature before heating to 60 °C for 6 d.

**Reaction code:** TK-487 (TIM230420m3a035)

*5.6.44.2 Cyclohexene sulfide*

In a 10 mL Schlenk vessel, 115.3 mg (1.010 mmol, 4.74 eq.) of cyclohexene sulfide were added to a suspension of 97.7 mg (0.213 mmol, 1.00 eq.) **17c** in 5 mL toluene. The mixture was heated to 80 °C for 53 d before removing volatiles *in vacuo* ($10^{-2}$ mbar). The yellow residue was washed three times with 2 mL *n*-pentane each and dried *in vacuo* ($10^{-2}$ mbar).

**Reaction code:** TK-528 (TIM230821p5a006)

**Molecular formula:** $C_{18}H_{24}N_2O_2P_2S_4$

**Molecular weight:** 522.71 g/mol

**MS** (pos. ESI, selected data): m/z (%): 525.014 (20) $[M+3H]^{+\bullet}$, 491.009 (100) $[M–S+H]^{+\bullet}$, 459.037 (65) $[M–2S+H]^{+\bullet}$.

**HRMS** (pos. ESI) for $C_{18}H_{24}N_2P_2S_6H$ theor./exp. 522.9812/522.9820 $[M+H]^{+\bullet}$.

**IR** (ATR Diamond, selected data): $\tilde{\nu}$ / $cm^{-1}$ = 2857 (w, *v*(CH)), 2929 (w, *v*(CH)), 2961 (w, *v*(CH)).

**$^1$H NMR** (500.0 MHz, 298.0 K, THF-d8): δ / ppm = 0.98 (t, 6H, $^3J_{H,H}$ = 7.38 Hz, $CH_2CH_2\mathit{CH_3}$), 1.14 (t, 6H, $^3J_{H,H}$ = 7.46 Hz, $CCH_2\mathit{CH_3}$), 1.71-1.74 (m, 4H, $CH_2\mathit{CH_2}CH_2$), 2.82-2.95 (m, 4H, $C\mathit{CH_2}CH_3$), 4.55-4.67 (m, 4H, $\mathit{CH_2}CH_2CH_3$).

**$^{13}$C{$^1$H} NMR** (125.8 MHz, 298.0 K, THF-d8): δ / ppm = 10.8 (s, $CH_2CH_2\mathit{CH_3}$), 14.6 (s, $CCH_2\mathit{CH_3}$), 23.3 (s, $CH_2\mathit{CH_2}CH_3$), 24.0 (t, $^2J_{P,C}$ = 10.9 Hz, $C\mathit{CH_2}CH_3$), 49.6 (s, $\mathit{CH_2}CH_2CH_3$), 133.1 (m, P*C*S), 148.8 (m, P*C*N), 155.7 (m, P*C*$CH_2CH_3$), 190.8 (m, *C*=S).

**$^{31}$P{$^1$H} NMR** (202.4 MHz, 298.0 K, THF-d8): δ / ppm = −3.91 (s) (83% by integration).

**$^{31}$P NMR** (202.4 MHz, 298.0 K, THF-d8): δ / ppm = −3.91 (m) (83% by integration).

### 5.6.45 Synthesis of *rel*-(9*S*,10*R*)-3,7-di-*n*-propyl-4,8-[1',2']-cyclohexano-4,8-di-λ$^5$-phosphanethiono[1,4]diphosphinino[2,3-d:5,6-d']bis[1,3]thiazole-2,6-dithione (24b)

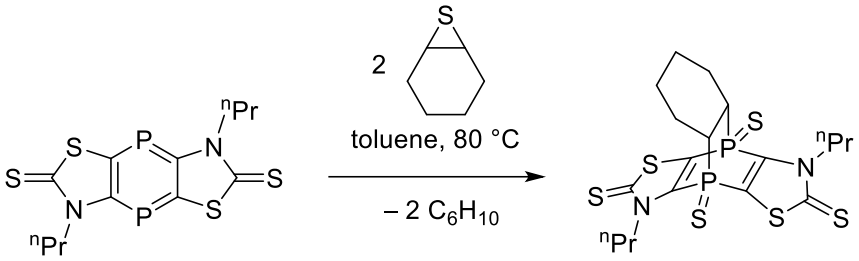


**1** **24b**

In a 10 mL Schlenk vessel, 99 mg (0.867 mmol, 13.72 eq.) cyclohexene sulfide were added to a suspension of 23.8 mg (0.063 mmol, 1.00 eq.) of **1** in 5 mL toluene. The mixture was stirred for 20 d at 80 °C before removing volatiles *in vacuo* ($10^{-2}$ mbar) and washing three times with 2 mL of *n*-pentane each. The residue was extracted twice with 0.7 mL THF and again washed with *n*-pentane.

**Reaction code:** TK-512 (TIM230621p5a044)

**Molecular formula:** $C_{18}H_{24}N_2P_2S_6$

**Molecular weight:** 522.71 g/mol

**Yield:** 15.7 mg; (0.03 mmol; 48%)

**Melting point:** 97 °C

**MS** (LIFDI, selected data): m/z (%): 522.0 $[M]^{+\bullet}$.

**HRMS** (pos. ESI) for $C_{18}H_{24}N_2P_2S_6$ theor./exp. 522.9812/522.9809 $[M+H]^{+\bullet}$.

**IR** (ATR Diamond, selected data): $\tilde{\nu}$ / $cm^{-1}$ = 2853 (w, *v*(CH)), 2929 (m, *v*(CH)), 2961 (w, *v*(CH)).

**$^1$H NMR** (500.0 MHz, 298.0 K, THF-d8): δ / ppm = 0.89 (t, 6H, $CH_2CH_2CH_3$), 0.96 (t), 1.22–1.35 (br. s., $CH_2CH_2CH_3$), 2.86–2.94 (m, PC*H*), 1.50–1.64 (br. s., PCHC$H_2$), 2.93–3.10 (br. s., $CH_2CH_2CH_3$).

**$^{13}$C{$^1$H} NMR** (176.1 MHz, 298.0 K, THF-d8): δ / ppm = 10.9 (s, $CH_2CH_2CH_3$), 10.9 (s, $CH_2CH_2CH_3$), 20.7 (d, $^nJ_{P,C}$ = 20.8 Hz, PCH$CH_2$), 20.8 (d, $^nJ_{P,C}$ = 20.8 Hz, PCH$CH_2$), 20.9 (d, $^nJ_{P,C}$ = 1.61 Hz, $CH_2CH_2CH_3$), 21.0 (s, ), 42.9 (dd, $^1J_{P,C}$ = 46.1 Hz, $^2J_{P,C}$ = 2.02 Hz, P*C*H), 44.3 (dd, $^1J_{P,C}$ = 48.2 Hz, $^2J_{P,C}$ = 1.88 Hz, P*C*H), 51.0 (d, $^3J_{P,C}$ = 10.2 Hz, $CH_2CH_2CH_3$), 51.1 (d, $^3J_{P,C}$ = 10.4 Hz, $CH_2CH_2CH_3$), 127.1 (dd, $^1J_{P,C}$ = 61.2 Hz, $^2J_{P,C}$ = 14.4 Hz, P*C*S), 127.5 (dd, $^1J_{P,C}$ = 61.2 Hz, $^2J_{P,C}$ = 14.3 Hz, P*C*S), 142.0 (dd, $^1J_{P,C}$ = 64.5 Hz, $^2J_{P,C}$ = 11.7 Hz P*C*N), 143.0 (dd, $^1J_{P,C}$ = 69.4 Hz, $^2J_{P,C}$ = 13.3 Hz, P*C*N), 192.0–192.2 (m, *C*=S).

**$^{31}$P{$^1$H} NMR** (202.4 MHz, 298.0 K, THF-d8): δ / ppm = 8.19 (d, $^3J_{P,P}$ = 82.1 Hz), 8.79 (d, $^3J_{P,P}$ = 82.3 Hz).

**$^{31}$P NMR** (202.4 MHz, 298.0 K, THF-d8): δ / ppm = 8.48 (m).

### 5.6.46 Attempted synthesis of 9-ethylcarboxy-3,7-di-*n*-propyl-4,8-ethano[1,4]diphosphinino[2,3-d:5,6-d']bis[1,3]thiazole-2,6-diylidene (26a)

*5.6.46.1 Potassium*

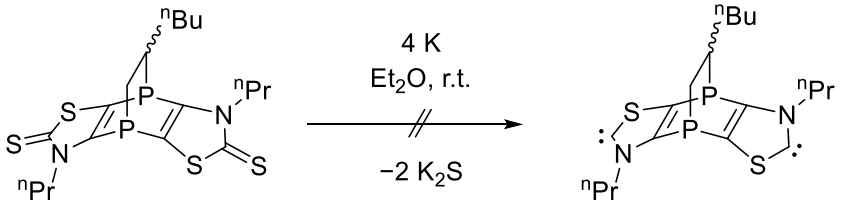


**18c** **26a**

In a 10 mL vial, 8.0 mg (0.205 mmol, 7.3 eq.) of potassium metal were added to a suspension of 13.0 mg (0.028 mmol, 1.00 eq.) of **18c** in 2 mL diethyl ether. The mixture was stirred for 4 h at ambient temperature before $^{31}P\{^{1}H\}$ NMR spectroscopic experiments were carried out.

**Reaction code:** TK-289 (31p5c020.21)

*5.6.46.2 Tri-n-butylphosphane*

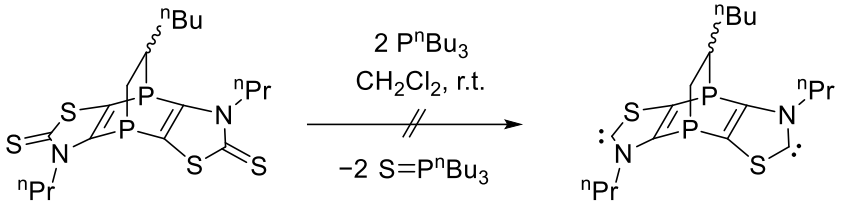


**18c** **26a**

In a 10 mL Schlenk vessel, 0.02 mL (0.081 mmol, 3.52 eq.) of tri-*n*-butylphosphane were added to a solution of 10.7 mg (0.023 mL, 1.00 eq.) of **18c** in 2 mL dichloromethane. The reaction mixture was stirred for 3 d at ambient temperature.

**Reaction code:** TK-286 (30.3b035.21, 31t4a014.21)

*5.6.46.3 Tris(diethylamino)phosphane*

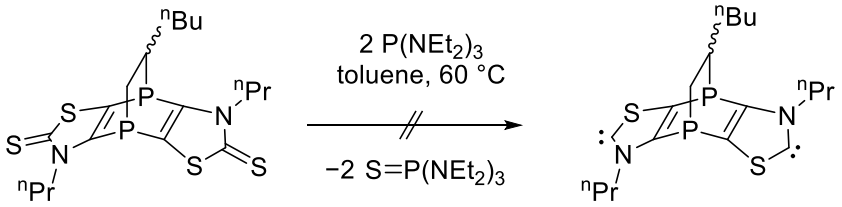


**18c** **26a**

In a 10 mL Schlenk vessel, 0.02 mL (0.073 mmol, 7.85 eq.) of tris(diethylamino)phosphane were added to a suspension of 4.3 mg (0.009 mmol, 1.00 eq.) of **18c** in 2 mL toluene. The reaction mixture was stirred for 22 h at ambient temperature before stirring for 24 h at 60 °C.

**Reaction code:** TK-287 (31p5a049.21, 31m3a014.21)

*5.6.46.4 Tri-n-butylphosphite*

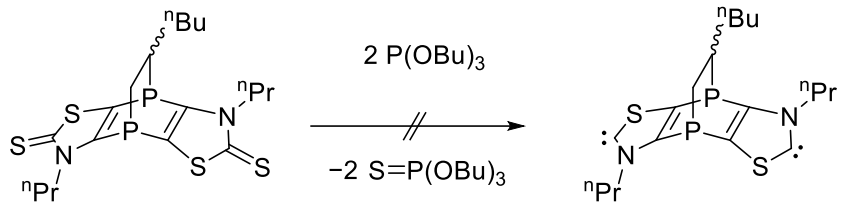


**18c** **26a**

In a 10 mL Schlenk vessel, 0.02 mL (0.074 mmol, 4.90 eq.) of tri-*n*-butylphosphite were added to a suspension of 7.0 mg (0.015 mmol, 1.00 eq.) of **18c** in 2 mL toluene. The reaction mixture was stirred for30 h at 60 °C.

**Reaction code:** TK-288 (31m3a018.21, 31m3a028.21)

In a 10 mL Schlenk vessel, 17 mg (0.037 mmol, 1.00 eq.) of **18c** were added to 2 mL of tri-*n*-butylphosphite. The reaction mixture was heated to 150 °C for 19 h.

**Reaction code:** TK-306 (47m3a043.21, 47t4b051.21, 47m3b034.21)

### 5.6.47 Attempted synthesis of 9,10-diethyl-3,7-di-*n*-propyl-4,8-etheno[1,4]diphosphinine[2,3-d:5,6-d']bis[1,3]thiazole-2,6-diylidene (26b)

*5.6.47.1 Potassium graphite*

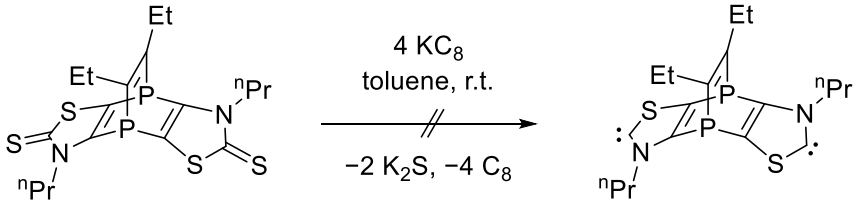


**17c** **26b**

In a 5 mL vial, a solution of 6.8 mg (0.050 mmol, 3.84 eq.) potassium graphite in 2 mL toluene was added to a suspension of 6.0 mg (0.013 mmol, 1.00 eq.) of **17c** in 1.5 mL toluene. The reaction mixture was stirred at ambient temperature for 4 d before the addition of a further 7.2 mg (0.053, 4.08 eq.) of potassium graphite.

**Reaction code:** TK-K-8 (TK-8-1, TK-8-2, TK-8-3, TK-8-4, TK-8-5, TK-8-7)

*5.6.47.2 Magnesium*

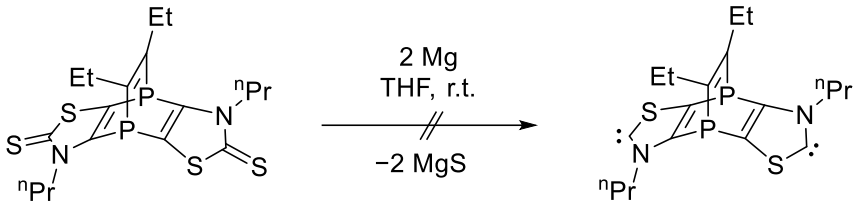


**17c** **26b**

In a 10 mL vial, 2 mL THF were added to a mixture of 1.2 mg (0.049 mmol, 1.12 eq.) magnesium granulate and of 20.2 mg (0.044 mmol, 1.00 eq.) of **17c**. The suspension was vigorously stirred at ambient temperature for 25 h.

**Reaction code:** TK-506 (TIM230509t4a046)

*5.6.47.3 Sodium dispersion in sodium chloride*

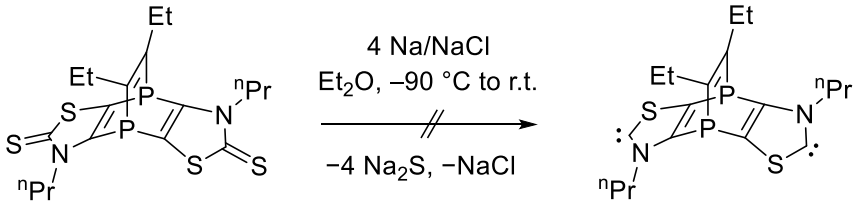


**17c** **26b**

In a 10 mL vial, a suspension of 69.6 mg (0.156 mmol, 4.32 eq.) of a dispersion of sodium in sodium chloride (5.77 wt.%) in 2.5 mL diethyl ether was added to a suspension of 16.6 mg (0.036 mmol, 1.00 eq.) **17c** in 2.5 mL diethyl ether at −90 °C. The reaction mixture was stirred for 23 h while slowly warming up to room temperature.

**Reaction code:** TK-440 (51m3a033.22, 51m3a038.22)

*5.6.47.4 Tri-n-butylphosphite*

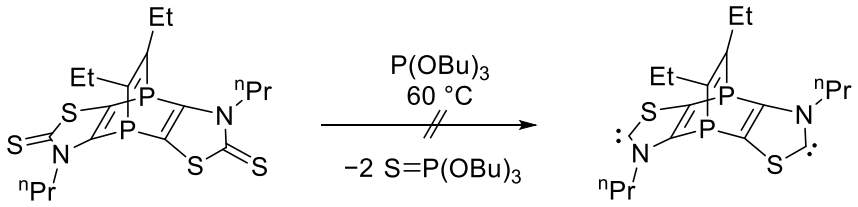


**17c** **26b**

In a 10 mL Schlenk vessel, a spatula tip's worth of **17c** was added to 1 mL of tri-*n*-butylphosphite. The mixture was stirred for 30 d at 60 °C

**Reaction code:** TK-403 (39m3a034.22, 39p5a016.22, 40p5a027.22, 43p5b009.22)

*5.6.47.5 Trimethylphosphane*

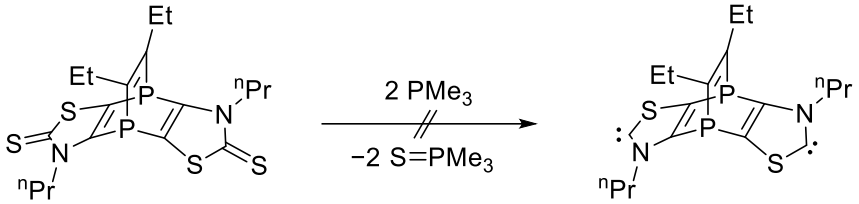


**17c** **26b**

0.03 mL (0.292 mmol, 10.84 eq.) of trimethylphosphane were added to a suspension of 12.3 mg (0.027 mmol, 1.00 eq.) of **17c** in 5 mL toluene in a sealed high-pressure vessel. The mixture was heated to 80 °C for 14 d.

**Reaction code:** TK-346 (11c5b003.22, 12p5a044.22, 13p5a031.22)

A spatula tip's worth of **17c** was added to 1 mL of trimethylphosphane in a sealed high-pressure vessel and the mixture was heated to 80 °C for 30 d.

**Reaction code:** TK-402 (39p5a015.22, 40p5a028.22, 43p5b010.22)

*5.6.47.6 1,3-Dimethylimidazole-2-ylidene*

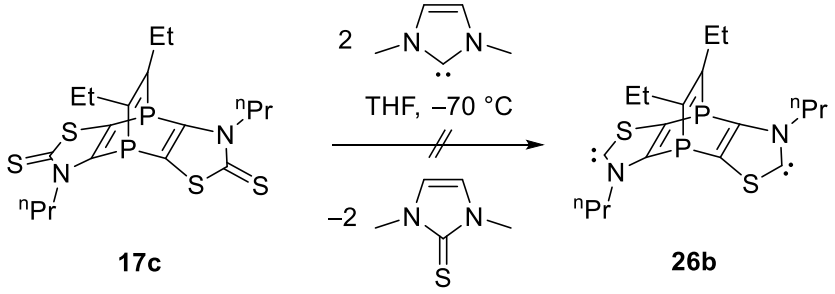


**17c** **26b**

In a 10 mL Schlenk vessel, a solution of 21.6 mg (0.225 mmol, 2.10 eq.) of $IMe_2$ in 1.5 mL THF were added to a suspension of 49.2 mg (0.107 mmol, 1.00 eq.) of **17c** in 1 mL THF at −70 °C. The reaction mixture was stirred for 1 h while slowly warming up to room temperature.

**Reaction code:** TK-363 (14m3a035.22)

*5.6.47.7 Trimethylsilyldiazomethane*

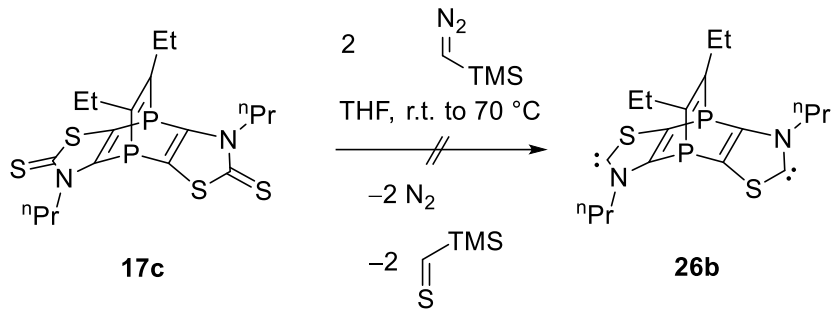


**17c** **26b**

In a 10 mL Schlenk vessel, 0.11 mL (0.22 mmol, 2.02 eq.) of a 2 M solution of TMS-diazomethane were added to a suspension of 49.5 mg (0.108 mmol, 1.00 eq.) of **17c** in 2.5 mL THF at ambient temperature. The mixture was stirred for 3 h at room temperature before heating to 70 °C for 24 h.

**Reaction code:** TK-380 (31p5b009.22, 31p5b025.22, 31p5b038.22)

*5.6.47.8 NacNacAl*

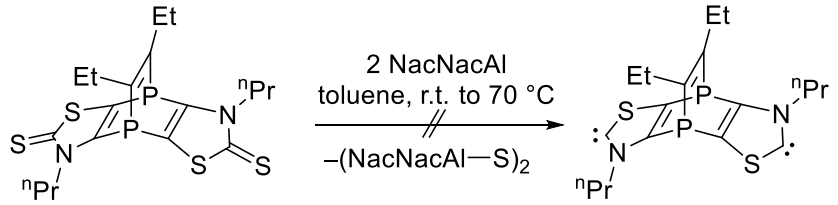


**17c** **26b**

In a 5 mL vial, a suspension of 4.6 mg (0.010 mmol, 1.00 eq.) of **17c** in 0.6 mL toluene was added to 9.0 mg (0.020 mmol, 2.00 eq.) of NacNacAl at ambient temperature. The mixture was stirred for 6 d at room temperature before heating to 70 °C for 7 d.

**Reaction code:** TK-K-10 (TK-10-1, TK-10-2, TK-10-3, TK-10-4, TK-10-5, TK-10-6, TK-10-7)

## 5.6.48 Synthesis of 3,7-di-*n*-propyl-9-ethylcarboxy-4,8-etheno[1,4]diphosphinino[2,3-d:5,6-d']-2,6-bis(methylsulfanyl)-bis[1,3]thiazolium trifluoromethane sulfonate (29a)

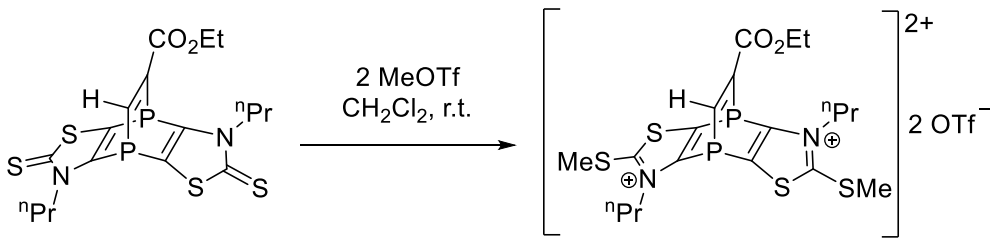


**17b** **29a**

In a 25 mL Schlenk vessel, 0.18 mL (1.645 mmol, 3.04 eq.) of methyl triflate were added to a solution of 256.7 mg (0.541 mmol, 1.00 eq.) **17b** in 9 mL dichloromethane at ambient temperature. The mixture was stirred for 3 h before removing the volatiles *in vacuo* ($10^{-2}$ mbar) at room temperature. The residue was washed once with 5 ml of *n*-pentane and three times with 2 mL of *n*-pentane. After drying *in vacuo* ($10^{-2}$ mbar), **29a** was obtained as a beige solid.

**Reaction code:** TK-112 (26p5a001.19, 26s7a012.19) —

**Molecular formula:** $C_{21}H_{24}F_6P_2N_2O_8S_6$

**Molecular weight:** 802.74 g/mol

**Yield:** 334.4 mg (0.417 mmol, 77%)

**Melting point:** 79 °C

| **Elemental analysis:** | | | | | |
|---|---|---|---|---|---|
| | calculated / % | C 31.42 | H 3.26 | N 3.49 | S 23.96 |
| | found / % | C 28.21 | H 3.48 | N 3.06 | S 23.00 |

**MS** (pos. ESI, selected data): m/z (%): 252.017 (100, z = 2) $[M]^{+\bullet}$.
(neg. ESI, selected data): m/z (5): 148.8 (100) $[OTf]^{-\bullet}$.

**IR** (ATR Diamond, selected data): $\tilde{\nu}$ / $cm^{-1}$ = 1704 (m, *v*(CO)), 2879 (w, *v*(CH)), 2934 (w, *v*(CH)), 2972 (w, *v*(CH)).

**$^1$H NMR** (500.1 MHz, 298.0 K, $CDCl_3$): δ / ppm = 1.05 (t, 3H, $^3J_{H,H}$ = 7.33 Hz, $CH_2CH_2CH_3$), 1.06 (t, 3H, $^3J_{H,H}$ = 7.33 Hz, $CH_2CH_2CH_3$), 1.33 (t, 3H, $^3J_{H,H}$ = 7.12 Hz, $OCH_2CH_3$), 1.87–1.99 (m, 4H, $CH_2CH_2CH_3$), 2.91 (s, 3H, $SCH_3$), 2.92 (s, 3H, $SCH_3$), 4.24 – 4.37 (m, 2H, $OCH_2CH_3$), 4.42 – 4.51 (m, 2H, $CH_2CH_2CH_3$), 4.70 – 4.78 (m, 2H, $CH_2CH_2CH_3$), 8.99 (dd, 1H, $^2J_{P,H}$ = 61.0 Hz, $^3J_{P,H}$ = 7.76 Hz, P*CH*).

**$^{13}$C{$^1$H} NMR** (125.8 MHz, 298.0 K, $CDCl_3$): δ / ppm = 11.2 (d, $^5J_{P,C}$ = 1.83 Hz, $CH_2CH_2CH_3$), 11.3 (d, $^5J_{P,C}$ = 1.83 Hz, $CH_2CH_2CH_3$), 14.1 (s, $OCH_2CH_3$), 19.1 (s, $SCH_3$), 19.1 (s, $SCH_3$), 22.5 (d, $^4J_{P,C}$ = 3.25 Hz, $CH_2CH_2CH_3$), 22.7 (d, $^4J_{P,C}$ = 3.25 Hz, $CH_2CH_2CH_3$), 55.9 (d, $^3J_{P,C}$ = 10.7 Hz, $CH_2CH_2CH_3$), 56.0 (d, $^3J_{P,C}$ = 10.5 Hz, $CH_2CH_2CH_3$), 63.2 (s, $OCH_2CH_3$), 120.3 (q, $^1J_{F,C}$ = 320.1 Hz, $CF_3$), 145.8 (dd, $^1J_{P,C}$ = 27.0 Hz, $^2J_{P,C}$ = 5.83 Hz, P*C*S), 146.0 (dd, $^1J_{P,C}$ = 27.5 Hz, $^2J_{P,C}$ = 5.86 Hz, P*C*S), 154.1 (dd, $^2J_{P,C}$ = 5.60 Hz, $^3J_{P,C}$ = 7.84 Hz, $CCO_2Et$), 159.9 (d, $^1J_{P,C}$ = 23.9 Hz, P*C*H), 163.7 (dd, $^1J_{P,C}$ = 34.8 Hz, $^2J_{P,C}$ = 3.87 Hz, $CCO_2Et$), 167.0 (dd, $^1J_{P,C}$ = 23.5 Hz, $^2J_{P,C}$ = 2.48 Hz, P*C*N), 167.9 (d, $^1J_{P,C}$ = 23.4 Hz, P*C*N), 177.9 (s, $CSCH_3$).

**$^{31}$P{$^1$H} NMR** (202.5 MHz, 298.0 K, $CDCl_3$): δ / ppm = −89.3 (d, $^3J_{P,P}$ = 25.40 Hz), −84.6 (d, $^3J_{P,P}$ = 25.40 Hz).

**$^{31}$P NMR** (202.5 MHz, 298.0 K, $CDCl_3$): δ / ppm = −89.3 (dd, $^3J_{P,H}$ = 7.76 Hz, $^3J_{P,P}$ = 25.4 Hz), −84.6 (dd, $^2J_{P,H}$ = 61.0 Hz, $^3J_{P,P}$ = 25.4 Hz).

### 5.6.49 Synthesis of 9,10-diethyl-3,7-di-*n*-propyl-4,8-etheno[1,4]diphosphinino[2,3-d:5,6-d']-2,6-bis(methylsulfanyl)-bis[1,3]thiazolium trifluoromethane sulfonate (29b)

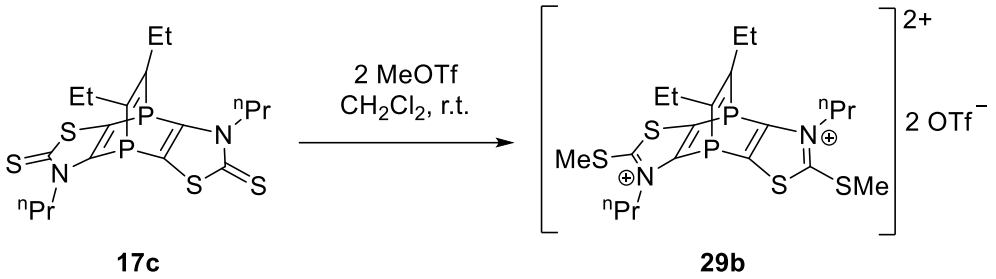


**17c** **29b**

In a 20 mL Schlenk vessel, 0.05 mL (0.457 mmol, 2.10 eq.) of methyl triflate were added to a suspension of 100 mg (0.218 mmol, 1.00 eq.) **17c** in 8 mL dichloromethane at ambient temperature. The mixture was stirred for 20 h before removing volatiles *in vacuo* ($10^{-2}$ mbar) at room temperature. After washing with *n*-pentane and drying *in vacuo* ($10^{-2}$ mbar), **29b** was obtained as a while solid.

**Reaction code:** TK-323 (07p5a032.22)

**Molecular formula:** $C_{22}H_{30}N_2P_2S_6O_6F_6$

**Molecular weight:** 786.78 g/mol

**Yield:** 134.0 mg (0.170 mmol, 78%)

**Melting point:** 71 °C

| | | | | |
|---|---|---|---|---|
| **Elemental analysis:** | calculated / % | C 35.67 | H 4.08 | N 1.89 |
| | found / % | C 32.25 | H 3.83 | N 3.11 |

**MS** (pos. ESI, selected data): m/z (%): 244.038 (100, z = 2) $[M–H]^{2+\bullet}$.
(neg. ESI, selected data): m/z (5): 148.9 (100) $[OTf]^{-\bullet}$.

**HRMS** (pos. ESI) for $C_{20}H_{30}N_2P_2S_4$ theor./exp. 244.0378/244.038 $[M−H]^{2+}$.

**IR** (ATR Diamond, selected data): $\tilde{\nu}$ / $cm^{-1}$ = 2878 (w, *v*(CH)), 2931 (m, *v*(CH)), 2970 (w, *v*(CH)).

**$^1$H NMR** (500.0 MHz, 298.0 K, $CDCl_3$): δ / ppm = 1.09 (t, 6H, $^3J_{H,H}$ = 7.370 Hz, $CH_2CH_2CH_3$), 1,13 (t, 6H, $^3J_{H,H}$ = 7.44 Hz, $CCH_2CH_3$), 1,92 (m, 4H, $CH_2CH_2CH_3$), 2,73 (m, 6H, $CCH_2CH_3$), 2,93 (s, 6H, $SCH_3$) 4,58 (m, 4H, $CH_2CH_2CH_3$).

**$^{13}C\{^1H\}$ NMR** (125.8 MHz, 298.0 K, $CDCl_3$): δ / ppm = 11.4 (s, $CH_2CH_2\mathit{CH_3}$), 13.4 (s, $CCH_2\mathit{CH_3}$), 19.2 (s, $S\mathit{CH_3}$) 22.7 (s, $CH_2\mathit{CH_2}CH_3$) 28.4 (d, $^2J_{P,C}$ = 44.1 Hz, $CC\mathit{H_2}CH_3$), 56.0 (dd, $^3J_{P,C}$ = 5.00 Hz, $^4J_{P,C}$ = 5.00 Hz, $\mathit{CH_2}CH_2CH_3$), 120.5 (q, $^1J_{P,F}$ = 320.4 Hz, $F_3\mathit{C}SO_3^-$), 146.4 (d, $^1J_{P,C}$ = 39.2 Hz, P*C*S), 156.4 (m, P*C*N), 177.4 (s, *C*-$SCH_3$).

**$^{31}P\{^1H\}$ NMR** (202.4 MHz, 298.0 K, $CDCl_3$): δ / ppm = −73.9 (s).

**$^{31}P$ NMR** (202.4 MHz, 298.0 K, $CDCl_3$): δ / ppm = −73.9 (m).

### 5.6.50 Synthesis of *rel*-(9*S*,10*R*)-9,10-bis(ethylcarboxy)-3,7-di-*n*-propyl-4,8-ethano[1,4]-diphosphinino[2,3-d:5,6-d']-2,6-bis(methylsulfanyl)-bis[1,3]thiazolium trifluoromethane sulfonate (29c)

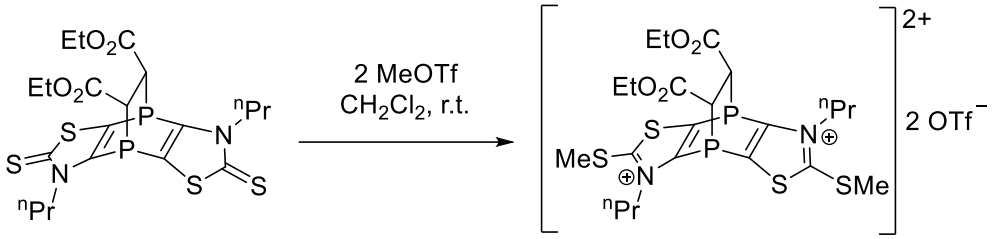


**18a** **29c**

In a 10 mL Schlenk vessel, 0.06 mL (0.548 mmol, 3.45 eq.) of methyl triflate were added to a solution of 87.2 mg (0.159 mmol, 1.00 eq.) of **18a** in 6 mL dichloromethane at ambient temperature. The mixture was stirred for 2 h and volatiles were removed *in vacuo* ($10^{-2}$ mbar) at ambient temperature. The residue was washed three times with 1.5 mL of *n*-pentane each and dried *in vacuo* ($10^{-2}$ mbar). **29c** was obtained as a white solid.

**Reaction code:** TK-128 (28p5a044.19)

**Molecular formula:** $C_{24}H_{32}F_6N_2O_{10}P_2S_6$

**Molecular weight:** 876.82 g/mol

**Yield:** 85.0 mg (0.097 mmol, 61%)

**Melting point:** 58 °C

| | | | | | |
|---|---|---|---|---|---|
| **Elemental analysis:** | calculated / % | C 32.88 | H 3.68 | N 3.19 | S 21.94 |
| | found / % | C 31.04 | H 3.66 | N 2.93 | S 21.35 |

**MS** (pos. ESI, selected data): m/z (%): 289.035 (100, z = 2) $[M]^{2+\bullet}$, 202.998 (78, z = 2) $[M-C_8H_{12}O_4]^{2+\bullet}$.

(neg. ESI, selected data): m/z (5): 149.2 (100) $[OTf]^{-\bullet}$.

**IR** (ATR Diamond, selected data): $\tilde{\nu}$ / cm$^{-1}$ = 1721 (s, *v*(CO)), 2881 (w, *v*(CH)), 2937 (w, *v*(CH)), 2976 (w, *v*(CH)).

**$^{1}$H NMR** (500.1 MHz, 298.0 K, $CDCl_3$): δ / ppm = 1.07 (t, 3H, $^{3}J_{H,H}$ = 7.50 Hz, $CH_2CH_2CH_3$), 1.09 (t, 3H, $^{3}J_{H,H}$ = 7.31 Hz, $CH_2CH_2CH_3$), 1.23 (t, 3H, $^{3}J_{H,H}$ = 7.00 Hz, $OCH_2CH_3$), 1.25 (t, 3H, $^{3}J_{H,H}$ = 7.00 Hz, $OCH_2CH_3$), 1.88–2.02 (m, 4H, $CH_2CH_2CH_3$), 2.93 (s, 3H, $SCH_3$), 2.95 (s, 3H, $SCH_3$), 3.97–4.06 (m, 2H, $OCH_2CH_3$), 4.06–4.15 (m, 2H, $OCH_2CH_3$), 4.18 (ddd, 1H, $^{2}J_{P,H}$ = 3.61 Hz, $^{3}J_{P,H}$ = 6.01 Hz, $^{3}J_{H,H}$ = 9.90 Hz, P*CH*), 4.40 (ddd, 1H, $^{2}J_{P,H}$ = 4.28 Hz, $^{3}J_{P,H}$ = 7.28 Hz, $^{3}J_{H,H}$ = 9.90 Hz, P*CH*), 4.42–4.50 (m, 2H, $CH_2CH_2CH_3$), 4.50–4.58 (m, 1H, $CH_2CH_2CH_3$), 4.60–4.70 (m, 1H, $CH_2CH_2CH_3$).

**$^{13}$C{$^{1}$H} NMR** (125.8 MHz, 298.0 K, $CDCl_3$): δ / ppm = 11.2 (s, $CH_2CH_2CH_3$), 11.3 (s, $CH_2CH_2CH_3$), 14.0 (s, $OCH_2CH_3$), 14.1 (s, $OCH_2CH_3$), 19.1 (s, $SCH_3$), 19.2 (s, $SCH_3$), 22.1 (d, $^{4}J_{P,C}$ = 3.51 Hz, $CH_2CH_2CH_3$), 22.2 (d, $^{4}J_{P,C}$ = 2.76 Hz, $CH_2CH_2CH_3$), 43.6 (dd, $^{1}J_{P,C}$ = 12.5 Hz, $^{2}J_{P,C}$ = 3.82 Hz, P*C*H), 44.3 (dd, $^{1}J_{P,C}$ = 12.6 Hz, $^{2}J_{P,C}$ = 3.06 Hz, P*C*H), 55.6 (d, $^{3}J_{P,C}$ = 9.33 Hz, $CH_2CH_2CH_3$), 55.8 (d, $^{3}J_{P,C}$ = 9.37 Hz, $CH_2CH_2CH_3$), 120.2 (q, $^{1}J_{F,C}$ = 319.9 Hz, $CF_3$), 139.7 (dd, $^{1}J_{P,C}$ = 24.6 Hz, $^{2}J_{P,C}$ = 8.20 Hz, P*C*S), 140.1 (dd, $^{1}J_{P,C}$ = 26.4 Hz, $^{2}J_{P,C}$ = 11.4 Hz, PC*S*), 157.8 (dd, d, $^{1}J_{P,C}$ = 16.5 Hz, $^{2}J_{P,C}$ = 6.54 Hz, P*C*N), 159.2 (dd, $^{1}J_{P,C}$ = 22.3 Hz, $^{2}J_{P,C}$ = 5.97 Hz, P*C*N), 170.2 (dd, $^{2}J_{P,C}$ = 1.50 Hz, $^{3}J_{P,C}$ = 8.58 Hz, C*C*O$_2$Et), 170.8 (dd, $^{2}J_{P,C}$ = 1.63 Hz, $^{3}J_{P,C}$ = 9.07 Hz, C*C*O$_2$Et), 179.7 (d, $^{3}J_{P,C}$ = 1.56 Hz, *C*SCH$_3$), 180.7 (d, $^{3}J_{P,C}$ = 1.86 Hz, *C*SCH$_3$).

**$^{31}$P{$^{1}$H} NMR** (202.5 MHz, 298.0 K, $CDCl_3$): δ / ppm =−75.4 (d, $^{3}J_{P,P}$ = 28.1 Hz), −75.2 (d, $^{3}J_{P,P}$ = 28.2 Hz).

**$^{31}$P NMR** (202.5 MHz, 298.0 K, $CDCl_3$): δ / ppm = −75.5–−75.1 (m).

### 5.6.51 Synthesis of 3,7-di-*n*-propyl-9-*n*-butyl-4,8-ethano[1,4]diphosphinino[2,3-d:5,6-d']-2,6-bis(methylsulfanyl)-bis[1,3]thiazolium trifluoromethane sulfonate (29d)

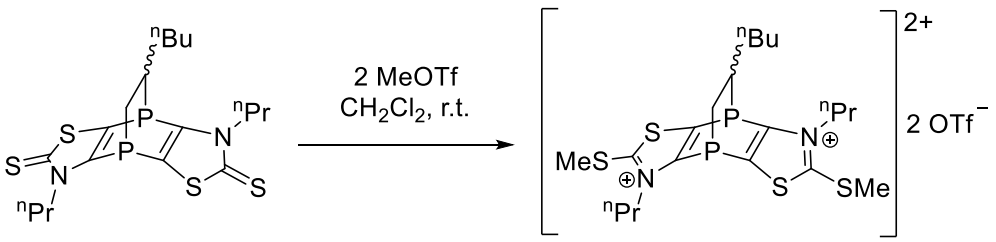


**18c** **29d**

In a 10 mL Schlenk vessel, 0.02 mL (0.183 mmol, 3.37 eq.) of methyl triflate were added to a solution of 25.0 mg (0.054 mmol, 1.00 eq.) of **18c** in 2 mL dichloromethane at 0 °C. The mixture was stirred for 23 h and volatiles were removed *in vacuo* ($10^{-2}$ mbar) at ambient

temperature. The residue was washed with 2 mL of *n*-pentane and dried *in vacuo* ($10^{-2}$ mbar). **29d** was obtained as a white solid.

**Reaction code:** TK-295 (45p5a022.21)

**Molecular formula:** $C_{22}H_{32}F_6N_2O_6P_2S_6$

**Molecular weight:** 788.80 g/mol

**Yield:** 85.0 mg (0.097 mmol, 61%)

**Melting point:** 87 °C

**MS** (pos. ESI, selected data): m/z (%): 245.045 (100, z = 2) $[M-H]^{2+\bullet}$.
(neg. ESI, selected data): m/z (5): 149.0 (100) $[OTf]^{-\bullet}$.

**HRMS** (pos. ESI) for $C_{20}H_{32}N_2P_2S_4$ theor./exp. 245.0456/245.0456 $[M-H]^{2+\bullet}$.

**IR** (ATR Diamond, selected data): $\tilde{\nu}$ / $cm^{-1}$ = 2927 (w, *ν*(CH)).

**$^1$H NMR** (700.4 MHz, 298.0 K, $CD_2Cl_2$): δ / ppm = 0.88–0.92 (m, 6H, $CH_2CH_2CH_2CH_3$), 1.04–1.11 (m, 12H, $CH_2CH_2CH_3$), 1.30–1.37 (m, 5H, $CH_2CH_2CH_2CH_3$), 1.38–1.46 (m, 2H, $CH_2CH_2CH_2CH_3$), 1.47–1.66 (m, 7H, $CH_2CH_2CH_2CH_3$ (4H), $CH_2CH_2CH_2CH_3$ (2H), $PCH_2$ (1H)), 1.71–1.76 (m, 1H, $PCH_2$), 1.82–2.00 (m, 7H, $CH_2CH_2CH_3$), 2.54–2.61 (m, 2H, PC*H*$^n$Bu, PC*H*$^n$Bu *isomer*), 2.64–2.70 (m, 1H, $PCH_2$), 2.78–2.85 (m, 1H, $PCH_2$), 2.94 (s, 1.7H, $SCH_3$ *isomer*), 2.95 (s, 3H, $SCH_3$), 2.97 (s, 3H $SCH_3$), 2.98 (s, 1.7H, $SCH_3$ *isomer*), 4.31–4.36 (m, 0.5H, $CH_2CH_2CH_3$), 4.44–4.56 (m, 3H, $CH_2CH_2CH_3$), 4.57–4.66 (m, 2H, $CH_2CH_2CH_3$), 4.68–4.74 (m, 0.5H, $CH_2CH_2CH_3$).

**$^{13}$C{$^1$H} NMR** (176.1 MHz, 298.0 K, $CD_2Cl_2$): δ / ppm = 11.4 (s, $CH_2CH_2CH_3$ *isomer*), 11.4 (m, $CH_2CH_2CH_3$), 14.1 (s, $CH_2CH_2CH_2CH_3$ *isomer*), 14.2 (s, $CH_2CH_2CH_2CH_3$), 19.6 (s, $SCH_3$, *isomer*)19.7 (s, $SCH_3$), 19.7 (s, $SCH_3$ *isomer*), 19.8 (s, $SCH_3$), 22.8 (s, $CH_2CH_2CH_3$), 22.9 (s, $CH_2CH_2CH_3$ *isomer*), 22.9 (d, $^4J_{P,C}$ = 3.40 Hz, $CH_2CH_2CH_3$, $CH_2CH_2CH_3$ *isomer*), 23.0 (d, $^4J_{P,C}$ = 3.31 Hz, $CH_2CH_2CH_2CH_3$ *isomer*), 23.0 ($^4J_{P,C}$ = 3.34 Hz, $CH_2CH_2CH_2CH_3$), 23.3 ($^4J_{P,C}$ = 2.87 Hz, $CH_2CH_2CH_2CH_3$), 26.0 (dd, $^1J_{P,C}$ = 13.7 Hz, $^2J_{P,C}$ = 2.71 Hz, $PCH_2$ isomer), 26.3 (dd, $^1J_{P,C}$ = 13.6 Hz, $^2J_{P,C}$ = 2.77 Hz, $PCH_2$), 31.4 (d, $^4J_{P,C}$ = 16.0 Hz, $CH_2CH_2CH_2CH_3$), 31.6 (d, $^4J_{P,C}$ = 15.5 Hz, $CH_2CH_2CH_2CH_3$ *isomer*), 34.8 (dm, $^4J_{P,C}$ = 10.7 Hz, P*C*H$^n$Bu), 34.9 (dd, $^4J_{P,C}$ = 17.6 Hz, $^4J_{P,C}$ = 1.04 Hz, $CH_2CH_2CH_2CH_3$), 35.2 (dd, $^4J_{P,C}$ = 10.9 Hz, $^4J_{P,C}$ = 1.01 Hz, P*C*H$^n$Bu *isomer*), 35.4 (dd, $^4J_{P,C}$ = 16.8 Hz, $^4J_{P,C}$ = 1.08 Hz, $CH_2CH_2CH_2CH_3$ *isomer*), 55.5 (d, $^3J_{P,C}$ = 11.3 Hz, $CH_2CH_2CH_3$ *isomer*), 55.7 (d, $^3J_{P,C}$ = 11.1 Hz, $CH_2CH_2CH_3$), 55.8 (d, $^3J_{P,C}$ = 10.9 Hz, $CH_2CH_2CH_3$), 55.8 (d, $^3J_{P,C}$ = 10.9 Hz, $CH_2CH_2CH_3$ *isomer*), 120.9 (q, $^1J_{F,C}$ = 315.8 Hz, $F_3CSO_3^-$), 139.0 (dd, $^1J_{P,C}$ = 36.9 Hz, $^2J_{P,C}$ = 6.28 Hz, P*C*S), 140.2 (dd, $^1J_{P,C}$ = 31.7 Hz, $^2J_{P,C}$ = 6.21 Hz, P*C*S), 142.3 (dd, $^1J_{P,C}$ = 30.5 Hz, $^2J_{P,C}$ = 6.82 Hz, P*C*S *isomer*),

142.5 (dd, $^{1}J_{P,C}$ = 31.8 Hz, $^{2}J_{P,C}$ = 5.90 Hz, P*C*S *isomer*), 158.9 (dd, $^{1}J_{P,C}$ = 30.6 Hz, $^{2}J_{P,C}$ = 3.98 Hz, P*C*N *isomer*), 159.6 (dd, $^{1}J_{P,C}$ = 24.2 Hz, $^{2}J_{P,C}$ = 3.96 Hz, P*C*N *isomer*), 161.5 (dd, $^{1}J_{P,C}$ = 24.3 Hz, $^{2}J_{P,C}$ = 3.67 Hz, P*C*N), 161.7 (dd, $^{1}J_{P,C}$ = 23.4 Hz, $^{2}J_{P,C}$ = 4.61 Hz, P*C*N), 179.8 (d, $^{3}J_{P,C}$ = 1.48 Hz, *C*-$SCH_3$ *isomer*), 180.0 (d, $^{3}J_{P,C}$ = 1.48 Hz, *C*-$SCH_3$), 180.1 (m, *C*-$SCH_3$ *isomer*), 180.2 (m, *C*-$SCH_3$).

**$^{31}P\{^{1}H\}$ NMR** (202.4 MHz, 298.0 K, $CD_2Cl_2$): δ / ppm = −74.6 (d, $^{3}J_{P,P}$ = 23.1 Hz, *P*$CH_2$, *isomer*), −74.3 (d, $^{3}J_{P,P}$ = 22.8 Hz, *P*$CH_2$), −71.8 (d, $^{3}J_{P,P}$ = 22.8 Hz, *P*$CH^{n}Bu$), −71.4 (d, $^{3}J_{P,P}$ = 23.1 Hz, *P*$CH^{n}Bu$, *isomer*).

**$^{31}P$ NMR** (202.4 MHz, 298.0 K, $CD_2Cl_2$): δ / ppm = −74.6 (dt, $^{3}J_{P,P}$ = 23.1 Hz, $^{2}J_{P,H}$ = 7.97 Hz, *P*$CH_2$, *isomer*), −74.3 (dt, $^{3}J_{P,P}$ = 22.8 Hz, $^{2}J_{P,H}$ = 8.10 Hz, *P*$CH_2$), −71.8 (m, *P*$CH^{n}Bu$), −71.4 (m, *P*$CH^{n}Bu$, *isomer*).

### 5.6.52 Attempted synthesis of 9,10-diethyl-3,7-di-*n*-propyl-4,8-etheno[1,4]diphosphinino[2,3-d:5,6-d']-bis[1,3]thiazolium trifluoromethane sulfonate (30)

*5.6.52.1 Sodium borohydride*

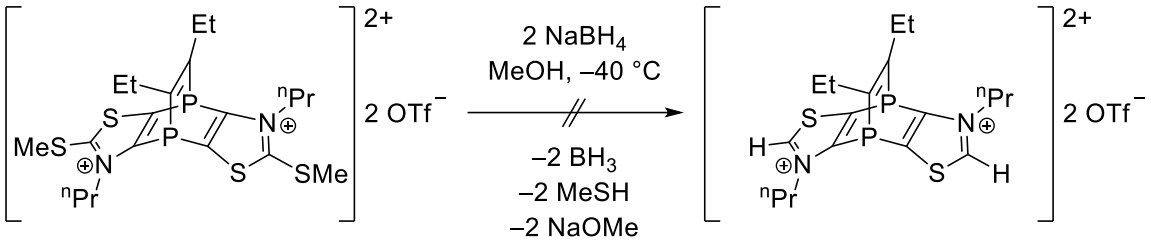


**29b** **30**

In a 20 mL Schlenk vessel, 24.0 mg (0.634 mmol, 4.56 eq.) of sodium borohydride were added to a solution of 102.7 mg (0.139 mmol, 1.00 eq.) of **29b** in 6 mL methanol at −40 °C. The mixture was stirred at −40 °C before removing volatiles *in vacuo* ($10^{-2}$ mbar) at the same temperature. The orange residue was extracted four times with 3 mL dichloromethane each, before washing with 3 mL *n*-pentane.

**Reaction code:** TK-353 (12m3b009.22, 12m3b021.22)

*5.6.52.2 Sodium borohydride, triethylammonium chloride*

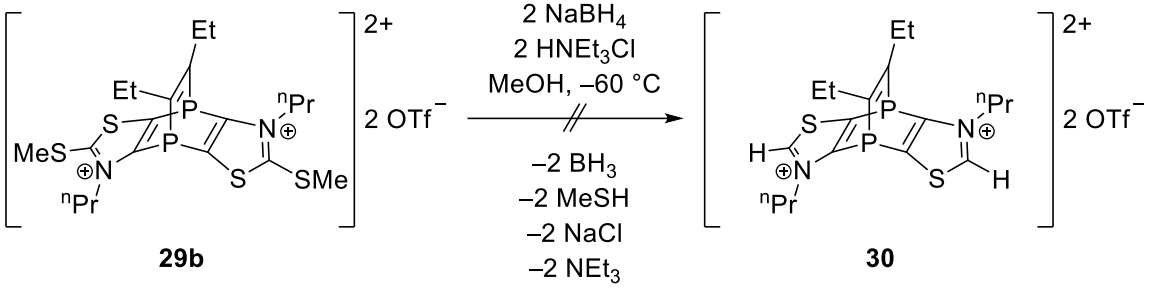


**29b** **30**

In a 20 mL Schlenk vessel, 32.1 mg (0.849 mmol, 5.98 eq.) of sodium borodydride were added to a solution of 105.3 mg (0.124 mmol, 1.00 eq.) of **29b** in 6 mL methanol at −60 °C. After stirring for 2 min, 81.7 mg (0.594 mmol, 4.18 eq.) of triethylammonium chloride were added and the mixture was stirred for another 3 h before removing volatiles *in vacuo* ($10^{-2}$ mbar) at ambient temperature. The orange residue was filtered through silica (Ø = 2 cm, 3 cm $SiO_2$) with 60 mL THF to remove the salt and volatiles were removed *in vacuo* ($10^{-2}$ mbar) again. After extracting five times with 5 mL dichloromethane each, volatiles were removed and the residue was dried *in vacuo* ($10^{-2}$ mbar).

**Reaction code:** TK-355 (12t4a009.22, 13m3a014.22)

*5.6.52.3 L-selectride*

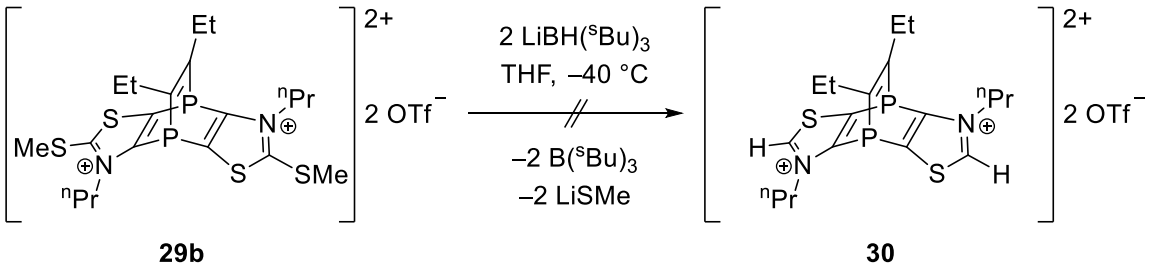


**29b** **30**

In a 10 mL Schlenk vessel, 0.07 mL (0.07 mmol, 2.33 eq.) of a 1 M solution of L-selectride in THF were added to a suspension of 22.3 mg (0.03 mmol, 1.00 eq.) **29b** in 2.5 mL THF at −40 °C. After an immediate colour change from colourless to red and then yellow, the mixture was stirred for 2.5 h while slowly warming up to room temperature.

**Reaction code:** TK-332 (09m3a002.22, 09m3a007.22)

*5.6.52.4 L-selectride, triethylammonium chloride*

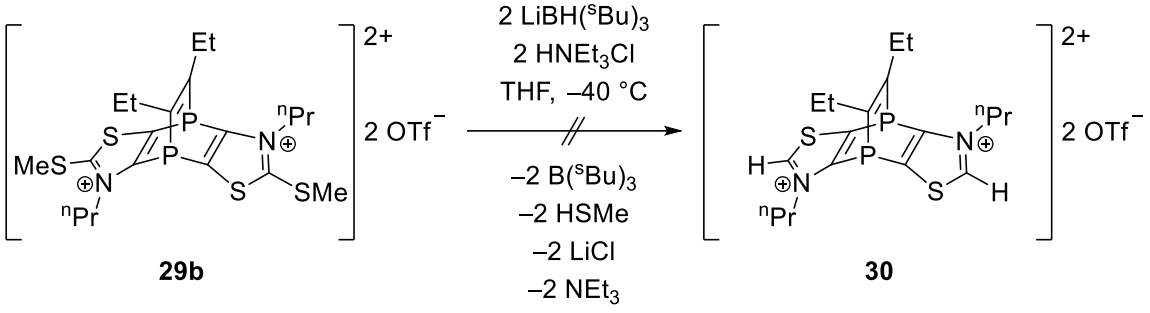


In a 10 mL Schlenk vessel, 0.13 mL (0.130 mmol, 2.13 eq.) of a 1 M solution of L-selectride in THF were added to a suspension of 45.0 mg (0.061 mmol, 1.00 eq.) **29b** in 2.5 mL THF at −40 °C. After stirring for 30 s, 17.0 mg (0.124 mmol, 2.02 eq.) of triethylammonium chloride were added and the mixture was stirred for 1.5 h while slowly warming up to room temperature.

**Reaction code:** TK-372 (19m3a039.22)

*5.6.52.5 L-selectride, triflic acid*

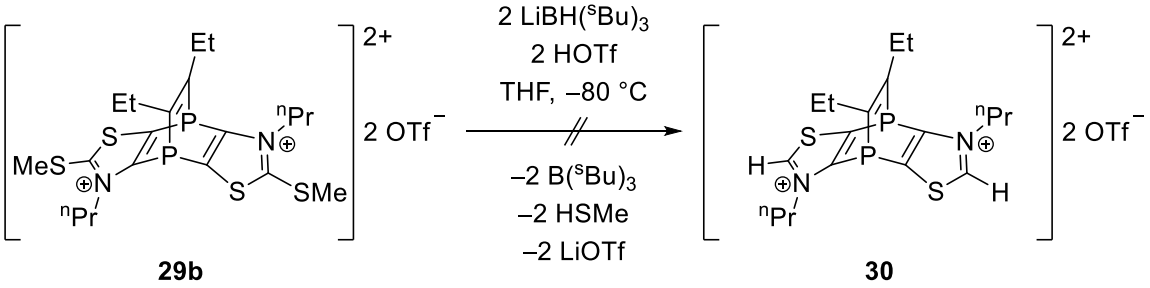


In a 10 mL Schlenk vessel, 0.06 mL (0.06 mmol, 2.31 eq.) of a 1 M solution of L-selectride in THF were added to a suspension of 18.9 mg (0.026 mmol, 1.00 eq.) **29b** in 2.5 mL THF at −80 °C. After stirring for 8 h while slowly warming up the mixture was again cooled to −80 °C and 0.13 mL (0.042 mmol, 2.03 eq.) of a 0.3245 M solution of triflic acid in THF were added at this temperature. The reaction was stirred for a further 15 min at −80 °C.

**Reaction code:** TK-338 (10m3a026.22, 10m3a035.22, 10m3a047.22)

*5.6.52.6 L-selectride, methanol*

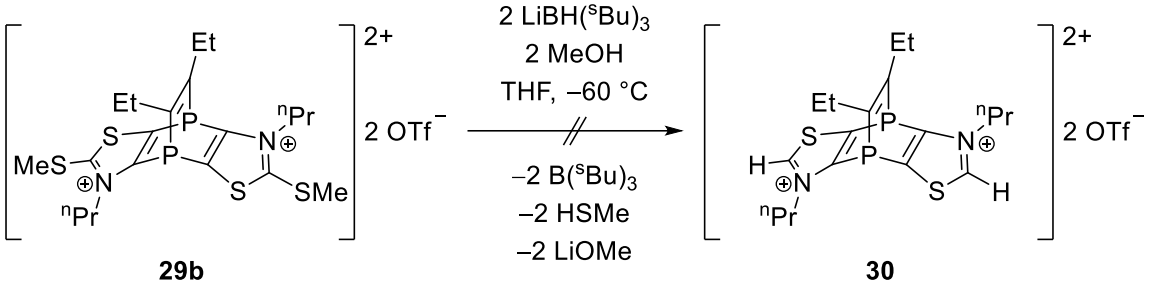


**29b** **30**

In a 10 mL Schlenk vessel, 0.10 mL (0.100 mmol, 2.04 eq.) of a 1 M solution of L-selectride in THF were added to a suspension of 36.6 mg (0.049 mmol, 1.00 eq.) **29b** in 2.5 mL THF at −60 °C. The mixture was stirred for 15 min before adding one drop of methanol and stirring for a further 1.5 h.

**Reaction code:** TK-351 (12m3a027.22)

## 5.6.53 Attempted synthesis of 9,10-diethyl-3,7-di-*n*-propyl-4,8-etheno[1,4]diphosphinino[2,3-d:5,6-d']bis[1,3]thiazole-2,6-diylidene from 29b (26b)

*5.6.53.1 Potassium*

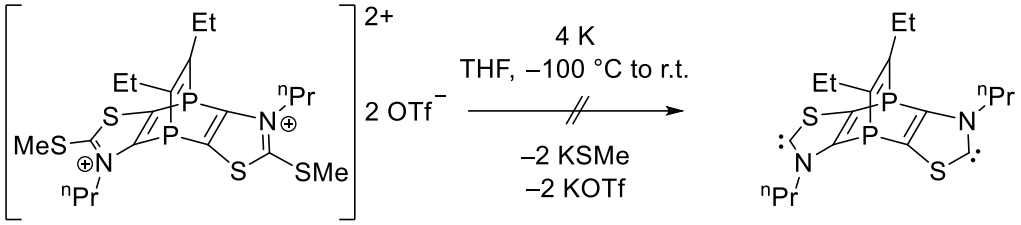


**29b** **26b**

In a 10 mL Schlenk vessel, 34.5 mg (0.047 mmol, 1.00 eq.) **29b** and 1.5 mL THF were added to a mirror of 7.6 mg (0.194 mmol, 4.12 eq.) of potassium at −196 °C. The mixture was warmed up to −100 °C and then stirred for 18 h while slowly warming up to room temperature.

**Reaction code:** TK-434 (48t4c002.22)

*5.6.53.2 Potassium graphite*

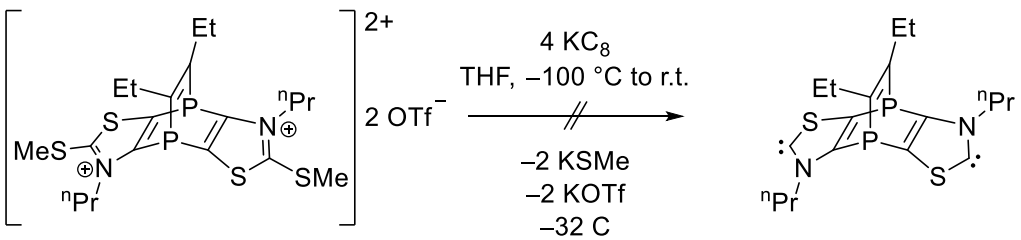


**29b** **26b**

In a 10 mL Schlenk vessel, 1.5 mL of THF were added to a mixture of 17.8 mg (0.024 mmol, 1.00 eq.) **29b** and 13.7 mg (0.101 mmol, 4.12 eq.) of potassium graphite at −196 °C. The mixture was warmed up to −100 °C and then stirred for 18 h while slowly warming up to room temperature.

**Reaction code:** TK-433 (48t4c004.22, 48m3a059.22)

### 5.6.54 Synthesis of 3-*n*-propylthiazolium iodide (35)

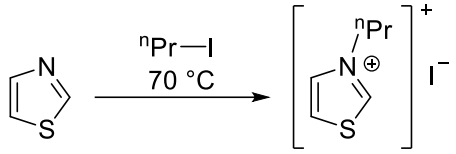


**34** **35**

In a 10 mL Schlenk vessel, 3.3 mL (33.97 mmol, 1.20 eq.) of 1-iodopropane was added to 2.0 mL (28.20 mmol, 1.00 eq.) of thiazole and heated to 70 °C for 18 h. The resulting white solid was washed three times with 6 mL toluene each and dried *in vacuo* ($10^{-2}$ mbar).

**Reaction code:** TK-389 (36m3a030.22)

**Yield:** 6.1 g (22.68 mmol, 80%)

**$^1$H NMR** (300.1 MHz, 299.5 K, $CD_2Cl_2$): δ / ppm = 1.03 (t, 3H, $^3J_{H,H}$ = 7.39 Hz, $CH_2CH_2CH_3$), 2.01–2.16 (m, 2H, $CH_2CH_2CH_3$), 4.73–4.81 (m, 2H, $CH_2CH_2CH_3$), 8.21 (dd, 1H, $^3J_{H,H}$ = 3.13 Hz, $^4J_{H,H}$ = 3.13 Hz, $C^4H$), 8.29, (dd, 1H, $^3J_{H,H}$ = 3.74 Hz, $^4J_{H,H}$ = 1.41 Hz, $C^5H$), 11.02 (d, 1H, $^4J_{H,H}$ = 1.75 Hz, $C^2H$).

### 5.6.55 Attempted synthesis of 2,3-dihydro-2-[3'-(*n*-propyl)-2'(3'*H*)-thiazolylidene]-3-(*n*-propyl)-thiazole (36)

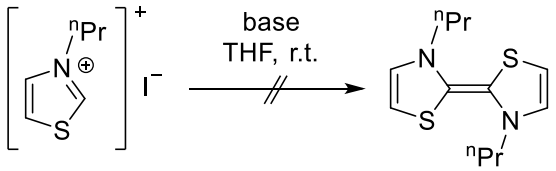


**35** **36**

*5.6.55.1 Potassium Hydride*

In a 30 mL Schlenk vessel, 211.7 mg (5.279 mmol, 1.01 eq.) of potassium hydride were slowly added to a suspension of 1.329 g (5.209 mmol, 1.00 eq.) of **35** in 15 mL THF. The mixture was stirred at ambient temperature for 2 h.

**Reaction code:** TK-387 (32m3b047.22)

*5.6.55.2 Triethylamine*

In a 30 mL Schlenk vessel, 0.65 mL (4.664 mmol, 4.75 eq.) of triethylamine were added to a suspension of 364.0 mg (0.982 mmol, 1.00 eq.) of **35** in 15 mL THF. The mixture was stirred for 20 h at ambient temperature.

**Reaction code:** TK-394 (37t4a065.22)

*5.6.55.3 Potassium t-butoxide*

In a 30 mL Schlenk vessel, three drops of potassium *t*-butoxide were added to a suspension of 364.0 mg (0.982 mmol, 1.00 eq.) of **35** in 15 mL THF. The mixture was stirred for 2 h at ambient temperature.

**Reaction code:** TK-394 (38m3a020.22)

*5.6.55.4 1,8-Diazabicyclo(5.4.0)undec-7-ene*

In a 10 mL Schlenk vessel, 0.07 mL (0.570 mmol, 1.11 eq.) of DBU were added to a suspension of 115.6 mg (0.513 mmol, 1.00 eq.) of **35** in 2 mL THF. The mixture was stirred for 30 min at ambient temperature.

**Reaction code:** TK-400 (38m3a015.22)

### 5.6.56 Attempted synthesis of 5-bis(diethylamino)phosphanyl-1,3-thiazole (39)

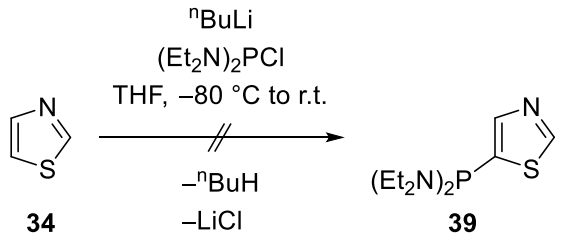


In a 20 mL Schlenk vessel, 1.7 mL (2.72 mmol, 1.13 eq.) of a 1.6 M solution of $^{n}$BuLi in *n*-hexane were added to a solution of 0.17 mL (2.40 mmol, 1.00 eq.) **34** in 3 mL THF at −80 °C. The mixture was stirred for 2 h at a temperature below −50 °C before the addition of 0.52 mL (2.62 mmol, 1.09 eq.) of $(Et_2N)_2PCl$ at −50 °C. The mixture was stirred for further 1 h while slowly warming up to ambient temperature and another 4 d at this temperature.

**Reaction code:** TK-406 (39m3b002.22, 40m3a007.22, 40m3a013.22)

### 5.6.57 Synthesis of 5-trimethylsilyl-1,3-thiazole (42a)[140]

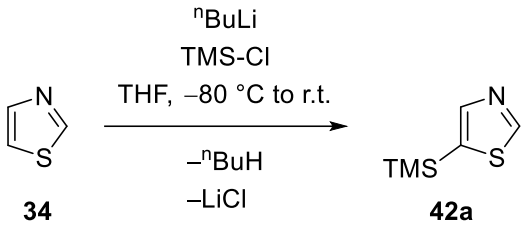


**34** **42a**

In a 250 mL flask, 20 mL (32 mmol, 1.14 eq.) of a 1.6 M solution of $^{n}$BuLi in *n*-hexane were added to 2 mL (28.19 mmol, 1.00 eq.) of **34** in 40 mL THF at −70 °C. The mixture was stirred for 1 h before cooling to −80 °C and adding a solution of 4.0 mL (31.44 mmol, 1.12 eq.) of TMS-Cl in 5 mL THF. After stirring the reaction mixture for 18 h while slowly warming up, the reaction was quenched using 100 mL saturated sodium carbonate solution. The aqueous phase was extracted three times with 80 mL ethyl acetate each, before washing three times with 20 mL water each and drying the organic phases over magnesium sulfate for 1 h. The solution was filtered and volatiles were evaporated *in vacuo* (20 mbar).

**Reaction code:** TK-414 (42m3b018.22)

**Yield:** 3.00 g (19.07 mmol, 68%)

**$^{1}$H NMR** (300.1 MHz, 298.0 K, $CDCl_3$): δ / ppm = 0.37 (s, 9H, $Si(CH_3)_3$), 7.97 (s, 1H, $C^4H$), 9.04 (s, 1H, $C^2H$).

### 5.6.58 Attempted synthesis of 5-bis(diethylamino)phosphanyl-1,3-thiazole (39)

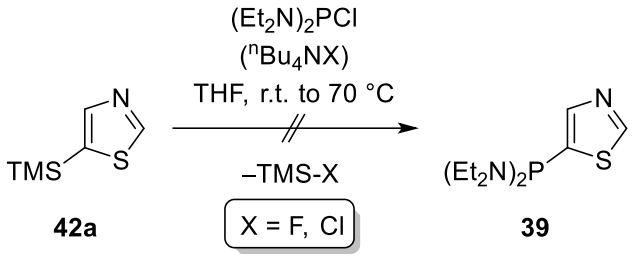


**42a** **39**

*5.6.58.1 Chlorobis(diethylamino)phosphane*

In a 10 mL Schlenk vessel, 0.26 mL (1.31 mmol, 1.12 eq.) $(Et_2N)_2PCl$ were added to a solution of 184 mg (1.17 mmol, 1.00 eq.) of **42a** in 3 mL THF. The mixture was heated to 70 °C and stirred for 8 d.

**Reaction code:** TK-417 (43t4b026.22, 43m3a037.22, 44m3a035.22)
TK-415 (42m3a029.22, 42m3a037.22, 43m3a004.22, 43t4c024.22)

*5.6.58.2 Chlorobis(diethylamino)phosphane, tetra-n-butylammonium chloride*

In a 10 mL Schlenk vessel, 0.2 mL (1.01 mmol, 1.11 eq.) $(Et_2N)_2PCl$ were added to a solution of 142 mg (0.90 mmol, 1.00 eq.) **42a** in 3 mL THF. After stirring at ambient temperature for 30 min, 247 mg (0.91 mmol, 1.01 eq.) of $^nBu_4NCl$ were added and the mixture was stirred for 45 min at ambient temperature before heating to 80 °C for 24 h.

**Reaction code:** TK-424 (44t4b002.22, 45m3a003.22)

*5.6.58.3 Chlorobis(diethylamino)phosphane, tetra-n-butylammonium fluoride*

In a 10 mL Schlenk vessel, 0.23 mL (1.16 mmol, 1.12 eq.) $(Et_2N)_2PCl$ were added to a solution of 162.5 mg (1.03 mmol, 1.00 eq.) of **42a** in 3 mL THF. After stirring at ambient temperature for 1 h, 1.05 mL (1.05 mmol, 1.02 eq.) of a 1 M solution of $^nBu_4NF$ in THF were added and the mixture was stirred for 1 h at ambient temperature before heating to 80 °C for 23 h.

**Reaction code:** TK-423 (44t4a060.22, 45p5a001.22)

### 5.6.59 Synthesis of 3-*n*-propyl-5-trimethylsilyl-thiazolium iodide (44)

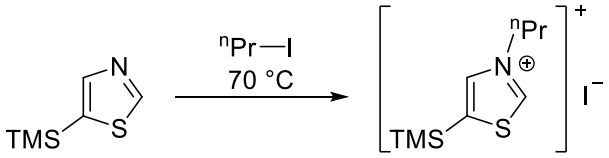


**42a** **44**

In a 10 mL Schlenk vessel, 0.17 mL (1.74 mmol, 1.20 eq.) of 1-iodopropane were added to 227.5 mg (1.45 mmol, 1.00 eq.) **42a**. The mixture was heated to 70 °C for 21 h before removing volatiles *in vacuo* ($10^{-2}$ mbar). The residue was washed twice with 4 mL diethyl ether each and dried *in vacuo* ($10^{-2}$ mbar).

**Reaction code:** TK-426 (45p5a055.22)

**$^1$H NMR** (500.0 MHz, 298.0 K, DMSO-d6): δ / ppm = 0.41 (s, 9H, $Si(CH_3)_3$), 0.87 (t, 3H, $^3J_{H,H}$ = 7.43 Hz, $CH_2CH_2CH_3$), 1.92 (m, 2H, $CH_2CH_2CH_3$), 4.53 (m, 2H, $CH_2CH_2CH_3$), 8.70 (d, 1H, $^4J_{H,H}$ = 1.17 Hz, $C^4H$), 10.42 (d, 1H, $^4J_{H,H}$ = 1.14 Hz, $C^2H$).

### 5.6.60 Attempted synthesis of 2,3-dihydro-2-[3'-(*n*-propyl)-5'-trimethylsilyl-2'(3'*H*)-thiazolylidene]-3-(*n*-propyl)-5-trimethylsilyl-thiazole (45)

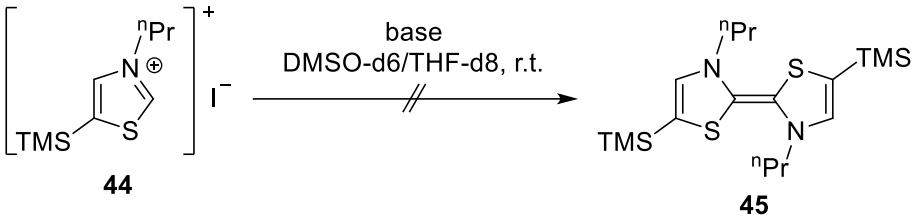


**44** **45**

*5.6.60.1 Triethylamine*

In a J Young NMR tube, 2 drops of triethylamine were added to a solution of **44** in DMSO-d6. The mixture was stirred for 5 h at ambient temperature.

**Reaction code:** TK-428 (45m3b051.22)

*5.6.60.2 Potassium hydride*

In a J Young NMR tube, 2.3 mg (0.057 mmol, 1.11 eq.) of KH were added to a solution of 16 mg (0.052 mmol, 1.00 eq.) of **44** in 0.5 mL THF-d8. The mixture was stirred for 3 d at ambient temperature.

**Reaction code:** TK-429 (45t4a037.22, 46m3a017.22)

### 5.6.61 Attempted synthesis of 5-bis(diethylamino)phosphanyl-3-*n*-propyl-thiazolium iodide (46)

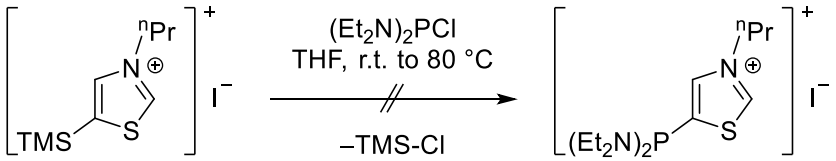


**44** **46**

In a 10 mL Schlenk vessel, 0.03 mL (0.151 mmol, 1.41 eq.) of $(Et_2N)_2PCl$ were added to a solution of 41.2 mg (0.107 mmol, 1.00 eq.) of **44** in 2.5 mL THF. The mixture stirred at ambient temperature for 15 h and then heated to 80 °C and stirred for 24 h before 1 drop of $^n$BuLi was added and the reaction was stirred for a further 3.5 h.

**Reaction code:** TK-438 (50t4c023.22, 50m3c006.22, 50m3b019.22, 50m3b022.22, 50m3b046.22)

# 6 REFERENCES


1 J. A. Tully, *The devil's milk*. *A social history of rubber*, Monthly Review Press, New York, **2011**.

2 E. P. Wilkinson, *Chinese history*. *A new manual,* Vol. 3, Harvard University Asia Center, Cambridge, Mass., **2013**.

3 E. J. Holmyard, *Alchemy,* Vol. 1, Dover Publications, New York, **1990**.

4 F. Krafft, *Angew. Chem. Int. Ed.* **1969**, *8*, 660–671; *Angew. Chem.* **1969**, *81*, 634–645.

5 a) A. Hantzsch, J. H. Weber, *Ber. Dtsch. Chem. Ges.* **1887**, *20*, 3118–3132; b) O. Widman, *J. Prakt. Chem.* **1888**, *38*, 185–201.

6 a) in *The IUPAC Compendium of Chemical Terminology* (Ed.: V. Gold), International Union of Pure and Applied Chemistry (IUPAC), Research Triangle Park, NC, **2019**; b) H. A. Favre, W. H. Powell, *Nomenclature of Organic Chemistry*, The Royal Society of Chemistry, **2013**.

7 S. De, A. Kumar S K, S. K. Shah, S. Kazi, N. Sarkar, S. Banerjee, S. Dey, *RSC Adv.* **2022**, *12*, 15385–15406.

8 S. Maity, A. Bera, A. Bhattacharjya, P. Maity, *Org. Biomol. Chem.* **2023**, *21*, 5671–5690.

9 B. Turovska, I. Goba, A. Lielpetere, V. Glezer, *J. Solid State Electr.* **2023**, *27*, 1717–1729.

10 M. Yoshifuji, S. Ito, *Science of Synthesis* **2004**, *16*, 1399.

11 F. A. Carey, *Advanced organic chemistry,* Vol. 5, Springer, New York, NY, **2008**.

12 J. A. Joule, K. Mills, *Heterocyclic chemistry,* Vol. 5, Wiley, Chichester, West Sussex, **2010**.

13 a) J.-Y. Zhang, Y. Ma, A.-L. Cheng, Q. Yue, Q. Sun, E.-Q. Gao, *Dalton Trans.* **2008**, 2061–2066; b) R. K. Ujjinamatada, P. Phatak, A. M. Burger, R. S. Hosmane, *J. Med. Chem.* **2008**, *51*, 694–698; c) I. Ortín, J. F. González, E. d. La Cuesta, C. Manguan-García, R. Perona, C. Avendaño, *Bioorg. Med. Chem.* **2008**, *16*, 9065–9078; d) B. P. Karsten, R. A. J. Janssen, *Org. Lett.* **2008**, *10*, 3513–3516; e) A. Busch, A. Turck, N. Plé, *J. Heterocycl. Chem.* **2008**, *45*, 417–424.

14 S. G. Patra, N. Mandal, *Int. J. Quantum Chem.* **2020**, *120*.

15 A. Kekulé, *Bull. Soc. chim. Paris* **1865**, 98–110.

16 a) E. Hückel, *Z. Physik* **1931**, *70*, 204–286; b) E. Hückel, *Z. Physik* **1931**, *72*, 310–337; c) E. Hückel, *Z. Physik* **1933**, *83*, 632–668.

17 G. Märkl, *Chem. Unserer Zeit* **1982**, *16*, 139–148.

18 P. R. Schleyer, *Chem. Rev.* **2001**, *101*, 1115–1118.

19 a) M. Solà, A. I. Boldyrev, M. K. Cyrański, T. M. Krygowski, G. Merino, *Aromaticity and Antiaromaticity*, Wiley, **2022**; b) M. K. Cyrański, *Chem. Rev.* **2005**, *105*, 3773–3811.

20 M. K. Cyrański, P. v. R. Schleyer, T. M. Krygowski, H. Jiao, G. Hohlneicher, *Tetrahedron* **2003**, *59*, 1657–1665.

21 a) T. M. Krygowski, *J. Chem. Inf. Comput. Sci.* **1993**, *33*, 70–78; b) E. M. Arpa, B. Durbeej, *Phys. Chem. Chem. Phys.* **2023**, *25*, 16763–16771.

22 A. D. Becke, K. E. Edgecombe, *J. Chem. Phys.* **1990**, *92*, 5397–5403.

23 P. v. R. Schleyer, C. Maerker, A. Dransfeld, H. Jiao, N. J. R. van Eikema Hommes, *J. Am. Chem. Soc.* **1996**, *118*, 6317–6318.

24 a) G. Merino, M. Solà, I. Fernández, C. Foroutan-Nejad, P. Lazzeretti, G. Frenking, H. L. Anderson, D. Sundholm, F. P. Cossío, M. A. Petrukhina et al., *Chem. Sci.* **2023**, *101*, 1115; b) J. Pedersen, K. V. Mikkelsen, *RSC Adv.* **2022**, *12*, 2830–2842.

25 a) Z. Chen, C. S. Wannere, C. Corminboeuf, R. Puchta, P. v. R. Schleyer, *Chem. Rev.* **2005**, *105*, 3842–3888; b) L. Nyulászi, *Chem. Rev.* **2001**, *101*, 1229–1246.

26 I. Alkorta, J. Elguero, *Magn. Reson. Chem.* **2010**, *48*, S32-S37.

27 A. Stanger, *J. Org. Chem.* **2006**, *71*, 883–893.

28 A. Stanger, *J. Org. Chem.* **2010**, *75*, 2281–2288.

29 A. Stanger, *J. Phys. Chem. A* **2019**, *123*, 3922–3927.

30 A. Stanger, *Eur. J. Org. Chem.* **2020**, *2020*, 3120–3127.

31 a) R. Gershoni-Poranne, A. Stanger, *Chem. Eur. J.* **2014**, *20*, 5673–5688; b) A. Stanger, *Org. Lett.* **2022**, *24*, 1243–1246.

32 A. Stanger, *ChemPhysChem* **2023**, *24*, e202300080.

33 J. B. Dumas, E. Peligot, *Ann. Chim. Phys.* **1835**, *58*, 5–74.

34 H.-W. Wanzlick, E. Schikora, *Angew. Chem.* **1960**, *72*, 494.

35 A. Igau, H. Grutzmacher, A. Baceiredo, G. Bertrand, *J. Am. Chem. Soc.* **1988**, *110*, 6463–6466.

36 A. J. Arduengo, R. L. Harlow, M. Kline, *J. Am. Chem. Soc.* **1991**, *113*, 361–363.

37 P. de Frémont, N. Marion, S. P. Nolan, *Coord. Chem. Rev.* **2009**, *253*, 862–892.

38 W. A. Herrmann, *Angew. Chem.* **2002**, *114*, 1342; *Angew. Chem. Int. Ed.* **2002**, *41*, 1290–1309.

39 A. J. Arduengo, R. Krafczyk, R. Schmutzler, H. A. Craig, J. R. Goerlich, W. J. Marshall, M. Unverzagt, *Tetrahedron* **1999**, *55*, 14523–14534.

40 A. J. Arduengo, J. R. Goerlich, W. J. Marshall, *J. Am. Chem. Soc.* **1995**, *117*, 11027–11028.

41 L. Jafarpour, E. D. Stevens, S. P. Nolan, *J. Organomet. Chem.* **2000**, *606*, 49–54.

42 T. L. Amyes, S. T. Diver, J. P. Richard, F. M. Rivas, K. Toth, *J. Am. Chem. Soc.* **2004**, *126*, 4366–4374.

43 A. W. Waltman, T. Ritter, R. H. Grubbs, *Organometallics* **2006**, *25*, 4238–4239.

44 N. Kuhn, T. Kratz, *Synthesis* **1993**, *1993*, 561–562.

45 F. E. Hahn, L. Wittenbecher, R. Boese, D. Bläser, *Chem. Eur. J.* **1999**, *5*, 1931–1935.

46 T. Chu, S. F. Vyboishchikov, B. Gabidullin, G. I. Nikonov, *Angew. Chem. Int. Ed.* **2016**, *55*, 13306–13311.

47 M. N. Hopkinson, F. Glorius in *N-heterocyclic carbenes in organocatalysis*. *With a foreword by Ronald Breslow* (Eds.: A. T. Biju, R. Breslow), Wiley-VCH, Weinheim, **2019**, pp. 1–35.

48 H. V. Huynh, *Chem. Rev.* **2018**, *118*, 9457–9492.

49 M. Melaimi, R. Jazzar, M. Soleilhavoup, G. Bertrand, *Angew. Chem.* **2017**, *129*, 10180–10203; *Angew. Chem. Int. Ed.* **2017**, *56*, 10046–10068.

50 S. Gründemann, A. Kovacevic, M. Albrecht, J. W. Faller, R. H. Crabtree, *Chem. Commun.* **2001**, 2274–2275.

51 E. Aldeco-Perez, A. J. Rosenthal, B. Donnadieu, P. Parameswaran, G. Frenking, G. Bertrand, *Science (New York, N.Y.)* **2009**, *326*, 556–559.

52 a) W. A. Herrmann, C. Köcher, L. J. Gooßen, G. R. J. Artus, *Chem. Eur. J.* **1996**, *2*, 1627–1636; b) T. Chen, X.-G. Liu, M. Shi, *Tetrahedron* **2007**, *63*, 4874–4880; c) A. A. Danopoulos, S. Winston, W. B. Motherwell, *Chem. Commun.* **2002**, 1376–1377; d) M. Poyatos, J. A. Mata, E. Falomir, R. H. Crabtree, E. Peris, *Organometallics* **2003**, *22*, 1110–1114; e) F. E. Hahn, M. C. Jahnke, V. Gomez-Benitez, D. Morales-Morales, T. Pape, *Organometallics* **2005**, *24*, 6458–6463.

53 D. M. Khramov, A. J. Boydston, C. W. Bielawski, *Angew. Chem. Int. Ed.* **2006**, *45*, 6186–6189.

54 J. W. Kamplain, C. W. Bielawski, *Chem. Commun.* **2006**, 1727–1729.

55 A. Prades, E. Peris, M. Alcarazo, *Organometallics* **2012**, *31*, 4623–4626.

56 H. Valdés, M. Poyatos, E. Peris, *Organometallics* **2015**, *34*, 1725–1729.

57 A. G. Tennyson, R. J. Ono, T. W. Hudnall, D. M. Khramov, J. A. V. Er, J. W. Kamplain, V. M. Lynch, J. L. Sessler, C. W. Bielawski, *Chem. Eur. J.* **2010**, *16*, 304–315.

58 S. Gonell, E. Peris, M. Poyatos, *Eur. J. Inorg. Chem.* **2019**, *2019*, 3776–3781.

59 N. R. Naz, G. Schnakenburg, Z. Kelemen, D. Gál, L. Nyulászi, R. T. Boeré, R. Streubel, *Dalton Trans.* **2021**, *50*, 689–695.

60 N. R. Naz, G. Schnakenburg, A. Mikeházi, Z. Kelemen, L. Nyulaszi, R. Boeré, R. Streubel, *Chem. Commun.* **2020**, 2646–2649.

61 S. J. Cristol, D. C. Lewis, *J. Am. Chem. Soc.* **1967**, *89*, 1476–1483.

62 M. Poyatos, E. Peris, *Dalton Trans.* **2021**, *50*, 12748–12763.

63 D. Tapu, Z. McCarty, C. McMillen, *Chem. Commun.* **2014**, *50*, 4725–4728.

64 T. Terschüren, G. Schnakenburg, R. Streubel, *Dalton Trans.* **2024**, *53*, 5043–5050.

65 A. J. Arduengo, J. R. Goerlich, W. J. Marshall, *Liebigs Ann./Recl.* **1997**, *1997*, 365–374.

66 D. Guérin, R. Carlier, M. Guerro, D. Lorcy, *Tetrahedron* **2003**, *59*, 5273–5278.

67 a) D. C. Graham, K. J. Cavell, B. F. Yates, *J. Phys. Org. Chem.* **2005**, *18*, 298–309; b) Z. Kelemen, O. Hollóczki, J. Oláh, L. Nyulászi, *RSC Adv.* **2013**, *3*, 7970; c) H. Prinzbach, H. Berger, A. Lüttringhaus, *Angew. Chem.* **1965**, *77*, 453–454.

68 Z. Časar, D. Lorcy, I. Leban, A. Majcen-Le Maréchal, *Acta Chim. Slov.* **2002**, *49*, 871–883.

69 I. Piel, M. D. Pawelczyk, K. Hirano, R. Fröhlich, F. Glorius, *Eur. J. Org. Chem.* **2011**, *2011*, 5475–5484.

70 J. Pesch, K. Harms, T. Bach, *Justus Liebigs Ann. Chem.* **2004**, *2004*, 2025–2035.

71 J. F. Binder, A. M. Corrente, C. L. B. Macdonald, *Dalton Trans.* **2016**, *45*, 2138–2147.

72 H.-W. Wanzlick, H.-J. Kleiner, I. Lasch, H. U. Füldner, H. Steinmaus, *Liebigs Ann. Chem.* **1967**, *708*, 155–169.

73 S. Eid, M. Guerro, T. Roisnel, D. Lorcy, *Org. Lett.* **2006**, *8*, 2377–2380.

74 G. Märkl, *Angew. Chem.* **1966**, *78*, 907–908; *Angew. Chem. Int. Ed.* **1966**, *5*, 846–847.

75 A. J. Ashe, *J. Am. Chem. Soc.* **1971**, *93*, 3293–3295.

76 C. Müller, L. E. E. Broeckx, I. de Krom, J. J. M. Weemers, *Eur. J. Inorg. Chem.* **2013**, *2013*, 187–202.

77 M. H. Habicht, F. Wossidlo, M. Weber, C. Müller, *Chem. Eur. J.* **2016**, *22*, 12877–12883.

78 S. Holand, L. Ricard, F. Mathey, *J. Org. Chem.* **1991**, *56*, 4031–4035.

79 A. Loibl, I. de Krom, E. A. Pidko, M. Weber, J. Wiecko, C. Müller, *Chem. Commun.* **2014**, *50*, 8842–8844.

80 P. Le Floch, F. Mathey, *Coord. Chem. Rev.* **1998**, *178-180*, 771–791.

81 F. Mathey, P. Le Floch, *Science of Synthesis* **2005**, *15*, 1097–1156.

82 R. Streubel, *Science of Synthesis* **2005**, *15*, 1157–1179.

83 A. J. Ashe, *Acc. Chem. Res.* **1978**, *11*, 153–157.

84 G. Märkl, C. Martin, W. Weber, *Tetrahedron Lett.* **1981**, *22*, 1207–1210.

85 G. Märkl, A. Merz, *Tetrahedron Lett.* **1968**, *9*, 3611–3614.

86 a) K. Dimroth, W. Städe, *Angew. Chem. Int. Ed.* **1968**, *7*, 881–882; b) A. Hettche, K. Dimroth, *Chem. Ber.* **1973**, *106*, 1001–1011.

87 N. T. Coles, A. Sofie Abels, J. Leitl, R. Wolf, H. Grützmacher, C. Müller, *Coord. Chem. Rev.* **2021**, *433*, 213729.

88 a) O. Diels, K. Alder, *Ann. Chem. Pharm.* **1928**, *460*, 98–122; b) J. Sauer, *Angew. Chem. Int. Ed.* **1967**, *6*, 16–33; c) K. C. Nicolaou, S. A. Snyder, T. Montagnon, G. Vassilikogiannakis, *Angew. Chem. Int. Ed.* **2002**, *41*, 1668–1698; d) M. Gregoritza, F. P. Brandl, *Eur. J. Pharm. Biopharm.* **2015**, *97*, 438–453; e) J.-A. Funel, S. Abele, *Angew. Chem. Int. Ed.* **2013**, *52*, 3822–3863; f) K. N. Houk, F. Liu, Z. Yang, J. I. Seeman, *Angew. Chem. Int. Ed.* **2021**, *60*, 12660–12681; g) B. Briou, B. Améduri, B. Boutevin, *Chem. Soc. Rev.* **2021**, *50*, 11055–11097.

89 L. Hu, D. Mahaut, N. Tumanov, J. Wouters, L. Collard, R. Robiette, G. Berionni, *Dalton Trans.* **2021**, *50*, 4772–4777.

90 a) G. Märkl, F. Lieb, *Angew. Chem.* **1968**, *80*, 702–703; *Angew. Chem. Int. Ed.* **1968**, *7*, 733; b) A. J. Ashe, M. D. Gordon, *J. Am. Chem. Soc.* **1972**, *94*, 7596–7597; c) G. Märkl, F. Lieb, C. Martin, *Tetrahedron Lett.* **1971**, *12*, 1249–1252; d) H. Tanaka, S. Motoki, *BCSJ* **1986**, *59*, 2047–2049.

91 a) E. Fuchs, M. Keller, B. Breit, *Chemistry* **2006**, *12*, 6930–6939; b) C. Wallis, P. G. Edwards, M. Hanton, P. D. Newman, A. Stasch, C. Jones, R. P. Tooze, *Dalton Trans.* **2009**, 2170–2177.

92 Y. van den Winkel, J. van der Laarse, F. J. J. de Kanter, T. van der Does, F. Bickelhaupt, W. J. J. Smeets, A. L. Spek, *Heteroat. Chem.* **1991**, *2*, 17–28.

93 E. Fluck, B. Neumueller, G. Heckmann, W. Plass, P. G. Jones, *New J. Chem.* **1989**, *13*, 383–388.

94 D. Böhm, F. Knoch, S. Kummer, U. Schmidt, U. Zenneck, *Angew. Chem. Int. Ed.* **1995**, *34*, 198–201.

95 G. Jochem, A. Schmidpeter, *Zeitschrift für Naturforschung B* **1996**, *51*, 773–777.

96 M. A. Hofmann, H. Heydt, M. Regitz, *Synthesis* **2001**, *2001*, 463–467.

97 Y. Kobayashi, I. Kumadaki, A. Ohsawa, H. Hamana, *Tetrahedron Lett.* **1976**, *17*, 3715–3716.

98 C. G. Krespan, *J. Am. Chem. Soc.* **1961**, *83*, 3432–3433.

99 A. Koner, G. Pfeifer, Z. Kelemen, G. Schnakenburg, L. Nyulászi, T. Sasamori, R. Streubel, *Angew. Chem.* **2017**, *129*, 9359–9363; *Angew. Chem. Int. Ed.* **2017**, *56*, 9231–9235.

100 I. Begum, G. Schnakenburg, Z. Kelemen, L. Nyulászi, R. T. Boeré, R. Streubel, *Chem. Commun.* **2018**, *54*, 13555–13558.

101 A. Gese, S. Kermanshahian, G. Schnakenburg, Z. Kelemen, L. Nyulaszi, A. E. Ferao, R. K. Streubel, *Inorg. Chem.* **2021**, *60*, 13029–13040.

102 S. Kermanshahian, T. Kalisch, Z. Kelemen, G. Schnakenburg, L. Nyulászi, R. T. Boeré, R. Streubel, *Dalton Trans.* **2023**, *52*, 9356–9367.

103 D. Rottschäfer, B. Neumann, H.-G. Stammler, T. Sergeieva, D. M. Andrada, R. S. Ghadwal, *Chemistry* **2021**, *27*, 3055–3064.

104 D. Welideniya, M. R. K. Ramachandran, T. Kalisch, R. Streubel, *Dalton Trans.* **2021**, *50*, 9345–9366.

105 A. Koner, Z. Kelemen, G. Schnakenburg, L. Nyulászi, R. Streubel, *Chem. Commun.* **2018**, *54*, 1182–1184.

106 A. Koner, B. M. Gabidullin, Z. Kelemen, L. Nyulászi, G. I. Nikonov, R. Streubel, *Dalton Trans.* **2019**, *48*, 8248–8253.

107 a) M. W. Grafflin in *Advances in chemistry series*, no. 14, AMERICAN CHEMICAL SOCIETY, Washington, **1955**, pp. 1–11; b) W. E. Parham, W. T. Hunter, R. Hanson, T. Lahr, *J. Am. Chem. Soc.* **1952**, *74*, 5646–5648.

108 H. E. Zimmerman, R. M. Paufler, *J. Am. Chem. Soc.* **1960**, *82*, 1514–1515.

109 M. R. K. Ramachandran, G. Schnakenburg, M. Majumdar, Z. Kelemen, D. Gál, L. Nyulászi, R. T. Boeré, R. K. Streubel, *Inorg. Chem.* **2022**, *61*, 4639–4646.

110 I. Begum, *Ph.D. thesis: From C-phosphanylated thiazole-2-thiones to phosphaalkenes and tricyclic 1,4-diphosphinines*. University of Bonn, **2019**.

111 G. I. Nikonov, A. Koner, T. Kalisch, R. Streubel, *unpublished results*.

112 D. Vincze, P. Ábrányi-Balogh, P. Bagi, G. Keglevich, *Molecules* **2019**, *24*.

113 Y. Kobayashi, H. Hamana, S. Fujino, A. Ohsawa, I. Kumadaki, *J. Am. Chem. Soc.* **1980**, *102*, 252–255.

114 Y. Kobayashi, S. Fujino, I. Kumadaki, *J. Am. Chem. Soc.* **1981**, *103*, 2465–2466.

115 C. Garot, G. Etemad-Moghadam, J.-P. Declercq, A. Dubourg, M. Koenig, *Angew. Chem. Int. Ed.* **1992**, *31*, 625–626.

116 M. L. Sierra, N. Maigrot, C. Charrier, L. Ricard, F. Mathey, *Organometallics* **1991**, *10*, 2835–2838.

117 P. Majewski, *Phosphorus, Sulfur, Silicon Relat. Elem.* **1991**, *55*, 185–194.

118 N. Rauf Naz, *Ph.D. thesis: Synthesis and reactions of Janus-type bis(NHCs), tuned by phosphorus bridges*, **2021**.

119 a) S. Yogendra, S. S. Chitnis, F. Hennersdorf, M. Bodensteiner, R. Fischer, N. Burford, J. J. Weigand, *Inorg. Chem.* **2016**, *55*, 1854–1860; b) G. Hogarth, J. Kilmartin, *J. Organomet. Chem.* **2007**, *692*, 5655–5670.

120 a) N. Burford, P. J. Ragogna, K. N. Robertson, T. S. Cameron, N. J. Hardman, P. P. Power, *J. Am. Chem. Soc.* **2002**, *124*, 382–383; b) A. Seifert, D. Scheid, G. Linti, T. Zessin, *Chem. Eur. J.* **2009**, *15*, 12114–12120.

121 a) *Advances in Inorganic Chemistry* (Eds.: C.-S. Liu, T.-L. Hwang), Elsevier, **1985**; b) R. S. Ghadwal, R. Azhakar, H. W. Roesky, *Acc. Chem. Res.* **2013**, *46*, 444–456; c) B. Gehrhus, M. F. Lappert, *J. Organomet. Chem.* **2001**, *617-618*, 209–223.

122 R. S. Ghadwal, H. W. Roesky, S. Merkel, J. Henn, D. Stalke, *Angew. Chem. Int. Ed.* **2009**, *48*, 5683–5686.

123 a) D. Wang, K. Wurst, M. R. Buchmeiser, *J. Organomet. Chem.* **2004**, *689*, 2123–2130; b) O. Jacquet, X. Frogneux, C. Das Neves Gomes, T. Cantat, *Chem. Sci.* **2013**, *4*, 2127.

124 B. Gehrhus, M. F. Lappert, J. Heinicke, R. Boese, D. Bläser, *J. Chem. Soc., Chem. Commun.* **1995**, 1931–1932.

125 a) G. Köbrich, *Angew. Chem.* **1973**, *85*, 314; *Angew. Chem. Int. Ed.* **1973**, *12*, 252–253; b) A. Velian, W. J. Transue, C. C. Cummins, *Organometallics* **2015**, *34*, 4644–4646; c) S. P. Kolesnikov, A. I. Ioffe, O. M. Nefedov, *Russ. Chem. Bull.* **1975**, *24*, 896.

126 A.-R. Ai-Soudani, A. G. Massey, *Applied Organom Chemis* **1988**, *2*, 553–556.

127 A. Ishii, R. Yoshioka, J. Nakayama, M. Hoshino, *Tetrahedron Lett.* **1993**, *34*, 8259–8262.

128 J. A. Werra, K. Wurst, P. Löwe, F. Dielmann, *ChemPlusChem* **2023**, *88*, e202200458.

129 I. Begum, T. Kalisch, G. Schnakenburg, Z. Kelemen, L. Nyulászi, R. Streubel, *Dalton Trans.* **2020**, *49*, 12776–12779.

130 L. Merzoud, F. Guégan, H. Chermette, C. Morell, *J. Comput. Chem.* **2021**, *42*, 1364–1372.

131 A. Espinosa Ferao, R. Streubel, *Inorg. Chem.* **2020**, *59*, 3110–3117.

132 T. P. A. Ruberu, H. R. Albright, B. Callis, B. Ward, J. Cisneros, H.-J. Fan, J. Vela, *ACS nano* **2012**, *6*, 5348–5359.

133 K. Moedritzer, L. Maier, L. C. D. Groenweghe, *J. Chem. Eng. Data* **1962**, *7*, 307–310.

134 E. Fluck, H. Binder, *Z. anorg. allg. Chem.* **1967**, *354*, 139–148.

135 A. Kornath, F. Neumann, H. Oberhammer, *Inorg. Chem.* **2003**, *42*, 2894–2901.

136 a) P. Tomar, T. Braun, E. Kemnitz, *Chem. Commun.* **2018**, *54*, 9753–9756; b) S. Wei, X.-G. Wei, X. Su, J. You, Y. Ren, *Chem. Eur. J.* **2011**, *17*, 5965–5971; c) K. Kureja, J. Zinke, C. Bruhn, U. Siemeling, *Chem. Commun.* **2019**, *55*, 9705–9708; d) M. Raynal, C. S. J. Cazin, C. Vallée, H. Olivier-Bourbigou, P. Braunstein, *Dalton Trans.* **2009**, 3824–3832.

137 K. Izod, A. M. Madlool, A. Craig, P. G. Waddell, *Chem. Ber.* **2022**, *2022*.

138 F. G. Bordwell, A. V. Satish, *J. Am. Chem. Soc.* **1991**, *113*, 985–990.

139 I. Begum, G. Schnakenburg, Z. Han, A. Franconetti, A. Frontera, D. P. Gates, R. Streubel, *Chem. Ber.* **2019**, *2019*, 1697–1705.

140 A. Zambon, G. Borsato, S. Brussolo, P. Frascella, V. Lucchini, *Tetrahedron Lett.* **2008**, *49*, 66–69.

141 K. Shen, Y. Fu, J.-N. Li, L. Liu, Q.-X. Guo, *Tetrahedron* **2007**, *63*, 1568–1576.

142 A. Gese, M. Akter, G. Schnakenburg, A. García Alcaraz, A. Espinosa Ferao, R. Streubel, *New J. Chem.* **2020**, *44*, 17122–17128.

143 A. Espinosa Ferao, A. R. Planells, *Chemistry* **2023**, e202302243.

144 a) A. Dworkin, R. Naumann, C. Seigfred, J. M. Karty, Y. Mo, *J. Org. Chem.* **2005**, *70*, 7605–7616; b) P. Gund, *J. Chem. Educ.* **1972**, *49*, 100.

145 W. L. F. Armarego, *Purification of laboratory chemicals,* Vol. 6, Elsevier/BH, Oxford, **2009**.

146 H. E. Gottlieb, V. Kotlyar, A. Nudelman, *J. Org. Chem.* **1997**, *62*, 7512–7515.

147 O. V. Dolomanov, L. J. Bourhis, R. J. Gildea, J. A. K. Howard, H. Puschmann, *J. Appl. Cryst.* **2009**, *42*, 339–341.

148 V. Lavallo, Y. Canac, C. Präsang, B. Donnadieu, G. Bertrand, *Angew. Chem. Int. Ed.* **2005**, *44*, 5705–5709; *Angew. Chem.* **2005**, *117*, 5851–5855.

149 C. Cui, H. W. Roesky, H.-G. Schmidt, M. Noltemeyer, H. Hao, F. Cimpoesu, *Angew. Chem. Int. Ed.* **2000**, *39*, 4274–4276.

150 N. J. Hardman, B. E. Eichler, P. P. Power, *Chem. Commun.* **2000**, 1991–1992.

151 A. J. Arduengo, H. V. R. Dias, R. L. Harlow, M. Kline, *J. Am. Chem. Soc.* **1992**, *114*, 5530–5534.

152 D. I. Schuster, L. Wang, J. M. van der Veen, *J. Am. Chem. Soc.* **1985**, 7045–7053.

153 J. R. VanWazer, L. Maier, *J. Am. Chem. Soc.* **1964**, *86*, 811–814.

154 F. Gaudemar-Bardone, M. Gaudemar, *Synthesis* **1979**, *1979*, 463–465.

155 W. Rüdorff, E. Schulze, *Z. anorg. allg. Chem.* **1954**, *277*, 156–171.

156 N. D. Scott, J. F. Walker, V. L. Hansley, *J. Am. Chem. Soc.* **1936**, *58*, 2442–2444.

157 Y. S. Goldberg, E. Abele, E. Liepins, M. V. Shimanskaya, *Zh. Org. Khim.* **1989**, *25*, 1099–1102.

158 R. R. Renshaw, F. K. Bell, *J. Am. Chem. Soc.* **1921**, *43*, 916–919.

159 P. A. Fowell, C. T. Mortimer, *J. Chem. Soc.* **1959**, 2913.

160 M. D. Hanwell, D. E. Curtis, D. C. Lonie, T. Vandermeersch, E. Zurek, G. R. Hutchison, *J. Cheminform.* **2012**, *4*, 17.

161 F. Neese, F. Wennmohs, U. Becker, C. Riplinger, *J. Chem. Phys.* **2020**, *152*, 224108.

162 J. Tao, J. P. Perdew, V. N. Staroverov, G. E. Scuseria, *Phys. Rev. Lett.* **2003**, *91*, 146401.

163 a) S. Grimme, J. Antony, S. Ehrlich, H. Krieg, *J. Chem. Phys.* **2010**, *132*, 154104; b) S. Grimme, S. Ehrlich, L. Goerigk, *J. Comput. Chem.* **2011**, *32*, 1456–1465.

164 F. Weigend, R. Ahlrichs, *Phys. Chem. Chem. Phys.* **2005**, *7*, 3297–3305.

165 M. Cossi, N. Rega, G. Scalmani, V. Barone, *J. Comput. Chem.* **2003**, *24*, 669–681.

166 a) M. Sierka, A. Hogekamp, R. Ahlrichs, *J. Chem. Phys.* **2003**, *118*, 9136–9148; b) F. Weigend, *Phys. Chem. Chem. Phys.* **2006**, *8*, 1057–1065.

167 G. Henkelman, B. P. Uberuaga, H. Jónsson, *J. Chem. Phys.* **2000**, *113*, 9901–9904.

168 Y. Zhao, D. G. Truhlar, *J. Phys. Chem. A* **2005**, *109*, 5656–5667.

169 F. Weigend, *J. Comput. Chem.* **2008**, *29*, 167–175.

170 E. F. Pettersen, T. D. Goddard, C. C. Huang, G. S. Couch, D. M. Greenblatt, E. C. Meng, T. E. Ferrin, *J. Comput. Chem.* **2004**, *25*, 1605–1612.

171 P. J. Stephens, F. J. Devlin, C. F. Chabalowski, M. J. Frisch, *J. Phys. Chem.* **1994**, *98*, 11623–11627.

172 *OriginPro*, OriginLab Corporation, Northampton, MA, USA.

173 T. Lu, F. Chen, *J. Comput. Chem.* **2012**, *33*, 580–592.

# 7 APPENDIX

## 7.1 ABBREVIATIONS

| | |
|---|---|
| $(Et_2N)_2PCl$ | chlorobis(diethylamino)phosphane |
| $\Delta_r G$ | free reaction enthalpy |
| δ | chemical shift |
| 12-crown-4 | 1,4,7,10-tetraoxacyclodecane |
| Ad | adamantly, $C_{10}H_{16}$ |
| AICD | anisotropy of the current density |
| Ar | aryl |
| ASE | aromatic stabilisation energy |
| br. s | broad singlet |
| CAAC | (alkyl)(amino)carbene |
| $CAAC^{Pr,Me}$ | 1-(2,6-di-i-propylphenyl)-3,3,5,5-tetramethylazolidine-2-ylidene |
| d | doublet |
| DEAD | diethylacetylene dicarboxylate |
| dec. | decomposition |
| DMPO | 5,5-dimethyl-1-pyrrolidine-*N*-oxide |
| DMSO | dimethylsulfoxide |
| dt | doublet of triplets |
| DTDAF | dithiadiazafulvalene(s) |
| EA | elemental analysis |
| EI | electron ionisation |
| ELF | electron localisation function |
| eq. | equivalent(s) |
| $Et_2O$ | diethylether |
| HCl | hydrogen chloride |
| HMDS | bis(trimethylsilyl)amide |
| HOMA | harmonic oscillator model of aromaticity |
| HOMO | highest occupied molecular orbital |
| HRMS | high resolution mass spectrometry |
| $IMe_2$ | 1,3-dimethylimidazole-2-ylidene |
| $IMe_4$ | 1,3,4,5-tetramethylimidazole-2-ylidene |
| IR | infrared |
| ISCP | isochemical shielding contour plot(s) |
| $KC_8$ | potassium graphite |

| | |
|---|---|
| KHMDS | potassium bis(trimethylsilyl)amide |
| KO$^t$Bu | potassium *t*-butoxate |
| LDA | lithium di-*i*-propylamide |
| LUMO | lowest unoccupied molecular orbital |
| *m* | meta |
| M | molar, mol/L |
| m | multiplet |
| Me | methyl |
| MIC | mesoionic carbene |
| MO | molecular orbital(s) |
| MS | mass spectronomy |
| NaBAr$^F$ | sodium tetrakis(3,5-bis(trifluoromethyl)phenyl)borate |
| NacNacAl | 1,2-dihydro-1,3-bis(2,6-di-*i*-propylphenyl)-4,6-dimethyl-1,3,2-diazaaluminine |
| NacNacGa | 1,2-dihydro-1,3-bis(2,6-di-*i*-propylphenyl)-4,6-dimethyl-1,3,2-diazagallinine |
| $^n$Bu | *n*-butyl |
| $^n$Bu$_4$NCl | tetra-*n*-butylammonium chloride |
| $^n$Bu$_4$NF | tetra-*n*-butylammonium fluoride |
| NHC | *N*-heterocyclic carbene |
| NHSi | *N*-heterocyclic silylene |
| NICS | nucleus independent chemical shift |
| NMR | nuclear magnetic resonance |
| Np | neopentyl |
| *o* | ortho |
| OTf | trifluoromethanesulfonate |
| *p* | para |
| Ph | phenyl, $C_6H_5$ |
| ppm | part(s) per million |
| r.t. | room temperature |
| s | singlet |
| SOM | s -only model |
| t | triplet |
| THF | tetrahydrofurane |
| TMS | trimethylsilyl |
| TMS-Cl | trimethylsilyl chloride |
| TMS-F | trimethylsilyl fluoride |
| triflate | trifluoromethanesulfonate |
| tt | triplet of triplets |
| TTF | tetrathiafulvalene(s) |

## 7.2 ADDITIONAL TABLES AND FIGURES

*Table 12:* Additional desulfurisation reactions of **17c** and **29b** which were not discussed in detail.

| starting material | reagent(s) | solvent | T / °C | observation ($^{31}P\{^{1}H\}$ NMR) |
|---|---|---|---|---|
| **17c** | 2.0 eq. $Cp_2Ti(btmsa)$[a] | toluene | r.t. | −71.4 ppm (**18c**), −13.1 ppm (s), −53.6/−34.7 ppm (d, 24.6 Hz) |
| **17c** | 3.0 eq. $COCl_2$, 3.6 eq. Mg | toluene | r.t. | no reaction |
| **17c** | 3.0 eq. $COCl_2$,1 drop $P^nBu_3$ | toluene | 80 °C | no reaction |
| **17c** | 4.0 eq. sodium naphthalide | THF | −50 °C | unselective reaction |
| **17c** | 4.1 eq. sodium naphthalide | THF | −100 °C | unselective reaction |
| **17c** | 5.7 eq. $Tf_2O$[a] | $CH_2Cl_2$ | r.t. | unselective reaction |
| **17c** | 3.1 eq. $Tf_2O$[a] | $Ch_2Cl_2$ | −80 °C | −101.6 ppm, −72.9 ppm (**18c**), 0.6 ppm |
| **17c** | 2.1 eq. $ZnEt_2$ | toluene | 80 °C | no reaction |
| **17c** | 2.2 eq. 9-BBN[a] | $Et_2O$ | −60 °C | no reaction |
| **29b** | 7.9 eq. KH | MeOH | −60 °C | unselective reaction |
| **29b** | 2.1 eq. MeLi | THF | −95 °C | empty $^{31}P\{^{1}H\}$ NMR spectrum |
| **29b** | 2.1 eq. LiHMDS[a] | THF | r.t. | empty $^{31}P\{^{1}H\}$ NMR spectrum |

[a] Cp: cyclopentadienyl, btmsa: bis(trimethylsilyl)acetylene, $Tf_2O$: trifluoromethanesulfonic anhydride, 9-BBN: 9-borabicyclo(3.3.1)nonane, LiHMDS: lithium bis(trimethylsilyl)amide

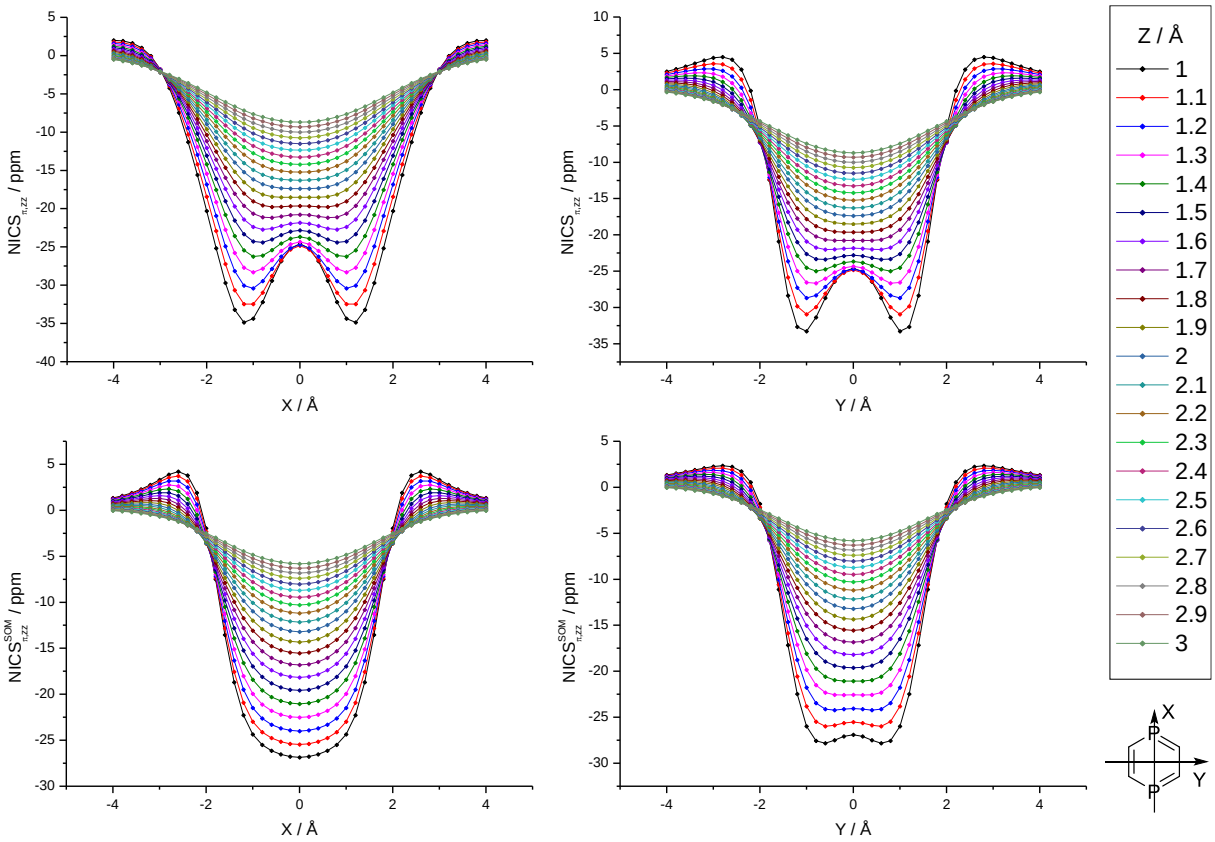


*Figure 69:* XZ (top left), XZ-SOM (bottom left), YZ (top right) and YZ-SOM (bottom right) scans of **C**.

*Table 13:* NICS(1)$^{SOM}_{\pi,zz}$ and $\int$ NICS$^{SOM}_{\pi,zz}$ values of monocyclic **A–D** and tricyclic **Ea,b,f,j**.

| | NICS(1)$^{SOM}_{\pi,zz}$/ ppm | $\int$ NICS$^{SOM}_{\pi,zz}$ / ppm·Å | % of $C_6H_6$ | $R^2$ |
|---|---|---|---|---|
| **A** | –28.4 ± 1.6 | –78.7 ± 4.8 | 100.0 | 0.996 |
| **B** | –28.0 ± 1.4 | –78.0 ± 4.2 | 99.1 | 0.996 |
| **C** | –27.4 ± 1.2 | –77.0 ± 3.7 | 97.8 | 0.997 |
| **D** | –26.0 ± 1.3 | –72.3 ± 3.7 | 91.9 | 0.997 |
| **Ea** | –24.2 ± 1.1 | –67.5 ± 3.5 | 85.8 | 0.997 |
| **Eb** | –24.6 ± 1.2 | –68.6 ± 3.5 | 87.1 | 0.997 |
| **Ef** | –22.3 ± 1.0 | –61.1 ± 2.8 | 77.6 | 0.998 |
| **Ej** | –19.0 ± 0.7 | –51.6 ± 1.9 | 65.5 | 0.999 |

*Table 14:* $\int NICS_{\pi,zz}^{SOM}$ of central and five-membered (fused and free) heterocycles of **Ea–e,h,i,k,m**.

| | Central | | | Outer | | | | | |
|---|---|---|---|---|---|---|---|---|---|
| | $\int NICS_{\pi,zz}^{SOM}$ / ppm·Å | % of $C_6H_6$ | $R^2$ | $\int NICS_{\pi,zz}^{SOM}$ / ppm·Å | | % of $C_6H_6$ | | $R^2$ | |
| | | | | fused | free | fused | free | fused | free |
| **Ea** | –67.5 ± 3.5 | 85.8 | 0.997 | –9.9 ± 1.0 | –11.2 ± 2.0 | 12.6 | 14.2 | 0.946 | 0.972 |
| **Eb** | –68.6 ± 3.5 | 87.1 | 0.997 | –9.8 ± 1.6 | –9.1 ± 1.8 | 12.4 | 11.5 | 0.858 | 0.967 |
| **Ec** | –71.9 ± 3.7 | 91.3 | 0.997 | –10.3 ± 2.5 | —[a] | 13.1 | —[a] | 0.721 | —[a] |
| **Ed** | –63.6 ± 4.0 | 80.8 | 0.994 | –29.2 ± 2.1 | –45.1 ± 3.7 | 37.1 | 57.3 | 0.990 | 0.994 |
| **Ee** | –64.0 ± 4.1 | 81.2 | 0.994 | –27.7 ± 1.9 | –37.3 ± 2.9 | 35.2 | 47.4 | 0.991 | 0.995 |
| **Eh** | –60.7 ± 4.1 | 77.1 | 0.994 | –28.0 ± 1.8 | –46.1 ± 3.2 | 35.6 | 58.5 | 0.992 | 0.996 |
| **Ei** | –61.4 ± 4.1 | 78.0 | 0.993 | –19.9 ± 5.9 | –38.2 ± 2.4 | 25.3 | 48.5 | 0.860 | 0.996 |
| **Ek** | –61.2 ± 4.4 | 77.7 | 0.993 | –29.1 ± 1.7 | –59.8 ± 3.6 | 37.0 | 75.9 | 0.993 | 0.997 |
| **Em** | –55.9 ± 4.1 | 71.0 | 0.993 | –40.0 ± 2.7 | –46.7 ± 2.5 | 50.9 | 59.3 | 0.993 | 0.997 |

[a]no exponential fit to the calculated data could be applied

*Table 15:* $\int NICS_{\pi,zz}^{SOM}$ of central and five-membered (fused and free) heterocycles of **Ef–i**.

| | Central | | | Outer | | | | | |
|---|---|---|---|---|---|---|---|---|---|
| | $\int NICS_{\pi,zz}^{SOM}$ / ppm·Å | % of $C_6H_6$ | $R^2$ | $\int NICS_{\pi,zz}^{SOM}$ / ppm·Å | | % of $C_6H_6$ | | $R^2$ | |
| | | | | fused | free | fused | free | fused | free |
| **Ef** | –61.1 ± 2.8 | 77.6 | 0.998 | —[a] | 3.7 ± 0.4 | —[a] | −4.7 | —[a] | 0.995 |
| **Eg** | –94.4 ± 3.1 | 119.9 | 0.999 | –12.8 ± 0.2 | –24.4 ± 2.2 | 16.2 | 31.0 | 0.999 | 0.991 |
| **Eh** | –60.7 ± 4.1 | 77.1 | 0.994 | –28.0 ± 1.8 | –46.1 ± 3.2 | 35.6 | 58.5 | 0.992 | 0.996 |
| **Ei** | –61.4 ± 4.1 | 78.0 | 0.993 | –19.9 ± 5.9 | –38.2 ± 2.4 | 25.3 | 48.5 | 0.860 | 0.996 |

[a]no exponential fit to the calculated data could be applied

*Table 16:* $\int NICS_{\pi,zz}^{SOM}$ of five-membered heterocycles of **Ff–i**.

| | $\int NICS_{\pi,zz}^{SOM}$ / ppm·Å | % of benzene | $R^2$ |
|---|---|---|---|
| **Ff** | 6.0 ± 1.1 | –7.6 | 0.9723 |
| **Fg** | –19.0 ± 2.6 | 24.1 | 0.9844 |
| **Fh** | –44.3 ± 3.1 | 56.3 | 0.995 |
| **Fi** | –35.2 ± 2.0 | 44.8 | 0.9971 |

*Table 17:* HOMA values of central and five-membered (fused and free) rings of **A–D** and **Ea–m** as well as 1,4-diphosphabarrelenes **Ff–i**.

| | Central | | Outer | | | |
|---|---|---|---|---|---|---|
| | | | fused | | free | |
| | HOMA | % of $C_6H_6$ | HOMA | % of $C_6H_6$ | HOMA | % of $C_6H_6$ |
| **A** | 0.978 | 100 | — | — | — | — |
| **B** | 0.923 | 94.3 | — | — | — | — |
| **C** | 0.844 | 86.3 | — | — | — | — |
| **D** | 0.762 | 77.8 | — | — | — | — |
| **Ea** | 0.708 | 72.4 | 0.785 | 80.2 | 0.813 | 83.1 |
| **Eb** | 0.706 | 72.2 | 0.770 | 78.7 | 0.795 | 81.3 |
| **Ec** | 0.710 | 72.6 | 0.717 | 73.3 | 0.706 | 72.2 |
| **Ed** | 0.721 | 73.7 | 0.784 | 80.1 | 0.873 | 89.3 |
| **Ee** | 0.727 | 74.3 | 0.758 | 77.5 | 0.789 | 80.6 |
| **Ef** | 0.726 | 74.2 | 0.639 | 65.3 | 0.693 | 70.8 |
| **Eg** | 0.746 | 76.2 | 0.736 | 76.9 | 0.803 | 82.0 |
| **Eh** | 0.746 | 76.3 | 0.752 | 76.9 | 0.865 | 88.4 |
| **Ei** | 0.759 | 77.5 | 0.662 | 67.7 | 0.745 | 76.2 |
| **Ej** | 0.743 | 75.9 | 0.547 | 56.0 | 0.633 | 64.7 |
| **Ek** | 0.787 | 80.4 | 0.557 | 56.9 | 0.768 | 78.5 |
| **Em** | 0.728 | 74.4 | 0.759 | 77.6 | 0.902 | 92.1 |
| **Ff** | — | — | 0.703 | 71.9 | — | — |
| **Fg** | — | — | 0.816 | 83.4 | — | — |
| **Fh** | — | — | 0.884 | 90.3 | — | — |
| **Fi** | — | — | 0.769 | 78.6 | — | — |

*Table 18:* $ELF_\pi$ bifurcation values of central and five-membered (fused and free) rings of **A–D** and **Ea–m** as well as 1,4-diphosphabarrelenes **Ff–i**.

| | Central | | Outer | | | |
|---|---|---|---|---|---|---|
| | | | fused | | free | |
| | $ELF_\pi$ | % of $C_6H_6$ | $ELF_\pi$ | % of $C_6H_6$ | $ELF_\pi$ | % of $C_6H_6$ |
| **A** | 0.89 | 100 | — | — | — | — |
| **B** | 0.90 | 101.1 | — | — | — | — |
| **C** | 0.91 | 101.9 | — | — | — | — |
| **D** | 0.90 | 101.1 | — | — | — | — |
| **Ea** | 0.78 | 87.6 | 0.63 | 70.6 | 0.65 | 84.0 |
| **Eb** | 0.76 | 85.4 | 0.58 | 65.2 | 0.70 | 78.7 |
| **Ec** | 0.79 | 88.8 | 0.55 | 62.2 | 0.60 | 67.0 |
| **Ed** | 0.84 | 94.0 | 0.65 | 73.0 | 0.75 | 84.0 |
| **Ee** | 0.78 | 88.0 | 0.66 | 73.9 | 0.73 | 81.6 |
| **Ef** | 0.79 | 89.1 | 0.56 | 62.5 | 0.61 | 68.1 |
| **Eg** | 0.82 | 91.8 | 0.56 | 63.1 | 0.69 | 77.1 |
| **Eh** | 0.81 | 91.0 | 0.67 | 75.1 | 0.76 | 85.6 |
| **Ei** | 0.82 | 92.1 | 0.65 | 73.3 | 0.73 | 81.8 |
| **Ej** | 0.83 | 92.9 | 0.51 | 57.5 | 0.59 | 66.1 |
| **Ek** | 0.82 | 92.5 | 0.69 | 77.5 | 0.79 | 88.3 |
| **Em** | 0.83 | 93.3 | 0.67 | 75.3 | 0.75 | 84.0 |
| **Ff** | — | — | 0.49 | 45.6 | — | — |
| **Fg** | — | — | 0.44 | 49.2 | — | — |
| **Fh** | — | — | 0.72 | 81.1 | — | — |
| **Fi** | — | — | 0.58 | 65.4 | — | — |

## 7.3 CRYSTAL DATA AND STRUCTURE REFINEMENTS

### 7.3.1 9,10-diethyl-3,7-di-n-propyl-4,8-etheno[1,4]diphosphinino[2,3-d:5,6-d']bis-[1,3]thiazole-2,6-dithione (17c)

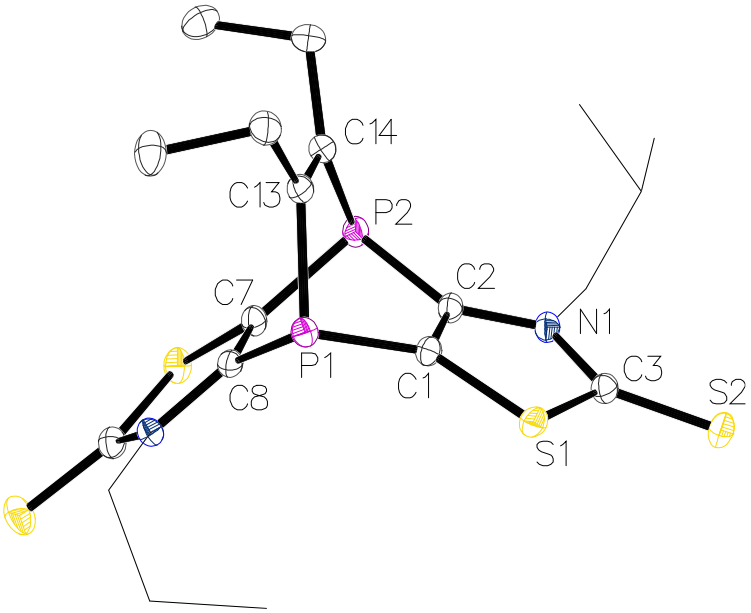


*Figure 70:* Molecular structure of **17c** in the single crystal lattice at 100 K. Thermal ellipsoids are set at 50% probability level. Hydrogen atoms were omitted and N-*n*-propyl groups are shown as wire-frames for clarity.

*Table 19:* Crystal data and structure refinement for **17c**.

| | |
|---|---|
| Identification code | GSTR751, TK-326 // GXraymo_6824f |
| Crystal Habitus | clear colourless block |
| Device Type | Bruker D8 Venture |
| Empirical formula | $C_{18}H_{24}N_2P_2S_4$ |
| Moiety formula | $C_{18}H_{24}N_2P_2S_4$ |
| Formula weight / g/mol | 458.57 |
| T / K | 100 |
| Crystal system | triclinic |
| Space group | $P\bar{1}$ |
| a / Å | 7.2842(5) |
| b / Å | 9.9259(6) |
| c / Å | 15.0111(9) |
| α / ° | 94.948(3) |
| β / ° | 94.001(3) |
| γ / ° | 96.798(3) |
| V / Å$^3$ | 1070.17(12) |
| Z | 2 |
| $\rho_{calc}$ / g/cm$^3$ | 1.423 |
| μ / mm$^{-1}$ | 0.600 |
| F(000) | 480.0 |

| | |
|---|---|
| Crystal size / $mm^3$ | 0.24 × 0.22 × 0.1 |
| Absorption correction | empirical |
| $T_{min}$; $T_{max}$ | 0.6744; 0.7460 |
| Radiation | MoKα (λ = 0.71073) |
| 2Θ range for data collection / ° | 4.152 to 59.932° |
| Completeness to Θ | 0.996 |
| Index ranges | −10 ≤ h ≤ 10, −13 ≤ k ≤ 13, −21 ≤ l ≤ 21 |
| Reflections collected | 20653 |
| Independent reflections | 6196 [$R_{int}$ = 0.0426, $R_{sigma}$ = 0.0400] |
| Data/restraints/parameters | 6196/226/250 |
| Goodness-of-fit on $F^2$ | 1.023 |
| Final R indexes (I≥2σ (I)) | $R_1$ = 0.0297, ω$R_2$ = 0.0712 |
| Final R indexes (all data) | $R_1$ = 0.0354, ω$R_2$ = 0.0747 |
| Largest diff. peak/hole / e/$Å^3$ | 0.46/−0.28 |

*Table 20:* Bond lengths for **17c**.

| Atom | Atom | Length/Å | Atom | Atom | Length/Å |
|---|---|---|---|---|---|
| S1 | C1 | 1.7349(13) | N2 | C8 | 1.3886(16) |
| S1 | C3 | 1.7457(14) | N2 | C9 | 1.3673(16) |
| S2 | C3 | 1.6664(14) | N2 | C10 | 1.4674(16) |
| S3 | C7 | 1.7327(13) | C1 | C2 | 1.3491(18) |
| S3 | C9 | 1.7424(14) | C4 | C5 | 1.523(2) |
| S4 | C9 | 1.6630(14) | C5 | C6 | 1.496(2) |
| P1 | C1 | 1.8193(13) | C5 | C6A | 1.496(3) |
| P1 | C8 | 1.8458(13) | C7 | C8 | 1.3484(18) |
| P1 | C13 | 1.8682(14) | C10 | C11 | 1.5292(19) |
| P2 | C2 | 1.8493(13) | C11 | C12 | 1.524(2) |
| P2 | C7 | 1.8177(14) | C13 | C14 | 1.338(2) |
| P2 | C14 | 1.8713(14) | C13 | C15 | 1.5084(19) |
| N1 | C2 | 1.3907(16) | C14 | C17 | 1.5168(19) |
| N1 | C3 | 1.3687(17) | C15 | C16 | 1.534(2) |
| N1 | C4 | 1.4717(17) | C17 | C18 | 1.529(2) |

*Table 21:* Bond angles for **17c**.

| Atom | Atom | Atom | Angle/˚ | Atom | Atom | Atom | Angle/˚ |
|---|---|---|---|---|---|---|---|
| C1 | S1 | C3 | 92.21(6) | N1 | C4 | C5 | 112.61(11) |
| C7 | S3 | C9 | 92.43(6) | C6 | C5 | C4 | 115.06(13) |
| C1 | P1 | C8 | 94.52(6) | C6A | C5 | C4 | 114.4(7) |
| C1 | P1 | C13 | 96.19(6) | S3 | C7 | P2 | 127.41(8) |
| C8 | P1 | C13 | 96.01(6) | C8 | C7 | S3 | 110.13(10) |
| C2 | P2 | C14 | 95.36(6) | C8 | C7 | P2 | 122.45(10) |
| C7 | P2 | C2 | 95.05(6) | N2 | C8 | P1 | 125.56(9) |

| | | | | | | | |
|---|---|---|---|---|---|---|---|
| C7 | P2 | C14 | 96.35(6) | C7 | C8 | P1 | 120.35(10) |
| C2 | N1 | C4 | 123.86(11) | C7 | C8 | N2 | 114.06(11) |
| C3 | N1 | C2 | 114.66(11) | S4 | C9 | S3 | 123.98(8) |
| C3 | N1 | C4 | 121.48(11) | N2 | C9 | S3 | 108.71(9) |
| C8 | N2 | C10 | 123.77(11) | N2 | C9 | S4 | 127.31(10) |
| C9 | N2 | C8 | 114.66(11) | N2 | C10 | C11 | 112.37(11) |
| C9 | N2 | C10 | 121.56(11) | C12 | C11 | C10 | 113.97(11) |
| S1 | C1 | P1 | 127.11(8) | C14 | C13 | P1 | 121.03(10) |
| C2 | C1 | S1 | 110.41(10) | C14 | C13 | C15 | 125.63(13) |
| C2 | C1 | P1 | 122.45(10) | C15 | C13 | P1 | 113.28(10) |
| N1 | C2 | P2 | 125.90(10) | C13 | C14 | P2 | 120.71(10) |
| C1 | C2 | P2 | 120.21(10) | C13 | C14 | C17 | 124.86(13) |
| C1 | C2 | N1 | 113.89(11) | C17 | C14 | P2 | 113.93(10) |
| S2 | C3 | S1 | 123.45(8) | C13 | C15 | C16 | 111.93(12) |
| N1 | C3 | S1 | 108.82(9) | C14 | C17 | C18 | 109.37(12) |
| N1 | C3 | S2 | 127.72(11) | | | | |

### 7.3.2 9,9-diethyl-3,7-di-*n*-propyl-4,8-ethano[1,4]diphosphinino[2,3-d:5,6-d']bis-[1,3]thiazole-2,6-dithione (18f)

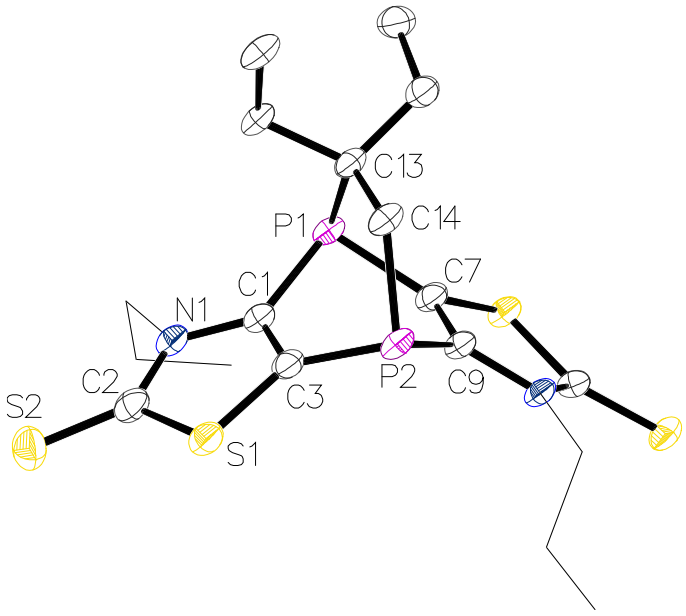


*Figure 71:* Molecular structure of **18f** in the single crystal lattice at 100 K. Thermal ellipsoids are set at 50% probability level. Hydrogen atoms were omitted and N-*n*-propyl groups are shown as wire-frames for clarity.

*Table 22:* Crystal data and structure refinement for **18f**.

| | |
|---|---|
| Identification code | GSTR797, KT-374 // GXray7140 |
| Crystal Habitus | clear colourless plank |
| Device Type | STOE Stadivari |
| Empirical formula | $C_{18}H_{26}N_2P_2S_4$ |

| | |
|---|---|
| Moiety formula | $C_{18}H_{26}N_2P_2S_4$ |
| Formula weight / g/mol | 460.62 |
| T / K | 100 |
| Crystal system | triclinic |
| Space group | $P\bar{1}$ |
| a / Å | 8.3076(3) |
| b / Å | 10.2906(4) |
| c / Å | 15.3615(6) |
| α / ° | 102.542(3) |
| β / ° | 101.566(3) |
| γ / ° | 106.023(3) |
| V / Å$^3$ | 1183.70(8) |
| Z | 2 |
| $\rho_{calc}$ / g/cm$^3$ | 1.292 |
| μ / mm$^{-1}$ | 5.00 |
| F(000) | 484.0 |
| Crystal size / mm$^3$ | 0.2 × 0.1 × 0.05 |
| Absorption correction | multi-scan |
| $T_{min}$; $T_{max}$ | 0.2631; 0.4032 |
| Radiation | CuKα (λ = 1.54186) |
| 2Θ range for data collection / ° | 9.342 to 141.228° |
| Completeness to Θ | 0.994 |
| Index ranges | −9 ≤ h ≤ 10, −12 ≤ k ≤ 12, −10 ≤ l ≤ 18 |
| Reflections collected | 27308 |
| Independent reflections | 4455 [$R_{int}$ = 0.0418, $R_{sigma}$ = 0.0251] |
| Data/restraints/parameters | 4455/0/239 |
| Goodness-of-fit on F$^2$ | 1.051 |
| Final R indexes (I≥2σ (I)) | |
| Final R indexes (all data) | |
| Largest diff. peak/hole / e/Å$^3$ | |

*Table 23:* Bond lengths for **18f**.

| Atom | Atom | Length/Å | Atom | Atom | Length/Å |
|---|---|---|---|---|---|
| S1 | C2 | 1.747(2) | N2 | C8 | 1.354(3) |
| S1 | C3 | 1.729(2) | N2 | C9 | 1.397(3) |
| S2 | C2 | 1.659(2) | N2 | C10 | 1.473(3) |
| S3 | C7 | 1.733(2) | C1 | C3 | 1.351(3) |
| S3 | C8 | 1.744(2) | C4 | C5 | 1.529(3) |
| S4 | C8 | 1.669(2) | C5 | C6 | 1.516(3) |
| P1 | C1 | 1.832(2) | C7 | C9 | 1.352(3) |
| P1 | C7 | 1.818(2) | C10 | C11 | 1.516(3) |
| P1 | C13 | 1.903(2) | C11 | C12 | 1.525(3) |
| P2 | C3 | 1.824(2) | C13 | C14 | 1.554(3) |
| P2 | C9 | 1.837(2) | C13 | C15 | 1.552(3) |

| | | | | | |
|---|---|---|---|---|---|
| P2 | C14 | 1.861(2) | C13 | C17 | 1.543(3) |
| N1 | C1 | 1.394(3) | C15 | C16 | 1.530(3) |
| N1 | C2 | 1.362(3) | C17 | C18 | 1.530(3) |
| N1 | C4 | 1.479(3) | | | |

*Table 24:* Bond angles for **18f**.

| **Atom** | **Atom** | **Atom** | **Angle/˚** | **Atom** | **Atom** | **Atom** | **Angle/˚** |
|---|---|---|---|---|---|---|---|
| C3 | S1 | C2 | 92.36(11) | N1 | C4 | C5 | 112.39(17) |
| C7 | S3 | C8 | 92.08(10) | C6 | C5 | C4 | 114.9(2) |
| C1 | P1 | C13 | 96.35(10) | S3 | C7 | P1 | 126.42(12) |
| C7 | P1 | C1 | 95.11(10) | C9 | C7 | S3 | 110.27(16) |
| C7 | P1 | C13 | 98.31(9) | C9 | C7 | P1 | 123.28(17) |
| C3 | P2 | C9 | 94.54(10) | S4 | C8 | S3 | 123.41(13) |
| C3 | P2 | C14 | 96.38(10) | N2 | C8 | S3 | 109.35(15) |
| C9 | P2 | C14 | 96.60(10) | N2 | C8 | S4 | 127.24(16) |
| C1 | N1 | C4 | 124.20(18) | N2 | C9 | P2 | 125.14(16) |
| C2 | N1 | C1 | 114.85(18) | C7 | C9 | P2 | 121.17(16) |
| C2 | N1 | C4 | 120.91(19) | C7 | C9 | N2 | 113.68(19) |
| C8 | N2 | C9 | 114.59(17) | N2 | C10 | C11 | 111.70(18) |
| C8 | N2 | C10 | 121.75(17) | C10 | C11 | C12 | 111.3(2) |
| C9 | N2 | C10 | 123.57(17) | C14 | C13 | P1 | 114.38(14) |
| N1 | C1 | P1 | 124.61(16) | C15 | C13 | P1 | 104.58(14) |
| C3 | C1 | P1 | 121.70(17) | C15 | C13 | C14 | 110.71(17) |
| C3 | C1 | N1 | 113.6(2) | C17 | C13 | P1 | 106.59(14) |
| S2 | C2 | S1 | 124.20(14) | C17 | C13 | C14 | 108.33(18) |
| N1 | C2 | S1 | 108.71(17) | C17 | C13 | C15 | 112.23(17) |
| N1 | C2 | S2 | 127.10(18) | C13 | C14 | P2 | 120.95(15) |
| S1 | C3 | P2 | 126.69(13) | C16 | C15 | C13 | 114.60(19) |
| C1 | C3 | S1 | 110.44(17) | C18 | C17 | C13 | 116.59(19) |
| C1 | C3 | P2 | 122.80(18) | | | | |

## 7.4 OVERVIEW OF ISOLATED NOVEL COMPOUNDS IN THIS WORK

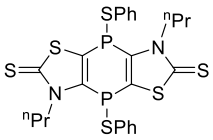

**2**

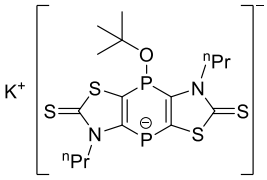

**5e**

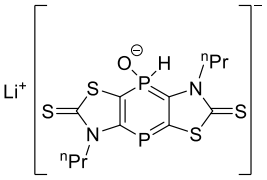

**5f'**

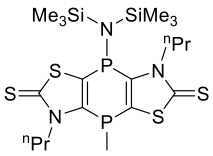

**6c**

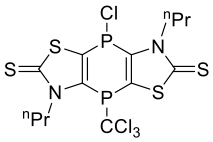

**12**

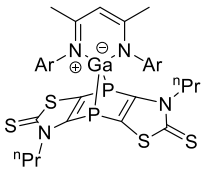

**14a**

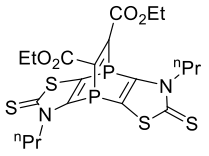

**17a**

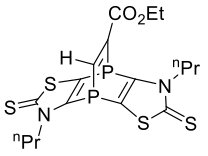

**17b**

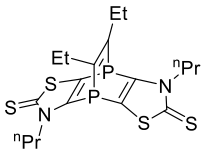

**17c**

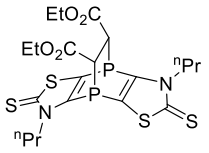

**18a**

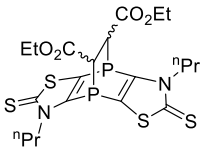

**18a'**

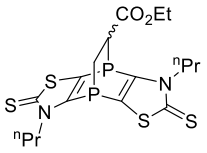

**18b**

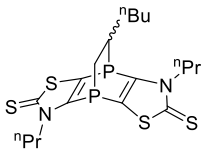

**18c**

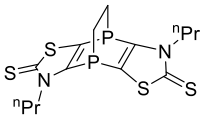

**18d**

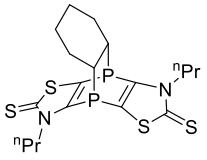

**18e**

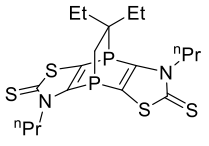

**18f**

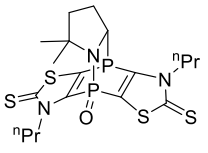

**19**

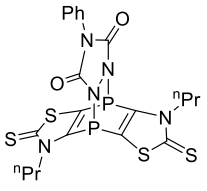

**20**

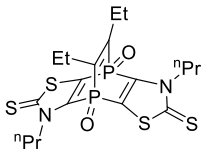

**22b**

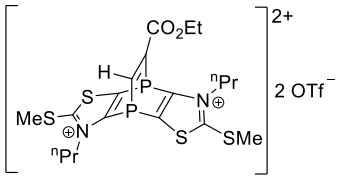

**29a**

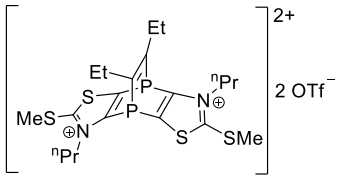

**29b**

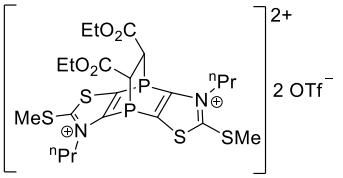

**29c**

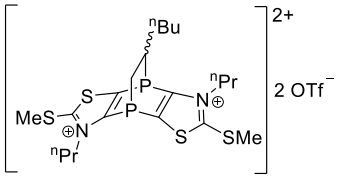

**29d**

## 7.5 LIST OF FIGURES

## 7.6 LIST OF SCHEMES

## 7.7 LIST OF TABLES